

NOTE TO USERS

This reproduction is the best copy available.

UMI[®]

**MODELING IMBIBITION OF LIQUIDS INTO RIGID AND
SWELLING POROUS MEDIA**

by

Reza Masoodi

A Dissertation Submitted in
Partial Fulfillment of the
Requirements for the Degree of

Doctor of Philosophy

in Engineering

at

The University of Wisconsin-Milwaukee

May 2010

UMI Number: 3437981

All rights reserved

INFORMATION TO ALL USERS

The quality of this reproduction is dependent upon the quality of the copy submitted.

In the unlikely event that the author did not send a complete manuscript and there are missing pages, these will be noted. Also, if material had to be removed, a note will indicate the deletion.



UMI 3437981

Copyright 2011 by ProQuest LLC.

All rights reserved. This edition of the work is protected against unauthorized copying under Title 17, United States Code.



ProQuest LLC
789 East Eisenhower Parkway
P.O. Box 1346
Ann Arbor, MI 48106-1346

**MODELING IMBIBITION OF LIQUIDS INTO RIGID AND
SWELLING POROUS MEDIA**

by

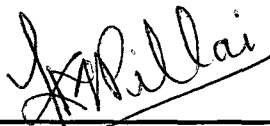
Reza Masoodi

A Dissertation Submitted in
Partial Fulfillment of the
Requirements for the Degree of
Doctor of Philosophy
in Engineering

at

The University of Wisconsin-Milwaukee

May 2010



Major Professor

5/10/2010

Date



Graduate School Approval

8-10-10

Date

ABSTRACT

MODELING IMBIBITION OF LIQUIDS INTO RIGID AND SWELLING POROUS MEDIA

by

Reza Masoodi

The University of Wisconsin-Milwaukee, 2010

Under the Supervision of Dr. Krishna M Pillai

In porous media studies, imbibition is the spontaneous movement of a liquid into a porous medium under the influence of capillary forces. It is also known by the name wicking, and can sometimes be aided by an external pressure, as in the case of forced infiltration of liquid polymers into a bed of fibermats. In this study, the imbibition of liquids into porous media in important engineering applications is studied. A relatively new approach of using the single-phase flow behind a clearly-defined liquid front in a porous medium has been adopted in this work to model imbibition or wicking. Such an approach employs Darcy's law in conjunction with the continuity equation to model the liquid flow behind the front.

First the modeling of liquid flow in polymer wicks is undertaken. A new formula to predict the capillary suction-pressure at the liquid fronts in commercial wicks made of sintering the polymer beads was proposed. Later, a more general formula was derived and verified for estimating the capillary suction pressure in any kind of porous substance. We compared the performance of the proposed Darcy's-law based approach with that of

the Lucas-Washburn equation; some new methods were suggested to improve the accuracy of these two dominant methods for modeling the liquid transport in aforementioned wicks.

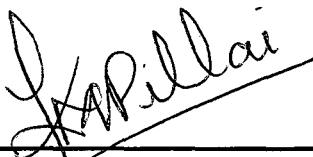
Our Darcy's law based modeling approach is superior to the previous Washburn Equation based approaches as the former can be easily extended to 2-D and 3-D unlike the latter. The 3-D liquid flow in the wicks was studied numerically using PORE-FLOW[®], an in-house computer program to model porous-media flows. For the first time, the finite element/control volume (FE/CV) algorithm is employed to solve the moving-boundary problem encountered in wicking. A good validation is achieved against the 1-D wicking-flow analytical solution as well as a 3-D wicking experiment involving a wick with two different cross-sections.

A special case of wicking, in which both the external hydrodynamic pressure as well as the capillary suction-pressure are the drivers, was studied experimentally and modeled analytically. Both the Darcy's-law based approach as well as the Washburn-equation based approach were used as models. The former was shown to work better at zero or low external pressures, while the latter displayed good predictive capabilities at higher imposed pressures.

We also studied flow in non-rigid swelling porous media. The continuity equation was modified to include the liquid-absorption and swelling effects, and then Darcy's law was employed to model wicking in paper stripes made from cellulose and superabsorbent polymers. The proposed model showed very good agreement with previous experimental results. It was shown that the wicking predictions by the newly proposed model are

identical to the predictions of another theoretical model in which Washburn equation was modified to include the swelling effects.

The wicking in swelling paper stripes was also modeled numerically using PORE-FLOW[®]. Once again the continuity equation, modified to include the liquid-absorption and swelling effects, coupled with the Darcy' s law formed the governing equations. The porosity and hence permeability in a swelling medium are a function of time in such a situation. A new method was proposed to estimate the local permeability in such swelling media from the absorbed-mass-vs-time plot to enable the numerical simulation of such a wicking process. The numerical results compared well with the experimental data and it proved the effectiveness of our suggested local-permeability estimation method as well as our wicking model for the swelling media.



Major Professor

5/10/2010

Date

© Copyright by Reza Masoodi, 2010
All Rights Reserved

This dissertation is dedicated to:

Fatemeh

and

Milad

Without their patience, understanding, support, and most of all love, the completion of this work would not have been possible.

TABLE OF CONTENTS

ABSTRACT	iii
TABLE OF CONTENTS	ix
LIST OF FIGURES	xvi
LIST OF TABLES	xxii
NOMENCLATURE	xxiv
ACKNOWLEDGEMENTS	xxviii
Chapter 1: INTRODUCTION	1
1.1 Imbibition	1
1.2 Mathematical Modeling of Imbibition	1
1.2.1 The Darcy's Law Based Approach	4
1.2.2 Washburn Equation	5
1.3 Capillary Pressure	6
1.4 Swelling Effects	8
1.5 Study of Special Cases	9
1.5.1 Darcy's Law-Based Model for Wicking in Polymer Wicks	9
1.5.2 A Washburn Equation Based Model for Wicking in Polymer Wicks	10
1.5.3 FEM Modeling of Wicking in Altered Polymer Wicks	11
1.5.4 Effect of External Pressure on Wicking into Paper Wipes	12

1.5.5 Darcy's Law Based Model for Wicking in Paper-Like Swelling	
Porous Media	12
1.5.6 A General Formula for Capillary Pressure	13
1.5.7 Flow Modeling in Natural-Fiber Preforms Used in Liquid	
Composite Molding	14
1.5.8 FEM Modeling of Flow in Paper-Like Swelling Porous Media	15
References	15
Chapter 2: DARCY'S LAW BASED MODEL FOR WICKING IN POLYMER	
WICKS	18
2.1 Introduction	18
2.2 Mathematical Theory	21
2.2.1 Washburn equation	21
2.2.2 Darcy's Law based Wicking Formulation	23
2.3. Experimental Procedure	31
2.3.1 Porosity (ε)	33
2.3.2 Permeability (K)	34
2.3.3 Mean Pore Radius of Wicks (R_p)	37
2.3. 4 Surface Tension and Contact Angle	38
2.3. 5 Tortuosity (τ)	40
2.3. 6 Effective Bead Radius (R_e)	40
2.4 Results and Discussion	42
2.4.1 Wicking Tests and Comparison with the Predictions of Various	
Models	45

2.5 Summary and Conclusion	51
References	53
Chapter 3: ROLE OF HYDRAULIC AND CAPILLARY RADII IN	
IMPROVING THE EFFECTIVENESS OF CAPILLARY MODEL IN	
WICKING	55
3.1 Introduction	55
3.2 Theory of Wicking	57
3.2.1 Capillary Model	58
3.2.2 Darcy Model	61
3.2.3 Improving the Capillary Model Through the Capillary and Hydraulic Radii	61
3.3 Experimental Measurements	61
3.3.1 Measuring the capillary radius (R_c)	62
3.3.2. Wicking tests	63
3.4 Results and Discussions	64
3.5 Summary and Conclusion	71
References	72
Chapter 4: DARCY'S LAW BASED NUMERICAL SIMULATION FOR	
MODELING 3-D LIQUID ABSORPTION INTO WICKS	
4.1 Introduction	73
4.2 Geometry of Plain and Altered Wicks	76
4.3 Theory of Wicking	77
4.3.1 Analytical Solution for a Single Cross-Section Wick	79

4.3.2 Analytical Solution for an Altered Wick Using Darcy's Law	80
4.3.3 Analytical Solution for a Simple Wick Using the Modified Capillary Model	83
4.4 Numerical Approach	84
4.4.1 FE/CV method	85
4.5 Results and Discussions	90
4.6 Summary and Conclusion	103
References	104
Chapter 5: EFFECT OF EXTERNALLY APPLIED LIQUID PRESSURE ON WICKING IN PAPER WIPES	106
5.1 Introduction	106
5.2 Mathematical Description of Wicking Models	109
5.2.1 Capillary Model	109
5.2.2 Darcy Model	112
5.3 Experimental Study	115
5.3.1 Measuring the Wicking Parameters	116
5.3.2 Measuring the Wicking Rate under Hydrodynamic Pressure	124
5.4 Results and Discussions	125
5.5 Summary and Conclusion	136
References	137
Chapter 6: DARCY'S LAW BASED MODEL FOR WICKING IN PAPER- LIKE SWELLING POROUS MEDIA	138
6.1 Introduction	138

6.2 Theoretical Details	141
6.2.1 Wicking in Rigid Porous Media	141
6.2.2 Wicking in Non-Rigid, Swelling Porous Media	143
6.3 Results and Discussions	150
6.3.1 An Experimental Study	150
6.3.2 Permeability	154
6.3.3 Wicking Predictions	159
6.4 Summary and Conclusions	162
References	164
Chapter 7: A GENERAL FORMULA FOR CAPILLARY SUCTION-	
PRESSURE IN POROUS MEDIA	167
7.1 Introduction	167
7.2 Derivation of a General Formula for Capillary Suction-Pressure	171
7.3 Verification of the Capillary-Pressure Relation	176
7.3.1 Flow in the Porous Media with a Constant Ratio of the Volume to Wetted Area in Particles	176
7.3.2 Flow along Capillary Tubes with a Fixed Radius	178
7.3.3 Flow along a Bank of the Same-Radius Fibers	179
7.3.4 Flow across a Bank of the Same-Radius Fibers	179
7.3.5 Flow across a Porous Medium Made of Spherical Particles	180
7.3.6 Flow in Woven Fibermats	183
7.4 Applications of the Suggested Formula	183
7.4.1 Deriving New Expressions for Capillary Pressure	183

7.4.2 Using Experimental Measurements to Estimate the Capillary Suction-Pressure	186
7.4.3 Study Changes in the Capillary Suction-Pressure	187
7.5 Summary and Conclusion	192
References	193
 Chapter 8: FLOW MODELING IN NATURAL-FIBER PREFORMS USED IN LIQUID COMPOSITE MOLDING	
8.1 Imbibition	196
8.2 Mathematical Theory	197
8.2.1 Flow Modeling in Rigid Porous Media	197
8.2.2 Flow Modeling in Non-Rigid, Swelling, Porous Media	198
8.3 Experimental Study	200
8.3.1 Measuring the Porosity and Permeability	202
8.3.2 Measuring the Liquid-Front Position	205
8.4 Results and Discussion	205
8.5 Summary and Conclusion	208
References	209
 Chapter 9: DARCY'S LAW BASED NUMERICAL SIMULATION FOR MODELING 2-D LIQUID ABSORPTION INTO PAPER-LIKE SWELLING POROUS MEDIA	
9.1 Introduction	211
9.2 Experimental Study	213
9.3 Theory of Wicking	215

9.4 Numerical Simulation	217
9.4.1 Estimating the Wicking Parameters	219
9.4.2 Estimating the Local Permeability Change	221
9.5 Results and Discussion	224
9.6 Summary and Conclusions	229
References	230
Chapter 10: SUMMARY, CONTRIBUTIONS, AND FUTURE WORK	232
10.1 Summary	232
10.2 Contributions	234
10.3 Future Work	235
References	237
Appendix A: CAPILLARY PRESSURE FOR AN ISOTROPIC POROUS MEDIA WHEN THE RATIO OF VOLUME TO SURFACE AREA OF PARTICLES IS A CONSTANT	239
Appendix B: PERMEABILITY OF A HYBRID SYSTEM	242
Appendix C: DERIVATION OF THE MODIFIED WASHBURN EQUATION FOR SWELLING MEDIA	244
Appendix D: DERIVATION OF THE VOLUME-AVERAGED CONTINUITY EQUATION FOR LIQUID-ABSORBING, SWELLING POROUS MEDIA	244
Appendix F: PRESSURE CHANGE UNDER A FLAT WIPE AT A SMALL ANGLE OF ATTACK	248
CURRICULUM VITAE	253

LIST OF FIGURES

No.	Description	Page
1.1	Two imbibition phenomena showing sharp liquid fronts	3
1.2	Meniscus (or liquid front) in a capillary tube	7
2.1	A typical micrograph of wick C (PP) and the visual description of a method used for measuring tortuosity ($\tau = (L_e / L)^2$).....	22
2.2	A photo and schematic of the real setup developed using DCA for the wicking and contact angle tests.....	23
2.3	A photo and schematic of the Falling Head Permeameter used for measuring the permeability and mean pore radius of the polymer wicks.....	34
2.4	The experimental plot used for estimating the permeability in wick A (PC)	37
2.5	Micrographs of wicks A (PC) and B (PE) showing the shape and size variations in the individual beads	41
2.6	Frequency distribution corresponding to bead radius for wick C (PP)	42
2.7	Scattering test on wick C (PP) with HDEC, scatter bars show confidence interval of 95%	44
2.8	Mass absorption rate in wick A (PC) with three different liquids.....	46
2.9	Mass absorption rate in wick B (PE) with three different liquids.....	47
2.10	Mass absorption rate in wick C (PP) with three different liquids	49
3.1	A schematic of the test setup and liquid front position in the wick	57
3.2	Mass absorption plots using wick A (PC) with the three liquids.....	66
3.3	Mass absorption plots using wick B (PE) with the three liquids.....	67
3.4	Mass absorption plots using wick C (PP) with the three liquids.....	69
4.1	a) A photo of a cylindrical polymer wick. b) An altered-wick section showing changes in its cross-sectional area as well as various associated dimensions.....	76
4.2	Different regions and liquid-front location in a altered wick with two different cross-sectional areas.....	80
4.3	A schematic describing a typical finite element mesh along with the	

surrounding control volumes for application with the FE/CV method to model the motion of liquid front in the wicks.....	85
4.4 A flow chart describing the FE/CV algorithm	88
4.5 A comparison of the numerical prediction with the experimental result and analytical solution for the case of wicking in a simple wick.....	91
4.6 For wicking in wick 'D', a comparison of the numerical prediction with the analytical solutions corresponding to the one and two different cross-sections for wick, and the experimental result.....	92
4.7 The finite element meshes generated for the wicks B, C, D, and E.....	94
4.8 Pattern of liquid-front movement in the wick C.....	95
4.9 Pattern of liquid-front movement in the wick D.....	95
4.10 A comparison of evolution of the dimensionless and numerically predicted liquid-front height (h_f / L_w) in the wicks A, C, and E.....	97
4.11 A comparison of evolution of the dimensionless and numerically predicted liquid-front height (h_f / L_w) in the wicks A, B, and D.....	99
4.12 A comparison of evolution of the dimensionless and numerically predicted liquid-front height (h_f / L_w) in the wicks A, B, and D.....	100
4.13 A comparison of evolution of the dimensionless and numerically predicted liquid-front height (h_f / L_w) in the wicks B, C, D, and E	102
5.1 A schematic and photo of the testing setup used to study the effect of externally imposed liquid-pressure on the wicking rate in a wipe-stack.....	107
5.2 The detail of cutting paper wipes and stacking layers in the cylinder.....	108
5.3 Micrography of the structure of the wipes	117
5.4 A schematic of the test-setup for measuring the permeability and hydraulic pore-radius of the hybrid system consisting of the fritted glass plate and stack of wipes.....	118
5.5 The fitted trend-line for the estimation of the permeability in wipe C.....	119
5.6 A scatter estimation on the wipe C with Windex experiment with scatter bars showing confidence interval of 95%.....	125
5.7 Wicking rate in wipe A when water was used under three different externally-imposed liquid pressures.....	126

5.8	Wicking rate in wipe B when water was used under three different externally-imposed liquid pressures.....	127
5.9	Wicking rate in wipe C when Windex was used under three different externally-imposed liquid pressures.....	129
5.10	The effect of externally imposed liquid pressure on the absorption time for wipes A, B and C when the three wipes absorbed the same volume of liquid...	131
5.11	The effect of externally-imposed liquid pressure on the absorption times for wipes A, B and C when the three wipes absorbed the same volume of liquid...	133
5.12	The effect of externally-imposed liquid pressure on the absorption time when absorbing a fixed volume of liquid (using the non-dimensional pressure and time for wipes A, B and C).....	135
6.1	A schematic of the wicking setup and the wicking (or liquid-front) height in a porous wick.....	142
6.2	Wicking height vs. time plot for water absorption in the 13%FC CMC/Cellulose composite-paper strip [22].....	149
6.3	Relative porosity $\varepsilon_f / \varepsilon_{f_0}$ versus time plot for the 13%FC CMC/Cellulose composite-paper.....	152
6.4	Dimensionless fiber diameter D_{fb} / D_{fb_0} versus porosity plot for the 13%FC CMC/Cellulose composite-paper.....	153
6.5	Dimensionless fiber-diameter D_{fb} / D_{fb_0} versus time plot for the composite 13%FC CMC/Cellulose paper.....	154
6.6	Wicking height vs. time plot for water absorption in the 13%FC CMC/Cellulose composite-paper strip using the capillary-model permeability and different values for the absorption coefficient b . Experimental data are from Ref [22].....	158
6.7	A comparison of predictions by the modified Washburn equation (Eq (6.4)) and the modified Darcy's law with ' $b=1$ ' (Eq (6.23)) while using the capillary-model permeability.....	160
6.8	Wicking height vs. time predictions for the wicking of water in the 13%FC CMC/Cellulose composite-paper strip using the Darcy's law-based model	

with different formula for the permeability of particulate porous media. The predicted values are compared with the modified Washburn-equation predictions and the experimental data of Schuchardt and Berg [22].....	160
Wicking height vs. time predictions for the wicking of water in the 13%FC	
6.9 CMC/Cellulose composite-paper strip using the proposed Darcy's law-based model with different formula for the permeability of <i>fibrous</i> porous media. The predicted values are compared with the modified Washburn-equation predictions and the experimental data of Schuchardt and Berg [22].....	162
7.1 A schematic of particles and void areas in a cross-section of the porous medium.....	173
7.2 Flow through a fiber-bank.....	178
7.3 Wicking predictions using the Darcy's law and different models for the capillary suction-pressure. The wick was put in contact with a liquid at one end while the other end was connected to a microbalance to measure the weight of the wick changing as a function of time. The E.B. Model with gravity, where the capillary pressure was estimated using Eq (7.34), predicted the best results [16]. The variable m is the absorbed mass in grams and t is time in seconds.....	181
7.4 A previous experimental study on the estimation of the capillary pressure in woven fiber-mats [28] showed a linear relation between the capillary pressure and $(1 - \varepsilon)/\varepsilon D_f$. Here different types of woven fiber-mats were used to measure the capillary pressure using the method of rising liquid-front.....	182
7.5 Change in the dimension-less capillary radius (\bar{R}_c) with porosity.....	187
7.6 Changes in the solid-based equivalent capillary radius with the porosity and the solid-based significant length.....	188
7.7 Changes in the void-based equivalent capillary radius with the porosity and the void-based significant length.....	191
7.8 The relation between the dimensionless capillary pressure and the porosity.....	192
8.1 The experimental setup used for permeability measurement and liquid front tracking during 1-D flow in a flat RTM mold.....	200

8.2	Estimation of fiber volume (which is used later to measure porosity) by measuring the difference in liquid volumes in a graduated cylinder before and after the submergence of fiber mats.....	202
8.3	The permeability change predicted by Eq (8.10).....	203
8.4	Estimation of liquid-front location in jute fiber mats during 1-D flow in the test setup.....	204
8.5	A comparison of the theoretical prediction of liquid-front location as a function of time with the experimental observations for the case of using motor oil as test liquid in the absence of fiber swelling.....	205
8.6	A comparison of theoretical predictions for the cases of non-swelling and swelling fibers using the constant and variable K models, respectively.....	206
8.7	A comparison of the theoretical prediction of liquid-front location as a function of time with the experimental observations for the case of using diluted corn-syrup as test liquid which is accompanied by fiber swelling.....	207
9.1	Wicking distance vs. time for n-Octane. (○) 0% CMC; (□) 10% CMC; (◇) 20% CMC; (Δ) 30% CMC [7].....	214
9.2	Wicking distance vs. time for water. (○) 0% CMC; (□) 10% CMC; (◇) 20% CMC; (Δ) 30% CMC [7].....	215
9.3	A schematic of the wicking setup and 2-D mesh used in numerical simulation.	217
9.4	The permeabilities of the first and second parts at time $t = t_2$ along with the average permeability of the system at time $t = t_2$	222
9.5	The experimental data and numerical prediction for 0% CMC.....	225
9.6	The experimental data and numerical prediction for 10% CMC.....	226
9.7	The experimental data and numerical prediction for 20% CMC.....	227
9.8	The experimental data and numerical prediction for 30% CMC.....	228
A-1	A schematic of particles and void areas in the cross-section of a porous medium.....	238
D-1	A schematic showing a spherical representative elementary volume (REV), the solid particles, the fluid region, and the unit normal vector \vec{n}_{fs} (which is on the fluid-solid interface and is directed from the fluid phase to the solid phase) in a porous medium.....	244

F-1	A schematic of cleaning a surface by a flat wipe at a small angle of attack.....	247
F-2	Predicted pressure distribution for a wipe using Eqn (F-19).....	250

•

LIST OF TABLES

No.	Description	Page
1.1	Some practical situations where imbibition is important.....	2
2.1	Characteristics of the test wicks (R_p , R_b , τ and K are presented with the 95% confidence interval range [32]).....	30
2.2	Equations for the height of liquid front h_f as predicted by different models.....	31
2.3	Properties of the test liquids [29, 30, and 31].....	33
3.1	Properties of the test wicks (R_h and R_c are presented with the 95% confidence interval ranges [10]).....	63
4.1	Values of the dimensions shown in Fig 1b for all the five wicks studied in this paper. (Fig. 8 provides an easy visualization of the geometries B, C, D and E.)	77
4.2	Characteristics of the wicks and the liquid used in our validation experiments: The wick was made from polypropylene while the liquid was hexadecane.....	90
4.3	Exact and relative time for liquid front to reach height of 0.07m in different wicks.....	103
5.1	Properties of the test liquids.....	115
5.2	Characteristics of the wipes (the \pm shows 95% confidence interval range [6]).	116
5.3	Contact angles of the wipe-liquid systems (with the 95% confidence interval range [6]).....	123
6.1	The characteristics of test liquid (distilled water) and the values of R_θ and α measured by Schuchardt [21].....	150
6.2	Different suggested relations for $\phi(\varepsilon_f)$ for porous media consisting of packed particles, where c is an arbitrary constant that depends on the structure of porous media.....	155
6.3	Different suggested relations for $\phi(\varepsilon_f)$ for porous media consisting of packed fibers, where c is an arbitrary constant that depends on the structure of	156

porous media.....	
6.4 The final forms of permeability relations (obtained using $\phi(\varepsilon_f)$ and Eq (6.30)) for porous media consisting of packed particles.....	157
6.5 The final forms of permeability relations (obtained using $\phi(\varepsilon_f)$ and Eq (6.30)) for porous media consisting of packed fibers.....	158
9.1 The properties of test liquids [5].....	219
9.2 The wicking parameters of test specimen estimated from Figure 9.1 plots.....	220
9.3 The estimated equations for permeability change in the first part (assumed to be identical to the permeability of each wetted element) when water was used as the wicking liquid.....	224

NOMENCLATURE

Roman Letters

<i>A</i>	Area [m ²], also coefficient matrix
<i>a</i>	A constant ratio related to the rate of decreasing pore radius [<i>I/s</i>]
<i>b</i>	Absorption coefficient (proportional to liquid absorption into matrix) [<i>I/s</i>]
<i>C</i>	Perimeter
<i>D</i>	Diameter [m]
<i>E</i>	Energy
<i>F</i>	Force [N], also coefficient matrix
<i>f</i>	Friction coefficient, also filling factor, also parameter related to each element
<i>g</i>	Acceleration due to gravity [m/s ²]
<i>G</i>	A set of defined function
<i>h</i>	Height [m]
<i>H</i>	Head [m], also total length of porous media [<i>m</i>]
<i>K</i>	Permeability [m ²]
<i>L</i>	Length [m]
<i>l</i>	Length [m]
<i>m</i>	Mass kg], also number of fibers per unit area
<i>M</i>	Number of solid particles
<i>MC</i>	Material constant
<i>N</i>	Number of particles or voids, also element shape function
<i>n</i>	Unit vector, also number of pores per unit area
<i>P</i>	Modified pressure ($P = p + \rho gh$) [Pa]
<i>p</i>	Liquid pressure [<i>Pa</i>]
<i>q</i>	A flow related quantity
<i>Q</i>	Volume flow rate [m ³ /s]
<i>R</i>	Radius [m]
<i>r</i>	Radius [m]
<i>Re</i>	Reynolds number

s	Surface area [m^2]
S	Sink term in the modified continuity equation [l/s]
t	Time [s]
u	x component of velocity [m/s]
v	Darcy velocity [m/s]
V	Velocity vector [m/s]
Vol	Volume [m^3]
W	Work [J]
w	weight function
x	x coordinate
y	y coordinate

Greek Letters

θ	Contact angle [<i>degree</i>]
γ	Surface tension [N/m]
μ	Viscosity of liquid [$kg/m.s$]
Γ	Ratio of volume to surface area [m], surface area of control volume [m^2]
ε	Porosity
η	A parameter in Bruschke and Advanis' permeability model
τ	Tortuosity
ρ	Density of the liquid [kg/m^3]
ϕ	Probability density function
ξ	A coordinate axis
λ	Significant length scale, also a parameter

Subscripts

a	Inertia [Eq (1)]
atm	Atmosphere
b	Bead
c	Capillary
cs	Cross-section

<i>ds</i>	Dry surface
<i>e</i>	Effective
<i>f</i>	Fluid or pore areas in porous media
<i>fb</i>	Fiber
<i>fs</i>	Corresponding to fluid-solid interface
<i>g</i>	Gravity
<i>h</i>	Hydraulic
<i>i</i>	Corresponding to the solid particle or void space i
<i>int</i>	Interface surface of dry and wet matrix
<i>j</i>	Corresponding to the solid particle or void space j
<i>k</i>	Kinetic, also element number
<i>lf</i>	Liquid front
<i>l</i>	Liquid
<i>L</i>	Loss
<i>m</i>	Mechanical
<i>nw</i>	Non-wetting
<i>nsw</i>	Non-swelling parameter
<i>p</i>	Pore
<i>rs</i>	Reservoir
<i>s</i>	Suction, also correspond to solid phase
<i>ss</i>	Steady State
<i>sat</i>	Saturated
<i>sp</i>	Spherical particles
<i>t</i>	Total
<i>sw</i>	Swelling parameter
<i>v</i>	Void space
<i>vs</i>	Viscosity
<i>ws</i>	Wet surface
<i>w</i>	Wetting, also wipe
<i>wk</i>	Wick
<i>0</i>	Initial value

- 1 An index
- 2 An index
- 3 An index

Superscripts

- f fluid or pore areas in porous media
- e related to an element
- t_n n^{th} time step
- ' Dummy variable

Other Symbols

- $\langle \rangle$ volume-averaged quantity
- $\langle \rangle^f$ pore-averaged quantity

ACKNOWLEDGMENTS

I would like to express my deepest gratitude to my advisor, Dr. Krishna Pillai, for his continuous guidance, care, patience, support, and providing me with an excellent atmosphere for doing research. I believe, I was truly fortunate to have such an exceptional teacher and scientist as my mentor and advisor in my Ph.D. study. His high standards on research and teaching and his commitment towards students made it a privilege to work with him. In addition, I express my sincere gratitude to Dr. Padma Varansi for providing me with financial support during the first year of my study at UWM.

I sincerely appreciate my dissertation committee members: Prof. Tien-Chien Jen, Prof. Ryoichi Amano, Dr. Andrei Skliarov, and Dr. Padma Varanasi for their support, patient, insights and suggestions. I am also grateful for their time and efforts in evaluating this research work. I would like to thank Dr. Marjorie Piechowski for her help in editing my papers and also this thesis.

I would like to thank my good friends, Hua Tan, Ehsan M Languri, and Saman Beyhaghi who were always willing to help and give their best suggestions. Many thanks to Andrew Vechart, Mike Verhagen, Grover Bennett, Russell Moore, and other undergraduate students worked in the Laboratory for Flow and Transport Studies in Porous Media for helping me in the experiments. My research would not have been possible without their helps.

I would also like to thank my parents, my sisters, brothers, and in-law family, especially my father in-law. They were always supporting me and encouraging me with their best wishes.

Above all, I would like to thank my wife, Fatemeh Sadry. She was always there cheering me up and stood by me through the good times and bad. This success was not possible without her support and strength during several years of my study. I also thank my sweet son, Milad, who is a constant source of pride, joy, and solace.

Chapter 1

INTRODUCTION

1.1 Imbibition

Imbibition is defined as the displacement of one fluid by another immiscible and more viscose viscous fluid in a porous medium [1]. If this phenomenon happens as a result of the capillary suction pressure, it called wicking or absorption [2]. It may also happen as a result of an external pressure [3]. Examples of wicking applications pertain to liquid absorbing materials, such as wipes, diapers, and commercial wicks [4]. An example of imbibition due to an external pressure is the Liquid Composite Molding (LCM) process for making polymer composites, in which the liquid resin is forced to fill the inter-fiber gaps in a fiber preform [5-7].

In this chapter, some practical scenarios, where the imbibition plays a role, are listed in Table 1.1. Next, the general mathematical theories used in the modeling of the imbibition of liquids are presented. Finally some special cases in detail are presented in the following chapters.

1.2 Mathematical Modeling of Imbibition

The liquid flow through porous media is a very complicated phenomenon. As the flow takes place at the level of the pores, it is often not possible to predict flow in each and every pore of a porous medium. In order to predict the fluid flow in a reasonably sized domain of a porous medium, one has to resort to the

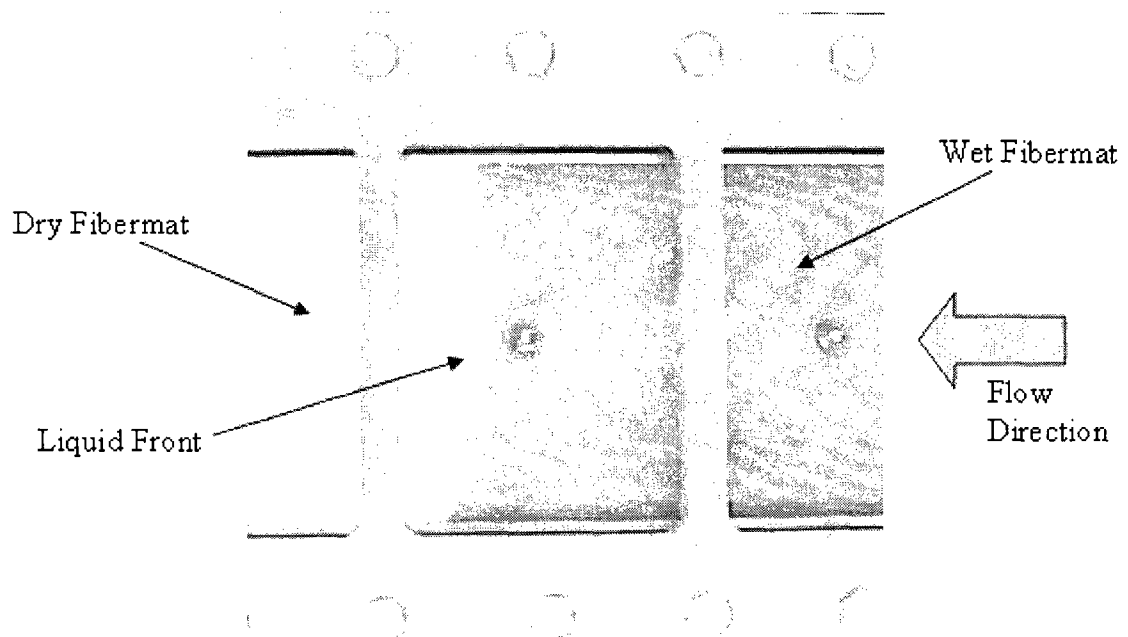
volume averaging approach [26], which means that the averaged velocity or other physical quantities (averaged over a small volume) are used to describe the flow and transport.

Table 1.1 Some practical situations where imbibition is important

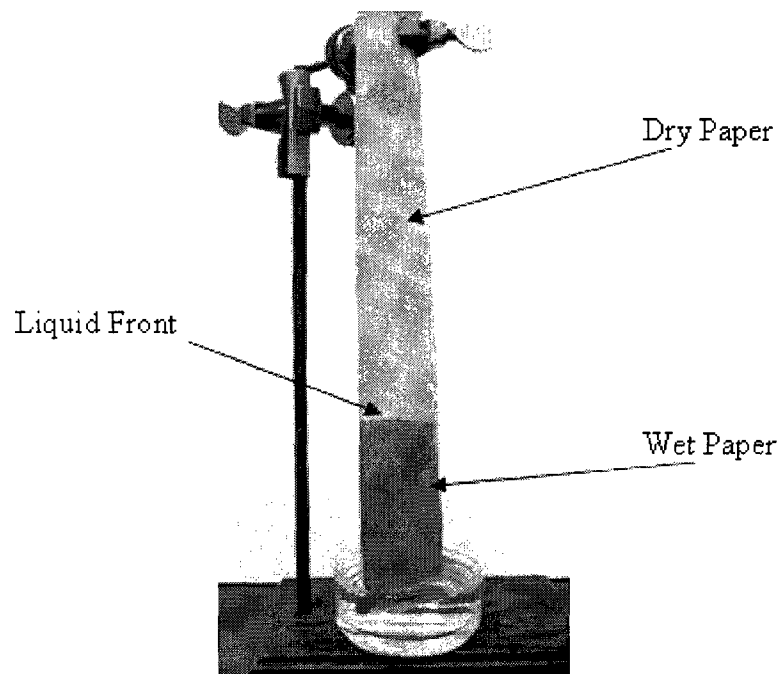
Application	Description
Oil recovery	Displacement of oil by another immiscible liquid [8, 9]
Polymer composites	Invasion of voids in a preform by a resin [5-7]
Textiles	Interaction of liquids and garments [10]
Hydrology	Moving groundwater from wet to dry areas of the soil [11]
Absorption	Removing liquids from a surface [12-15]
Printing process	Ink penetration into paper or coating a paper [16-18]
Food	Wine filtering [19]
Plants	Transport of water and minerals in plants [20, 21]
Air fresheners	Dispensing air fresheners into the air [2, 22, 23]
Insect repellents	Dispensing insect repellents into the air [2, 23,24]
Surface chemistry	Contact angle measurement [25]

The flow of liquid during imbibitions can be treated with two different approaches. One approach is to treat the flow of air and the displacing liquid as a two-phase flow where the volume-averaged flow equations for the two phases is written separately using the generalized form of Darcy's law¹ and the separate continuity equation for the two flowing phases [27,28]. In this approach, the saturation (defined as the percentage of the pore volume occupied by the flowing liquid) usually changes gradually from 100% in the liquid-saturated region to 0% in the completely dry region. There is another approach where the displacement of air by the liquid is seen to be characterized by the presence of a clear liquid-air

¹ Darcy's law is an empirical formula published in 1856 by Henry Darcy based on the results of his experiments on the flow of water through beds of sand [28].



a) A clear liquid-front propagating in a 1-D flow mold through compressed fiber mats



b) A clear liquid-front in a paper absorbing water.

Figure 1.1 Two of the imbibition phenomena showing sharp liquid-fronts

interface (see Figure 1.1). In other words, a clear demarcation exists between the wetted and the dry portions of the porous medium, and such a situation is marked by a sudden drop in saturation from 100% to 0% at the interface. In such a case, the flow of liquid in the wetted portion of the porous medium can be modeled as a single-phase flow through porous media. The flow physics is characterized by the Darcy's law for momentum balance and the single-phase continuity equation. It is this latter type of flow that we will be modeling in the present work.

There are two theories to model the single-phase flow in porous media: the Darcy's law based approach [28] and the Washburn equation [29, 30]. The former a relatively new approach that has been developed fully in the present work; the latter, though based on an out-dated capillary model for liquid flows in porous media, has been the model of choice for researchers investigating wicking and liquid absorption.

1.2.1 The Darcy's Law Based Approach

The single-phase flow of a Newtonian liquid in an isotropic and rigid porous medium is governed by Darcy's law and the following form of the continuity equation:

$$\text{Darcy's Law:} \quad \langle \vec{V} \rangle = -\frac{K}{\mu} \vec{\nabla} \langle P \rangle^f \quad (1.1)$$

$$\text{Continuity Equation:} \quad \vec{\nabla} \cdot \langle \vec{V} \rangle = 0 \quad (1.2)$$

Here $\langle \vec{V} \rangle$ and $\langle P \rangle^f$ are volume-averaged liquid velocity and pore-averaged modified pressure, respectively, and K is the permeability of the porous medium. The variables $\langle \vec{V} \rangle$ and $\langle P \rangle^f$ are obtained after integrating the point-wise liquid velocity and pressure in an averaging volume several times bigger than the particles of a porous medium [28][31].

Using the terminology of the well-known volume averaging method used for deriving the volume-averaged flow and transport equations in porous media [26], the volume average (also called the phase average) and the pore average (also called the intrinsic phase average) for any quantity q_f in a porous medium are defined, respectively, as

$$\langle q_f \rangle = \frac{1}{Vol} \int_{Vol_f} q_f dVol \quad (1.3)$$

$$\langle q_f \rangle^f = \frac{1}{Vol_f} \int_{Vol_f} q_f dVol \quad (1.4)$$

where q_f is integrated over an averaging volume (Vol) called the representative elementary volume or REV².

1.2.2 Washburn Equation

In the Washburn equation, also called the Lucas-Washburn equation, the porous medium is assumed to consist of a bundle of parallel capillary tubes of constant radii. The flow through the capillary-tube bundle is considered to be equivalent to the porous-medium flow. This model uses a one-dimensional flow

² REV is typically much bigger than the solid constituents (particles or fibers) in a porous medium.

as its basis since the flow can just move along the axis of the assumed capillary tubes. For such an idealized porous medium, the Hagen-Poiseuille law [32] for laminar flow through pipes can be employed to find the equation of motion for the porous-medium flow. The Hagen-Poiseuille law states that the volumetric flow-rate is proportional to the pressure drop along the tube length, i.e.,

$$\Delta p = \frac{8\mu L Q}{\pi R_c^4} \quad (1.5)$$

where Q is the volume flow-rate, R_c is the tube radius, μ is the fluid viscosity, L is the length of the wetted tube, and ΔP is the net driving pressure (pressure drop across L). If the only driving pressure is the capillary pressure, then

$$\Delta p = \frac{2\gamma \cos \theta}{R_c} \quad (1.6)$$

where γ is the surface tension of liquid and θ is the contact angle. Note that the volume flow-rate in a tube can be expressed in terms of the rate of change of the wetted length of the tube as

$$Q = \pi R_c^2 \frac{dL}{dt} \quad (1.7)$$

Upon replacing ΔP and Q in Eq (1.5) using Eqs (1.6) and (1.7), we have the following equation for the length of the wetted region as a function of time:

$$L = \sqrt{\frac{R_c \gamma \cos \theta}{2\mu} t} \quad [1.8]$$

This equation is commonly known as the Washburn equation [29, 30] and is used quite frequently in wicking applications [4].

1.3 Capillary Pressure

As mentioned before, the imbibition of liquid into porous media is often modeled as a fully saturated flow behind a clearly-defined fluid front. In such a moving-boundary problem, the driving force, which comes from the capillary

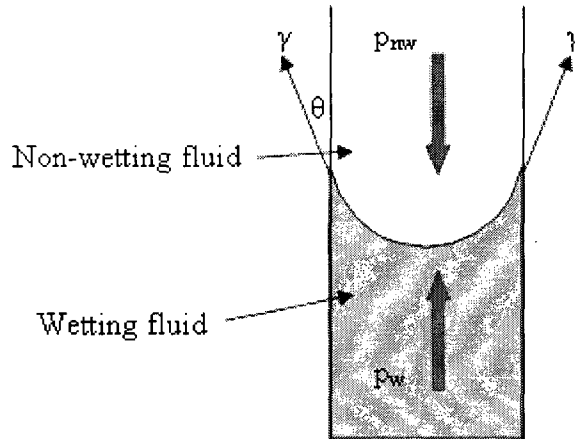


Figure 1.2 Meniscus (or liquid front) in a capillary tube

suction-pressure, pulls the liquid-front during such an imbibition. In fluid statics, the capillary pressure is the difference in pressure across the interface between two immiscible fluids, and thus is defined as

$$p_c = p_{nw} - p_w \quad (1.9)$$

where p_{nw} is the pressure in a non-wetting fluid and p_w is the pressure in a wetting fluid. Consider the capillary tube shown in Figure 1.2; the force balance over the liquid front leads to

$$p_{nw} \pi R_c^2 = p_w \pi R_c^2 + \gamma \cos \theta (2\pi R_c) \quad (1.10)$$

where R_c is the radius of the capillary tube. Combining Eqs (1.9) and (1.10) leads to the following relation, the famous Young–Laplace equation³, for the capillary pressure in tubes:

$$p_c = \frac{2\gamma \cos \theta}{R_c} \quad (1.11)$$

1.4 Swelling Effects

Most of the natural fiber materials (such as cellulose) undergo swelling when a wetting liquid such as water comes in contact with the fibers. It is generally accepted that the crystallinity of such material plays a major role in the swelling process. The amount of water retained by swollen fibers varies from 6% to 100% of dry weight of fibers. This retained water changes the capillary pore-radius, the porosity, and the permeability of porous media made from natural fibers [35].

Swelling starts with the wetting of fibers and ends when the fibers reach an equilibrium state. So it is a time-related process that causes the above-mentioned parameters of the porous medium to vary in each location once the flow-front passes through that location. In the other words, the porosity, capillary pore-radius, and permeability are functions of time and spatial location within the porous media as a result of swelling. Since the parameters of the porous media

³ The Young–Laplace equation is named after Thomas Young, who developed the qualitative theory of surface tension in 1805 [33], and Pierre-Simon Laplace, who published the mathematical description later [34]. It might also be called the Young–Laplace–Gauss equation, as Gauss unified the work of Young and Laplace, by deriving the governing differential equation and boundary conditions using Bernoulli's principles [34].

change due to swelling, then the governing equations (Darcy's law, continuity equation, and Washburn equation) should also be modified to include the swelling effects. An attempt to modify the Washburn equation has already been made in the literature; in this thesis, the modifications implemented in the continuity equation to include the swelling effects in the Darcy's law based flow-model will be presented.

1.5 Study of Special Cases

Because the imbibition is a broad area, some important cases have been selected for a detailed study in this thesis. In each of these studied cases, development of some new ideas, some of them already published in peer-reviewed scientific journals or presented at international conferences, will be described. Following are the studied topics.

1.5.1 Darcy's Law-Based Model for Wicking in Polymer Wicks

In chapter 2, wicking of liquids in polymer wicks made of sintered polymer beads is studied experimentally where three different polymer wicks (made from Polycarbonate, Polyethylene and Polypropylene) and three different well-characterized liquids (Hexadecane, Decane and Dodecane) are used to plot the mass of wicked liquid as a function of time. The experimental results are compared with the predictions from the Washburn equation as well as a Darcy's law based formulation. The suction pressure needed to pull the liquid up a wick in

the formulation is modeled using a new energy balance (E.B.) method and a capillary method. In the former, the released surface energy during wetting is equated to the viscous losses during liquid motion; in the latter, the suction pressure is obtained by treating the wick pore-space as a bundle of capillary tubes. The Darcy's law-based formulation also considers the effect of gravity in its predictions. The newly proposed E.B. method in conjunction with gravity yields the most satisfying predictions. All parameters used in the proposed model were measured independently and no fitting parameters were used. The success of this method is especially notable for a large-pore polypropylene wick where it was the only model to predict the final steady-state height for the liquid column.

1.5.2 A Washburn Equation Based Model for Wicking in Polymer Wicks

In chapter 3, the liquid absorption under capillary pressure, or wicking, in cylindrical polymer wicks made of sintered polymer beads is studied experimentally and theoretically. Three different polymer wicks (made from Polycarbonate, Polyethylene and Polypropylene) and three different well-characterized liquids (Hexadecane, Decane and Dodecane) are used in the present experimental study. These experimental results are then compared with the predictions of the capillary model. The capillary and hydraulic radii used in the model are found to behave like two independent wicking parameters and are needed to be measured separately to improve the accuracy of the capillary model in predicting wicking in the wicks. Accurate measuring of the capillary

radius ensured good predictability of the final steady-state height in the large-pore wicks by the capillary model.

1.5.3 FEM Modeling of Wicking in Altered Polymer Wicks

In chapter 4, liquid imbibition into polymer wicks, where a clear liquid-front can be seen rising during the wicking process, is modeled using the concepts of flow in porous media. The flow of liquid behind the moving liquid-front is modeled using the physics of single-phase flow in a porous medium where Darcy's law is combined with the continuity equation and a capillary suction-pressure pressure is imposed at the liquid front. A novel numerical simulation PORE-FLOW[®] based on the finite element/control volume (FE/CV) method is used to model such imbibitional flows in wicks of complex shapes. A validation of the simulation is obtained by achieving an excellent comparison of its predictions with an experimental result, the analytical solution, and the Washburn equation for the case of wicking against gravity in a cylindrical wick. The simulation is also used to predict flow in a case of three-dimensional wicking in the altered cylindrical wicks with two different cross-sectional areas. Once again an excellent match is obtained with the experimental results, while analytical solutions for the single and double cross-section cases along with the Washburn equation fail to predict the three dimensional wicking. Later some other types of altered wicks with sharp changes in their cross sectional areas were analyzed numerically for their wicking behavior. It was observed that the height of liquid front in a vertical wick as a function of time, which is proportional to the history of liquid imbibed, is

strongly dependent on the extent of reduction in the wick cross-section area as well as its location vis-à-vis the wick entrance.

1.5.4 Effect of External Pressure on Wicking into Paper Wipes

In chapter 5, wicking of liquid under externally applied liquid pressure into three paper wipes is studied. Darcy's law and capillary-flow or Washburn equation form the basis of two separate theoretical models that were tested through experiments. The wicking and wetting parameters of the tested wipes were measured independently to enable such a comparison without the use of any fitting parameters. Darcy's model is found to work better under zero hydraulic pressure, i.e., pure wicking; however, the capillary model is more accurate when the incoming liquid is pressurized. An increase in the applied pressure led to an increase in the liquid absorption rate and a decrease in the saturation time. However, its relative effect on the absorption rate and saturation time was found to decrease with an increase in its magnitude.

1.5.5 Darcy's Law Based Model for Wicking in Paper-Like Swelling Porous

Media

In chapter 6, the wicking of liquid into a paper-like, swelling porous medium made from cellulose and superabsorbent fibers was modeled using Darcy's law. The work is built on a previous study in which the Washburn equation, modified to account for swelling, was used to predict wicking in a

composite of cellulose and superabsorbent fibers. In a new wicking model proposed here, Darcy's law for flow in porous media is coupled with the mass conservation equation with an added sink term to account for matrix swelling and liquid absorption. The wicking-rate predicted by the new model compares well with the previous experimental data, as well as the modified Washburn equation predictions. The effectiveness of various permeability models used with the new wicking model is also investigated.

1.5.6 A General Formula for Capillary Pressure

In chapter 7, a simple, general formula has been developed for the capillary suction-pressure in porous media, which relates the capillary pressure to the micro-structure of various porous media. The energy-balance principle is applied during the wicking process to develop this expression for the capillary pressure in a general porous-medium. The proposed formula can be applied to both the homogeneous as well as inhomogeneous porous media. To validate the suggested theory, six different cases of the capillary suction-pressure from the literature are considered. It is shown that the new formula leads to an identical expression for the capillary suction-pressure for each of the studied cases. Later, the formula is used to derive some expressions for capillary pressure in different porous media where the complexity of microstructure is taken into account. The expressions for the equivalent capillary radius are derived as functions of the significant length of microstructure in porous media and the porosity. It is discovered that the equivalent capillary radius increases with the porosity or the

significant length of solid particles, thereby leading to a reduction in the suction pressure. The proposed equation can also be used to estimate the local capillary suction-pressure using the macrographs of a porous medium.

1.5.7 Flow Modeling in Natural-Fiber Preforms Used in Liquid Composite

Molding

Natural fibers are being increasingly used as substitutes for artificial glass and carbon fibers in polymer composites. However, not much is known about the flow of resins and test liquids through a preform made from natural fibers. The swelling of natural fibers, due to liquid absorption, adds a new dimension to the conventional flow modeling in Liquid Composite Molding (LCM). Swelling of natural fibers causes the permeability and porosity of LCM fibermats to be variable (not constant as assumed for the artificial carbon or glass fibers) during the mold-filling process.

Chapter 8 presents details of an experimental investigation into the flow of liquids through a porous medium made of natural fibers. Two different test liquids, motor oil and water-diluted corn syrup, are used to infiltrate a bed of jute fibers. The latter liquid causes swelling in jute fibers due to the absorption of water, while the former liquid has no similar effect on them. Analytical models to predict 1-D, constant-pressure infiltration into a flat rectangular mold under swelling and non-swelling conditions are compared with experiments. For the swelling case, it is observed that the traditional constant-permeability approach with the conventional continuity equation does not work as well as the new

approach involving variable permeability with a modified continuity equation that incorporates the effect of fiber swelling due to liquid absorption.

1.5.8 FEM Modeling of Flow in Paper-Like Swelling Porous Media

The wicking of water into wet-formed paper strips was studied numerically in chapter 9. The work is built on a previous research in which wicking into four paper stripes, consisting of cellulose fibers and four different percentages of the powdered carboxymethyl cellulose (CMC) superabsorbent, was studied experimentally. Due to the swelling of cellulose fibers and CMC powder on coming in contact with water, the wicking was accompanied by a swelling of the matrix. PORE-FLOW[®], a finite element/control volume (FE/CV) based computer code, was used to model the wicking in such swelling porous medium. The simulation employed an altered form of continuity equation, which included the effects of liquid absorption and matrix swelling, in conjunction with the Darcy's law to model the single-phase flow behind a clearly-defined liquid front. A novel method of estimating the time-varying permeability of the paper, based on the absorbed liquid mass versus time plots, was proposed. Later, this time-dependent permeability was employed in the numerical simulation to change the permeability in finite elements behind the moving liquid-front as a function of the time the element has been wetted by the liquid since the passage of the front. The numerical prediction of the wicking-front location as a function of time compared reasonably well with the previous absorbed-mass-versus-time plots.

References

1. Mikko Alava, Martin Dubé, and Martin Rost, "Imbibition in disordered media," *Advances in Physics*, 53, 83-175, 2004.
2. Masoodi, R., Pillai, K.M. and Varanasi, P.P., "Darcy's Law based Models for Liquid Absorption in Polymer Wicks," *AIChE Journal*, 53,11, 2769-2782, 2007.
3. Masoodi, R., Pillai, K.M. and Varanasi, P.P., "The Effect of Hydraulic Pressure on the Wicking Rate into the Wipes," to appear in *Journal of Engineered Fibers and Fabrics*.
4. P.K Chatterjee and B.S. Gupta. *Absorbent Technology*. Amsterdam. Elsevier. 2002.
5. Krishna M. Pillai, "Governing Equations for Unsaturated Flow in Woven Fiber Mats: Part 1 Isothermal Flows," *Composites Part A: Applied Science and Manufacturing*, 33, 1007-1019, 2002.
6. K.M. Pillai, "Unsaturated flow in liquid composite molding processes: a review and some thoughts," *Journal of Composite Materials*, 38, 23, 2097-2118, Dec 2004.
7. T. Roy and K.M. Pillai, "Characterization of dual-scale fiber mats for unsaturated flow in liquid composite molding," *Polymer Composites*, 26, 6, 756-769, Dec 2005.
8. Sorbie, K. S.; Wu, Y. Z.; McDougall, S. R. The Extended Washburn Equation and Its Application to the Oil/Water Pore Doublet Problem. *J. Colloid Interface Sci.*, 174, 289, 1995.
9. K. M. Pillai and K. Muralidhar, "Numerical Modeling of Enhanced Oil Recovery Using Water Injection Method," *The Journal of Institution of Engineers (India)*, 1992.
10. A. Patniak, R.S. Rengasamy, V.K. Kothari and A. Ghosh. *Wetting and Wicking in Fibrous Materials*. *Textile Progress*. Woodhead, 38, 1, 2006.
11. Martin Hendriks, *Introduction to Physical Hydrology*, Oxford University Press, 2010.
12. N. Mao and S.J. Russell. *Prediction of Liquid Absorption in Homogeneous Three Dimensional Nonwoven Structures*. *Int. Nonwoven Tech. Con. Atlanta*. 2002.
13. N. Mao and S.J. Russell. *Anisotropic Liquid Absorption in Homogeneous Two Dimensional Nonwoven Structures*. *J. Applied Phys.* 94(6), 4135-4138, 2003.
14. D.A. Lockington and J.Y. Parlange. *Anomalous Water Absorption in Porous Materials*. *J. Phys. D: Appl. Phys.* 36, 760-767, 2003.
15. P.A.C.Gane, C.J. Ridgway and J. Schoelkopf. *Absorption Rate and Volume Dependency on the Complexity of Porous Network Structures*. *Transport in Porous Media.*, 54, 79-106, 2004.

16. Schoelkopf, J.; Gane, P. A. C.; Ridgway, C. J.; Matthews, G. P. Influence of Inertia on Liquid Absorption into Paper Coating Structures. *Nordic Pulp Pap. Res. J.*, 15, 422, 2000.
17. Gane, P. A. C.; Schoelkopf, J.; Spielmann, D. C.; Matthews, G. P.; Ridgway, C. J. Fluid Transport into Porous Coating Structures: Some Novel Findings. *Tappi J.*, 83, 77, 2000.
18. Schoelkopf, J. Observation and Modelling of Fluid Transport into Porous Paper Coating Structures. Ph.D. Thesis, University of Plymouth, U.K., 2002.
19. M. Victoria Moreno-Arribas, Carmen Polo, M. Carmen Polo, *Wine Chemistry and Biochemistry*, Springer, 2009
20. <http://users.rcn.com/jkimball.ma.ultranet/BiologyPages/X/Xylem.html>
21. Oktavian Stanislavovich Ksenzhek and Alexander George Volkov, *Plant energetics*, Academic Press; 1st edition, 1998.
22. http://en.wikipedia.org/wiki/Air_freshener.
23. Masoodi, R., Pillai, K.M., and Varanasi, P.P., "Role of Hydraulic and Capillary Radii in Improving the Effectiveness of Capillary Model in Wicking," ASME Summer Conference, Jacksonville FL, USA, August 10-14, 2008.
24. James P. Wingo Timothy Martin, Gary Kessinger, Trevor Waghorn, *Wicks for Dispensers of Vaporizable Matrials*, US patent (#20100065653)
25. Berg, John C. "Wettability," New York, Marcel Dekker, 1993.
26. Whitaker, Stephen. *The Method of Volume Averaging*. Springer. 1998.
27. Adrian E. Scheidegger. *The physics of flow through porous media*. University of Toronto, 1974.
28. Jacob Bear. *Dynamics of Fluids in Porous Media*. Elsevier Science, 1972.
29. Lucas R Rate of Capillary Ascension of Liquids. *Kollid Z.*, 23, 15, 1918.
30. E.V. Washburn. *The Dynamics of Capillary Flow*. *Phys. Rev.* ,17, 273, 1921.
31. C.I. Tucker and R.B. Dessenberger. *Governing Equation for Flow and Heat Transfer in Stationary Fiber beds*. In: SG Advani *.Flow and Rheology in Polymer Composites Manufacturing*. Elsevier Science, Ch 8, 1994.
32. Sutura, Salvatore P. *The history of Poiseuille's law*. *Annual Review of Fluid Mechanics*. 25, 1-19, 1993.
33. Young, T. "An essay on the cohesion of fluids. *Philos. Trans,*" R. Soc. London 95, 65-87, 1805.
34. Finn, Robert "Capillary Surface Interfaces," *Notices of the AMS*, 46, 7, 770-781, 1999.
35. P.K. Chatterjee and B.S. Gupta. *Absorbent Technology*. Amsterdam. Elsevier. 2002.

Chapter 2

DARCY'S LAW BASED MODEL FOR WICKING IN POLYMER WICKS

2.1 Introduction

Wicking is the spontaneous transport of liquid into a porous medium through capillary suction. The capillary suction force arises as a result of the wetting of solid matrix by the invading liquid. Previous research on wicking can be divided into three groups: Study of the relation between the wicking rate and wicking time, study of the relation between the wicking rate and the porous medium characteristics, and study of the wettability of a liquid in terms of the contact angle.

The relation between wicking rate and time was studied by Lucas [1], Washburn [2], and Poiseuille [3]. They concluded that the relation between the wicking rate and the square root of time is linear, i.e. $L = k_0 t^m$ in which $m = 0.5$ and L is wicked mass or height. Some researchers [4] tried to find the exact value of m experimentally, where they estimated it to be between 0.46 to 0.48.

In the first few attempts to model the wicking of a liquid into a porous medium, the porous structure was treated as a bundle of capillary tubes, and the inertial and gravitational forces were neglected in the liquid motion modeling. These assumptions resulted in the simple Washburn equation for predicting of the wicking rate. Szekely et al. [5] took inertial and gravity forces into account

and developed a differential equation for the wicking rate. Unfortunately, the resulting equation is a non-linear, second order, ordinary differential equation that can not be solved analytically. In the most wicking applications, the Washburn equation is used when the inertial and gravitational energies can be neglected.

Study of the wicking rate relationship with the porous medium characteristics, especially the fiber orientation, was also a major direction of previous investigations. Chwastiak [6], Scher [7], and Hodgson and Berg [8] studied the wicking rate along fibers. The wicking rate across the fibers was studied by Fowkes [9], Williams et al. [10], and Pillai and Advani [11].

Wetting is an initial requirement for wicking. The parameter indicating wettability is the contact angle, which is the angle between the tangent lines of the liquid-air and solid-liquid interfaces at the solid-air-liquid contact line. The first notable work on wetting was done by T. Young [12] and Gauss [13]. They tried to find a mathematical equation for contact angle and concluded that the contact angle is a function of surface energies. Dussan and Davis [14] and Dussan [15] reviewed all previous works on the fields of dynamic and static contact angle. In recent years, You-Lo-Hsieh [16] studied liquid wetting and analyzed its relation to fiber morphology and chemistry. Although several researchers tried to find a theoretical equation to predict the magnitude of contact angle, it is still a poorly understood problem.

Wicking tests are used to evaluate the absorption efficiency and liquid transport in the porous materials [17, 18]. It is a function of porous media, time, and wettability (in terms of contact angle). Kissa [19] classified the important

previous works on the wetting and wicking. Miller [20] experimentally investigated the effect of gravity on upward wicking. Russel and Mao [21] proposed an apparatus and a method to investigate the in-plane anisotropic liquid absorption in nonwoven fabrics. Jeong [22] investigated the slip boundary condition on a porous wall using Stokes approximation. Mao and Russel [23] proposed a theoretical approach to predict the liquid absorption in homogeneous 3-D nonwoven structures. They also [24] presented a theoretical analysis of fluid flow in a 2-D nonwoven structure by using Darcy's law. Lockington and Parlange [25] presented a new approach to predict water absorption in porous materials based on sorptivity. Gane et al. [26] numerically and experimentally studied the absorption rate and volume dependency on the complexity of porous networks.

As one can see, a majority of the above mentioned research works is about fibrous materials or textiles where ways of predicting the liquid absorption or wicking into the materials by using the Darcy's law was attempted. The research focused on defining the porous media characteristics, such as the permeability, or the solid-liquid interaction (dynamic contact angle) in order to use the Darcy's law.

Nowadays, commercial wicks, made by sintering polymer beads, are used by consumer product companies to dispense volatile substances such as room fresheners or insect repellents into the air. For these polymer wicks, which have several important commercial applications, no significant research on their wicking characteristics has been reported. In this chapter, we used the Darcy's law to predict the liquid absorption in such wicks. A new expression for the

suction pressure in polymer wicks was developed, which in conjunction with the Darcy's law compares very well with the experimental results and is found to be superior to the conventional modeling approaches such as the Washburn equation.

2.2 Mathematical Theory

We studied the wicking of liquid through a few available commercial wicks in order to investigate the efficiency of the wicking models. In this regard, we used the following approaches.

2.2.1 Washburn equation

The modified Washburn equation can be used to predict the rise of the liquid front h_f as a function of time t ; for our wicking tests it can be expressed as

$$h_f = \left(\frac{R_h \gamma \cos(\theta)}{2\tau^2 \mu} \right)^{1/2} \sqrt{t} \quad (2.1)$$

where R_h is hydraulic radius, γ is the surface energy or surface tension of the liquid, θ is the contact angle, μ is the viscosity of liquid, and τ is the tortuosity of the porous wick obtained from

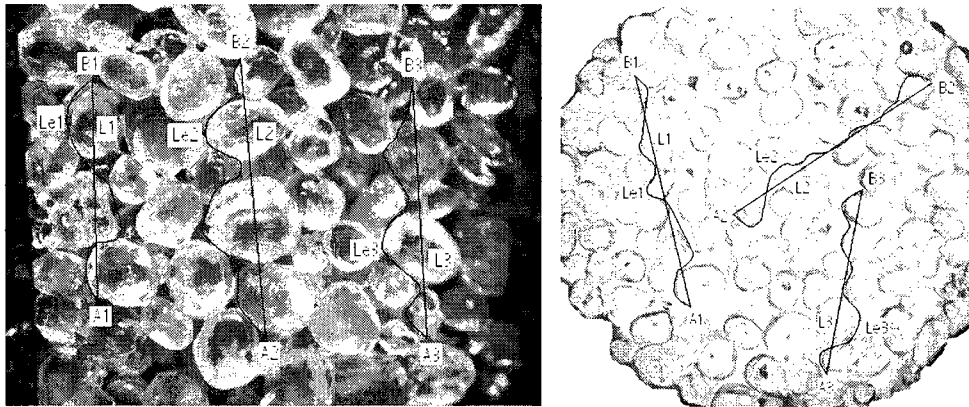
$$\tau = \left(\frac{L_c}{L} \right)^2 \quad (2.2)$$

where L_c is the length of the shortest fluid path through pores between two different points in the wick; L is the length of a straight line path between these two points (see Figure 2.1)

We used the definition of hydraulic radius as the ratio of the fluid volume filled in pores to the wetted surface area of pores to find the hydraulic radius R_h as

$$R_h = \frac{\varepsilon \pi R_{wk}^2 h}{2N\pi R_p h} \quad (2.3)$$

where R_w is wick radius, R_p is mean pore radius, h is height of the liquid within the wick, ε is porosity, and N is number of longitudinal capillaries passing through the wick.



a) Section along the wick axis b) Section across the wick axis
 Figure 2.1. A typical micrograph of wick C (PP) and the visual description of a method used for measuring tortuosity ($\tau = (L_e / L)^2$).

We also have the following equation for pores which is obtained by equating the pore volume in the wick with the total volume of the cylindrical tubes inside the wick:

$$N\pi R_p^2 h = \varepsilon \pi R_{wk}^2 h \quad (2.4)$$

After using Eq. (2.4) in Eq. (2.3) we have

$$R_h = \frac{R_p}{2} \quad (2.5)$$

Applying the Eq. (2.5) result in Eq. (2.1) gives the final form of Washburn equation as

$$h_f = \left(\frac{R_p \gamma \cos(\theta)}{4\tau^2 \mu} \right)^{1/2} \sqrt{t} \quad (2.6)$$

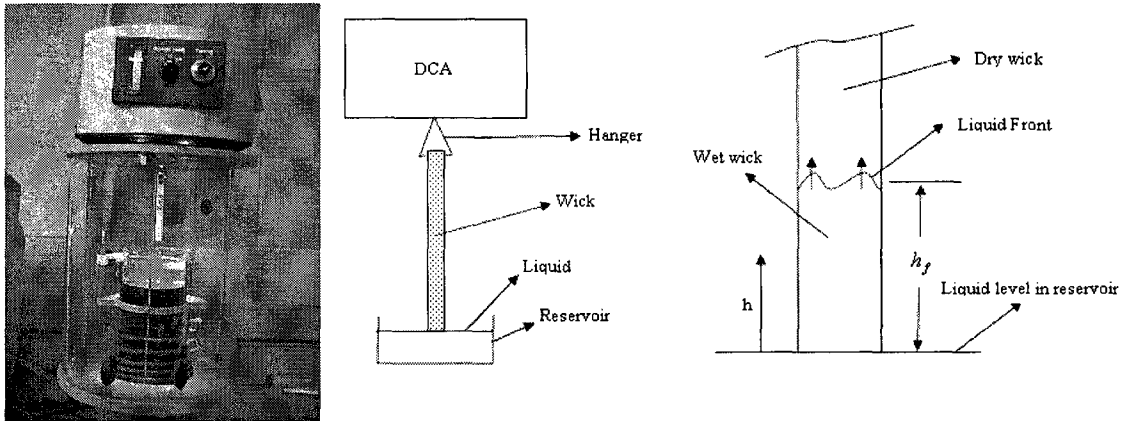


Figure 2.2. A photo and schematic of the real setup developed using DCA for the wicking and contact angle tests.

2.2.2 Darcy's Law based Wicking Formulation

The modified pressure P is defined in such a way so as to include the effects of gravity induced liquid motion in a porous medium and is combined with the pore averaged hydrodynamic pressure p as

$$P = p + \rho gh \quad (2.7)$$

where h is the height of a point within a fully saturated (or fully wetted) porous medium. We would now model the motion of a liquid within a porous polymer wick as shown in Figure. 2.2 The upward wicking of liquid in the vertical wick is characterized by a clearly defined and upwardly mobile liquid front. It is common to assume that the wick below the rising front is fully wet, i.e. all the pore spaces in the porous wick are occupied by the liquid after it has displaced air. As a

result, motion of liquid behind the rising front in the wet wick is governed by Eqs. (1.1) and (1.2). For the one dimensional (1-D) fluid motion described in Figure 2.2, the Darcy's law and continuity equation reduce to

$$V = -\frac{K}{\mu} \frac{dP}{dh} \quad (2.8)$$

and

$$\frac{dV}{dh} = 0 \quad (2.9)$$

The pressure distribution in the wetted wick is given by

$$\frac{d^2P}{dh^2} = 0 \quad (2.10)$$

which is obtained by combining Eqs. (2.8) and (2.9), and noting that K and μ are constants. Integration of Eq. (2.10) results into a general solution of the form $P(h) = Ah + B$ where the constants A and B are evaluated using the boundary conditions

$$p = p_{atm} \quad \text{at} \quad h = 0 \quad (2.11a)$$

and

$$p = p_{atm} - p_s \quad \text{at} \quad h = h_f \quad (2.11b)$$

that are in terms of the pore averaged hydrodynamic pressure p . Note that p_s is the suction pressure created at the liquid front due to the capillary action. Eqs. (2.11a) and (2.11b) can be transformed in terms of the modified pressure P as

$$P = p_{atm} \quad \text{at} \quad h = 0 \quad (2.12a)$$

$$P = (p_{atm} - p_s) + \rho g h_f \quad \text{at } h = h_f \quad (2.12b)$$

Use of the boundary conditions (2.12a) and (2.12b) with the general solution of Eq. (2.10) results into the following expression for the modified pressure:

$$P(h) = p_{atm} + \rho g h - p_s \frac{h}{h_f} \quad (2.13)$$

Note that this solution is valid for $0 \leq h \leq h_f(t)$ where the front height h_f is a function of time. An expression for h_f can be derived by relating front speed $\frac{dh_f}{dt}$

with the Darcy velocity [Eq. (2.8)] at front h_f as

$$\frac{dh_f}{dt} = \frac{V(h = h_f)}{\varepsilon} = -\frac{K}{\varepsilon \mu} \frac{dP}{dh} \quad (2.14)$$

which through the use of Eq.(2.13) results in

$$\frac{dh_f}{dt} = \frac{K}{\varepsilon \mu} \left(\frac{p_s}{h_f} - \rho g \right) \quad (2.15)$$

After separation of variables and integration with the initial value of $h_f(t = 0) = 0$, we have

$$p_s \ln \left| \frac{p_s}{p_s - \rho g h_f} \right| - \rho g h_f = \frac{\rho^2 g^2 K}{\varepsilon \mu} t \quad (2.16)$$

which is an implicit equation for the liquid-front height h_f in the wick. We can neglect the effect of gravity for wicking in smaller samples. After neglecting the gravity term, integration of Eq. (2.15) gives us

$$h_f = \sqrt{\frac{2K p_s t}{\varepsilon \mu}} \quad (2.17)$$

The rise of a liquid in a wick leads to rise in the mass of the wick. The plot of the wicked liquid mass versus time has been used to study and characterize wicking in the past. So note that the mass of fluid absorbed by the wick can be related to h_f through

$$m = \varepsilon \rho \pi R_{wk}^2 h_f \quad (2.18)$$

On studying Eqs. (2.16) and (2.17) for h_f , one notes that suction pressure p_s is an important parameter for predicting the evolution of h_f with time. We will now present two different ways of estimating the suction pressure p_s .

2.2.2.1 Capillary Model

Here the porous wick is assumed to be a bundle of vertically aligned capillary tubes, and the suction pressure is considered to be the capillary pressure. Based on the Young-Laplace equation, Eq. (1.11), the capillary pressure in a cylindrical tube is given by

$$p_c = \frac{2\gamma \cos(\theta)}{R_p} \quad (2.19)$$

Replacing of suction pressure in Eq. (2.16) with capillary pressure (i.e. $p_s = p_c$) leads to

$$p_c \ln \left| \frac{p_c}{p_c - \rho g h_f} \right| - \rho g h_f = \frac{\rho^2 g^2 K}{\varepsilon \mu} t \quad (2.20)$$

We obtain the final form of the liquid-front height (or the liquid-column height) in the wick for the case of neglecting the gravity effects after using the capillary pressure in a cylindrical tube, Eq. (2.19), as the suction pressure in Eq. (2.17):

$$h_f = \sqrt{\frac{4K\gamma \cos(\theta)}{\varepsilon\mu R_p}} \sqrt{t} \quad (2.21)$$

2.2.2.2. Energy Balance Model

Here in order to find an alternative expression for the suction pressure, we apply the energy balance principle to wicking. The amount of energy needed to raise the liquid in the wick is equal to the sum of the viscous energy dissipated by the fluid, the energy spent on accelerating the fluid from zero to the wicking speed, and the energy needed to overcome the gravity. The inertial energy can be neglected in these kinds of experiments as speed of the liquid is very small. We neglect the gravity effects at this stage as well, though we include it elsewhere through the Darcy's law and the modified pressure [Eqs. (2.8) and (2.9)]. So we balanced the reduction of free surface energy when a liquid moves within a wick with the viscous dissipation energy. As the liquid moves through a porous medium, it reduces the dry solid-air interface area and thus increases the wetted solid-liquid interface area. If γ_{ds} stands for the surface energy of the dry surface (or the solid-air interface), and γ_{ws} stands for surface energy of the wetted surface areas (or the solid-liquid interface), then energy balance leads to

$$(\gamma_{ds} - \gamma_{ws}) dA = -dW_{vs} \quad (2.22)$$

in which dA is the interfacial area and W_{vs} is viscous work done by the flow of the liquid. According to Young's equation [12], the relation between the contact angle and surface energy is given by

$$\cos \theta = \frac{\gamma_{ds} - \gamma_{ws}}{\gamma} \quad (2.23)$$

Based on Eq. (2.23), the term $(\gamma_{ds} - \gamma_{ws})$ in Eq. (2.22) can be replaced by $\gamma \cos \theta$.

So we have

$$-dW_{vs} = \gamma \cos \theta dA \quad (2.24)$$

Based on our initial investigation of pore structure by study the wick micrographs (Figure 2.1), we proposed that the porous wick be composed of spherical beads.

The number of beads with radii between r and $(r+dr)$ is given by $dM(r) = M\phi(r)dr$ where M is the total number of the beads in the wick and ϕ is the probability density function. Hence the total volume of beads is

$$Vol_b = \int_0^{\infty} \frac{4}{3} \pi r^3 dM(r) = \frac{4}{3} \pi M M_3, \quad \text{where} \quad M_3 = \int_0^{\infty} r^3 \phi(r) dr \quad (2.25)$$

If Vol_l is the total volume of the wick, then the wick porosity can be estimated as

$$\varepsilon = 1 - \frac{Vol_b}{Vol_l} = 1 - \frac{4\pi M M_3}{3A_{cs} L_w} \quad (2.26)$$

Similarly dA , the increase in the wetted surface area within the cylindrical wick as the liquid moves up by dh_f , is given by

$$dA = \int_0^{\infty} 4\pi r^2 dM(r) \left(\frac{dh_f}{L_{wk}} \right) = 4\pi M M_2 \left(\frac{dh_f}{L_{wk}} \right) \quad \text{where} \quad M_2 = \int_0^{\infty} r^2 \phi(r) dr \quad (2.27)$$

On replacing M in Eq. (2.27) with its equivalent expression from Eq. (2.26), we get

$$dA = 3A_{cs} (1 - \varepsilon) \frac{M_2}{M_3} dh_f \quad (2.28)$$

which allows the change in the wet interface area to be expressed in terms of the change in the liquid-column height. Substitution of dA from Eq. (2.29) into Eq. (2.24) gives the final form for the increment in dissipation energy as

$$dW_{vs} = -\frac{3A_{cs}(1-\varepsilon)\gamma \cos(\theta)}{R_e} dh_f \quad (2.29)$$

where effective radius R_e is defined as $R_e = \frac{M_3}{M_2}$. The mechanical work needed

to move the fluid by dh_f is $dW_m = F_p dh_f$ where F_p is the pulling force that 'pulls' the liquid front through the pores of the wick. As per the definition of suction pressure, this pulling force should be equal to $p_s \cdot \varepsilon \cdot A_{cs}$. As a result

$$dW_m = \varepsilon \cdot p_s A_{cs} dh_f \quad (2.30)$$

According to the energy balance principle, the total energy of system after moving the front liquid into the wick should be equal to its initial value which was zero. So the summation of the left sides of Eqs. (2.29) and (2.30) should be zero, i.e. $dW_{vs} + dW_m = 0$, which results in an expression for suction pressure as

$$p_s = \frac{3(1-\varepsilon)\gamma \cos(\theta)}{\varepsilon R_e} \quad (2.31)$$

Note that if all beads have the same radius of R_b in a simplified ideal case, then

$R_e = R_b$ and we have

$$p_s = \frac{3(1-\varepsilon)\gamma \cos(\theta)}{\varepsilon R_b} \quad (2.32)$$

We have made the following two assumptions in obtaining Eq (2.31):

1. Inertial energy is negligible.
2. Wicks are made up of spherical beads.

We have also made the assumption of neglecting gravity effects, but since the gravity can be included through Darcy's law, it is not listed above. Comparison of Eq (2.31) with Eq (2.19) gives the relation between the suction and capillary pressures as

$$p_s = \left(\frac{3}{2}\right) \left(\frac{R_p}{R_e}\right) \left(\frac{1-\varepsilon}{\varepsilon}\right) p_c \quad (2.33)$$

Table 2.1 Characteristics of the test wicks (R_p , R_b , τ and K are presented with the 95% confidence interval range [32]).

Type of wicks	A	B	C
Material	PC	PE	PP
Length of wick L [m]	0.076	0.075	0.075
Wick radius R_{wk} [m]	0.0036	0.0036	0.0036
Pore radius R_p [μm]	29.8 ± 7.1	36.7 ± 2.5	88.4 ± 4.4
Porosity ε	0.49	0.41	0.4
Average bead radius R_b [μm]	85.9 ± 9.9	133.1 ± 19.9	376.4 ± 30.1
Effective bead radius R_e [μm]	97.9	164.1	428.5
Tortuosity τ	2.38 ± 0.72	2.22 ± 0.81	1.58 ± 0.07
Permeability K [m^2]	$(5.46 \pm 2.3)e - 11$	$(6.84 \pm 1.16)e - 11$	$(3.9 \pm 0.4)e - 10$

Here the capillary pressure p_c , which acts solely inside the hypothetical capillary tubes, is moderated by a function of porosity ε (with $0 < \varepsilon < 1$), mean pore size R_p , and effective bead radius R_e . For our assumption of spherical shape for beads, it

turns out that $R_e > R_p$ (Table 2.1), and hence $p_s < p_c$. It is important to mention that if we assume the wicks to be a bundle of vertically aligned capillary tubes, we can still derive the expression for capillary pressure given in Eq (2.19) using the same approach as used for obtaining Eq (2.31). Substitution of p_s from Eq. (2.31) into Eqs. (2.16) and (2.17) allows us to derive expressions for liquid height h_f for the polymer wicks. The resulting equations, along with the corresponding equations are summarized in Table 2.2

Table 2.2 Equations for the height of liquid front h_f as predicted by different models.

Name of Model	Equation
Washburn Equation	$h_f = \left(\frac{R_p \gamma \cos(\theta)}{4\tau^2 \mu} \right)^{1/2} \sqrt{t}$
Capillary Model	$h_f = \sqrt{\frac{4K\gamma \cos(\theta)}{\varepsilon \mu R_p}} \sqrt{t}$
Capillary Model with gravity	$p_c \ln \left \frac{p_c}{p_c - \rho g h_f} \right - \rho g h_f = \frac{\rho^2 g^2 K}{\varepsilon \mu} t, \quad p_c = \frac{2\gamma \cos(\theta)}{R_p}$
Energy Balance (E.B.) Model	$h_f = \sqrt{\frac{6K(1-\varepsilon)\gamma \cos(\theta)}{\varepsilon^2 \mu R_e}} \sqrt{t}$
E.B. Model with gravity	$p_s \ln \left \frac{p_s}{p_s - \rho g h_f} \right - \rho g h_f = \frac{\rho^2 g^2 K}{\varepsilon \mu} t, \quad p_s = \frac{3(1-\varepsilon)\gamma \cos(\theta)}{\varepsilon R_e}$

2.3. Experimental Procedure

In order to study the wicking process through the commercial polymer wicks experimentally, some parameters about the wicks, the liquids, or the

interaction between wicks and liquids should be found carefully. These parameters are: wick porosity (ε), wick permeability (K), mean pore radius (R_p), mean bead radius (R_b), liquid surface tension (γ), and dynamic contact angle (θ). The experimental techniques and results obtained for the testing materials are described briefly in this section.

Different bead sizes in the wicks lead to different permeability and pore sizes in them. These kinds of wicks, made by sintering polymer beads, are often used for delivering active liquids such as fragrances and insecticides from a reservoir to ambient air or other regions of interest. The most important polymers used for making wicks are Polycarbonate (PC), Polyethylene (PE), Polypropylene (PP), and Ethylene Vinyl Acetate. Among these, the first three are the most commonly used and are hence chosen for this study. We also used three different well-characterized alkane hydrocarbon liquids in the forms of Hexadecane (HDEC), Decane (DEC) and Dodecane (DDEC) to see how variations in the liquid characteristics affect the wicking results. Alkane hydrocarbons are often the main solvents used for making insecticides/insect repellents by the consumer product companies; such solutions are released to the atmosphere through polymer wicks. Another reason for choosing the above alkane hydrocarbons as our test liquids was their low surface energies in comparison to the surface energies of chosen polymers, which cause their imbibition into the wicks to be spontaneous. (Due to the low surface energy of the polymers, these tests can not be done with liquids of high surface energy such as water. PC, PE and PP wicks are known to be hydrophobic as their contact angle

with water is greater than 90° .) The characteristics of the liquids and wicks used in our experiments are presented in Tables (2.1) and (2.3).

We used a Dynamic Contact-angle Analyzer (DCA) equipped with a sensitive balance with the accuracy of 0.0001 gram to measure the absorbed mass in the wicks. The DCA has the capability of recording the weight of the wicks versus time; so with its special software we were able to measure the wicking rates as well as the surface tension of the liquids and contact angles. The details of the experiments are described in the next few subsections.

Table 2.3 Properties of the test liquids [29, 30, and 31].

Type of liquid	Hexadecane (HDEC)	Decane (DEC)	Dodecane (DDEC)
Density [Kg/m^3]	773	730	750
Viscosity [$mPa.s$]	3.34	0.92	1.43
Surface tension [mJ/m^2]	27.47	23.83	25.35

2.3.1 Porosity (ε)

In this experiment, we used Gravimetric Test Method to find the mean porosity of wicks which is based on measuring the wicking rate. A DCA was used to accurately record the mass as a function of time and the amount of liquid absorbed by the wicks is plotted against time. This curve has a positive slope but this slope decreases with time and reaches zero at full saturation. Since all pores of the wetted wick are filled with the liquid at the final saturation stage, the mean porosity (ε) of the cylindrical wick can be determined by the equation

$$\varepsilon = \frac{m_{sat.}}{\rho \pi R_w^2 h_{f,ss}} \quad (2.34)$$

Note that $h_{f,ss} = L_w$ if the liquid traverses the complete wick length.

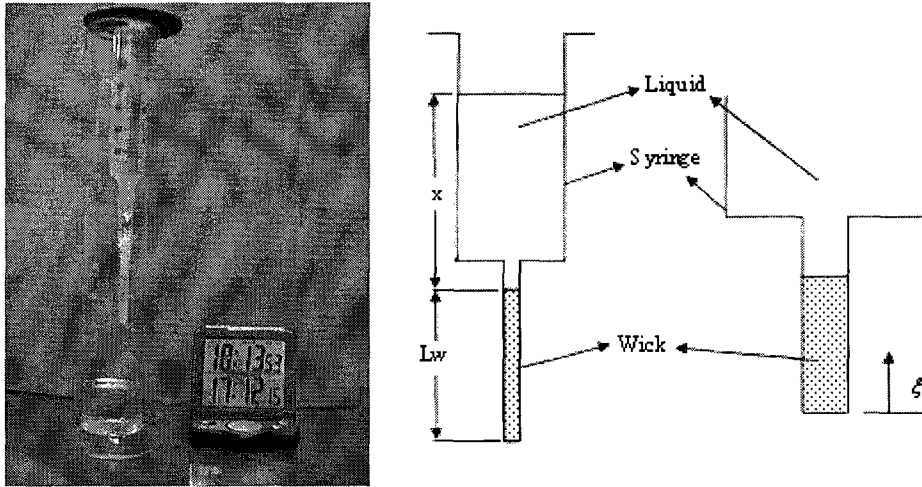


Fig. 2.3. A photo and schematic of the Falling Head Permeameter used for measuring the permeability and mean pore radius of the polymer wicks.

2.3.2 Permeability (K)

Falling Head Permeameter (FHP) is a simple and effective technique for measuring the permeability of porous materials such as wicks [28]. A photo and a schematic of our testing setup are presented in Figure 2.3. A syringe is filled with a hydrocarbon liquid of known density and viscosity, and the wick is attached to the output end of the syringe. The setup is held vertically to enable the gravity force the liquid down the wick. The permeability of the wick is measured by measuring the liquid flow-rate in terms of the speed with which the liquid level goes down in the syringe. Later a formula derived from Darcy's law is used to calculate the permeability of the wick. This technique does not use a high applied pressure and so does not lead to wick compaction (and hence to an alteration in

the distribution of the porosity and pore size in the wick), so it is suitable for quantifying the pore size and permeability of the wicks, especially for compressible wicks which could deform under high pressure. In order to get accurate results from this test, it was ensured that the test liquid did not flow over the sides of the wick by covering the wick surface with scotch tape completely.

Analysis presented here to estimate the permeability is almost identical to the derivation presented in Section 2.2.2 for wicking. However there is an important difference between the two: the current analysis is for the fully saturated flow in the wick, whereas the earlier analysis is for the flow behind a rising front which is *assumed* to be fully saturated. As shown in Figure 2.3, a liquid-column of depth x in the syringe applies the hydrostatic pressure at the bottom to force the liquid through the wick of length L_w . Darcy's law applied to the saturated wick is

$$V = -\frac{K}{\mu} \frac{dP}{d\xi} \quad (2.35)$$

where ξ is an upwardly oriented coordinate axis for the wick (Figure 2.3). This

combined with the equation of continuity $\frac{dV}{d\xi} = 0$ yields $\frac{d^2P}{d\xi^2} = 0$

where $P = p + \rho g \xi$. Therefore pressure distribution inside the wick is to be given

by $P(\xi) = A\xi + B$ where A and B are determined from the boundary conditions

$$P = p_{atm} \quad \text{at} \quad \xi = 0 \quad (2.36a)$$

$$P = p_{atm} + \rho g x \quad \text{at} \quad \xi = L_{wk} \quad (2.36b)$$

This results in

$$P(\xi) = \frac{\rho g x}{L_{wk}} \xi + P_{atm} \quad (2.37)$$

as the pressure distribution inside the wick. Use of this equation in the Darcy's law (Eq. 2.25) yields

$$V = -\frac{K}{\mu} \frac{\rho g x}{L_{wk}} \quad (2.38)$$

The flow rate in the wick is related to the magnitude of wicking velocity $|V|$ through the relation

$$Q = \varepsilon |V| \pi R_{wk}^2 \quad (2.39)$$

Through the mass conservation principle, the flow rate is also related to the rate of depletion of liquid in the burette as

$$Q = -\frac{dx}{dt} \pi R_{rs}^2 \quad (2.40)$$

where x is the height of the liquid. By multiplying Eq (2.38) by $\varepsilon \pi R_{wk}^2$ and using it with Eqs (2.39) and (2.40), the following equation is derived

$$\frac{dx}{dt} = -\frac{K \rho g R_{wk}^2}{\mu L_w R_{rs}^2} x \quad (2.41)$$

On separating the variables and integrating it, we get

$$\ln\left(\frac{x_0}{x}\right) = \frac{K \rho g R_{wk}^2}{\mu L_w R_{rs}^2} t \quad (2.42)$$

The initial condition of $x = x_0$ at $t = 0$ was applied in the integration. In a plot of

$\ln\left(\frac{x_0}{x}\right)$ versus time, the slope of the trend line is equal to $\frac{K \rho g R_{wk}^2}{\mu L_w R_{rs}^2}$. Since all the

other parameters in the 'slope' equation are known, the permeability K can be found. Each test was repeated four times to make sure that the slope of the line

had a repeatable value. The trend line and its slope for wick A (PC) is presented in Figure 2.4; and the test results are given in Table 2.1

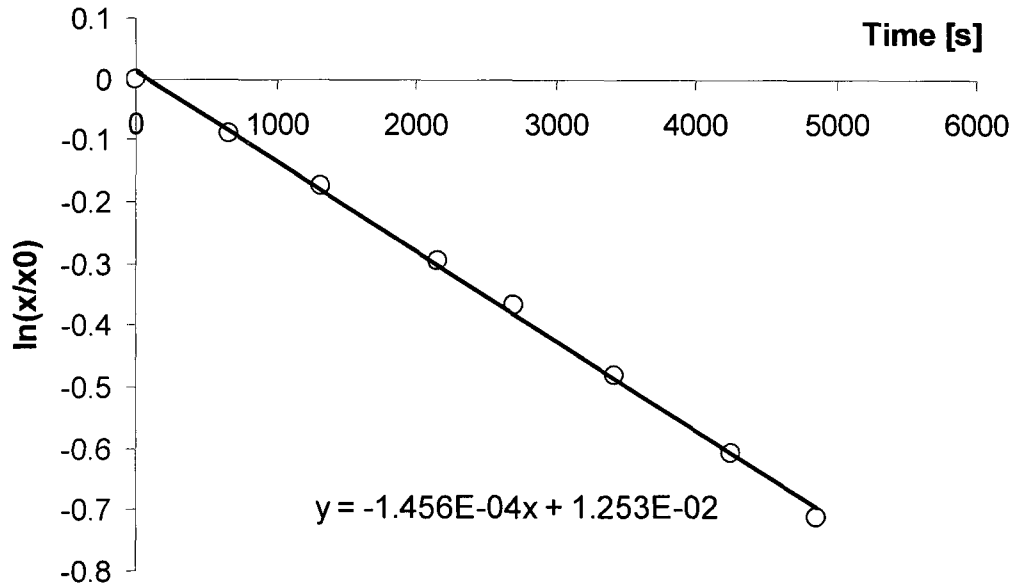


Fig. 2.4. The experimental plot used for estimating the permeability in wick A (PC)

2.3.3 Mean Pore Radius of Wicks (R_p)

The mean pore size of the wick, to be used with the capillary model, can be estimated by the same device that is used for measuring the permeability. We once again assume the wick to consist of parallel capillary tubes. By applying the Hagen-Poiseuille law, the flow rate Q through the wick can be described by

$$Q = N \frac{\pi \rho g R_p^4 (x + L_{wk})}{8 \mu L_{wk}} \quad (2.43)$$

After substituting Eq. (2.40) into Eq. (2.43), and integrating with the initial condition of $x = x_0$ at $t = 0$, the following equation is derived

$$\ln\left(\frac{x + L_{wk}}{x_0 + L_{wk}}\right) = -\frac{N\rho g R_p^4}{8R_s^2 \mu L_{wk}} t \quad (2.44)$$

Since N is the number of capillary tubes passing through the wick, so

$$N = \frac{\varepsilon \pi R_{wk}^2}{\pi R_p^2} \quad (2.45)$$

Substitution of Eq. (2.45) into Eq. (2.44) leads to

$$\ln\left(\frac{x_0 + L_{wk}}{x + L_{wk}}\right) = \frac{\varepsilon R_{wk}^2 R_p^2 \rho g}{8 \mu L_{wk} R_s^2} t \quad (2.46)$$

So by measuring the height of the fluid level, x , at various times and plotting

$\ln\left(\frac{x_0 + L_{wk}}{x + L_{wk}}\right)$ versus time, the slope of the trend line can be measured and pore

radius R_p can be computed from Eq. (2.46). The measured pore radii for the three

testing wicks are listed in Table 2.1.

2.3.4 Surface Tension and Contact Angle

The standard Wilhelmy plate method was used in a DCA to measure the surface tension of the three test liquids. DCA was also used to measure the dynamic contact angles of the wicks and liquids system. This new approach is based on the Washburn theory. According to Eqs. (2.1) and (2.18), the absorbed liquid mass into the pores of the wick obeys the relationship

$$m = \varepsilon \rho \pi R_{wk}^2 \left(\frac{R_h \gamma \cos(\theta)}{2\tau^2 \mu} \right)^{1/2} \sqrt{t} \quad (2.47)$$

Raising both sides to the power of two results in

$$m^2 = \frac{MC\rho^2 \gamma \cos(\theta)}{\mu} t \quad (2.48)$$

Where MC, the material constant, is equal to

$$MC = \frac{\varepsilon^2 \pi^2 R_w^4 R_h}{2\tau^2} \quad (2.49)$$

The experiments were performed and the mass of the absorbed liquid was measured versus time. The setup shown in Figure 2.2 was used to estimate the contact angles through this Washburn-theory based approach. A plot of m^2 versus t was used to find the slope of the best fitted line; this slope in turn was used to find the constant MC and contact angle for the testing wick. First, the experiments were performed with a liquid in which the contact angle is close zero, so that we could use the slope of the best fitted line to estimate MC. For this reason we used N-hexane, a liquid with a very low surface tension. It was then possible to perform the same experiments with the three test liquids, and estimate the contact angle for liquids and the wick through the use of Eq. (2.48).

This newly proposed method is valid when MC can be assumed to remain constant for a given wick from one experiment to the next. According to Eq. (2.44), the material constant MC is a geometry based term that is a function of the macro-geometric parameters (such as R_w) and the micro-geometric parameters (such as ε , R_h and τ). Because MC was assumed to be constant, we ensured that each wick sample has the same size, shape and pore orientation during these experiments.

Incidentally, the measured contact angles were found to be zero for all combinations of the considered testing liquids and wicks. This was to be expected since the surface energy of wicks was much higher than liquids.

2.3.5 Tortuosity (τ)

The micrographs of the wicks were used to estimate the tortuosity of the porous medium. Figure 2.1 shows two microscopic cross-sections of the wick C (PP) along and across its length, and shows our method to measure the tortuosity. Three pairs of points across the wick and another three pairs along the wick were considered to measure the mean tortuosity for each wick. The measured tortuosities, listed in Table 2.1, enabled us to use the modified Washburn equation, Eq. (2.6).

(Incidentally if we consider an idealized spherical geometry for polymer beads that constitute the wicks, the ratio of L_e/L will be equal to $\frac{\pi}{2}$ for a path wrapped around an individual bead, as it is the ratio of half of the circular section perimeter to its diameter. The resultant tortuosity τ obtained from Eq. 2.2 is 2.47, which is of the same order-of-magnitude as the values listed in Table 2.1)

2.3.6 Effective Bead Radius (R_e)

The micrographs of the wicks were also used to measure the bead sizes distribution and to observe the range of variations in bead shapes for different wicks (Figures 2.1 and 2.5). The frequency distribution of the measured bead radii was presented in the form of a histogram for all the three wicks. (The histogram for wick C (PP) is shown in Figure 2.6.) As described under Eq. (2.29), the effective radius should be estimated as

$$R_e = \frac{M_3}{M_2} = \frac{\int_0^{\infty} r^3 \phi(r) dr}{\int_0^{\infty} r^2 \phi(r) dr} \quad (2.50)$$

Since discrete frequencies are plotted in the histogram, so the corresponding discrete *probability density function* for each bead radius R_{b_i} can be determined by

$$\phi(R_{b_i}) = \frac{\text{frequency corresponding to } R_{b_i}}{T} \quad (2.51)$$

where T is the sum of all frequencies. The discrete form of Eq. (2.50) is

$$R_e = \frac{\sum_{R_{b_i}.min}^{R_{b_i}.max} R_{b_i}^3 \phi(R_{b_i})}{\sum_{R_{b_i}.min}^{R_{b_i}.max} R_{b_i}^2 \phi(R_{b_i})} \quad (2.52)$$

where the effective radius R_e can be obtained after using the ϕ estimated through Eq. (2.52). The measured effective and mean bead radii for the considered wicks are presented in Table 2.1.

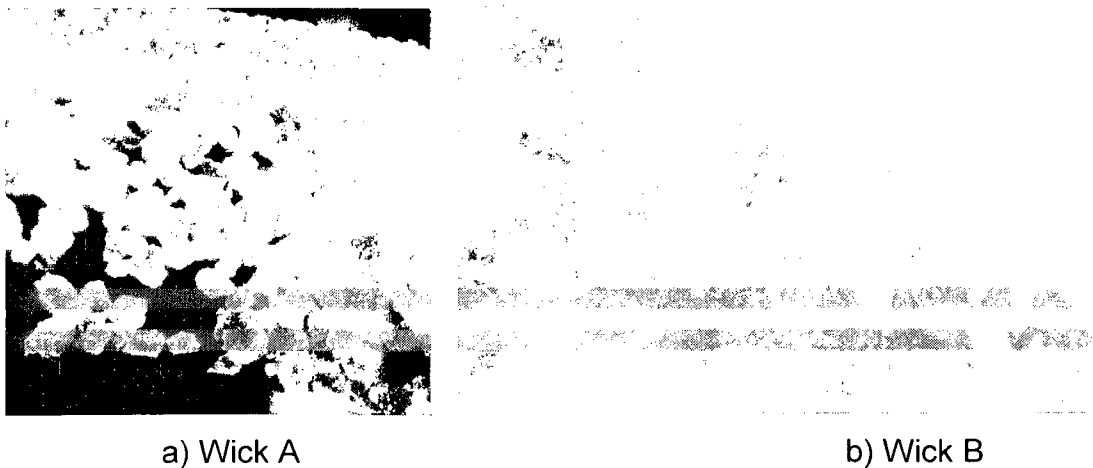


Figure 2.5 Micrographs of wicks A (PC) and B (PE) showing the shape and size variations in the individual beads

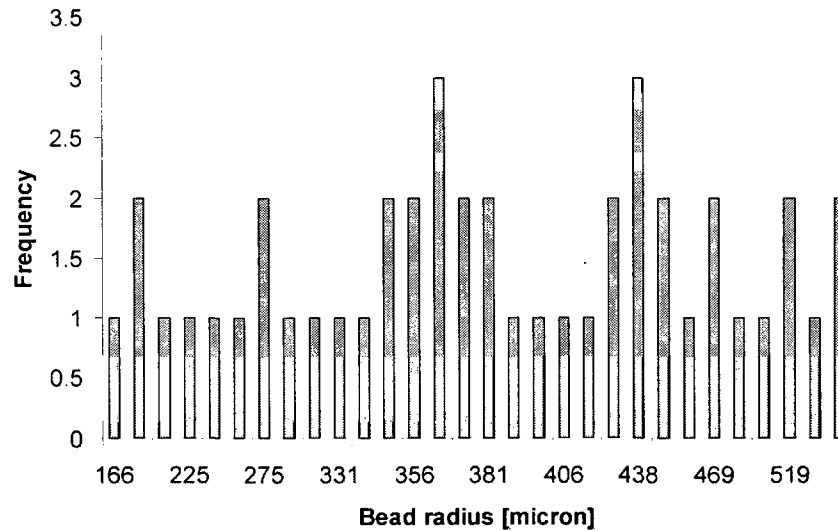


Figure 2.6 Frequency distribution corresponding to bead radius for wick C (PP)

2.4 Results and Discussion

To predict the absorbed mass into the wicks, we used the following five models and compared their predictions with the experimental results. Nomenclatures corresponding to the five models, details of which are listed in Table 1, are as follows:

1. The modified Washburn model, Eq. (2.6), would be named “Washburn Model”.
2. The capillary model without the gravity effect would be named “Capillary Model”.
3. The capillary model including the gravity effect would be named “Capillary Model with gravity”.
4. The energy balance model without the gravity effect would be named “E.B. Model”.

5. The energy balance model including the gravity effect would be named "E.B. Model with gravity".

As we mentioned before, we used three different polymer wicks with three different mean pore and effective bead radii. In the wicks A (PC) and B (PE) the pore radii are small enough such that the suction pressure can saturate all the length of the wick (lengths 0.074 m) after touching the liquid from one end of the wick. In the wick C (PP), the pore size is very large such that the suction pressure is not strong enough to saturate the wick completely. In this case, the liquid rises to a height that is less than the wick length and the downward pull due to gravity is equal to the upward pull of the suction pressure at this stage; the absorption stops at this point. It was noticed that around this stationary point, a little below and above this front position, the wick saturation was not complete or 100%. Over a certain length, the saturation was visually observed to gradually decrease from 100% before the front to 0% at slightly ahead of the front. Since all the above mentioned models are based on the assumption of complete saturation behind the front liquid, the presence of partial saturation near the front may contribute to some extent to the observed differences between the model predictions and the experimental observations.

We did a scatter-estimation test on the wick C (PP) to estimate the repeatability of the test results. Figure 2.7 shows the results of scatter-estimation tests on wick C (PP) with HDEC; the measured 95% confidence intervals [32] are shown with the help of scatter bars. (This interval is a range of the measured quantity in which the measured value is expected to fall 95% of the times.) The

smallness of these bars means that our experiments were very repeatable. We are confident that all experiments listed in this paper show similar repeatability patterns. One reason for this excellent repeatability could be the extremely consistent pore structure of the commercial polymer wicks chosen for this experiment.

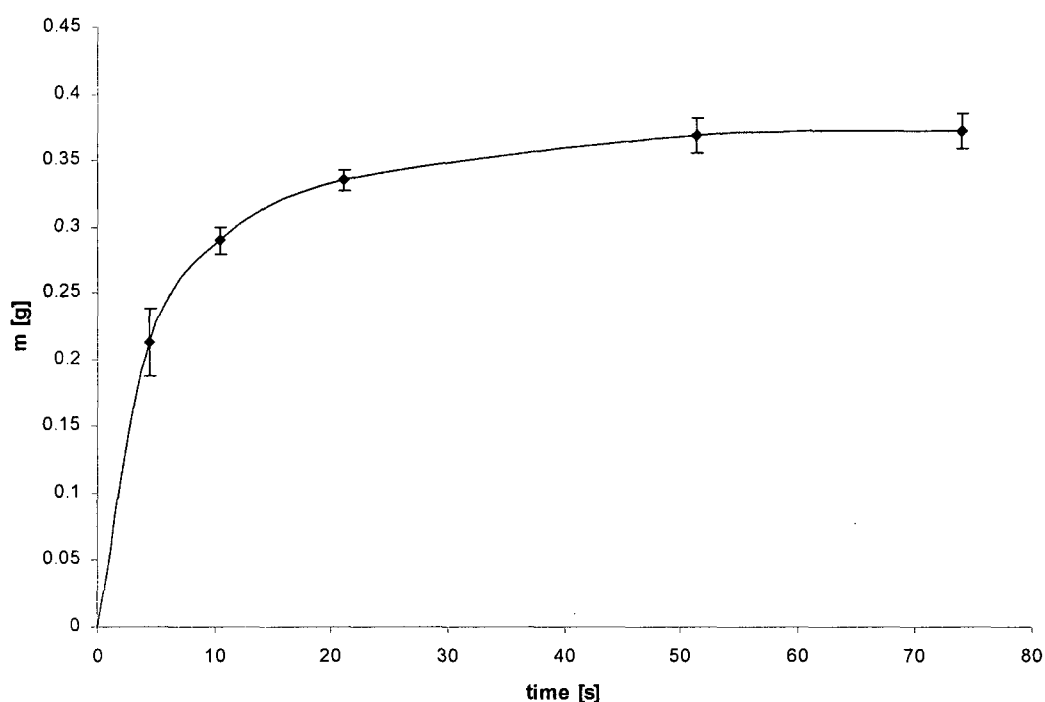


Figure 2.7 Scattering test on wick C (PP) with HDEC, scatter bars show confidence interval of 95%.

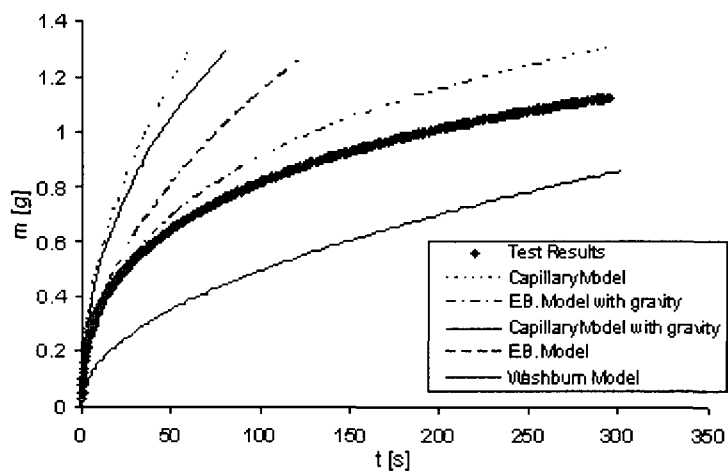
Similarly tests to measure various properties (Table 2.1) were often conducted multiple times to obtain more than one measured values. The scatter in the property values thus obtained was quantified through the use of the 95% confidence interval [32].

Note that the micrographs of the wicks were used to get a visual estimation for porosity and mean pore size to corroborate what we measured using the tests described in sections 2.3.1 and 2.3.3. The porosity was measured by dividing the pore area within an arbitrary rectangle by the total rectangle area. A typical pore size was estimated from the radius of the largest circle that can be fitted between the polymer beads. The porosity and mean pore size estimated through the two different methods were found to be quite close. As described in previous sections, the micrographs also were used to measure the tortuosity and bead sizes.

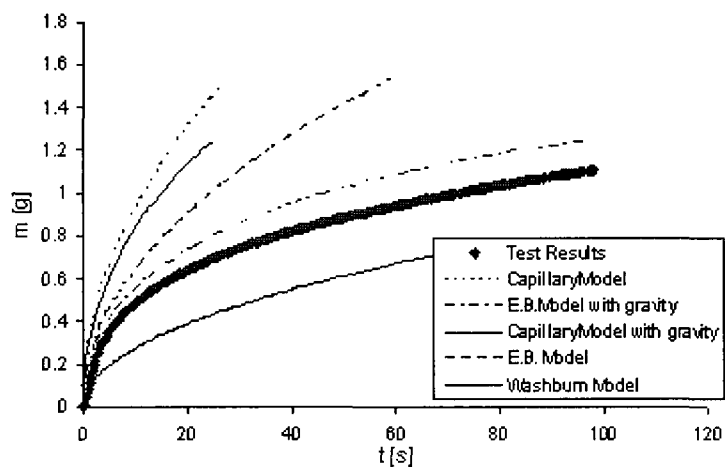
2.4.1 Wicking Tests and Comparison with the Predictions of Various Models

The results of wicking tests and the predictions for wick A (PC) are shown in Figure 2.8. As per the plots, the “E.B. Model with gravity” performs better than the other models. As the time increases, all predictions diverge away from the experimental results. Comparing of parts a, b and c of Figure 2.8 indicates that as the viscosity of the test liquid reduces [Table 2.3], the difference between the “E.B. Model with gravity” prediction and the experimental results also reduces. It is also to be noted that the liquid mass absorbed by wick A (PC) is the highest for the least viscous liquid, DEC.

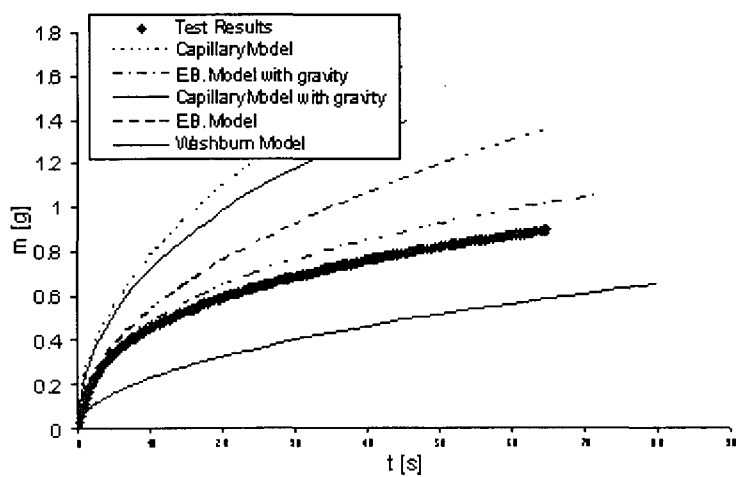
Figure 2.9 shows the test results and predictions for Wick B (PE). Again the “E.B. Model with gravity” performs better than the capillary models; surprisingly, predictions of the “Washburn Model” are perhaps equally good. The former,



a) With HDEC

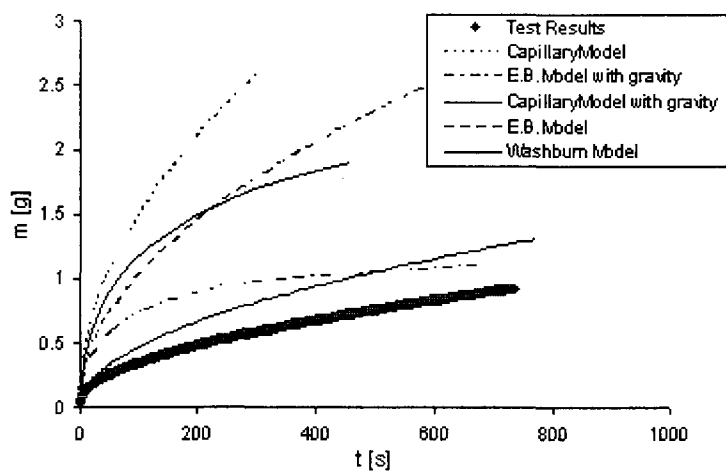


b) With DEC

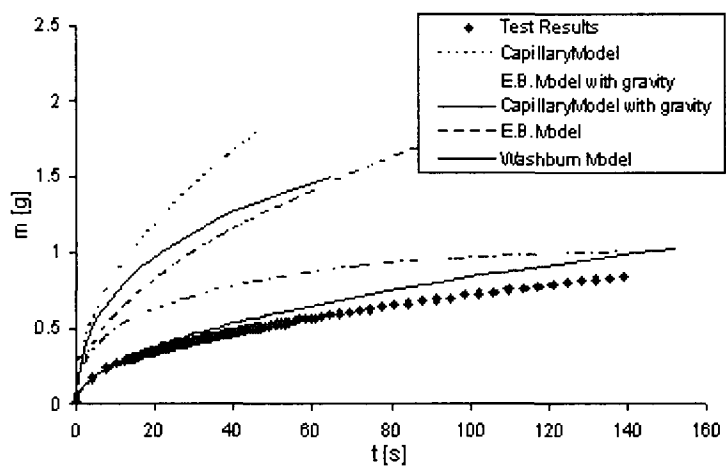


c) With DDEC

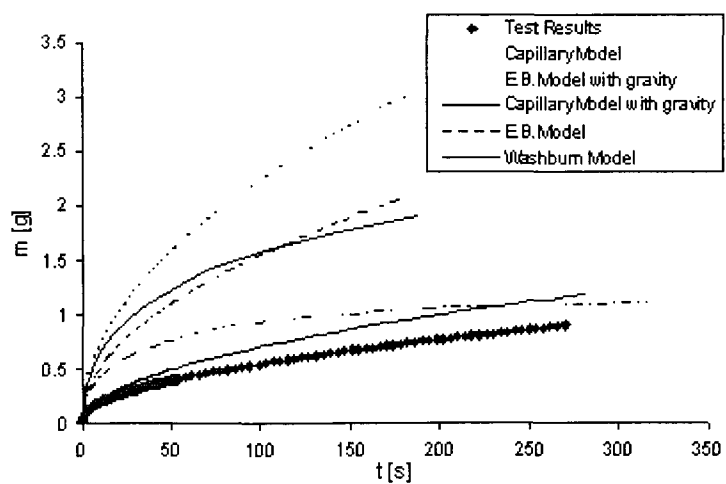
Figure 2.8 Mass absorption rate in wick A (PC) with three different liquids.



a) With HDEC



b) With DEC



c) With DDEC

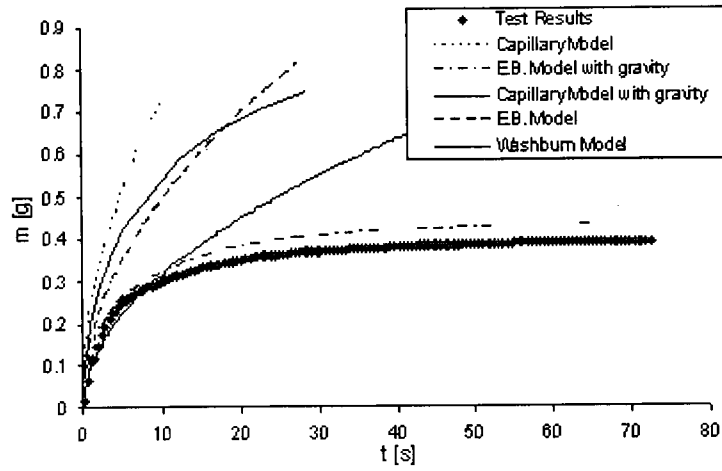
Figure 2.9 Mass absorption rate in wick B (PE) with three different liquids.

though inaccurate in the beginning of the wicking process, becomes more accurate with time. The latter, though more accurate in the beginning, progressively loses its accuracy with time. It is clear that the predictions of the capillary model, even after including the gravity effect, do not compare well with the experimental observations.

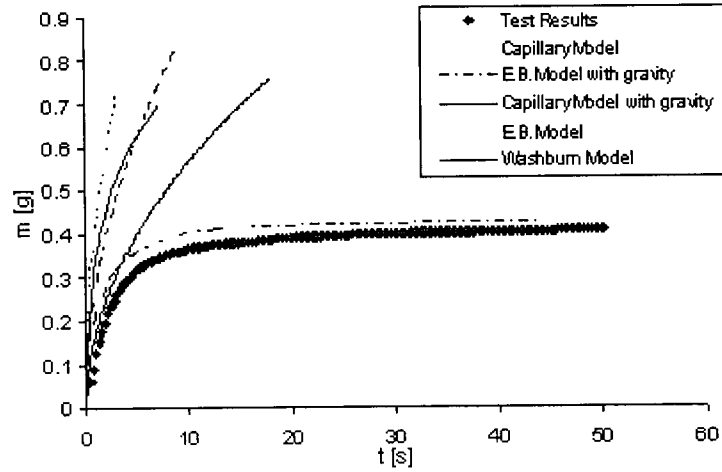
Figure 2.10 shows the predictions of various models and experimental observations for the wick C (PP). As described before, due to its large pore size, this wick could not be completely saturated along all of its length as the suction pressure at liquid front is not strong enough to raise the liquids to the top of the wick. Due to this effect, this is a good wick to test the predictions for the maximum absorbed mass under steady state condition. As shown in the figures, none of the models, except the newly proposed “E.B. Model with gravity” can predict the maximum mass absorbed in the wick. Since the absorbed mass in a wick is proportional to the height to which a liquid rises, the final steady-state height reached by the three liquids in this PP wick is only predicted by the “E.B. Model with gravity.” This heartening observation establishes that it might be the most accurate of all the models considered in this study.

(Incidentally our Darcy based approach allows us to compute steady-state height⁴ as $h_{f,ss} = p_s / \rho g$ for E.B. model with gravity, and $h_{f,ss} = p_c / \rho g$ for capillary model with gravity. As is clear from Eq. 2.33, $p_s < p_c$ and hence $h_{f,ss}$ for the E.B. model is smaller than that for the capillary model. The steady-state mass in wick C (Figure 10) that is thus

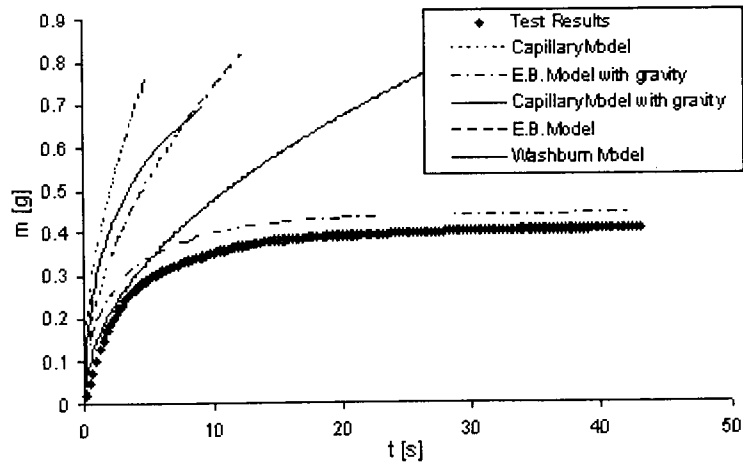
⁴ The steady state fluid-column height in a wick is obtained by noting that dh/dt in Eqn. 17 is equal to zero at the final state.



a) With HDEC



b) With DEC



c) With DDEC

Figure 2.10 Mass absorption rate in wick C (PP) with three different liquids

obtained from $h_{f,ss}$ can be shown to be very close to the large-time asymptotic value predicted by the E.B. model with gravity.)

A possible reason for the difference between the experimental results and the predictions of newly proposed E.B. model with gravity is the deviation of bead shapes from assumed spherical shape. Most beads in wick B have non-spherical irregular shapes, and that perhaps explains the difference between the experimental results and theoretical predictions of the E.B. model with gravity in Figure 2.9. A strong agreement of the model with experiment for wick C (Figure 2.10) may have something to do with the almost spherical shape of its beads shown in Figure 2.1.

As the only difference between the E.B. and capillary models is in the expression for the suction pressure, so this prediction indicates that the newly proposed suction-pressure expression works better than one applied with the conventional models for such polymer wicks. The reason could be the inclusion of porosity ε , effective bead radius R_e , and mean pore radius R_p , the three additional parameters related to the microstructural attributes of the wick, in the definition of the suction pressure in the E.B. models (Eq. 2.33). We anticipate that adding of more parameters related to wick microstructure, such as the bead shape distribution, in the suction-pressure expression will probably improve the prediction even more.

From the study of Figures 2.8, 2.9 and 2.10, it is clear that both the E.B. as well as the capillary models have a tendency to grossly over-predict the mass absorption rate. However they improve their predictions after inclusion of the

gravity effects. So gravity can not be neglected for our system of 7.5 cm long PC, PE, PP wicks and the alkane hydrocarbon liquids HDEC, DEC, and DDEC.

From the present experimental study, it is also clear that the capillary models are perhaps the worst of all the models considered, and an explanation of the failure of these models is in order here. In the polymer wicks made of small beads with irregular shapes and sizes, the capillary tube assumption of having a bundle of aligned fixed-diameter tubes is clearly not satisfied—the size and shape of the pores vary along any flow direction, and might even be different along and across the wick (Figure 2.1). Moreover numerous interconnections exist between the pores. So the capillary model can perhaps be improved if the effect of the shape and size variations in pores along with the inter-pore interconnections is somehow included in the definition of the suction pressure.

2.5 Summary and Conclusion

We use the Darcy's law to model the absorption of a liquid into a wick made from sintering polymer beads. A new expression for suction pressure at the liquid front inside the wick is formulated based on the balance of surface energy and viscous dissipation energy; such an expression is found to depend on both the mean bead size and the porosity of the wick. Another expression for suction pressure, which treats the porous wick as a bundle of capillary tubes, is also formulated. These two different expressions for the suction pressure, when implemented with the Darcy's law based formulation, lead to two different flow models: one the energy balance or E.B. model, and the other the capillary model.

Two further variants of these models were considered after incorporating the effect of gravity.

As a case study of these wicking models, a set of tests using three different polymer wicks [Polycarbonate (PC), Polyethylene (PE) and Polypropylene (PP)] and three different hydrocarbon liquids [Hexadecane (HDEC), Decane (DEC) and Dodecane (DDEC)] were conducted. In these tests, the mass absorbed through wicking is plotted as a function of time while all parameters used in the proposed model were measured accurately and no fitting parameters were used. The traditional Washburn's equation was also employed to predict the mass gain during wicking. Of all the different models used, the newly proposed E.B. method in conjunction with gravity yields the most satisfying predictions. The success of this method is especially notable for a large-pore PP wick where it was the only model to predict the final steady-state height of the liquid column.

This work is characterized with several novel features. The main original contribution is in the development of a new expression for suction pressure in polymer wicks based on the energy balance principle. The other important contribution is in the form of some new techniques that have been used to estimate the property parameters in the wicking models. For example, measurement of the wick permeability with the falling head permeameter is a novelty to the science of wicking. Similarly the use of wick micrographs to estimate parameters such as the porosity, the tortuosity, and the effective bead radius (through the use of histogram of bead size distribution), is new to the field of wicking studies. We have also proposed a new method to estimate the contact

angle of wicking liquids inside the wicks. As a result of the independent estimation of various model parameters, the proposed E.B. model with gravity model predicts the experimental results rather well without the use of any fitting parameters.

References

1. Lucas R .Rate of Capillary Ascension of Liquids. *Kolloid Z.* 1918; 23: 15
2. EV Washburn .The Dynamics of Capillary Flow. *Phys. Rev.* 1921;17: 273
3. Sauter, Salvatore P .The history of Poiseuille's law. *Annual Review of Fluid Mechanics.* 1993; 25: 1-19
4. PK Chatterjee .Absorbency. Amsterdam/New York. Elsevier. 1985
5. Szekely J, Neumann AW and Chuang YK .The Rate of Capillary Penetration and the Applicability of the Washburn Equation. *J. Colloid Interface Sci.* 1971; 35: 273-278
6. Chwastiak S .A Wicking Method for Measuring Wetting Properties of Carbon Yarn. *J. Colloid Interface Sci.* 1973; 42: 298-309
7. Scher KE .Master's Thesis. Dept. of Chemical Engineering. University of Washington. 1983
8. Hodgson KT and Berg JC .The Effect of Surfactants on Wicking Flow in Fiber Networks. *J. Colloid Interface Sci.* 1988;121 (1): 22-31
9. Fowkes FM .Role of Surface Active Agents in Wetting. *J. Phys. Chem.* 1953;57:98-103
10. Williams JG, Morris CM and Ennis BC .*Polym. Eng. Sci.* 1979;14(6): 413-419
11. KM Pillai and SG Advani .Wicking Across a Fiber-Bank. *J. Colloid and Interface Sci.* 1996; 183: 100-110
12. Young T .An essay on the cohesion of fluids. *Philos. Trans. R. Soc.* 1805; London 95: 65-87
13. Gauss K. 1829; *Gott. Gelehrte Anz.*:1641
14. EB Dussan V, B Davis SH .On the Motion of a Fluid-Solid interface Along a Solid Surface. *J. Fluid Mech.* 1974; 65: 71-95
15. EB Dussan V .On the Spreading of Liquids on Solid Surfaces: Static and Dynamic Contact Lines. *Ann. Rev. Fluid Mech.* 1979; 11: 371-400

16. You-Lo Hsieh .Novel Surface Chemistry and Geometric Features of Fibers: Regulation of Liquid Wetting and Absorption. INTC Int. Nonwovens Tech. Con., Millwinnium Hot; Sep 2005: 19-22
17. BS 3424 Method 21 .British Standard. 1973
18. DIN 53924 .German Standard. 1978
19. E Kissa .Wetting and Wicking. Textile Res. J. 1996; 66(10): 660-668
20. B Miller .Critical Evaluation of Upward Wicking Tests. Int. Nonwovwn J. 2000; 9(1): 79-87
21. SJ Russell and N Mao .Apparatus and Method for Assessment of In-Plane Anisotropic Liquid Absorption in Nonwoven Fabrics. AUTEX Res. J. 2000; 1(2)
22. JK Jeong .Slip Boundary Condition on an Idealized Porous Wall. Phys. Fluids. 2001; 13(7): 1884-1890
23. N Mao and SJ Russell .Prediction of Liquid Absorption in Homogeneous Three Dimensional Nonwoven Structures. Int. Nonwoven Tech. Con. Atlanta. 2002
24. N Mao and SJ Russell .Anisotropic Liquid Absorption in Homogeneous Two Dimensional Nonwoven Structures. J. Applied Phys. 2003; 94(6): 4135-4138
25. DA Lockington and JY Parlange .Anomalous Water Absorption in Porous Materials. J. Phys. D: Appl. Phys. 2003; 36: 760-767
26. PAC Gane, CJ Ridgway and J Schoelkopf .Absorption Rate and Volume Dependency on the Complexity of Porous Network Structures. Transport in Porous Media. 2004; 54: 79-106
27. CI Tucker and RB Dessenberger .Governing Equation for Flow and Heat Transfer in Stationary Fiber beds. In: SG Advani .Flow and Rheology in Polymer Composites Manufacturing. Elsevier Science, 1994: Ch8
28. Jacob Bear .Dynamics of Fluids in Porous Media. Elsevier Science, 1972
29. Material Database. In: Sigma 701 Tentiometer, KSV Instruments Ltd
30. DR Caudell, JPM Trusler, V Vesovie and WA Wakeham .The Viscosity and Density of n-Dodecane and n-Octadecane at Pressure up to 200 MPa and Temperatures up to 473 K. <http://symp15.nist.gov/pdf/p175.pdf>
31. Wikipedia the free encyclopedia, <http://en.wikipedia.org/wiki/Decane>
32. Anthony J Wheeler, Ahmad R Ganji .Introduction to Engineering Experimentation. Prentice Hall, 1996

Chapter 3

ROLE OF HYDRAULIC AND CAPILLARY RADII IN IMPROVING THE EFFECTIVENESS OF CAPILLARY MODEL IN WICKING

3.1 Introduction

Pore size and permeability are two very important parameters that are needed in the modeling of liquid transport into the porous media. Several methods have been developed by researchers to measure these two parameters. Maejima [1] used the centrifugal force to pressure a liquid into a porous media and thus measured its mean pore radius. Miller and Tyomkin [2] introduced liquid extrusion method for determining the pore volume distribution. Van Oss et al [3] used the low energy liquids, such as alkanes, to measure the contact angle and pore size of porous media.

Li et al. [4] used wicking techniques for measuring the pore size in ceramic materials where they used low energy liquids to ensure zero contact angle. After knowing the pore radius, they used the same technique to measure the contact angle as well. Bachmann et al [5] developed two new methods for measuring the contact angle and particle surface energy in porous media. Mercury porosimetry [6] is a standard method of pore size characteristic determination where the mercury is made to penetrate into a porous medium under pressure. As the surface energy of mercury is very high and contact angle for most cases is more

than 90 degrees, a high pressure-gradient is needed to drive it into the porous medium. Due to a high imposed pressure, mercury porosimetry is not appropriate for compressible materials as it leads to their deformation. The only method that does not impose high pressure in pore size measurement is the capillary rise method; Dang-vu and Hupka [7] used this method to measure the contact angle and pore size in porous media. A comprehensive review of experimental techniques for measuring the wetting and wicking parameters was conducted by Ghali et al [8].

The capillary model, which treats the porous media as a bundle of capillary tubes and of which the famous Washburn equation is a derivative, needs to rely on the average radius of the tubes as an important parameter. This radius is often quantified either as the capillary radius or the hydraulic radius. However while using the capillary model to predict wicking in porous materials, no previous researcher has made a distinction between the capillary and hydraulic radii. In this chapter, we experimentally study wicking while measuring the capillary and hydraulic radii separately. Later these measured wicking parameters are used to predict the wicking rate in certain commercial wicks made from polymers. These porous wicks, made by sintering polymer beads, are usually used by consumer product companies to dispense volatile substances such as room fresheners or insect repellents into room air. For such polymer wicks, not many studies on their wicking characteristics have been reported. In this chapter, we use the capillary model to predict the liquid absorption rate into these polymer wicks. It has shown

that the hydraulic and capillary radii are independent and must be measured separately to improve the predictions of the capillary model.

3.2 Theory of Wicking

As described in the literature survey, there are essentially two different models for the prediction of wicking in porous media: one is the capillary model which is based on Washburn equation and treats pores as capillary tubes, and the other model is based on using the Darcy's law to predict liquid motion. The two approaches have been used by the authors to predict wicking in polymer wicks and are described chapter 2. Here since we investigate the effect of treating the capillary and hydraulic radii as independent parameters in the former, we will describe it in some detail for the benefit of the reader.

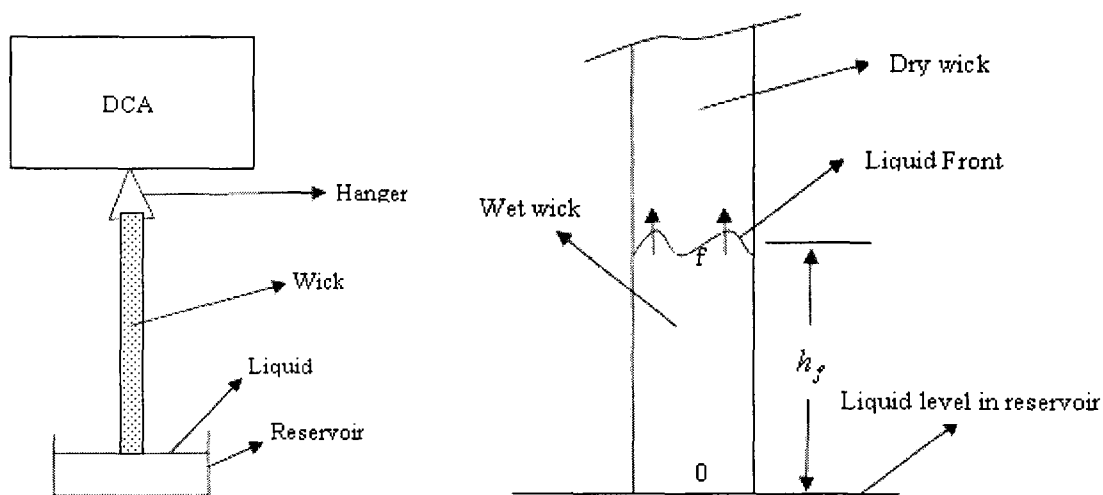


Figure 3.1 A schematic of the test setup and liquid front position in the wick

3.2.1 Capillary Model

A brief derivation of the capillary model is presented here to highlight the roles of the hydraulic and capillary radii. (In this chapter, please note that the terms capillary radius stand for the average radius of the capillary tubes constituting the porous medium, while the hydraulic radius stands for the average hydraulic radius of the same tubes.) We assume our porous medium, i.e. the polymer wick, to be equivalent to a bundle of vertically aligned capillary tubes.

The energy balance equation for liquid traveling in the imagined wetted capillary tubes of the porous wick behind the moving front (Figure 3.1) can be expressed as

$$\frac{p_0}{\rho g} + \frac{u_0^2}{2g} + h_0 = \frac{p_f}{\rho g} + \frac{u_f^2}{2g} + h_f + H_L \quad (3.1)$$

where h is the vertical coordinate, p is the pressure, u is the average velocity of fluid within a capillary tube, and H_L is the head loss. Subscript 0 indicates the initial reference value of each variable and subscript f indicates the value of the variable at the liquid front. As shown in Figure 3.1, h_f is the height of the liquid front within the wick. Since the velocity inside the capillary tubes during wicking is very small and h_0 is taken to be zero, the terms involving them can be neglected, and Eq (3.1) reduces to

$$p_0 - p_f = \rho g h_f + \rho g H_L \quad (3.2)$$

The initial gage pressure p_0 is zero and the front pressure p_f , which drives the liquid column up in the tubes during the wicking, is the capillary suction pressure

applied at the top of the liquid column with a -ve sign ($p_f = -p_c$). The capillary pressure for a tube can be obtained through the Young-Laplace equation as

$$p_c = \frac{2\gamma \cos(\theta)}{R_c} \quad (3.3)$$

To estimate H_L in Eq (3.2), we assume the flow to be laminar in the capillary tubes; so it can be estimated through the Darcy-Weisbach relation as

$$H_L = f \frac{h_f u_f^2}{D_h 2g} \quad (3.4)$$

As the flow is laminar, so $f = \frac{64}{\text{Re}}$ where $\text{Re} = \frac{\rho u_f D_h}{\mu}$. Use of this relation in Eq (3.4) results in

$$H_L = \frac{32u_f \mu h_f}{\rho g D_h^2} = \frac{32\mu h_f}{\rho g D_h^2} \frac{dh_f}{dt} \quad (3.5)$$

where the average velocity in the capillary tube is related to the rate of the liquid column rise through $u_f = dh_f/dt$. Using Eqs (3.3) and (3.5) in Eq (3.2) gives the final form of governing equation as

$$\frac{4\gamma \cos(\theta)}{D_c} = \frac{32\mu h_f}{D_h^2} \frac{dh_f}{dt} + \rho g h_f \quad (3.6)$$

If we neglect the gravity effects, last term vanishes, and an integration leads to the well-known Washburn equation:

$$h_f = \sqrt{\frac{\gamma D_e \cos(\theta)}{4\mu} t} \quad (3.7)$$

Here D_e , the effective pore radius, is obtained through

$$D_e = \frac{D_h^2}{D_c} \quad (3.8)$$

In general cases, where the gravity is included, Eq (3.6) can be used to derive a relation between the location of liquid front h_f and time t . After the separation of variables and the subsequent integration of Eq (3.6) along with the application of the initial condition $h_f(t = 0) = 0$, we obtain

$$\frac{4\gamma \cos(\theta)}{D_c} \ln \left| \frac{4\gamma \cos(\theta)}{4\gamma \cos(\theta) - \rho g h_f D_c} \right| - \rho g h_f = \frac{\rho^2 g^2 R_h^2}{8\mu} t \quad (3.9)$$

which is an implicit equation for the liquid-front height h_f in the wick. To use this equation we need to have a relation between the capillary and hydraulic radii $R_c (= D_c / 2)$ and $R_h (= D_h / 2)$, respectively. We used the regular definition of hydraulic radius as the ratio of the fluid volume inside the capillary tubes to the wetted surface area of the tubes to formulate the expression for R_h as

$$R_h = \frac{\varepsilon \pi R_w^2 h_f}{2N\pi R_p h_f} \quad (3.10)$$

where R_w is wick radius, R_p is pore radius, ε is porosity, and N is number of longitudinal capillaries passing through the wick. We also have the following equation for pores which is obtained by equating the pore volume in the wick with the total volume of the cylindrical tubes inside the wick:

$$N\pi R_p^2 h_f = \varepsilon \pi R_w^2 h_f \quad (3.11)$$

After using Eq. (3.11) in Eq. (3.10) we have

$$R_h = \frac{R_p}{2} \quad (3.12)$$

It is customary to assume $R_c = R_p$, so the relation between the capillary and hydraulic radii is

$$R_c = 2R_h \quad (3.13)$$

Eqs (3.12) and (3.13) are commonly used in the wicking applications; we will see the accuracy of these equations later.

3.2.2 Darcy Model

Darcy law based model for wicking modeling in commercial polymer wicks is described in detail in Chapter 2 (Section 2.2.2).

3.2.3 Improving the Capillary Model Through the Capillary and Hydraulic Radii

We are going to increase the accuracy of Eq (3.9) by making a distinction between the capillary and hydraulic radii. We suspect the accuracy of Eq. (3.13), and so we plan to measure each radius separately, instead of the customary method of measuring one of them and then using Eq (3.13) to estimate the other. This distinction can be considered to modify the capillary model, which, as we shall see later, leads to a better prediction of wicking rate in the polymer wicks.

3.3 Experimental Measurements

To study the wicking phenomenon through the commercial polymer wicks experimentally, some properties of the wicks, of the liquids, and of the interaction between wicks and liquids, should be measured carefully. These properties are

wick porosity (ε), hydraulic radius (R_h), capillary radius (R_c), liquid surface tension (γ), and dynamic contact angle (θ). The experimental techniques for all of the testing materials are described in chapter 2; only the technique for measuring the capillary radius (R_c) will be explained here. The measured properties of the liquids and wicks used in our experiments are presented in Tables 2.3 and 3.1.

3.3.1 Measuring the capillary radius (R_c)

The capillary radius will be measured when the upward pulling suction force is balanced by the downward force of gravity in a wick. A study of Eq (3.6) indicates that as h_f increases, the $\frac{dh_f}{dt}$ decreases, and a steady state height h_{ss} is attained when $\frac{dh_f}{dt}$ is zero. This is the condition in which the capillary pressure balances the gravity 'pressure', and Eq (3.6) yields an expression for the capillary radius as

$$R_c = \frac{2\gamma \cos(\theta)}{\rho g h_{ss}} \quad (3.14)$$

In my tests, we had to be sure that the steady state height h_{ss} is less than the length of the wick so we had to choose a particular 'liquid + porous medium' system to attain this criterion. According to Eq (3.14), the steady-state height is directly proportional to the liquid surface tension and cosine of the contact angle, but is inversely proportional to the liquid density. This relation enabled us to select appropriate liquid for a given porous wick. The wicks B and C were tested

using Hexadecane while Wick A was tested using a mixture of distilled water and Windex®. The capillary radii computed using Eq (3.14) are listed in Table 3.1.

Table 3.1 Properties of the test wicks (R_h and R_c are presented with the 95% confidence interval ranges [10]).

Name of wicks	A	B	C
Material	PC	PE	PP
Length of wick L [m]	0.076	0.073	0.075
Wick radius R_w [m]	0.0036	0.0035	0.0036
Porosity ε	0.49	0.5	0.4
Hydraulic radius R_h [μm]	29.8 ± 7.1	54.5 ± 4.5	88.4 ± 4.4
Capillary radius R_c [μm]	65.1 ± 9.3	150.1 ± 7.9	200.0 ± 11.4

3.3.2. Wicking tests

A set of wicking tests using three different polymer wicks [Polycarbonate (PC), Polyethylene (PE) and Polypropylene (PP)] and three different hydrocarbon liquids [Hexadecane (HDEC), Decane (DEC) and Dodecane (DDEC)] were conducted. The details of the experimental setup used for wicking test are described in chapter 2. We have used the experimental results from this cited paper for wicks A and C; we have replaced wick B it with another wick of the same material but with larger bead or pore sizes to enable us to study the theoretical predictions near the steady-state height h_{ss} . So we have used three different polymer wicks with three different mean pore radii. In the wick A (PC), the pore radii are small enough such that the suction pressure can saturate all the length of the wick (L= 0.074 m) after touching the liquid from one end of the

wick. In the wicks B (PE) and C (PP), the pore sizes are very large such that the suction pressure is not strong enough to saturate the wick completely. In these cases the liquid rises to a height that is less than the wick length and the downward pulling force due to gravity is equal to the upward pull of the suction pressure. The wick stops absorbing liquid at this point, and h_f asymptotically approaches the steady-state height h_{ss} .

Figure 3.7 shows the results of scatter-estimation tests conducted on wick C (PP) with the liquid HDEC to estimate the repeatability of our test results. The measured 95% confidence intervals are shown with the help of the scatter bars. (This interval is a range of the measured quantity in which the measured value is expected to fall 95% of the times.) The smallness of these bars indicates that these experiments were very repeatable. We are confident that all experiments listed in this paper show similar repeatability patterns. One reason for this excellent repeatability is the extremely consistent pore structure of the commercial polymer wicks chosen for this experiment. Similarly the tests measuring various properties (Table 3.1) were often conducted multiple times to obtain more than one measured values. The scatter in the property values thus obtained was quantified through the use of the 95% confidence interval [10].

3.4 Results and Discussions

We have used three different capillary ‘models’, that are described below, to theoretically predict the absorbed liquid mass into the wicks as a function of time, and later compare their predictions with the experimental results. In these three

models, first Eq (3.9) was used as the mathematical relation to predict the liquid-front position h_f as a function of time, and then the following equation was used to estimate the absorbed liquid mass as a function of time:

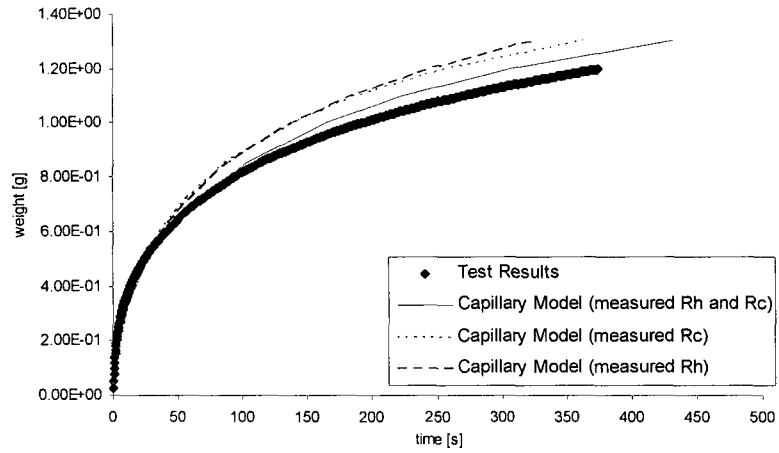
$$m = \varepsilon \rho \pi R_{wk}^2 h_f \quad (3.15)$$

Nomenclatures corresponding to the applied theoretical models are as follows:

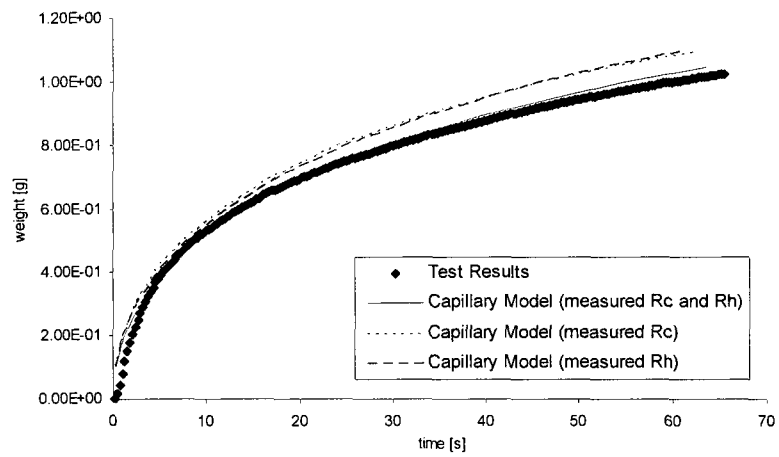
1. “Capillary Model (measured Rh)”: Measure the hydraulic radius R_h first, and then use Eq (3.13) to estimate the capillary radius R_c .
2. “Capillary Model (measured Rc)”: Measure the capillary radius R_c first, and then use Eq (3.13) to estimate the hydraulic radius R_h .
3. “Capillary Model (measured Rc and Rh)”: Measure both the capillary radius R_c and the hydraulic radius R_h independently.

Results of the wicking tests and the predictions of the three models for wick A (PC) with three different liquids are shown in Figures 3.2a to 3.2c. The plots indicate that the “Capillary Model (measured Rc and Rh)” performs better than other two models for all three cases. As the time increases, all predictions diverge away from the experimental

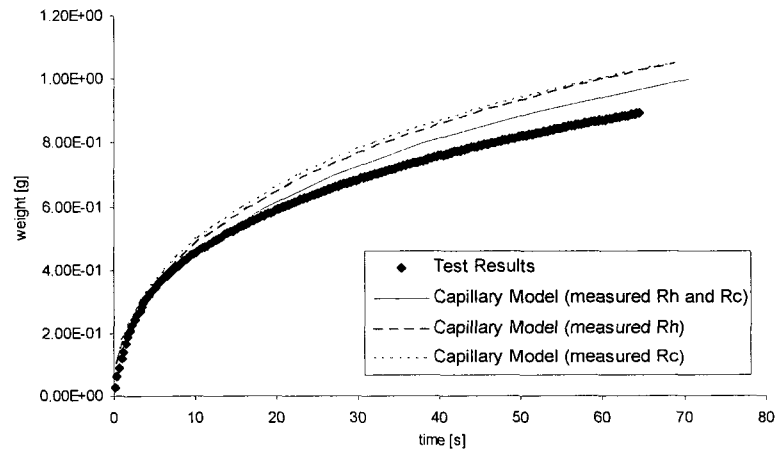
results but still the ‘measured Rc and Rh’ model behaves better than the other two. Comparing of parts a, b and c of Figure 3.2 indicates that as the viscosity of the test liquid reduces [Table (1): $\mu_{HDEC} > \mu_{DDEC} > \mu_{DEC}$], the difference between the ‘measured Rc and Rh’ model predictions and the experimental results also reduces. It is also to be noted that at any given time, the liquid mass absorbed by wick A (PC) is the highest for the least viscous liquid DEC.



a) With HDEC

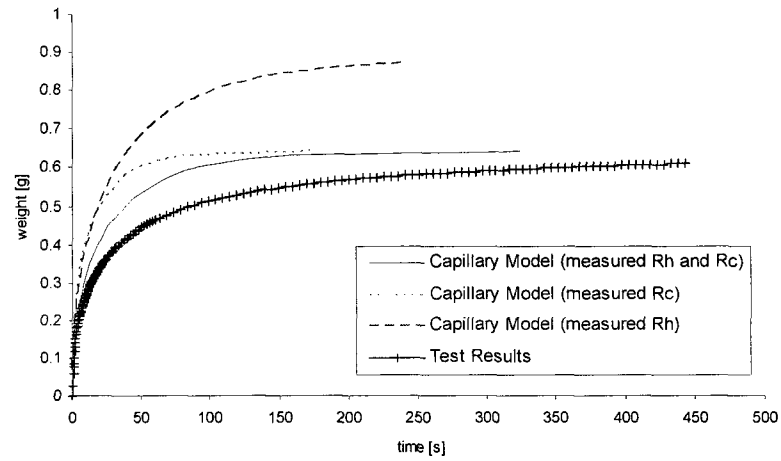


b) With DEC

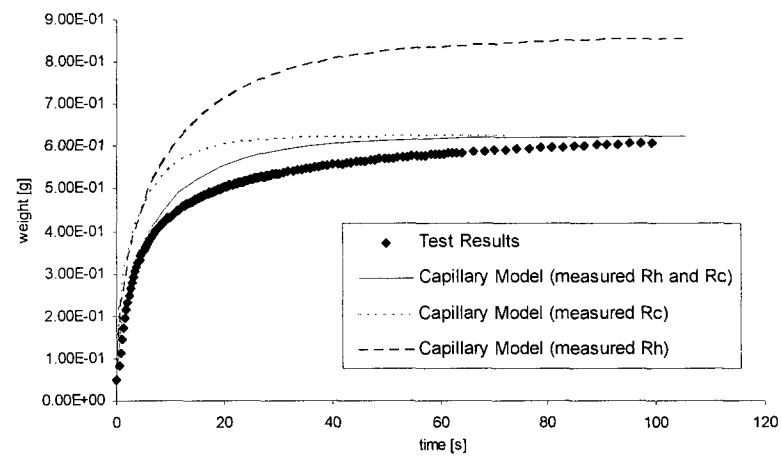


c) With DDEC

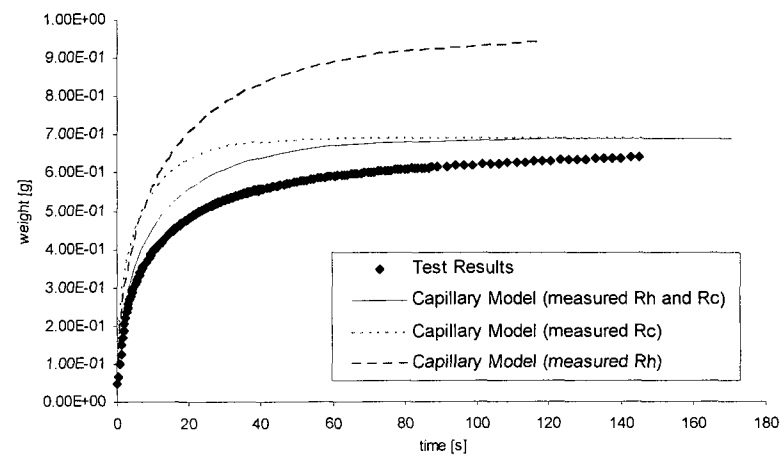
Figure 3.2 Mass absorption plots using wick A (PC) with the three liquids.



a) With HDEC



b) With DEC



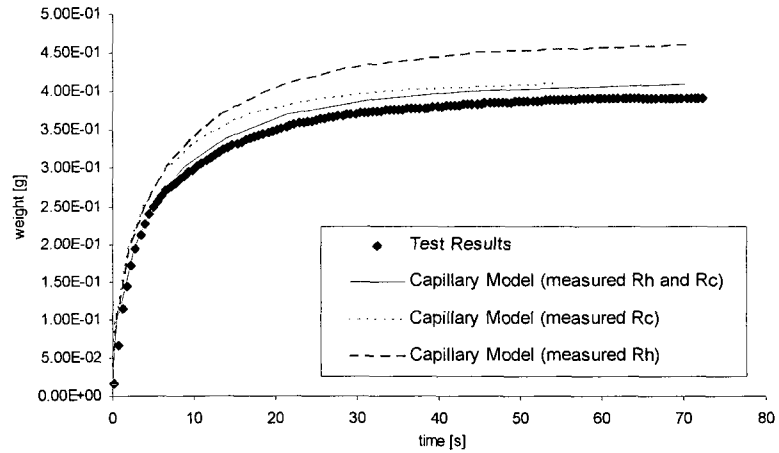
c) With DDEC

Figure 3.3 Mass absorption plots using wick B (PE) with the three liquids.

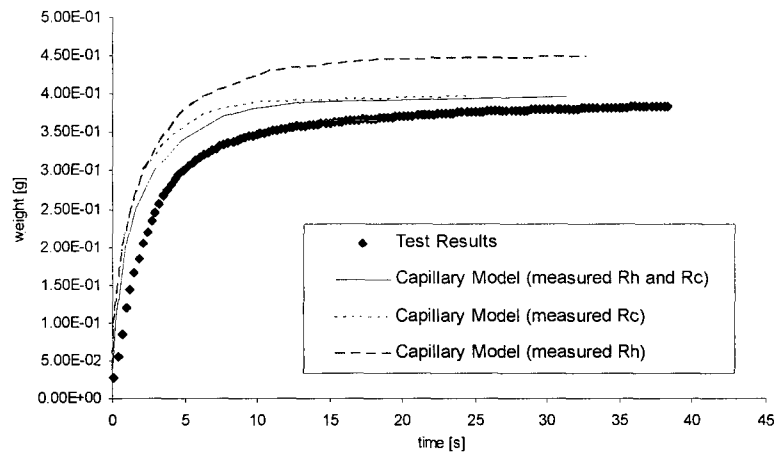
Figure 3.3 shows the test results and predictions for Wick B (PE). Once again the 'measured R_c and R_h ' model performs better than other models. As was described earlier, this wick could not be completely saturated along all of its length because, due to its large pore-size (and consequently large R_c), the suction pressure at liquid front (given by Eq. (3.3)) is not large enough to raise the liquid front to the top of the wick. Due to this effect, this is a good wick to test the predictions for the maximum absorbed mass under steady state condition. As shown in the figures, the 'measured R_c ' and 'measured R_c and R_h ' models do well toward the end and can predict the steady state mass quite accurately. We feel that this accuracy in prediction is related to the accuracy of the measured capillary radius value used in the models.

Figure 3.4 shows the predictions of various models and experimental observations for the wick C (PP); here also the wick could not be saturated completely. As shown in the figures, the 'measured R_c and R_h ' model can once again predict the maximum mass absorbed in the wick most accurately. Since the absorbed mass in a wick is proportional to the height to which a liquid rises, the final steady-state height reached by the three liquids in this wick can be predicted quite closely by both the 'measured R_c ' and 'measured R_c and R_h ' models. As before, their success could be related to the accuracy of the measured capillary radius value used in the models.

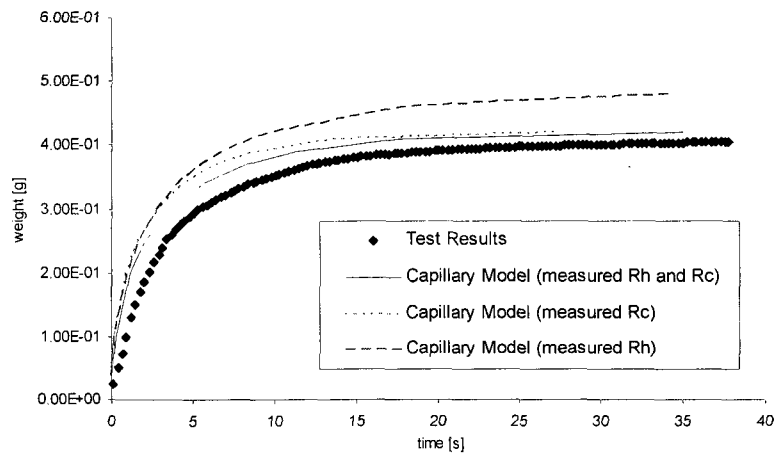
Let us try to explain the success of the 'measured R_c ' and 'measured R_c and R_h ' models near the final steady-state height. The capillary radius appears in the suction pressure or the driving force term in governing equation, Eq. (3.6),



a) With HDEC



b) With DEC



c) With DDEC

Figure 3.4 Mass absorption plots using wick C (PP) with the three liquids.

while the hydraulic radius and flow velocity appear in the fluid-flow friction term. It implies that when the wicking velocity goes to zero, such as when the flow-front height h_f approaches the steady-state height h_{ss} , the effect of hydraulic radius in the fluid-flow friction term of Eq. (3.6) is negligible (and hence its accuracy is unimportant) while the accuracy of the capillary radius in the dominant suction pressure term is significant always; this is why both the 'measured Rc' and 'measured Rc and Rh' type capillary models behave well near the steady state height. However accuracy of both the radii are expected to be important in the wicking process when the wicking rate is significant and the steady-state is not being approached, perhaps explaining the similar reasonably good performance of both the 'measured Rc' and 'measured Rh' type capillary models in Figure 3.2.

A possible reason for the difference between the experimental results and the predictions of theoretical models before reaching the final steady-state is the lack of interconnections between assumed capillary tubes in the capillary model. As a result, interconnections between pores in a porous medium are not reflected in the assumed structure of parallel capillary tubes of the capillary models. Another reason for this difference is that both the radii are perhaps not constant in the irregular pores of the wick, but they are considered as constants in the capillary model. We content that if the interconnections and variations in capillary-tube size could be somehow included in the capillary model, its accuracy would improve, especially with the approach of measuring both the capillary and hydraulic radii.

3.5 Summary and Conclusion

We used the capillary model to predict the absorption of liquids into wicks made from sintering polymer beads. . Of the two radii involved (capillary and hydraulic), it is customary to measure just one and use it to estimate the other; however we have shown that this is not the best approach for modeling liquid absorption in polymer wicks. It has been demonstrated here clearly that both the capillary and hydraulic radii should be measured independently for maximizing the accuracy of the capillary model.

A set of tests using three different polymer wicks [Polycarbonate (PC), Polyethylene (PE) and Polypropylene (PP)] and three different hydrocarbon liquids [Hexadecane (HDEC), Decane (DEC) and Dodecane (DDEC)] were conducted. In these tests, the mass absorbed through wicking is plotted as a function of time for each wick and the corresponding liquid. Based on how the capillary and hydraulic radii are estimated, three different cases of the capillary model were considered for prediction: 1) using the measured hydraulic radius and deriving the capillary radius from it, 2) using the measured capillary radius and deriving the hydraulic radius from it, and 3) measuring both the capillary and hydraulic radii independently. All other parameters used in the capillary model were measured accurately and no fitting parameters were used. Among the different models used here, the third case of the capillary model yielded the most satisfying predictions overall, while both the second and third cases of the capillary model were good in predicting the final mass absorbed by the large pore

PP and PE wicks at steady-state when the suction force is balanced by the gravity force

References

1. M Maejima .Applying Capillary to Estimation of Space Structure of Fabrics. *Textile Res. J.* 1983: 427-434
2. B Miller and I Tymokin .An Extended Range Liquid Extrusion Method for Determining Pore Size Distributions. *Textile Res. J.* 1986: 35-40
3. CJ Van Oss, RF Giese, Z Li, K Murphy, J Norris, MK Chaudhury and RJ Good .Determination of Contact Angles and Pore sizes of Porous Media by Column and Thin Layer Wicking. *J Adhesion Sci. Tech.* 1992 6(4): 413-428
4. Z Li, RF Giese, CJ Van Oss, HM Kerch and HE Burdette. Wicking Techniques for Determination of Pore Size in Ceramic Materials. *J. Am Ceramic Soc.* 1994; 77(8): 220-22
5. J Buchmann, S Woche, MO Goebel, MB Kirkham and R Horton .Extended methodology for Determining Wetting Properties of Porous Media. *Water Resources Res. J.* 2003; 39(12):1353
6. V Nagy LM Vas .Pore Characteristic Determination with Mercury Porosimetry in Polyester Staple Yarns. *Fibers & Textiles in Eastern Europe.* Jul/Sep 2005; 13(3): 21-26
7. T Dang-Vu and J Hupka .Characterization of Porous Materials by capillary Rise Method. *Physicochemical Problems of Mineral Processing.* 2005; 39: 47-65
8. K Ghali, B Jones and J Tracy .Experimental Techniques for Measuring Parameters Describing Wetting and Wicking in Fabrics. *Textile Res. J.* 1994; 64(2): 106-111
9. Masoodi, R., Pillai, K.M. and Varanasi, P.P., "The Effect of Hydraulic Pressure on the Wicking Rate into the Wipes," to appear in *Journal of Engineered Fibers and Fabrics.*
10. Anthony J Wheeler, Ahmad R Ganji .Introduction to Engineering Experimentation. Prentice Hall, 1996

Chapter 4

DARCY'S LAW BASED NUMERICAL SIMULATION FOR MODELING 3-D LIQUID ABSORPTION INTO WICKS

4.1 Introduction

In the previous chapter, we showed a method to improve the predictions of liquid absorption in the polymer wicks using the capillary model: the hydraulic and capillary radii were shown to be independent and were to be measured separately to improve the predictions. In general, the Washburn Equation has been studied extensively through experiments by several researchers, where the suggested equation was shown to be valid for most liquid absorbing materials [1]. An excellent review of the most important previous work on wetting and wicking has been conducted by Kissa [2]. Some more recent reviews of literature on wicking phenomenon are available in references [3] and [4].

Though the Washburn equation is an important relation that has been widely used for modeling absorption and wicking into porous substrates [1], it is important to reflect on its limitations. One of its chief drawbacks is that since it is based on the model of Hagen–Poiseuille flow through a bundle of aligned and parallel capillary tubes, it can predict only one-dimensional imbibitional flows along the direction of capillary tubes. It can not, due to the unidirectional nature of its flow model, predict the *two-dimensional* flows in wicks of complicated shapes. Moreover, the use of the Washburn equation implies that the

complicated flow paths of liquids in a real porous medium are replaced by straight and hypothetical flow paths through cylindrical tubes. Hence this model will always have a parameter, such as the hydraulic radius, which due to its origin in the pipe-flow physics, is physically irrelevant and is often used as a fitting parameter.

The flow physics based on the Darcy's law is quite well established in the porous media literature where it is regularly used to model flow in porous media [5-7]. Though relatively new in the field of wicking-flow modeling, the application of Darcy's law for modeling wicking flow in various types of porous media has been done in the recent past. Masoodi et al. [8] used Darcy's law based models for predicting liquid absorption in the polymer wicks where a clear liquid-front is discernible with only liquid flow behind the front, and the suction pressure at the liquid front is the primary flow driver. Similarly, Pillai and Advani [9] had used a similar approach to model flow across a bank of parallel fibers.

Sometimes a clearly marked liquid-front can not be discerned in porous wicks during wicking and there is a gradual change (over a finite distance) in saturation from 1 to 0 at the front⁵. For such situations, the unsaturated flow model has been employed to model changes in saturation during the liquid imbibition process [10-12]. A heat-equation like equation called the Richard's equation has been employed to model the time-dependent, diffusion-like migration of saturation during wicking. Since the Richard's equation can be derived from the generalized Darcy's law employed to model the simultaneous

⁵ Saturation is defined as the fraction of pore volume of the porous medium occupied by the invading liquid. As a result, the saturation takes a value between zero and unity.

flow of two different fluids through a porous medium [5], such an approach for modeling liquid imbibition in wicks can still be called a Darcy's law based approach. Incidentally, the Richard's equation approach has been quite successful in modeling moisture distributions in soils above a water table [5-7]. However, the approach has its difficulties as complex experiments need to be used to measure important parameters such as the relative permeability and capillary pressure so that the moisture diffusion coefficient can be estimated. In the absence of an easy estimation of the coefficient, very often an exponential or power-law form of the moisture diffusion coefficient is assumed while applying this approach [13].

In general, the use of the Darcy's law based flow-models not only raises the scientific level of a wicking flow-model and enables one to draw upon the vast research done in the area of porous-media flow and transport, but also makes it possible to predict two-dimensional wicking flows in porous wicks of complex shapes. In this chapter, we are going to model two-dimensional liquid flow in polymer wicks of complex shapes using the Darcy's law based approach employing the single-phase flow assumption behind a clearly defined liquid-front. PORE-FLOW[®], a computer program based on the finite element/control volume (FE/CV) method to model free-surface flows in porous media [14], is employed to solve the flow equations within the complex-shaped polymer wicks and to predict the location of liquid front. (It is the first time that such a FE/CV based flow-modeling software is employed to solve for such two-dimensional wicking flows.) Complex (altered) wicks are created from the ordinary cylindrical polymer wicks

by changing their diameters for certain lengths at certain axial locations. First, the experimental validation of our computational flow model will be undertaken for the simple and altered wicks. Then this numerical study will estimate how effective this technique (of altering the cross-sectional areas) is in controlling and reducing the liquid absorption rate in wicks.

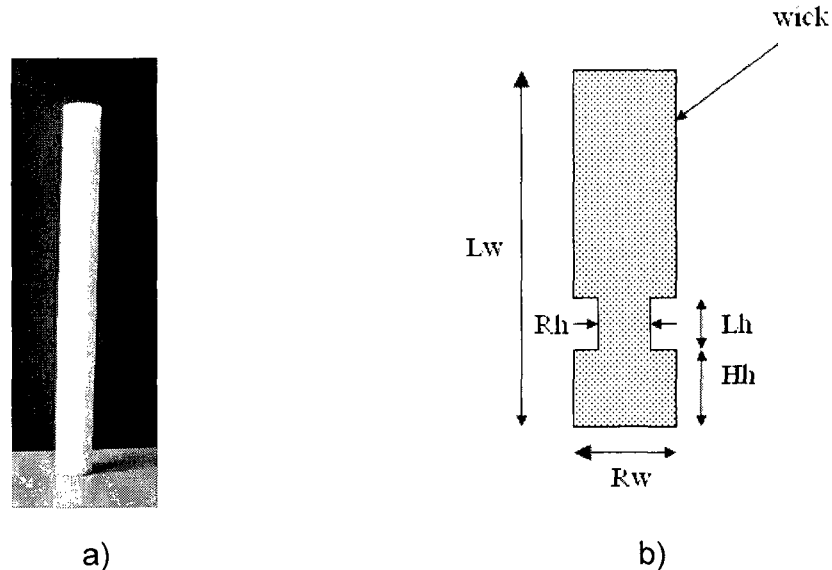


Figure 4.1 a) A photo of a cylindrical polymer wick. b) An altered-wick section showing changes in its cross-sectional area as well as various associated dimensions.

4.2 Geometry of Plain and Altered Wicks

As we can see in the Figure 4.1a, commercial polymer wicks are cylindrical in shape and have a constant diameter along their entire length. A typical diameter and a typical length of such wicks are 0.0072m and 0.075m, respectively. We created an altered wick by sharply changing the wick diameter along the wick length at several locations with the help of a milling machine. Figure 4.1b shows planned changes in the plain wick and the names assigned to the dimensions to be changed. Table 4.1 lists the values of these dimensions in

the five different altered wicks considered in the present study. In the table, wick A is a simple wick without any manipulation while wicks B, C, D, and E are altered wicks.

Table 4.1 Values of the dimensions shown in Fig 1b for all the five wicks studied in this paper. (Fig. 8 provides an easy visualization of the geometries B, C, D and E.)

Wick	Lw [mm]	Rw [mm]	Rh [mm]	Lh [mm]	Hh [mm]
A	75	7	0	0	0
B	75	7	3	5	10
C	75	7	5	5	10
D	75	7	3	15	0
E	75	7	5	15	0

4.3 Theory of Wicking

During a previously reported study [8], we tested ten different polymer wicks and discovered that six of them created a clear liquid front during the wicking process; in the other four wicks, a capillary fingering effect caused the liquid front to be unstable and no clear front could be discerned. In other words, the saturation changed from one to zero over a finite distance, unlike the case of a clear-liquid front where it jumps from one to zero over a very small distance. It means that we can use the single-phase Darcy's law models to study fluid flow in about 60% of the wicks, while its two-phase version will be needed for modeling the remaining 40%. The wicks that we have considered in this study belong to

the first group. Therefore, the theoretical approach presented here involves the single-phase flow inside porous wicks with a clear liquid front.

The momentum equation, also called the Darcy's law, for the flow of a single liquid in an isotropic porous medium under isothermal conditions is

$$\tilde{V} = -\frac{K}{\mu} \tilde{\nabla} P \quad (4.1)$$

where \tilde{V} is volume-averaged liquid velocity and P is the pore-averaged modified pressure⁶. Here K is the permeability of the porous medium while μ is the liquid viscosity. Another governing equation for the flow of an incompressible liquid in a solid porous medium is the macroscopic continuity or mass-balance equation:

$$\tilde{\nabla} \cdot \tilde{V} = 0 \quad (4.2)$$

The effect of gravity induced liquid motion in a porous medium and pore averaged hydrodynamic pressure p are included in the modified pressure P as

$$P = p + \rho gh \quad (4.3)$$

where h is the height of a point within the fully saturated porous medium. If the permeability and viscosity are considered to be constant, then a combination of Eq. (4.1) with Eq. (4.2) leads to a Laplace equation for the modified pressure as

$$\nabla^2 P = 0 \quad (4.4)$$

After solving Eq (4.4) for P in a domain, Eq (4.1) yields the velocity distribution, and subsequently the location of liquid front in the wick.

⁶ The macroscopic flow description in porous media seeks to average flow quantities over the pore-space of an averaging volume and thus create a continuum of such volume-averaged quantities for the purposes of flow modeling. The volume-average, also referred to as the phase average, and the pore averaged, also referred to as the intrinsic phase average, are two different types of averages used in porous media studies [10]. The former pertains to averaging a quantity over the whole of the averaging volume, while the latter refers to averaging over the pore space within the averaging volume.

4.3.1 Analytical Solution for a Single Cross-Section Wick

For now, we are going to consider the one dimensional (1-D) fluid motion in a simple wick as shown in Figure 1a with a constant cross-sectional area. Figure 2.2 shows the test setup consisting of the Dynamic Contact Angle Analyzer (DCA), which is usually used for the wicking tests. The analytical solution for the liquid motion will be presented in here—details of its derivation presented in Chapter 2.

$$p_s \ln \left| \frac{p_s}{p_s - \rho g h_f} \right| - \rho g h_f = \frac{\rho^2 g^2 K}{\varepsilon \mu} t \quad (4.5)$$

Once the location of liquid front h_f is known, following equation can be used to estimate the absorbed liquid mass as a function of time:

$$m = \varepsilon \rho \pi R_{wk}^2 h_f \quad (4.6)$$

Using the energy balance model suggested earlier for polymer wicks [8], one can estimate p_s as

$$p_s = \frac{3(1 - \varepsilon)\gamma \cos(\theta)}{\varepsilon R_e} \quad (4.7)$$

where R_e , the effective beads radius, can be computed using the equation

$$R_e = \frac{\int_0^\infty R_b^3 \phi(R_b) dR_b}{\int_0^\infty R_b^2 \phi(R_b) dR_b} \quad (4.8)$$

with $\phi(R_b)$ being the probability density function for bead radius⁷ R_b .

⁷ The polymer wicks are made from polymer beads through a sintering process. So on studying the wick cross-section under a microscope, one can not only estimate bead radii but also study their distribution [13].

4.3.2 Analytical Solution for an Altered Wick Using Darcy's Law

It turns out that the flow physics applied for developing an analytical solution for a plain cylindrical wick in Chapter 2 can also be used to fashion an analytical solution for wicking in an altered wick with step-like variations in its cross-sectional area.

For a wick with a sharp change in the cross-section area, such as the wick 'D' of Table 4.1, we have two regions: region 1 with a smaller wick-radius R_{w1} up to height h_i , and region 2 with larger wick-radius R_{w2} (see Figure 4.2).

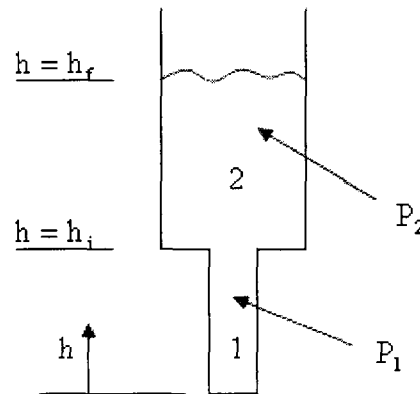


Figure 4.2 Different regions and liquid-front location in a altered wick with two different cross-sectional areas.

Fluid flow is expected to be 1-D (one dimensional) everywhere in the altered wicks except near the point of change in the wick cross-sectional area. If we assume the flow to be 1-D in the entire the wick, then there will be an error in our analytical solution due to the anticipated 3-D flow around the sharp change in the cross-section area. However, this error is expected to decrease as the front moves away from this point. If the difference between R_{w1} and R_{w2} is small, then this error is expected to be insignificant as well.

On imposing the 1-D flow assumption in each region of Figure 4.2, the Laplace equation for pressure, Eq (4.4), reduces to

$$\frac{d^2 P}{dh^2} = 0 \quad (4.9)$$

Solution of this equation in regions 1 and 2 can be expressed as

$$P_1 = B_1 h + C_1 \quad (4.10a)$$

$$P_2 = B_2 h + C_2 \quad (4.10b)$$

where subscripts 1 and 2 refer to the two wick regions. Now the four boundary conditions needed to find four constants in Eqs (4.10a) and (4.10b) are:

$$P_1 = p_{atm} \quad \text{at } h = 0 \quad (4.11a)$$

$$P_1 = P_2 \quad \text{at } h = h_i \quad (4.11b)$$

$$P_2 = p_{atm} - p_s + \rho g h_f \quad \text{at } h = h_f \quad (4.11c)$$

$$Q_1 = Q_2 \Rightarrow B_1 R_{wk1}^2 = B_2 R_{wk2}^2 \quad \text{at } h = h_i \quad (4.11d)$$

The last condition is obtained from the equality of mass flux at the common boundary of regions 1 and 2. The use of these four boundary conditions in Eqs (4.10) yields the following expressions for the four constants.

$$B_1 = \frac{R_{wk2}^2}{R_{wk1}^2} \frac{\rho g h_f - p_s}{h_f - h_i + h_i \frac{R_{wk2}^2}{R_{wk1}^2}} \quad (4.12a)$$

$$C_1 = p_{atm} \quad (4.12b)$$

$$B_2 = \frac{\rho g h_f - p_s}{h_f - h_i + h_i \frac{R_{wk2}^2}{R_{wk1}^2}} \quad (4.12c)$$

$$C_2 = p_{atm} - p_s + \rho g h_f - h_f \frac{\rho g h_f - p_s}{h_f - h_i + h_i \frac{R_{wk2}^2}{R_{wk1}^2}} \quad (4.12d)$$

On using Darcy's law in association with the front velocity in region 2, we get

$$\frac{dh_f}{dt} = - \frac{K}{\varepsilon \mu} \frac{dP_2}{dh} \Big|_{h=h_f} = - \frac{K}{\varepsilon \mu} \frac{\rho g h_f - p_s}{h_f - h_i + h_i \frac{R_{wk2}^2}{R_{wk1}^2}} \quad (4.13)$$

On integrating after separating the variables, and later assuming $h_f(t_i) = h_i$, we can derive following expression for region 2.

$$t = t_i + \frac{\varepsilon \mu}{K \rho g} \left[h_i - h_f + \frac{p_s - \rho g h_i \left(1 - \frac{R_{wk2}^2}{R_{wk1}^2}\right)}{\rho g} \ln \frac{p_s - \rho g h_i}{p_s - \rho g h_f} \right] \quad (4.14)$$

Note that we can get the equivalent relation for region 1 by imposing the condition $h_i = t_i = 0$ in Eq (20) and obtain an expression identical to Eq (4.5). We can develop the following compact form for the implicit expressions for $h_f(t)$ in both the wick regions.

$$t = \begin{cases} t_i + \frac{\varepsilon \mu}{K \rho g} \left[h_i - h_f + \frac{p_s - \rho g h_i \left(1 - \frac{R_{wk2}^2}{R_{wk1}^2}\right)}{\rho g} \ln \frac{p_s - \rho g h_i}{p_s - \rho g h_f} \right], & h_f > h_i \\ - \frac{\varepsilon \mu h_f}{K \rho g} + \frac{\varepsilon \mu p_s}{K \rho^2 g^2} \ln \frac{p_s}{p_s - \rho g h_f}, & h_f < h_i \end{cases} \quad (4.15)$$

Though we can develop a similar analytical solution for the other wick-type (wicks B and C of Table 4.1), we will confine the development of such an analytical

solution to the present case only. This is because we have used a wick of the type shown in Figure 4.2 for conducting experiments and used those results for validating our simulation. Hence the analytical solution will be useful in providing another point of reference for our code.

4.3.3 Analytical Solution for a Simple Wick Using the Modified Capillary Model

As mentioned in the introduction, the wicking model proposed by Washburn remains a powerful technique used by the research community to predict 1-D wicking in porous substrates. We intend to use it as the third analytical solution in order to highlight its limitation for the cases where 3-D flows are involved during wicking.

Under the Washburn's capillary model, the considered porous medium, a polymer wick, will be assumed to be equivalent to a bundle of vertically aligned capillary tubes. If the gravity effect is negligible, then the capillary model yields the well-known form of Washburn equation that predicts the location of liquid front h_f as a function of time t as

$$h_f = \sqrt{\frac{\gamma D_e \cos(\theta)}{4\mu} t} \quad (4.16)$$

where D_e , the effective pore diameter, is obtained through

$$D_e = \frac{D_h^2}{D_c} \quad (4.17)$$

such that D_c is the capillary diameter and D_h is the hydraulic diameter of the capillary tubes. (The capillary and hydraulic radii, R_c and R_h respectively, are half of these diameters.)

In general cases where the gravity is not negligible, one can derive an implicit relation between h_f and time t as

$$p_c \ln \left| \frac{p_c}{p_c - \rho g h_f} \right| - \rho g h_f = \frac{\rho^2 g^2 R_h^2}{8\mu} t \quad (4.18)$$

which can be termed as the alternate form of the Washburn equation with the gravity effects. The capillary (suction) pressure for capillary tubes p_c , a parameter in Eq. (4.18), is obtained with the help of the Laplace equation as

$$p_c = \frac{2\gamma \cos(\theta)}{R_c} \quad (4.19)$$

Since the right hand side of Eq. (4.18), a linear expression in t , is a function of the left-hand-side expression for h_f , it is very easy to estimate t for a given value of h_f .

4.4 Numerical Approach

We will now describe a finite element/control volume (FE/CV) method to solve for the two-dimensional wicking flow using the single-phase flow physics described in Sec. 4.2 by Eqs. (4.1) to (4.4). The FE/CV is a well-proven method to model free-surface flows in porous media. One of the chief applications of the method is in numerically simulating the transient mold-filling in the liquid composite molding processes used for the manufacture of composite materials

[16]. The FE/CV method will be employed here to model the transient free-surface problem encountered during wicking in porous wicks.

4.4.1 FE/CV method

In the proposed algorithm, the transient fluid flow in the wicks involving a moving-boundary is divided into multiple time steps. After assuming a quasi-steady condition during each time step, Eq (4.4) is first solved for modified pressure in the wick region that has been saturated by the moving liquid-front. We then use the computed pressure field to estimate the velocity field using Eqs (4.1) and (4.2), and then use the field to find the new location of liquid front at each time step.

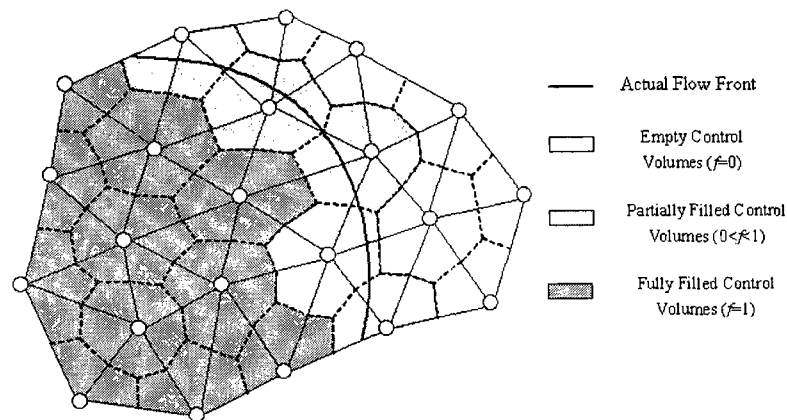


Figure 4.3 A schematic describing a typical finite element mesh along with the surrounding control volumes for application with the FE/CV method to model the motion of liquid front in the wicks.

Since the liquid front is moving, so the hybrid FE/CV method is employed to track the flow surface. This method uses an Eulerian fixed mesh to track the flow front, and is highly efficient computationally as it avoids frequent remeshing

of the flow domain as opposed to a Lagrangian algorithm. Eq (4.4) is first solved in the fully saturated region behind the moving front. As shown in Figure 4.3, P behind the moving wicking front is solved in the fixed finite element (FE) mesh. By applying the standard Galerkin weighted residual method to Eq (4.4) and integrating by parts, the weak formulation of pressure governing equation is given by

$$\int_{\Omega} \frac{K}{\mu} \left(\frac{\partial w}{\partial x} \frac{\partial p}{\partial x} + \frac{\partial w}{\partial y} \frac{\partial p}{\partial y} \right) dx dy = \oint_{\Gamma} w(\mathbf{v} \cdot \mathbf{n}) ds \quad (4.20)$$

where w is the weight function, \mathbf{v} is the Darcy velocity, and \mathbf{n} is the unit vector normal to the boundary [17]. The pressure is approximated by the shape function N and nodal pressure p as

$$p = \sum_{j=1}^n N_j(x, y) p_j \quad (4.21)$$

where n is the number of nodes in an element. On substituting Eq (4.21) into the weak formulation Eq (4.20) while using the relation $w_i = N_i$, we obtain a set of linear equations for one finite element as

$$\left[\sum_{j=1}^n \int_{\Omega^e} \frac{K}{\mu} \left(\frac{\partial N_i}{\partial x} \frac{\partial N_j}{\partial x} + \frac{\partial N_i}{\partial y} \frac{\partial N_j}{\partial y} \right) dx dy \right] p_j = \oint_{\Gamma^e} N_i(\mathbf{v} \cdot \mathbf{n}) ds \quad (4.22)$$

Since the domain is divided into a number of elements, the assembly of Eq (4.22) for each element results in a set of algebraic linear equations as

$$[\mathbf{A}]\{\mathbf{P}\} = \{\mathbf{F}\} \quad (4.23)$$

where the coefficient matrices are defined as

$$K_{ij}^e = \sum_{j=1}^n \int_{\Omega^e} \frac{K}{\mu} \left(\frac{\partial N_i}{\partial x} \frac{\partial N_j}{\partial x} + \frac{\partial N_i}{\partial y} \frac{\partial N_j}{\partial y} \right) dx dy \quad \mathbf{f}_i^e = \oint_c N_i(\mathbf{v} \cdot \mathbf{n}) ds \quad (4.24)$$

$$\mathbf{A} = \sum_{e=1}^{ne} K_{ij}^e \quad \mathbf{F} = \sum_{e=1}^{ne} \mathbf{f}_j^e$$

The velocity normal to the boundary is zero except at the inlet, where a non-zero value is automatically satisfied by the finite element method (often referred to as the natural boundary condition). The capillary suction-pressure p_s , obtained from Eq (4.7), will be used for imposing the modified pressure boundary condition at the front. The pressure boundary conditions implemented in our model are

$$P = p_{atm} \text{ at } h = 0 \quad (4.25a)$$

$$\frac{dP}{dn} = 0 \text{ at } R = R_{wk} \text{ for } h < h_f \quad (4.25b)$$

$$P = (p_{atm} - p_s) + \rho g h_f \text{ at } h = h_f \quad (4.25c)$$

Note that the hydrostatic variation in liquid pressure is accounted for in the modified pressure through the use of expression given in Eq (4.3).

The final set of linear algebraic equations corresponding to Eq (4.23) are solved by a large parallel sparse direct solver MUMPS [18]. Later the distribution of P behind the front is used to furnish V with the help of Darcy's law, Eq (4.1), at the interfaces of the control volumes (CV) defined around the node points, which is then used to determine the flow-front velocity and to advance the front after each time-step as follows.

We have defined a filling factor f_i which is used to track saturation in the CV defined around any element i and can be expressed as

$$f_i = 1 \quad \text{for CVs behind the liquid front that are filled with the liquid} \quad (4.26a)$$

$$0 \leq f_i \leq 1 \quad \text{for CVs near the liquid front that filled partially with the liquid} \quad (4.26b)$$

$$f_i = 0 \quad \text{for CVs beyond the liquid front in the dry region} \quad (4.26c)$$

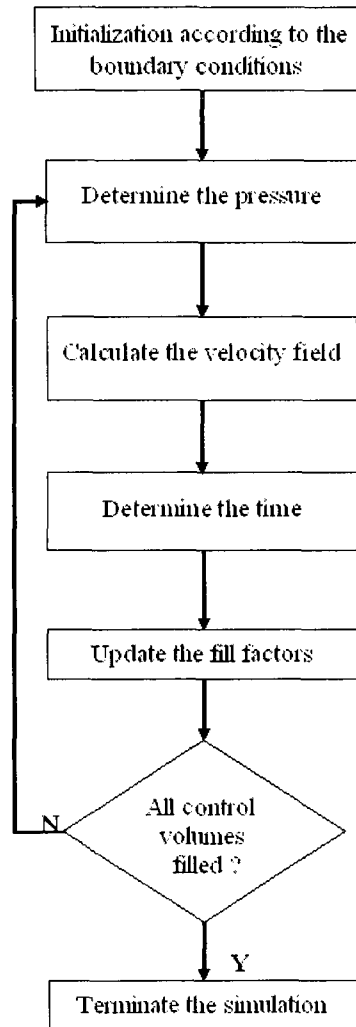


Fig.4.4. A flow chart describing the FE/CV algorithm

The time increment of each time step for advancing the flow front is determined by the shortest time to completely fill one control volume expressed as

$$\Delta t = \min \left[\frac{(1 - f_i) \varepsilon V_i}{Q_i} \right] \quad (4.27)$$

where Q_i is the flow rate related to control volume i , and can be computed by

$$Q_i = \int_{cv} -(\vec{V} \cdot \hat{n}) d\Gamma_{cv} = \sum_k \int_k -(\vec{V} \cdot \hat{n}) d\Gamma_k \quad (4.28)$$

After each time-step t_n , we have to update the filling factor before going into next time-step t_{n+1} ; the following expression is used to modify the filling factor for each time increment:

$$f_i^{t_{n+1}} = f_i^{t_n} + \frac{Q_i}{\varepsilon V_i} \Delta t \quad (4.29)$$

This finite element/control volume (FEM/CV) algorithm (described using a flow chart in Figure 4.4) is employed by PORE-FLOW[®], a computer program developed at University of Wisconsin-Milwaukee [19] for modeling liquid flow in porous media. Note that the FE/CV algorithm has been employed in the past to model wetting of fibrous porous media in liquid molding processes in polymer composites [16, 17, 19]; however, this is the first time that this technique is employed to model the flows in polymer wicks.

Note that since the flow is essentially one-dimensional along the wick length, except near places with sharp jumps in the cross-sectional area, a 2-D flow simulation is enough to capture fluid flow in the axi-symmetric geometry of the essentially cylindrical wicks. So even though a full 3-D flow simulation can be conducted by PORE-FLOW for more complex wick geometries, a 2-D flow simulation is sufficient in the modeling of wicking flow in the present paper. As a result, the meshes used here are flat, two-dimensional shell meshes. However,

a thickness is assigned to these meshes in order to conduct flow-rate computations while doing mass flow estimation into the CVs. The thickness is chosen in such a way that the cross-section area of the entrance of 2-D meshes matches the wick cross-section area—such a step ensures that Darcy velocities in the real wick and the 2-D finite element model are equal for a given flow rate.

Table 4.2 Characteristics of the wicks and the liquid used in our validation experiments⁸. The wick was made from polypropylene while the liquid was hexadecane.

Property	Value	Unit
Density of the liquid	773	Kg/m^3
Viscosity of the liquid	0.00334	$m Pa.s$
Surface tension of liquid ⁹	22.24	mJ/m^2
Length of wick L_{wk}	0.076	m
Wick radius R_{wk}	0.0036	m
Wick porosity ε	0.4	-
Effective bead-radius R_e	482	μm
Permeability K	$4.84e-10$	m^2
Contact angle θ	0	-

4.5 Results and Discussions

It is important to test the accuracy of our simulation. Therefore we tested our code against experimental results as well as the analytical solutions. The wicking experiments were conducted using a microbalance shown in Figure 4.1

⁸ The experimental procedures for measuring these parameters are explained in Ref [8].

⁹ Previously we had used a higher value for surface tension in Ref [8], which came from some other source (Ref [29]); while here we have measured the value of surface tension directly.

The cylindrical wick (simple or adapted) was suspended from the balance and made to touch the surface of a liquid; the wicking starts as soon as the contact was made. The weight gain in the wick due to liquid imbibition is recorded by the microbalance, and is recorded with the help of a computerized data acquisition system hooked to the microbalance. (Details of the wicking experiment are given in chapter 2.) The properties of the wick and liquid used in our experiments are listed in Table 4.2.

First, the case of one-dimensional wicking in a simple wick, as analyzed in Chapter 2, will be considered. The analytical solutions for this case are given by the Darcy's law approach [Eq (4.6)] and the Washburn equation [Eq (4.18)]. A plot of the front height predicted as a function of time is given in Figure 4.5—as we can see, the numerical prediction match very well with the analytical solutions, which in turn match very well with the experimental results. So it is heartening to see such a good validation of our numerical simulation.

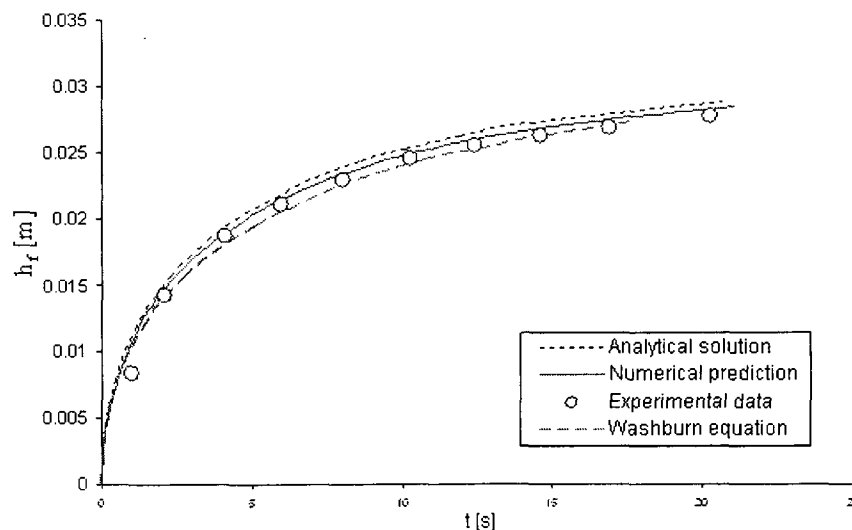
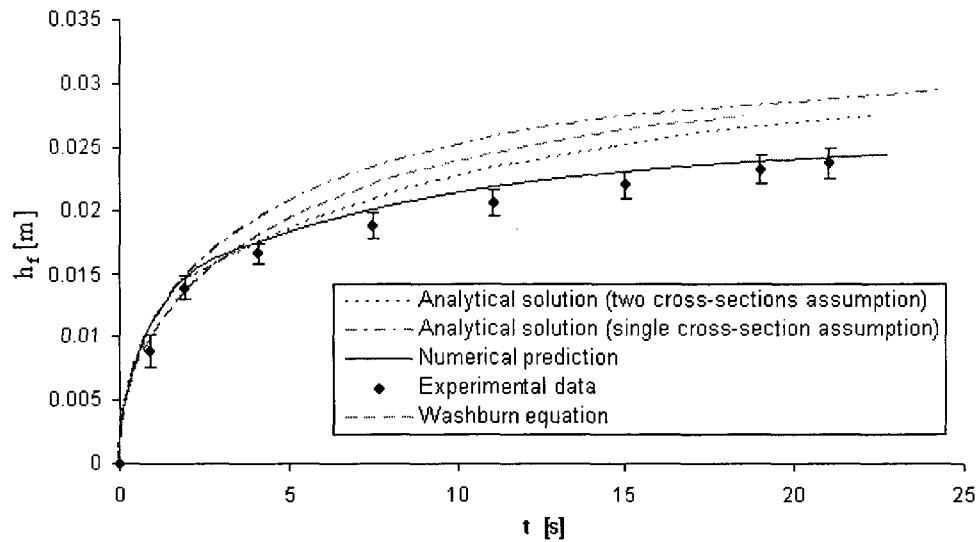
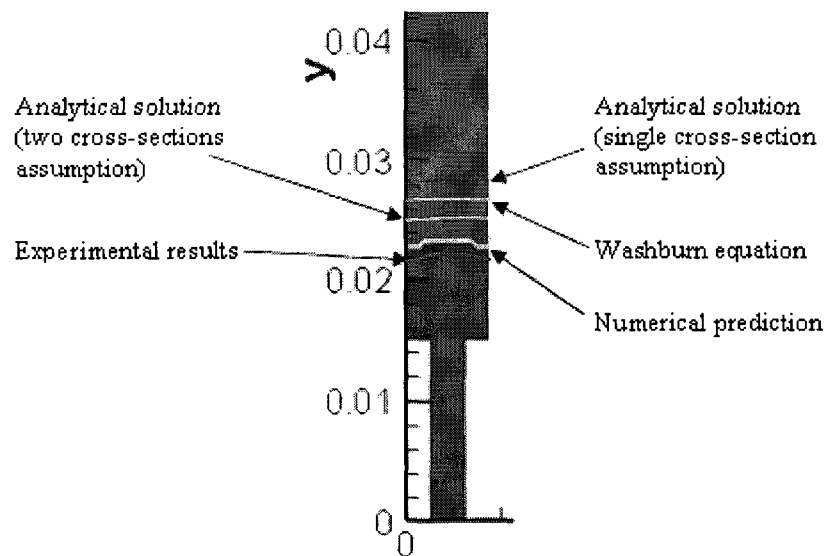


Figure 4.5 A comparison of the numerical prediction with the experimental result and analytical solution for the case of wicking in a simple wick.



a) A comparison of the flow-front height h_f versus time t plots. Scatter bars show confidence interval of 95%.



b) A comparison of the flow-front locations for the wick 'D' at time $t = 20$ s. Figure 4.6 For wicking in wick 'D', a comparison of the numerical prediction with the analytical solutions corresponding to the one and two different cross-sections for wick, and the experimental result.

Now we consider a more difficult case of wicking in a cylindrical wick with a single step-change in the diameter, i.e. wicking in wick D, for the validation of our code. Figure 4.6 shows a comparison of the numerical prediction of the flow-front height h_f as a function of time t with the analytical 1-D solutions developed

for one and two different cross-sections of the wick [Eqs. (4.6) and (4.15), respectively], the Washburn equation [Eq (4.18)], and the experimental data for wick 'D'. In the plot of experimental results, the confidence interval of 95% is shown by the scatter bars. Figure 4.6 shows that the use of the double cross-section model as compared to the single cross-section model improves the analytical prediction, but it is still not as good as the numerical prediction. Similarly the limitations of the 1-D approximation based Washburn equation are exposed in this case of the 3-D wicking flows where the equation over predict the flow-front height. Such a good validation for the cases of wicking in the simple 1-D flow and the altered 3-D flow wicks inspires confidence in the accuracy and correctness of our simulation POREFLOW[®].

Let us turn our attention to a parametric study done with the four different geometries of the altered wick listed in Table 4.1 and their FEM meshes shown in Figure 4.7 Numerical simulations for wicking were done for these four different altered wicks with four different sharp changes in their cross sectional areas. The results are compared with each other as well as with the predictions for the simple wick with a constant cross-sectional area.

Figures 4.8 and 4.9 show the liquid-front movements in the wicks C and D as predicted by POREFLOW[®]. Figure 4.8 shows that after entering the notched area, the liquid front near the boundaries is a little higher than the liquid front in the middle. The reason for this discrepancy is that the flow that is to go in the 'removed' pores must be distributed into all the remains pores; however, since the pores close to the boundaries are

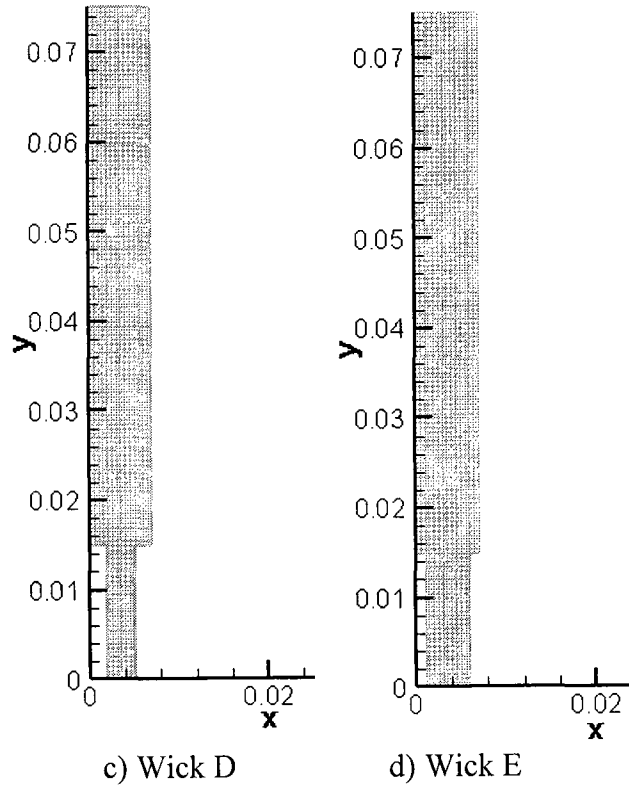
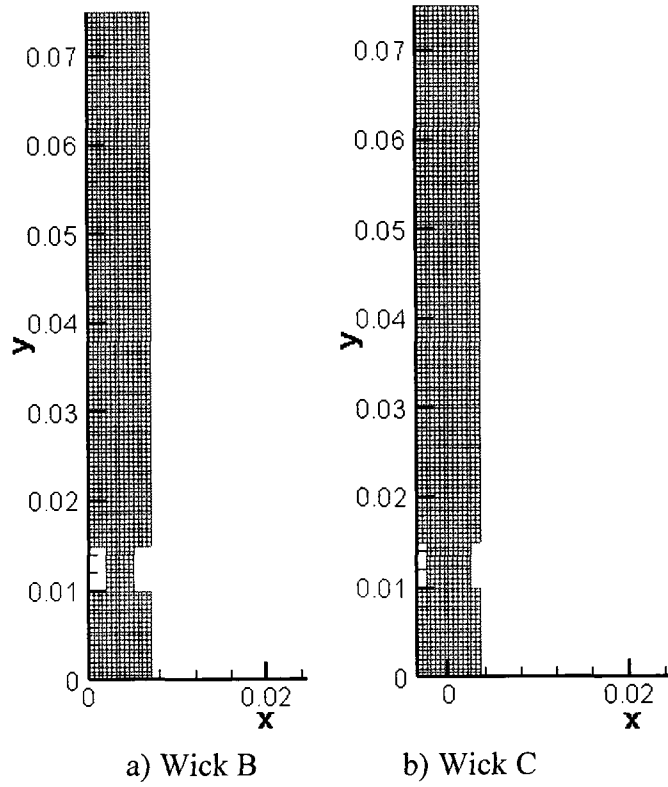


Figure 4.7 The finite element meshes generated for the wicks B, C, D, and E.

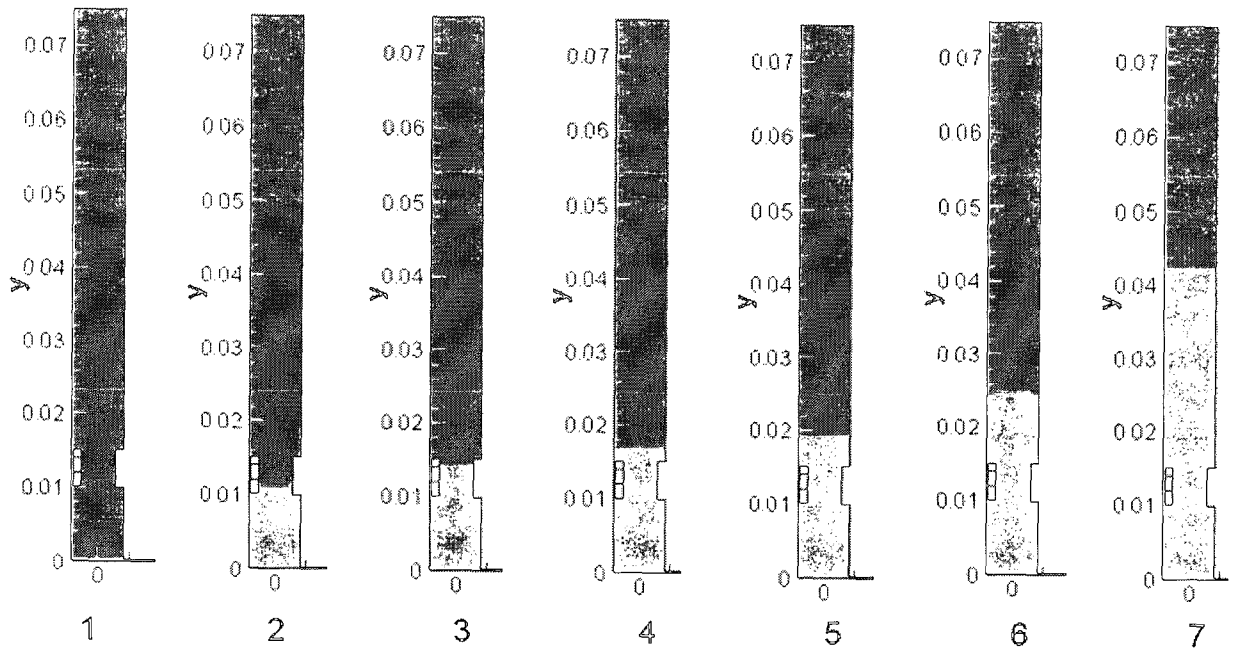


Figure 4.8 Pattern of liquid-front movement in the wick C

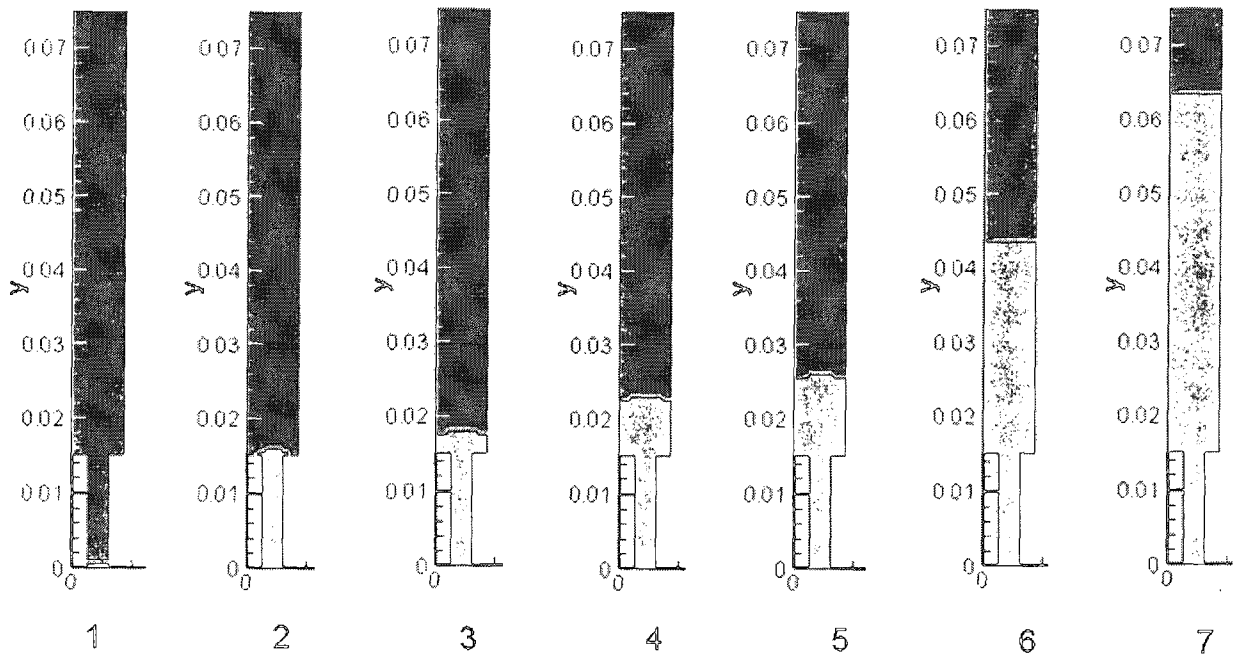


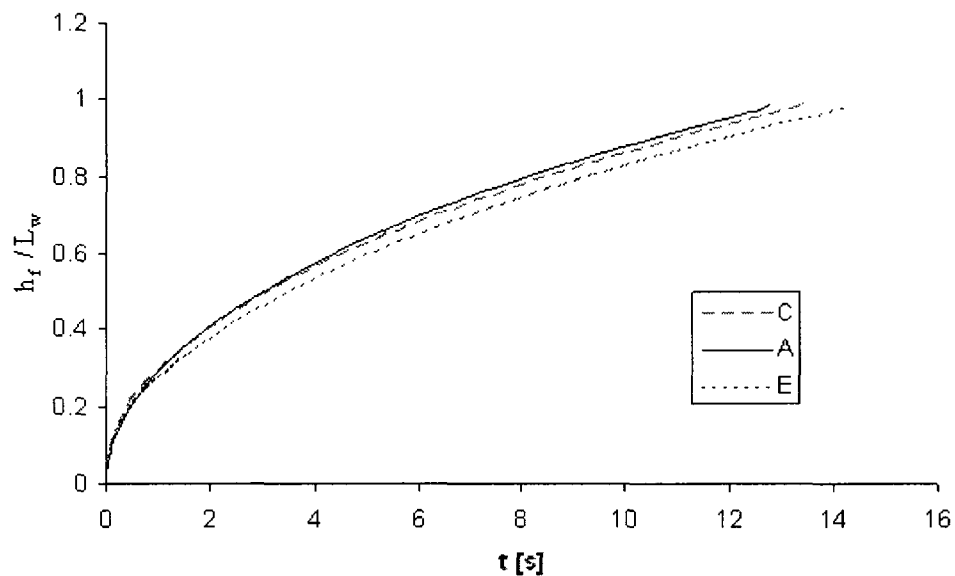
Figure 4.9 Pattern of liquid-front movement in the wick D

closest to the removed pores, so they have a higher flow-rate compared to the pores in the middle that are far away from the removed pores. Note that this

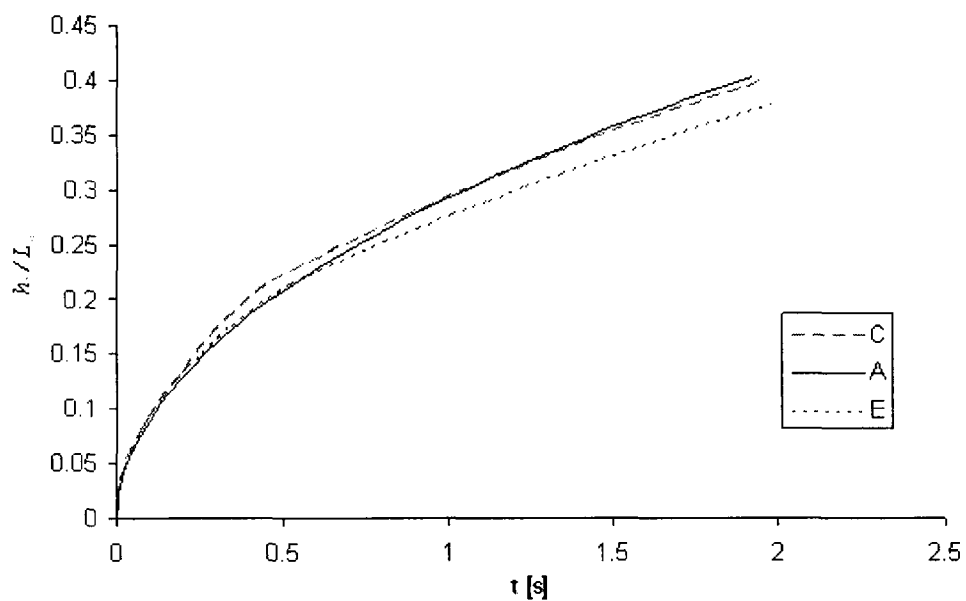
imbalance is corrected after a while as the flow-front becomes perfectly horizontal once again. We see an exactly opposite effect after the passage of the front through a constriction and into a wider cross-section. In the parts 4 and 6 of Figure 4.8 as well as in parts 2 to 5 of Figure 4.9, we can observe a little bulging of the front due to an enlargement in the cross-sectional area. It implies that the pores in the middle regions face higher flow-rates as compared to the pores in the border regions, and hence the liquid front is a little higher in the middle after the expansion of the wick cross-sectional area. This unbalance in the flow rate is compensated as the front moves away from the expansion point, and the liquid front acquires the perfectly horizontal profile during the later stages of the wicking process.

Figure 4.10a plots the evolution of the dimensionless liquid-front height (h_f / L_w) for the wick A, C, and E. Note that the slope of these plots is equal to the speed of the liquid front. It is clear that beyond $t = 1$ s, the liquid-front traveled has traveled the farthest in the simple wick A. However, the speeds of their liquid fronts are almost identical beyond $t = 5$ s; hence the curves are almost parallel beyond this point. It is clear that reduction in the distance traveled as well as reduction in the speed is related to 1) the reduction in the cross sectional area of these wicks, and 2) the length over which the reduced area is maintained. Though the diameter reduces by same amount in the wicks C and E, the smaller diameter is retained for a longer length in E. If we propose that these two factors are related to the resistance offered by a wick, then the resistance in the wick C is less than that in the wick E. As a result, the liquid front travels farther in the

wick C as compared to the wick E. Figure 4.10b give more details of the first two seconds of the absorption process. Initially, the wicking speeds in A, C and E are almost identical. This is understandable since the wicking process is purely one



a) The comparison till the time of full saturation



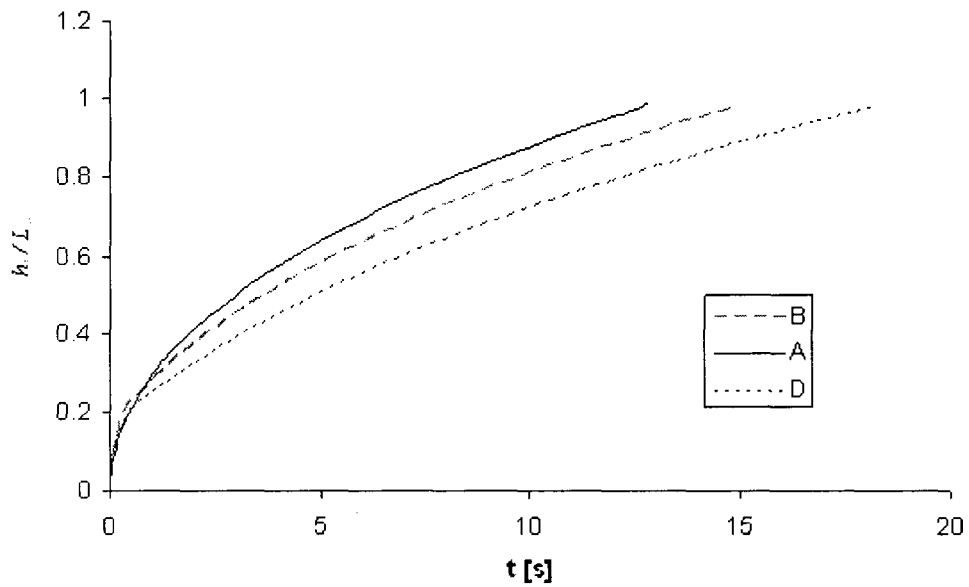
b) The comparison in the first two seconds

Figure 4.10 A comparison of evolution of the dimensionless and numerically predicted liquid-front height (h_f / L_w) in the wicks A, C, and E

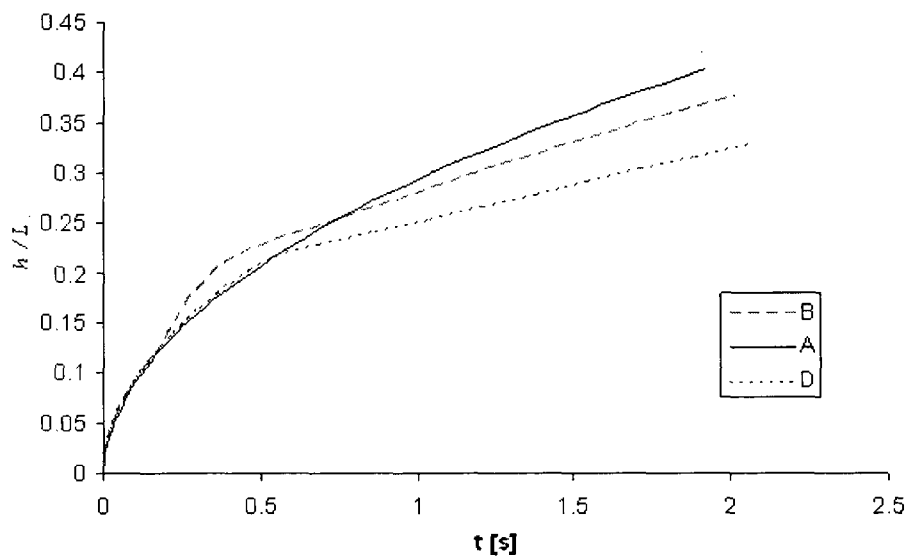
dimensional in all these wicks in the beginning, and hence variations in the cross-sectional areas are immaterial. However, the wicking speeds up in C at around $t = 0.25$ s when the front hits the first notch of the constriction in C. The C and E fronts are in the constricted region till $t = 0.5$ s; from this point onwards, the sectional area remains constant in these two wicks and hence we see a constant pattern for the C and E curves. Note that at $t = 0.45$ sec, the liquid-front height is about 9% higher in C compared to A.

Figure 4.11 plots the dimensionless liquid-front positions as a function of time for the wicks A, B and D. Since the wicks B and D are similar in shape to the wicks C and E, respectively, we see the same patterns as in Figure 4.10. However, the differences in terms of diameters between the altered wicks B and D with the simple wick A are more. Once again, in comparison to the simple wick A, the absorption speed has reduced in B and D due to a reduction in the cross-sectional area. As before, the reduction in diameter is the same in wicks B and D, but the length of the constriction is longer in D. According to Figure 4.11a, the curve of D is below the curve B, which implies that the wick D offers more resistance to wicking as compared to B. Figure 4.11b gives more detail of the first two seconds of absorption. The front is in the notched region till $t = 0.45$ s; from $t = 0.45$ sec onward, the sectional area remains constant for altered wicks and hence we see a constant, almost-linear pattern for each curve. Based on Figure 4.11b, the absorption rate in the wick D is similar to that of the wick A for up to $t = 0.5$ sec, and after that it decreases. The wick B has a higher liquid-front than the wick A from $t = 0.2$ sec to $t = 0.75$ sec. The liquid-front height in B is

about 18% higher than in A at $t = 0.39$ sec, but then B's front-speed decreases and its front height becomes 6% less than that of A after 12 sec.

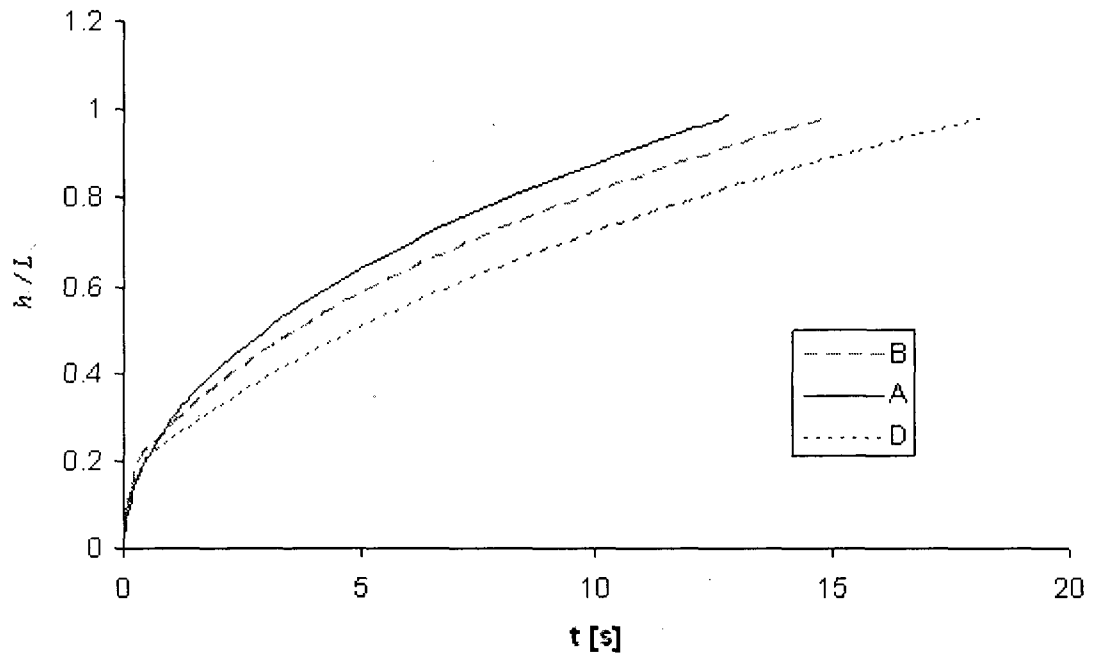


a) The comparison till the time of full saturation

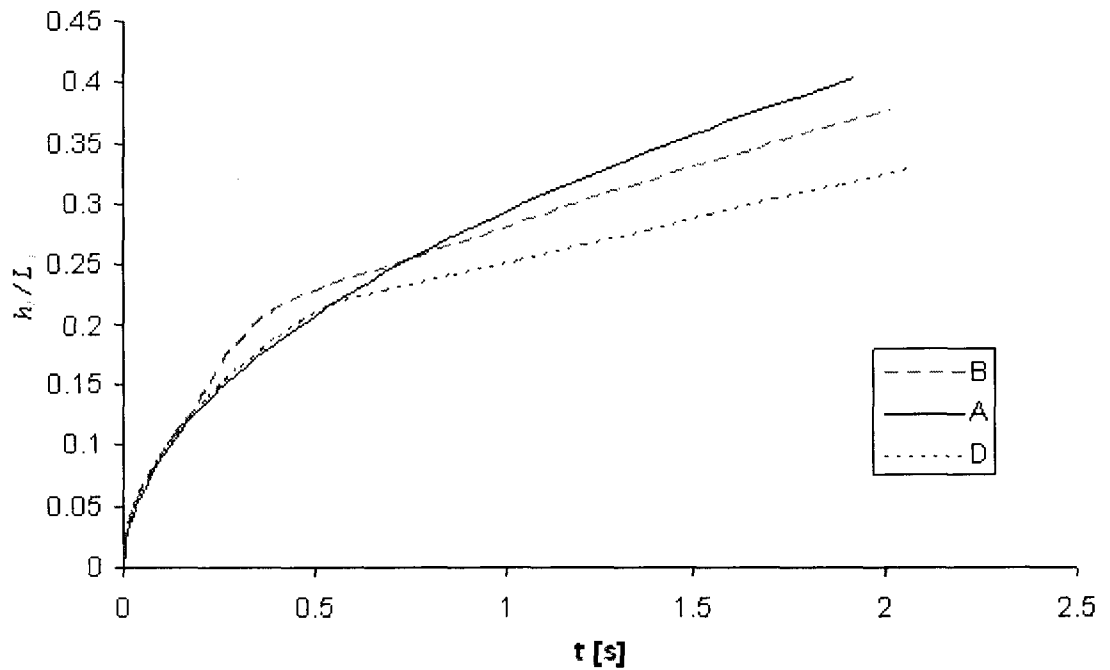


b) The comparison in the first two seconds

Figure 4.11 A comparison of evolution of the dimensionless and numerically predicted liquid-front height (h_f / L_w) in the wicks A, B, and D



a) The comparison till the time of full saturation



b) The comparison in the first two seconds

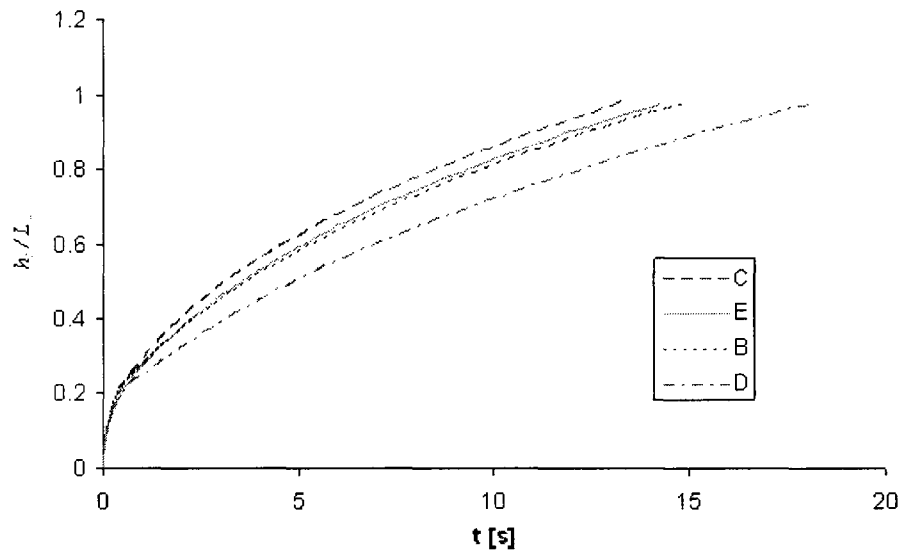
Fig. 12 A comparison of evolution of the dimensionless and numerically predicted liquid-front height (h_f/L_w) in the wicks A, B, and D

Figure 4.12 compares the dimensionless liquid-front heights as a function of time in all the four altered wicks. The wicks B and C have the same shape, but B has a smaller diameter in the constricted region. Similarly, the wicks D and E also have the same shape, but the diameter of the constricted region is smaller in D than in E. According to Figure 4.12a, the highest wicking rate is in wick C, while the lowest is in wick D. The time to traverse the whole length of the wick (0.075m) is surprisingly almost identical in the wicks B and E, even though they are completely different in terms of their shapes. According to Figure 4.12b, just after leaving the sharp changes in the cross sectional area (i.e., around $t = 0.4$ sec), the highest liquid front is in the wick B while the lowest liquid front is in the wick E.

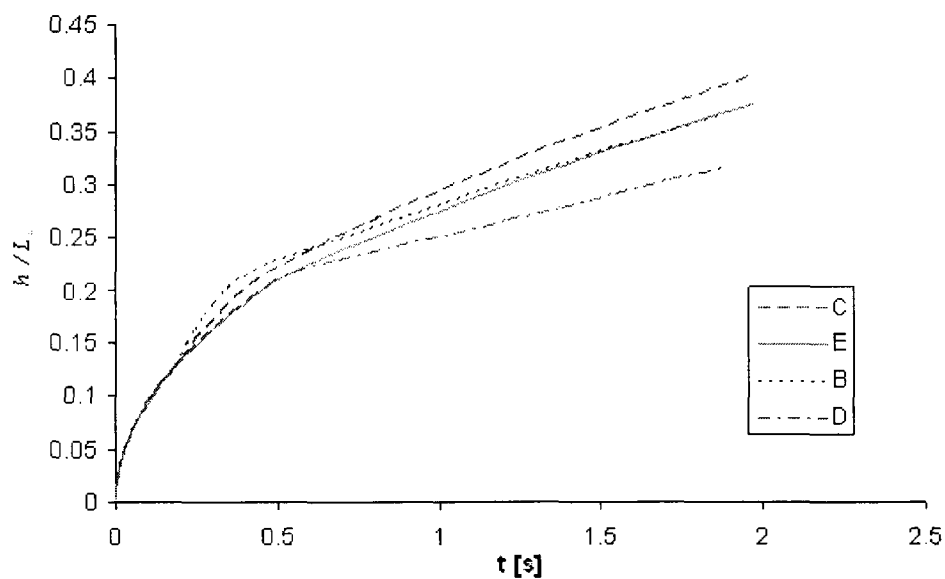
We would like to evaluate the relative performance of the altered wicks with respect to the simple wick in yet another way; the middle column of Table 4.3 lists the exact time needed for liquid front to reach the height of 0.07m. (Since the length of a commercial wick is between 0.07m to 0.075m, therefore we chose this final height for the comparison of wicking performance of different wicks.) As shown in the right-most column of Table 4.3 which lists the relative wick-wetting time with respect to the wick A, alteration of wick geometry causes delay in reaching the wick end by the liquid-front. All the altered wicks take more time to wet as compared to the simple wick. Note that the shortest and longest delays are in the wicks C and D, respectively.

Since the absorption rate (or absorption speed) is inversely proportional to the measured times, so the right-most column is also indicative of the relative

absorption rates in various wicks. It indicates that the wick alteration has reduced the absorption rate in general, and this reduction is related to the length and diameter of the altered regions. The wicks C and D with 4.2% and 44.9% increase in the wicking time have the smallest and the largest reduction in the absorption rate as compared to the simple wick A.



a) The comparison till the time of full saturation



b) The comparison in the first two seconds

Fig. 13 A comparison of evolution of the dimensionless and numerically predicted liquid-front height (h_f/L_w) in the wicks B, C, D, and E

Table 4.3 Exact and relative time for liquid front to reach height of 0.07m in different wicks

Wick	T7 (Time to reach hf = 0.07m) [s]	$\{[T7(A)-T7]/T7(A)\} * 100$ %
A	11.1471	0
B	13.091	-17.4
C	11.6152	-4.2
D	16.1555	-44.9
E	12.573	-12.8

4.6 Summary and Conclusion

Though the Washburn equation based approach to model wicking in porous substrates is well established, the approach is not accurate for modeling the 2-D and 3-D capillary-pressure driven imbibitional flows as it is based on the assumption of 1-D flow through a bundle of aligned tubes. We model the imbibition of liquids into polymer wicks, where a sharp flow-front is clearly visible during the wicking process, using the flow physics of single-phase flow in porous media for flow behind the front. A computer program called PORE-FLOW[®] based on the finite element / control volume (FE/CV) algorithm for the Darcy's law based single-phase flow is developed to model the 3-D wicking flows in complex-shaped wicks. The predictions of the program are first validated against the experimental results as well as the Darcy's law and Washburn equation based analytical solutions for the 1-D imbibition in a cylindrical wick—it is observed that the numerical predictions follow the experimental results and the analytical solutions very closely. Later the code is validated against the experimental

results pertaining to imbibition in a complex wick with two different diameters. While the numerical predictions follow once again the experimental results very closely, the analytical solutions based the Darcy's law and Washburn equation and employing the 1-D flow assumption, fail to be accurate. The excellent validation of our numerical simulation for the 1-D and 3-D wicking situations not only highlight the power of the single-phase Darcy's law based wicking model, but also point to another advantage of this model (*vis-à-vis* the Richard's equation approach described in the introduction) in terms of being able to measure the model parameters quite easily.

Later the code is then used to study wicking in four different wick shapes obtained by shaving off portions of cylindrical wicks. It is observed that these changes in the wick shape can have a significant impact on the mass of liquid imbibed into the wick, and reducing the wick diameter at appropriate places can be an effective way of controlling the wicking rate.

References

1. PK Chatterjee .Absorbency. Amsterdam/New York. Elsevier. 1985
2. E Kissa .Wetting and Wicking. Textile Res. J. 1996; 66(10): 660-668
3. PK Chatterjee and BS Gupta .Absorbent Technology. Amsterdam. Elsevier. 2002
4. N Pan and P Gibson .Thermal and Moisture Transport in Fibrous Materials. Cambridge. Woodhead. 2006
5. Jacob Bear .Dynamics of Fluids in Porous Media. Elsevier Science, 1972
6. Adrian E. Scheidegger . The physics of flow through porous media. University of Toronto, 1974
7. FAL Dullien .Porous Media: Fluid Transport and Pore Structure. Academic Press, 1992

8. R Masoodi, K M Pillai and P Varanasi. Darcy's Law based Models for Liquid Absorption in Polymer Wicks. *J. AIChE.* 2007; 53(11): 2769-2782
9. KM Pillai and SG Advani .Wicking Across a Fiber-Bank. *J. Colloid and Interface Sci.* 1996; 183: 100-110
10. DA Lockington, JY Parlange and M Lenkopane .Capillary Absorption in Porous Sheets and Surfaces Subjected to Evaporation. *Transp Porous Med.* 2007; 68:29-36
11. RJ Glass .Wetting Front Instability in Unsaturated Porous Media: A Three-Dimensional Study in Initially Dry Sand. *Transp Porous Med.* 1990; 5: 247-268
12. Wang Quan-Jiu, R Horton and Fan Jun .An Analytical Solution for One-Dimensional Water Infiltration and Redistribution in Unsaturated Soil. *Pedosphere.* 2009; 19(1): 104–110
13. John Crank .The Mathematics of Diffusion. Oxford University Press, 2nd Ed., 1980
14. <http://www4dev.uwm.edu/porous/>
15. Whitaker Stephen .The Method of Volume Averaging. Springer. 1998
16. Hua Tan and Krishna M Pillai .Processing composites for blast protection. in Blast protection of civil infrastructures and vehicles using composites. N Uddin ed. Cambridge Woodhead (in press).
17. Hua Tan, Krishna M. Pillai, Finite element implementation of stress-jump and stress-continuity conditions at porous-medium, clear-fluid interface, *Computers & Fluids*, Volume 38, Issue 6, June 2009, Pages 1118-1131
18. P. R. Amestoy, I. S. Duff and J.-Y. L Excellent, Multifrontal parallel distributed symmetric and unsymmetric solvers, in *Comput. Methods in Appl. Mech. Eng.*, 184, 501-520 (2000).
19. Hua Tan and Krishna M. Pillai, Effect of Fiber-Mat Anisotropy on 1D Mold Filling in LCM: A Numerical investigation, *Polymer Composites*, 2008, 29(8), 869-882.

Chapter 5

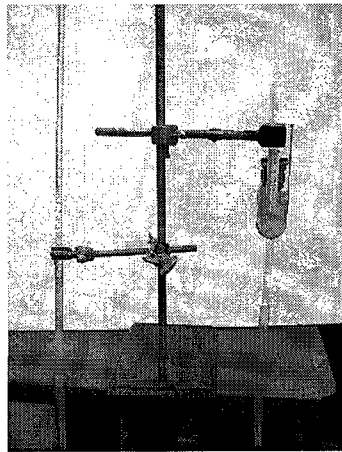
EFFECT OF EXTERNALLY APPLIED LIQUID PRESSURE ON WICKING IN PAPER WIPES

5.1 Introduction

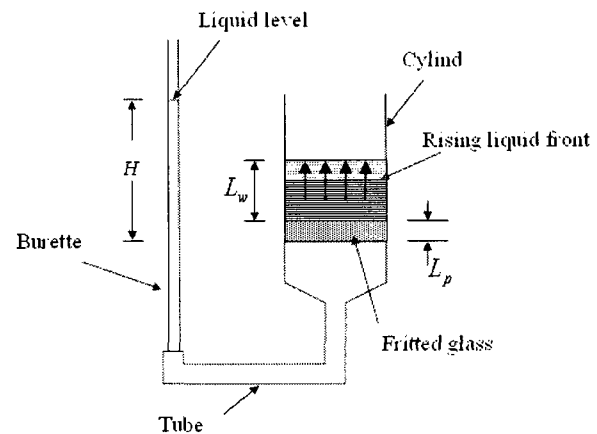
Absorption or wicking rate is the most important characteristic studied in the literature on absorbing technology [1]. When someone uses a stationary wipe to absorb liquid laid on a surface, the only driving force for wicking comes from the capillary pressure. However if somebody uses a wipe to clean a wet surface by moving the wipe over the surface, due to the forcing of liquid into the wedge created by the wipe and the surface, an extra hydrodynamic pressure in the wedge along with the capillary pressure inside the wipe drive the liquid absorption. This extra pressure facilitates the absorption and increases the wicking speed—we will refer to such a pressure as the external pressure. As is evident from the literature survey on wicking described in previous chapters, no previous study has evaluated the effect of external pressure on wicking rate in paper wipes. We plan to study the wicking of liquid into ordinary paper wipes under an externally applied liquid pressure where we will compare the experimental results with the predictions of two theoretical models based on the capillary-tube and Darcy's-law based flows. Different wicking parameters used in the two models are to be measured independently in this study. Liquid absorption

as a function of time as well as the time taken for a given volume of liquid to wick into the wiper are to be studied.

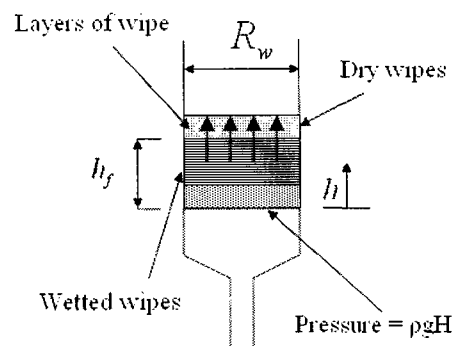
Figure 5.1 shows a photo and a schematic of the test setup where a liquid column was used to create an externally applied liquid pressure at the bottom of a stack of wiper.



a) A photo of the testing setup



b) A schematic of the testing setup



c) Details near the flow-front inside the stack of wiper

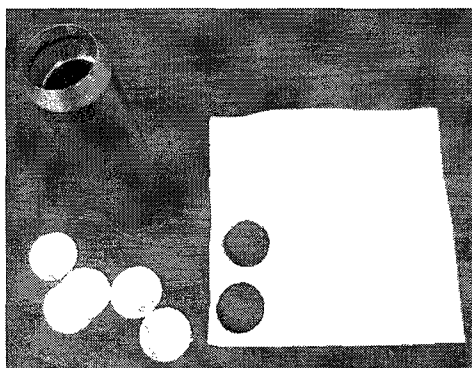
Figure 5.1 A schematic and photo of the testing setup used to study the effect of externally imposed liquid-pressure on the wicking rate in a wiper-stack.

Changing the height of the liquid column enabled us to study the effect of varying externally applied liquid pressure on wicking in the stack of wiper. Paper wiper,

which have cellulose as their main constituent and which are commonly used in the household, medical and industrial applications, were used in this study. Layers of paper towel or table napkin were stacked on top of a 'fritted glass' (a porous screen) in the cylinder (see Figure 5.2). The rate of reduction of liquid level in the burette was measured using a digital camera. Each film was reviewed several times to extract the exact position of the liquid level at different times during the wicking process. As the volume of liquid employed for wetting the stack of wipes was very small, changes in external pressure, which is related to the height of liquid column in the burette, could be neglected during the wipe-saturation process.



a) The layers of wipes stacked in the cylinder



b) The tool that was used to cut the wipes

Figure 5.2. The detail of cutting paper wipes and stacking layers in the cylinder

5.2 Mathematical Description of Wicking Models

As we reviewed in previous Chapters, there are essentially two conventional models that are popular in wicking studies: the Washburn model and the Darcy's law based model. We will use both of these two models to compare the experimental results with theoretical predictions.

5.2.1 Capillary Model

WE assume our porous medium created by wicks to be equivalent to a bundle of vertically aligned capillary tubes. The energy balance equation for liquid flow within the capillaries can be written as

$$\frac{p_0}{\rho g} + \frac{u_0^2}{2g} + h_0 = \frac{p_f}{\rho g} + \frac{u_f^2}{2g} + h_f + h_L \quad (5.1)$$

where h is the vertical coordinate in the porous medium, p is the pressure, u is the average velocity of fluid within a capillary tube, and h_L is the head loss.

Subscript 0 indicates the initial value of each parameter and subscript f indicates the value of parameters at the liquid front. Note that h_f is the length of the capillary tube filled with the liquid. Since the velocity is purely axial and constant in the capillary tubes (i.e. $u_0 = u_f$), Eq. (5.1) can be expressed as

$$p_0 - p_f = \rho g h_f + \rho g h_L \quad (5.2)$$

after recognizing that $h_0 = 0$. The pressure terms in Eq. (5.2) can be obtained through boundary conditions on the fluid as

$$p_0 = p(h=0) = p_h + p_{atm} \quad (5.3a)$$

$$p_f = p(h=h_f) = -p_c + p_{atm} \quad (5.3b)$$

So the left hand side of Eq. (5.2), which is the pressure drop driving the flow in the tube, can be expressed using the boundary conditions as

$$p_0 - p_f = p_h + p_c \quad (5.4)$$

The capillary suction pressure p_c , applied at the top of the liquid column, can be obtained through the Young-Laplace equation, Eq. (4.19).

To estimate h_L in Eq. (5.2), WE assume the flow to be laminar in the capillary tubes. So Eq (3.5) holds. Using Eqs. (5.4), (4.19) and (3.5) in (5.2) gives the final form of governing equation as

$$p_h + \frac{4\gamma \cos(\theta)}{D_c} = \frac{32\mu L_c}{D_h^2} \frac{dh_f}{dt} + \rho g h_f \quad (5.5)$$

If we neglect the gravity effects and take the imposed hydraulic pressure to be zero, then the first and last terms will vanish. Since $L_c = h_f$, an integration of the remaining equation leads to the well-known Washburn equation. For the general case when the gravity and hydraulic pressure are included, we use Eq. (5.5) to derive a relation between the location of liquid front h_f and time t . Using the schematic of the experimental setup shown in Figure 5.1 and noting that $p_h = \rho g H$ and $h_f = L_c$, Eq. (5.5) can be rewritten as

$$\rho g H + \frac{4\gamma \cos(\theta)}{D_c} = \frac{32\mu h_f}{D_h^2} \frac{dh_f}{dt} + \rho g h_f \quad (5.6)$$

where h_f is the height of the liquid front. Note that we use the hydrostatic pressure inside the tube and burette to claim that 1) the externally imposed liquid pressure under the fritted glass is equal to the pressure in the burette on the same horizontal plane, 2) the corresponding burette pressure is $\rho g H$. If the fritted

glass is saturated at the time of starting the test, a decrease in the volume of fluid within the burette can be related to an increase in the volume of fluid within the wiper through this equation

$$-\int_{H_0}^H \pi R_b^2 dH = \varepsilon_w \int_{L_p}^{h_f} \pi R_w^2 dh \quad (5.7)$$

where H_0 is position of fluid in the burette at the beginning of the test. Integration of Eq. (5.7) gives the relation between H and h_f as

$$H = H_0 - \varepsilon_w \left(\frac{R_w}{R_b} \right)^2 (h_f - L_p) \quad (5.8)$$

Using Eq. (5.8) in Eq. (5.6) leads to

$$\lambda_1 - \lambda_3 h_f = \lambda_2 h_f \frac{dh_f}{dt} \quad (5.9)$$

where

$$\lambda_1 = p_s + \rho g H_0 + \rho g L_p \varepsilon_w \left(\frac{R_w}{R_b} \right)^2 \quad (5.10a)$$

$$\lambda_2 = \frac{32\mu}{D_h^2} \quad (5.10b)$$

$$\lambda_3 = \rho g \left(1 + \varepsilon_w \left(\frac{R_w}{R_b} \right)^2 \right) \quad (5.10c)$$

Integration of Eq. (5.9) gives the final form of equation as

$$t = \frac{\lambda_2}{\lambda_3} \left[\frac{\lambda_1}{\lambda_3} \ln \left(\frac{\lambda_1}{\lambda_1 - \lambda_3 h_f} \right) - h_f \right] \quad (5.11)$$

For capillary model, we take $p_s = p_c$ in Eq. (5.10a) while using the Young-Laplace equation for capillary pressure p_c from Eq. 4.19.

5.2.2 Darcy Model

We would now use an alternative approach where the wetted wiper behind the rising liquid front is assumed to be completely saturated, and will be modeled using the Darcy's law for single-phase flow in porous media. As we explained in Chapter 2, it leads to Eq (2.10) for a 1-D flow such as what we have here:

$$\frac{d^2 P}{dh^2} = 0 \quad (2.12)$$

Note that this equation is valid in the stack of wet wiper as well as in the porous fritted glass underneath it. (As shown in Figure 5.1, the fritted glass and the stack of wipers above it form a hybrid porous media where these two different porous media of distinct porosities and permeabilities are in series.) Integration of Eq. (5.12) results into a general solution of the form $P_p(h) = Ah + B$ where $0 \leq h \leq L_p$ and $P_w(h) = Ch + D$ where $L_p \leq h \leq h_f$. Note that P_p is modified pressure within the porous fritted glass and P_w is modified pressure within the stack of the wipers. The constants A, B, C and D are evaluated using the boundary conditions

$$p_p = p_{atm} + p_h \quad \text{at } h = 0 \quad (5.13a)$$

$$p_w = p_{atm} - p_s \quad \text{at } h = h_f \quad (.5.13b)$$

$$p_w = p_p \quad \text{at } h = L_p \quad (5.13c)$$

$$V_w = V_p \quad (5.13d)$$

that are in terms of the pore averaged hydrodynamic pressure p . Eqs. (5.13a) to (5.13c) can be transformed in terms of the modified pressure P as

$$P_p = p_{atm} + p_h \quad \text{at } h = 0 \quad (5.14a)$$

$$P_w = (p_{atm} - p_s) + \rho g h_f \quad \text{at } h = h_f \quad (5.14b)$$

$$P_w = P_p \quad \text{at } h = L_p \quad (5.14c)$$

Use of the boundary conditions (5.14) and (5.13d) with the general solution of Eq. (5.12) results into the following expression for the modified pressure:

$$P_w(h) = \frac{\rho g(L_p - h_f) + p_s + p_h}{L_p(1 - \frac{K_w}{K_p}) - h_f} h + p_{atm} - p_s + h_f \left(\rho g - \frac{\rho g(L_p - h_f) + p_s + p_h}{L_p(1 - \frac{K_w}{K_p}) - h_f} \right) \quad (5.15)$$

Note that this solution is valid for $L_p \leq h \leq h_f$ with $P(h) = P_w(h)$; the front height h_f is a function of time. An expression for h_f can be derived by relating front speed dh_f/dt with the Darcy velocity [Eq. (2.28)] at front h_f as

$$\frac{dh_f}{dt} = \frac{V_w(h = h_f)}{\varepsilon_w} = - \frac{K_w}{\varepsilon_w \mu} \left. \frac{dP_w}{dh} \right|_{h=h_f} \quad (5.16)$$

which through the use of Eq.(5.15) results in

$$\frac{dh_f}{dt} = - \frac{K_w}{\varepsilon_w \mu} \left(\frac{\rho g(L_p - h_f) + p_s + p_h}{L_p(1 - \frac{K_w}{K_p}) - h_f} \right) \quad (5.17)$$

If the only external pressure is the hydrodynamic pressure, which based on Figure 5.1 is $p_h = \rho g H$, then the governing equation for the front speed can be expressed as

$$\frac{dh_f}{dt} = - \frac{K_w}{\varepsilon_w \mu} \left(\frac{\rho g(L_p - h_f) + p_s + \rho g H}{L_p(1 - \frac{K_w}{K_p}) - h_f} \right) \quad (5.18)$$

Using Eq. (5.8) in Eq. (5.18) to eliminate H leads to

$$\frac{dh_f}{dt} = -\frac{\lambda_1 + \rho g L_p - \lambda_3 h_f}{L_p \left(1 - \frac{K_w}{K_p}\right) - h_f} \left(\frac{K_w}{\varepsilon_w \mu}\right) \quad (5.19)$$

where λ_1 and λ_3 are defined in Eqs. (5.10a) and (5.10c). Integration of Eq. (5.19) leads to following equation as an explicit relation between time and location of liquid front.

$$t = \frac{\varepsilon_w \mu}{K_w \lambda_3} \left[\left(\frac{\lambda_1 + \rho g L_p}{\lambda_3} - L_p \left(1 - \frac{K_w}{K_p}\right) \right) \ln \left(\frac{\lambda_1 + \rho g L_p}{\lambda_1 + \rho g L_p - \lambda_3 h_f} \right) - h_f \right] \quad (5.20)$$

If there was just one material (i.e. only the stack of wipes) present in the cylinder, then $L_p = 0$, and a comparison of Eqs. (5.20) and (5.11) under this condition gives a relation between the permeability and the hydraulic pore diameter as

$$K_w = \frac{\varepsilon_w}{32} D_h^2 \quad (5.21)$$

This implies that if this equation is satisfied, and the permeabilities of the fritted glass and wipes are the same (or if we had just one material instead of two), the predictions of both the Darcy's law based model and the Capillary model are identical.

Note that p_s is the suction pressure created at the liquid front. The suction pressure is a function of the porous-medium microstructure, liquid surface-energy, and dynamic contact angle. If the porous medium is composed of spherical beads, it is a function of beads radius [3]; if the porous medium is a fabric, there are some other expressions for suction pressure [4,5]. we propose a novel, more general expression to estimate the suction pressure in paper-based porous media as

$$p_s = \frac{\gamma \cos(\theta) (1 - \varepsilon)}{\Gamma \varepsilon} \quad (5.22)$$

where Γ is the ratio of volume and wetted surface-area of the particles in a porous medium. Details of derivation of Eq. (5.22) appear in appendix A.

Table 5.1 Properties of the test liquids

Type of liquid	Distilled water	Windex®
Density [kg/m^3]	998	982
Viscosity [MPa.s]	0.982	1.5
Surface tension [MJ/m^2]	72.8	27.65

5.3 Experimental Study

The experimental study of wicking into the wipes is divided into two sections: in the first section, wicking parameters of wipes and wetting liquids will be measured in the testing systems; in the latter section, the wicking in the test setup will be explained. Cellulose wipes are commonly used in the household, medical and industrial applications. Two of the most important applications are paper towels and table napkins. We have chosen two different paper towels and a table napkin for this study. Water and cleaners are usually used as surfactants to clean the surfaces. We have used Windex®, a known common-use cleaner, and distilled water for this study. The reason for choosing distilled water instead of the regular tap water is that the chemical composition (and hence wettability) of different waters are not the same; so the results obtained with the water in a city may not be exactly the same as those obtained with the water from another

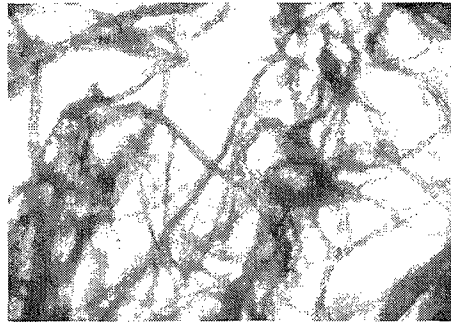
city or country. So we have chosen to use distilled water to increase the repeatability of our test results. Characteristics of the liquids and wipes are presented in Tables 5.1 and 5.2.

Table 5.2 Characteristics of the wipes (the \pm shows 95% confidence interval range [6]).

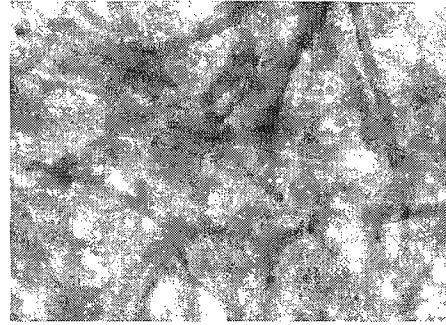
Designated name	A	B	C
Type of wipes	Paper towel	Paper towel	Table napkin
Brand Name	Bounty®	Scott®	Clarissa®
Cylinder radius R_w [m]	0.0155	0.0155	0.0155
Porosity of system ε	0.58	0.4	0.5
Parameter of Γ [μm]	47.9	53.3	35.8
Hydraulic radius of system R_h [μm]	14.6 ± 1.32	1.45 ± 0.7	2.5 ± 0.53
Permeability of system K [m^2]	$(1.55 \pm .4)$ $\times 10^{-11}$	(3.1 ± 0.86) $\times 10^{-13}$	(4.0 ± 0.48) $\times 10^{-13}$

5.3.1 Measuring the Wicking Parameters

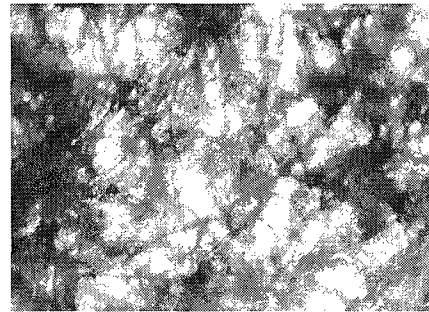
To compare the experimental results of wicking into wipes with the theoretical predictions, we need to measure some parameters used in the relations derived in previous sections. These parameters are: porosity of wipes (ε), permeabilities of the testing system (K) which includes the permeability of wipes (K_w) and that of the fritted glass (K_p), hydraulic pore radius of the testing system (R_h), capillary pore radius of wipes (R_c), surface tension of the liquids (γ), dynamic contact angle (θ), and suction pressure parameter (Γ). The experimental techniques for the testing materials and the results obtained are described briefly in this section.



a) Micrograph for wipe A



b) Micrograph for wipe B



c) Micrograph for wipe C

Figure 5.3 Micrography of the structure of the wipes

5.3.1.1 Micrography

Micrographs of the wipes were prepared to study the microstructure visually (Figure 5.3). Micrography was also used to study changes in the wipe microstructure with the wetting of wipes. It was seen that the microstructure of wipe C shrinks more than the other wipes during wetting. It was also observed that the rate of change of the micro-structure due to wetting was quite high in wipe C (a few seconds to reach the equilibrium) in comparison to wipes A and B (a few minutes to reach the equilibrium).

5.3.1.2 Porosity

The mean porosity ε of wipes is defined as the ratio of liquid occupied pore volume to the total bulk volume. If Q_{sat} is the volume of liquid absorbed by a

porous medium to saturate itself and Q_{tot} is its total volume in the dry state, then the porosity ε is given by

$$\varepsilon = \frac{Q_{sat}}{Q_{tot}} \quad (5.23)$$

Using dimensions shown in Figure 5.1, the final expression for porosity is

$$\varepsilon = \frac{Q_{sat}}{\pi R_w^2 L_w} \quad (5.24)$$

5.3.1.3 Permeability

We will now measure the permeability of system employed in the setup shown in Figure 5.4. We will impose a pressure on the wipe stack and measure the volume rate of the fluid passing through the wipes for such conditions. Here we will employ a well known method called the falling-head permeameter [3] to estimate the permeability. Assuming the system (wipes + fritted glass) to be fully saturated, we can employ Darcy's law to get

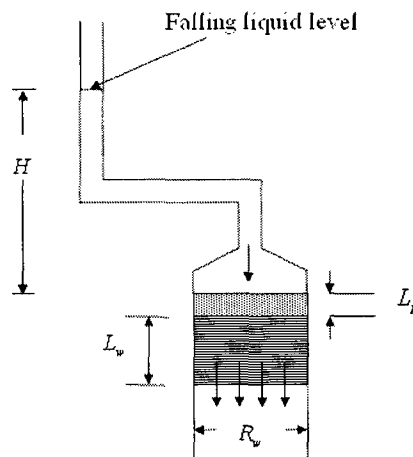


Figure 5.4 A schematic of the test-setup for measuring the permeability and hydraulic pore-radius of the hybrid system consisting of the fritted glass plate and stack of wipes

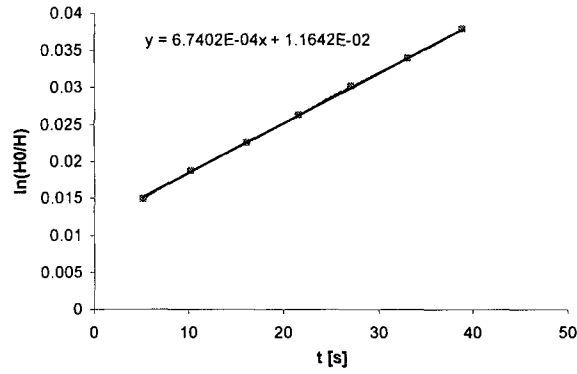


Figure 5.5 The fitted trend-line for the estimation of the permeability in wipe C.

$$V = \frac{K}{\mu} \frac{P}{(L_p + L_w)} \quad (5.25)$$

in which $P = p_h = \rho g H$ and K is the hybrid permeability of the system. The Darcy's velocity can be also be related to the falling liquid level (Figure 5.4) as

$$V = \frac{\pi R_b^2 \frac{dH}{dt}}{\pi R_w^2} \quad (5.26)$$

Combination of the above two relations results in

$$\frac{dH}{H} = \frac{K R_w^2 \rho g}{\mu (L_w + L_p) R_b^2} dt \quad (5.27)$$

On integrating Eq. (5.27) and using the initial condition $H(t=0) = H_0$, WE get

$$\ln \frac{H_0}{H} = \frac{K \rho g R_w^2}{\mu (L_w + L_p) R_b^2} t \quad (5.28)$$

In a plot of $\ln\left(\frac{H_0}{H}\right)$ versus time t , the slope of the trend line is equal to $\frac{K \rho g R_w^2}{\mu (L_w + L_p) R_b^2}$.

Since all the other parameters in the slope are known, the permeability K can be estimated. For our experiments, each test was repeated four times to make sure that the slope of the line had a repeatable value. A sample trend line and its slope are presented in Figure 5.5, and the test results for various wipes are given

in Table 5.2. The permeability measured was for the hybrid system consisting of the wipes and fritted glass. The method for estimating the permeability of the hybrid system is derived in detail in Appendix B.

5.3.1.4 Hydraulic pore radius

To measure the equivalent hydraulic pore-radius of the wipes + fritted glass system, we assume the hybrid system to consist of vertically aligned capillary tubes that are fully saturated. Based on Eq. (5.1), the fluid flow within wipes in the test setup shown in Figure 5.4 can be written as

$$\frac{P_{up}}{\rho g} + h_{up} = \frac{P_{down}}{\rho g} + h_{down} + h_L \quad (5.29)$$

Noting that $h_{up} - h_{down} = L_p + L_w$, $P_{up} = P_h = \rho g H$, and $P_{down} = 0$, this equation can be simplified to

$$H = h_L - (L_p + L_w) \quad (5.30)$$

To estimate h_L in Eq. (5.30), once again we assume the flow to be laminar in the assumed homogenous capillary tubes and use the Darcy-Weisbach relation [2]:

$$h_L = f \frac{L_p + L_w}{D_h} \frac{u^2}{2g} \quad (5.31)$$

Here u is the average liquid velocity within the capillary tubes that can be estimated through the mass conservation law (i.e., the flow rate is related to the rate of depletion of liquid column in the burette):

$$u = \frac{-\pi R_b^2 \frac{dH}{dt}}{\varepsilon \pi R_w^2} \quad (5.32)$$

Substituting Eq. (5.32) in Eq. (5.31) and using the definition of friction factor f for laminar flow in the tubes to be $f = 64/\text{Re}$ with $\text{Re} = \rho u D_h / \mu$, we get following relation for the head loss within the porous medium.

$$h_L = -\frac{32\mu R_b^2(L_p + L_w)}{\rho g \varepsilon R_w^2 D_h^2} \frac{dH}{dt} \quad (5.33)$$

Substitution of Eq. (5.33) in Eq. (5.30), and the subsequent separation of variables leads to

$$\frac{dH}{H + L_p + L_w} = -\frac{\rho g \varepsilon R_h^2 R_w^2}{8\mu(L_w + L_p)R_b^2} dt \quad (5.34)$$

Integration of Eq. (5.34) and use of the initial condition $H(t=0) = H_0$ gives the final form of the equation as

$$\ln \frac{H_0 + L_p + L_w}{H + L_p + L_w} = \frac{\varepsilon R_h^2 R_w^2 \rho g}{8\mu(L_w + L_p)R_b^2} t \quad (5.35)$$

So in a plot of $\ln\left(\frac{H_0 + L_p + L_w}{H + L_p + L_w}\right)$ versus time t , the slope of the fitted line is equal to $\frac{\varepsilon R_h^2 R_w^2 \rho g}{8\mu(L_w + L_p)R_b^2}$. Since all the other parameters in the slope are known through

independent measurements, the hydraulic pore radius R_h can be found. The test results are given in Table 5.2.

5.3.1.5 Capillary Pore Radius

To find a relation between the capillary and hydraulic pore radii, we used the definition of hydraulic radius as the ratio of net liquid volume inside capillary tubes to the wetted surface area of the tubes to formulate the expression for R_h as

$$R_h = \frac{N\pi R_c^2 h_f}{2N\pi R_c h_f} \quad (5.36)$$

where R_c is capillary pore radius and N is number of longitudinal capillaries passing through the porous medium. Eq. (5.36) reduces to the following relation for estimating the capillary pore radius R_c .

$$R_c = 2R_h \quad (5.37)$$

In the tests, enough layers of wipes were stacked in the cylinder to enable me to measure the saturation height. Since the capillary pore radius is also related to the compression ratio¹⁰ of the wiping material, we measured the density of wipes (i.e. number of the wipe layers in a unit length) in the cylinder during the test to maintain the same porosity and pore radius. To adjust the volume of the wipes to reach a desired wipe density, we used a special piston to compress them within the cylinder. The piston itself had a lot of pores in it, so the air could not be trapped under the piston as it was compressing the wipes.

5.3.1.6 Contact Angle and Surface Tension

The standard Wilhelmy plate method was used in a Dynamic Contact-angle Analyzer (DCA) to measure the surface tension of the testing liquid. The DCA was also used to measure the dynamic contact angles of the wipes and liquid system using the standard Wilhelmy plate method with a piece of flat rectangular paper replacing the metal plate. (To prevent the effect of absorption on the measuring angle, the testing sample was put into the liquid and allowed to

¹⁰ In compressible materials, the compression ratio is the ratio of their current volume under an external pressure to their initial volume under zero external pressure.

become fully saturated before the measuring of the contact angle.) The measured surface tension and contact angle are given in Tables 5.1 and 5.3.

Table 5.3 Contact angles of the wipe-liquid systems (with the 95% confidence interval range [6])

Type of liquid	Distilled water	Windex
Wipe A	55.9 ± 1.26	0
Wipe B	41 ± 0.71	0
Wipe C	$51. \pm 0.39$	0

5.3.1.7 Suction Pressure Parameter Γ

According to the newly proposed expression for the suction pressure as presented in Appendix A, the suction pressure parameter Γ is defined as the ratio of volume of particles/fibers in a porous medium to their wetted area (Eq. A-4). If we approximate the three-dimensional pore structure in paper as something generated by extruding a two dimensional micrograph along the vertical direction, this parameter can be equated to the ratio of the particle cross-sectional area to its perimeter. Thus we can use the micrographs of wipes given in Figure 5.3 to estimate the value of Γ for each wipe after measuring the cross-sectional area and perimeter of solid portions of the micrographs. Note that if we assume the porous medium to be a fibrous material, the value of Γ would be equal to fiber radius. Therefore one of the effective ways of estimating Γ is to measure the average radius of fibers in the micrographs.

5.3.2 Measuring the Wicking Rate under Hydrodynamic Pressure

As we have mentioned before, the capillary pore radius is related to the compression ratio of wiping material, so to get accurate results we measured the density of each stack of wipes in the cylinder to make sure it is constant in all the tests for each of the wipes¹¹. To adjust the volume of the wipes, a special piston was used to compress the stack of wipe layers within the cylinder (see Figure 5.1) to a desired height. At the start of each experiment, we have been saturating the fritted glass while the stacks of wipes were kept a few millimeters above the fritted glass. During the procedure, the end of the burette was closed to prevent the fluid from moving down. As the stack of wipes touch the fritted glass, the burette was opened to let the liquid move down the tube. A camcorder was used to record the height of liquid within the burette; the video film was reviewed later to extract the absorption rate into the wipes.

To make sure that our measurements were reliable, each test was repeated at least three times. We also did a scatter-estimation test on the wipe C to estimate the repeatability of the test results. Figure 5.6 shows the results of scatter-estimation tests on wipe C with Windex; the measured 95% confidence intervals are shown with the help of the scatter bars. (This interval is a range of the measured quantity in which the measured value is expected to fall 95% of the times [6].) The small bars (especially till $t = 6$ sec) mean that our experiments

¹¹ Since the number of layers was high, we weighed the stack of wipes to make sure that we were using the same number of layers in different experiments with the same wipe. The precision of the microbalance used was 0.01 g which was less than the weight of a single layer. (The weight of layers for the test materials A, B, and C were 1.37 g, 2 g, and 1.37 g, respectively.) Using this method and such a microbalance, we ensured that the number of layers remained constant from test to test.

were very repeatable. We are confident that all experiments listed in this paper show similar repeatability patterns. To get a good confidence level, it was necessary to avoid trapping of bubble under the fritted glass as the bubbles provide additional resistance to fluid moving upwards.

Similarly tests to measure wicking parameters (Tables 5.2 and 5.3) were often conducted multiple times to obtain more than one measured values. The scatter in the property values thus obtained was once again quantified through the use of the 95% confidence interval.

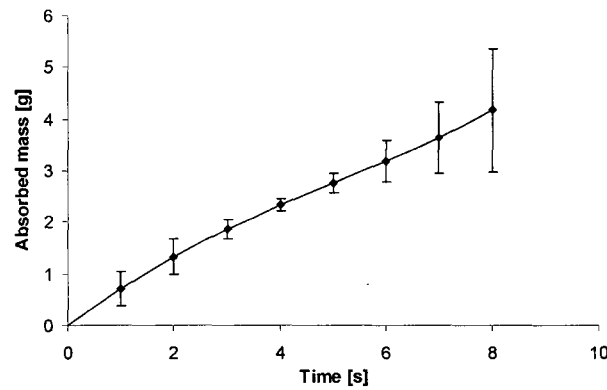


Figure 5.6 A scatter estimation on the wipe C with Windex experiment with scatter bars showing confidence interval of 95%

5.4 Results and Discussions

Since we had an explicit relation for time in terms of the liquid front position in Eqs. (5.11) and (5.20), we gave different values of the liquid-front position h_f from zero to L_w , and then calculated the corresponding time for each position using the mentioned equations. The position h_f was then converted into the liquid mass absorbed into the wipes through the relation

$$m = \varepsilon_w \rho \pi R_w^2 (h_f - L_p) \quad (5.38)$$

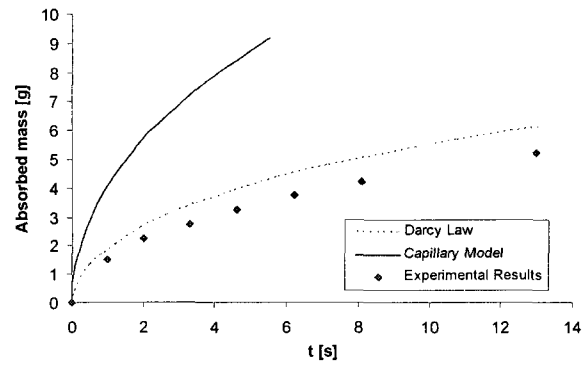
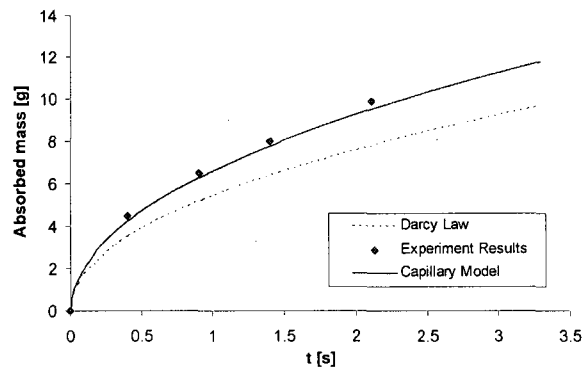
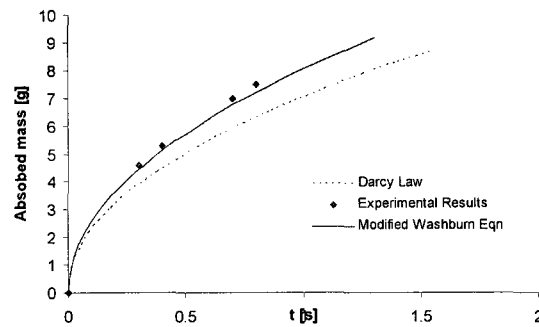
a) $p_h = 0 \text{ pa}$ b) $p_h \approx 2683 \text{ pa}$ ($H = 29 \text{ Cm}$)c) $p_h \approx 4758 \text{ pa}$ ($H = 49 \text{ Cm}$)

Figure 5.7 Wicking rate in wipe A when water was used under three different externally-imposed liquid pressures.

As seen in Figure 5.7, the experimental and capillary model results are not close when the externally imposed liquid pressure is zero (Figure 5.7a). But as the externally imposed liquid pressure increases, the theoretical predictions obtained from the capillary model grow closer to the experimental measurements (Figures

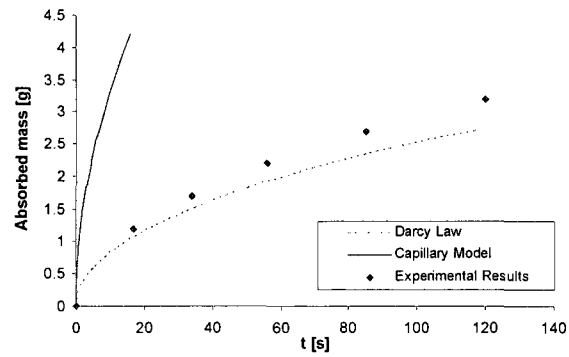
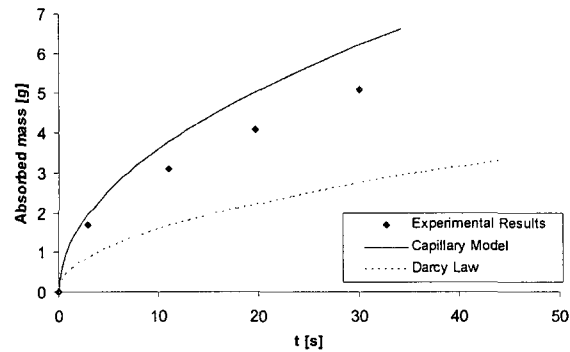
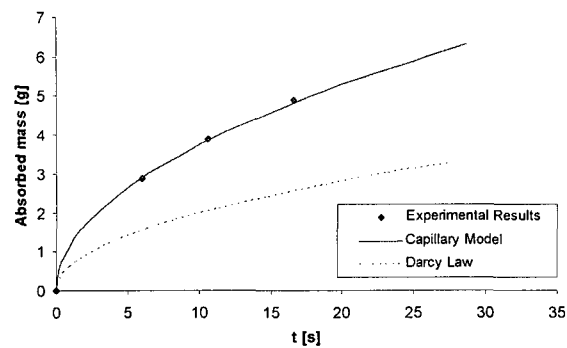
a) $p_h = 0 \text{ pa}$ b) $p_h = 2683 \text{ pa}$ ($H = 29 \text{ Cm}$)c) $p_h = 4758 \text{ pa}$ ($H = 49 \text{ Cm}$)

Figure 5.8 Wicking rate in wipe B when water was used under three different externally-imposed liquid pressures.

5.7b and 5.7c). As for the Darcy law results, it has the opposite effect, i.e., there is an excellent prediction when the external pressure is zero. However, there is an increasing deviation from experiments with a rise in the external pressure.

One possible reason for this progressive improvement of results for the capillary model is our method of measuring the hydraulic pore-radius. We measured this parameter while the materials were under the externally imposed liquid-pressure and as the imposed pressure compresses the material, the obtained parameters (permeability and hydraulic pore radius) are valid for the externally imposed liquid pressures equal to or close to the measuring pressure¹². So we expect that as the difference between the measuring pressure¹³ and testing pressure¹⁴ increases, the difference between the theoretical predictions and the experiment results would increase as well. This difference is more significant for those type materials that are more compressible or those that swell more as they get wet. This fact can explain why we have better theoretical results when an external liquid pressure is imposed during wicking.

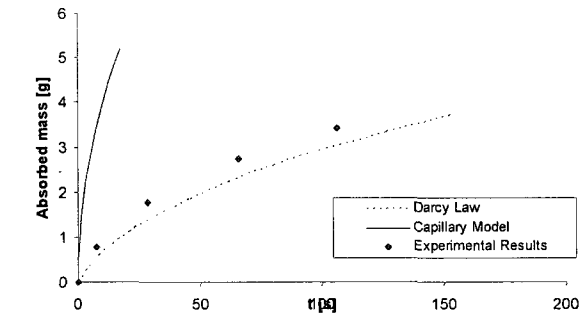
In Figure 5.8, we have used another type of paper towel with its compressibility lower than that of type A. As we can see in Figure 5.8a, theoretical results predicted using the capillary model for the case of pure wicking (no externally imposed liquid pressure) are way off the target once again, in fact more than the one seen for wipe A in Figure 5.7. So one might surmise that as the compressibility of wipes decreases, the accuracy of the capillary model predictions deteriorates for the pure wicking case. Theoretical predictions by the Darcy's law model are good as before for this case. However tables are turned as the external pressure is increased: performance of the capillary model

¹² Note, we are dealing with compressible materials, so the externally imposed liquid-pressure compresses them and changes their wicking parameters.

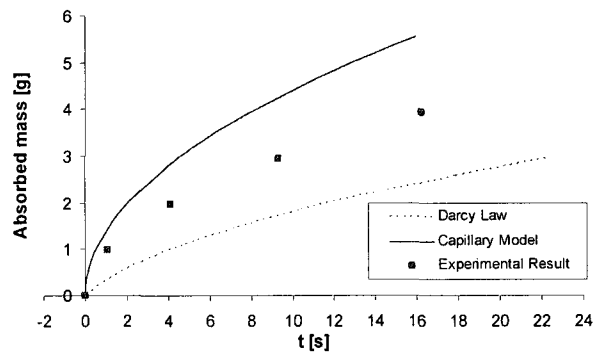
¹³ The externally imposed liquid-pressure at which the wicking parameters were measured

¹⁴ The externally imposed liquid-pressure under which the wicking rate is being measured

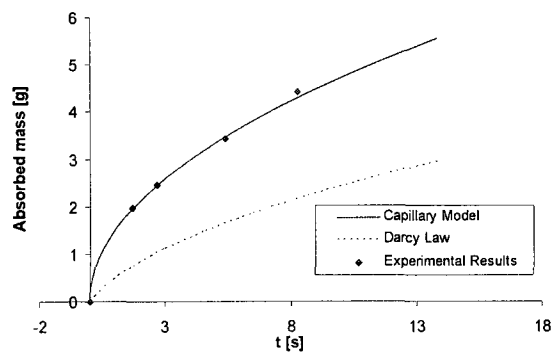
improves while predictions of the Darcy's-law based model deteriorate. In fact the former gives a very accurate prediction in part (C) of Figure 5.8, while the latter under-predicts the absorbed mass.



a) $p_h = 0 \text{ pa}$



b) $p_h = 2683 \text{ pa}$ ($H = 29 \text{ Cm}$)



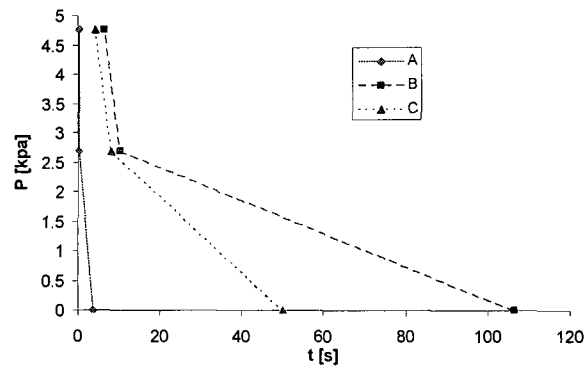
c) $p_h = 4758 \text{ pa}$ ($H = 49 \text{ Cm}$)

Figure 5.9 Wicking rate in wipe C when Windex was used under three different externally-imposed liquid pressures.

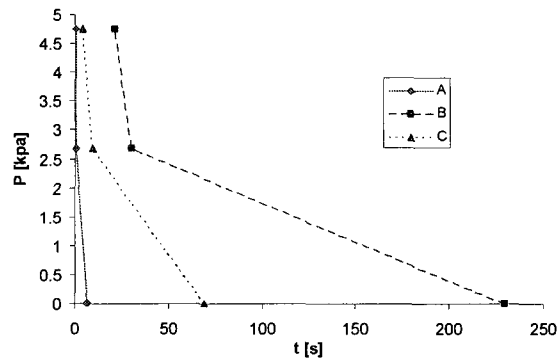
Figure 5.9 shows the results obtained for wipe C, a table napkin. In addition to having a higher compressibility, the napkins also swelled faster than the paper towel as they got wet. Again we can see a very large difference between the capillary model predictions and the experiment for the zero imposed pressure or pure wicking case (Figure 5.9a). Once again Darcy law predictions are quite accurate. However as the external pressure increases, predictions of the capillary model improve and approach the experimental results (Figures 5.9b and 5.9c); Darcy's law model predictions deteriorate as before.

It is clear from Figures 5.7, 5.8 and 5.9 that for wicking (of both the free and pressurized types) in swelling materials such as paper napkins and towels, the capillary and Darcy's law based models fail to perform consistently over the whole range of imposed pressures. For the lower imposed pressures, the Darcy's law based models perform better whereas for the higher imposed pressures, the capillary model are more accurate. This is in contrast to their sterling behavior in predicting wicking accurately in rigid polymer wicks [3,7]. The reason could lie in the fact that the measurement of certain wicking parameters (such as the hydraulic pore-radius, the wicking parameter M , and the permeability) may be affected by swelling of the cellulose-based porous medium. Experiments have shown that swelling of cellulose has a time-scale that matches the time-scale of the wicking process, so some wicking parameters in such materials might be a function of time and the location of liquid front in addition to other usual factors. As a result, the conventional methods for measuring wicking parameters, which rely on establishing steady-state conditions in porous media before the start of

measurement, may not be valid for swelling materials. In other words, the measured wicking parameters are expected to be reliable only when they are used at liquid pressures that are close to the imposed pressure used during the measurement.



a) Testing liquid is water



b) Testing liquid is Windex

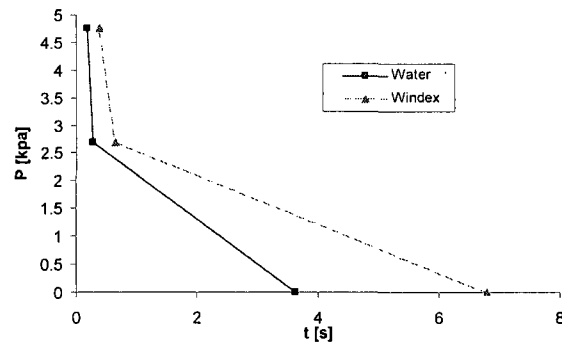
Figure 5.10 The effect of externally imposed liquid pressure on the absorption time for wiper A, B and C when the three wiper absorbed the same volume of liquid

Saturation time, which could be defined as the time needed for a liquid to make the stack of wiper fully wet or saturated, was measured next. Such a time could be measured from the recorded video films of the aforementioned wicking experiments. However since the volumes of liquid needed to make wiper fully wet were different for the three wiper, we defined a special fixed volume (which

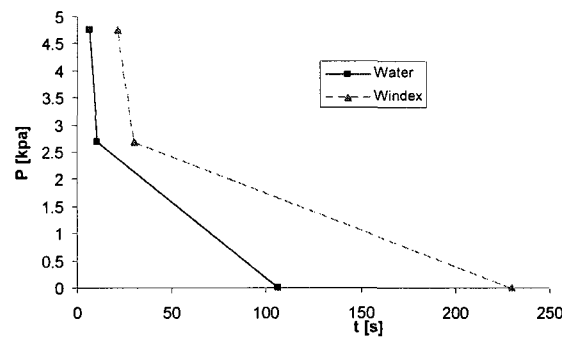
was less than the saturation volume for the least absorbent type of the testing wipes) to compare the absorption time. So, the time needed for each wipe to absorb a defined volume of selected liquids were measured and compared together to see how the hydrodynamic pressure may affect the absorption time in each of the tested wipes. (Note that since our theoretical approaches did not predict the experimental results consistently well, we have used only the experimentally measured saturation-times of the three tested wipes.) The effect of the externally imposed liquid-pressure on the absorption time for the three tested wipes is shown in Figure 5.10. It shows that as the imposed pressure increases, the effect of the capillary pressure grows less important in comparison to the imposed pressure; this is why we can see a convergence of the lines in Figure 5.10 with an increase in the imposed pressure. The pattern is repeated in both Figures 5.10a and 5.10b although the absorption time for Windex is more than that for the water. The changing of the test liquid merely changes the speed of absorption, but leaves the pattern of liquid absorption unchanged. Of course, some physical or chemical properties of the liquids (such as the polarity or chemical reactivity) and the solid-liquid interactions are different in the two cases, which consequently lead to minor differences in the absorption pattern. It might be the cause of a slight difference seen between Figures 5.10a and 5.10b.

In Figure 5.11, the change in the absorption times for each wipe are presented for the two test-liquids separately to show the effect of changing liquid properties on the absorption rate. The pattern of the liquid absorption is similar for both the liquids in wipes A and B (Figures 5.11a and 5.11b) while there is a

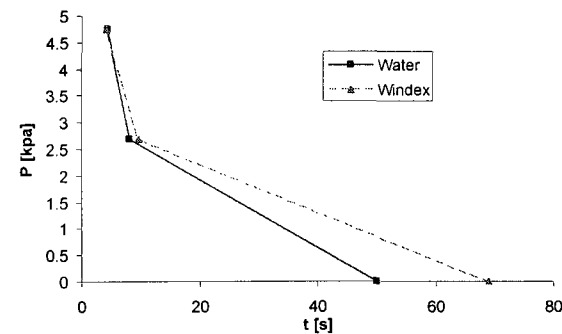
difference for wipe C (Figure 5.11c). It shows that when the liquid was switched in wipes A and B, the structural interaction between the new liquid and wipe



a) Wipe A



b) Wipe B



c) Wipe C

Figure 5.11 The effect of externally-imposed liquid pressure on the absorption times for wipes A, B and C when the three wipes absorbed the same volume of liquid

matrix was less than that in wipes B and C. All of the plots in Figures 5.10 and 5.11 show that as the externally imposed liquid-pressure increases, it enhances the absorption rate. But the effect of increasing the imposed pressure from zero to 2683 kPa is much higher than the effect of increasing it from 2683 kPa to 4758 kPa. For example, in wipe A with water, when the imposed pressure increases from zero to 2683 kPa, the saturation time decrease from 3.63 to 0.27 seconds, which means a decrease of 93 percents. On the other hand, increasing the imposed pressure from 2683 kPa to 4758 kPa (77 percent increase) decreases the saturation time from 0.27 to 0.19 seconds, which is merely 2.2 percent of its initial saturation time of 3.63 seconds. This important result shows that as the externally imposed liquid pressure increases, its relative effect on the absorption rate (or the wicking rate) decreases.

To consolidate the above argument, two non-dimensional parameters of 'relative pressure' and 'relative absorption time' are proposed:

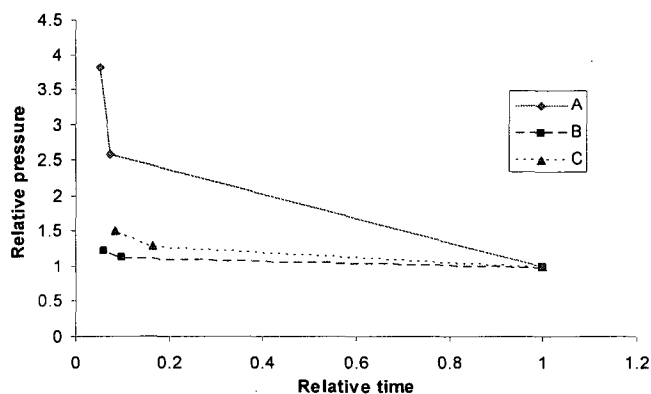
$$P_{re} = \frac{P_c + P_h}{P_c} \quad (5.39a)$$

$$T_{re} = \frac{\text{time of saturation when } P = P_c + P_h}{\text{time of saturation when } P = P_c} \quad (5.39b)$$

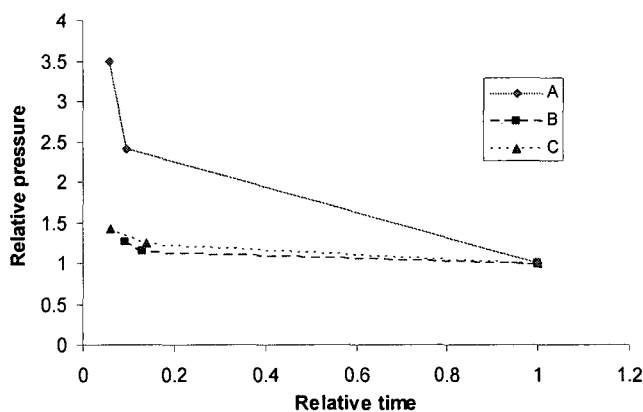
Figure 5.12 shows our previous point about the effect of the externally imposed liquid pressure. It shows that as the relative pressure P_{re} increases, the change in the relative time T_{re} decreases. This effect is more significant in wipes B and C than wipe A. In other words, both Figures 5.11 and 5.12 show that as the imposed pressure increases, its ability to decrease the absorption time decreases. A speculative explanation of this phenomenon can be attempted as

follows. When an externally applied liquid-pressure is imposed on the wiper, it compresses them and reduces their pore sizes, which in turn lead to two effects:

1) increase in the capillary suction pressure, 2) decrease in the permeability (or



a) Testing liquid is water



b) Testing liquid is Windex

Figure 5.12 The effect of externally-imposed liquid pressure on the absorption time when absorbing a fixed volume of liquid (using the non-dimensional pressure and time for wiper A, B and C)

increase in flow resistance) of wiper. During the first increase in P_{re} perhaps the first effect is dominant, and as a result, increase in the applied pressure as well as the capillary pressure provide higher motive force to the wicking liquid and thus cause the saturation times to decrease. During the second increase in P_{re}

perhaps the second effect is dominant, and the increase in the motive force due to an increased capillary pressure is cancelled by an increase in flow resistance, and as a result, the saturation time does not decrease as much.

In conclusion, we would like to mention that some wicking tests were also conducted with a special 'microfiber' wipes that were characterized by the presence of microscopic apertures to enhance wicking. However significant scatter in the absorbed-mass-vs-time plots were observed for this wipe. It was postulated that presence of microscopic apertures rendered the wipe microstructure a dual-scale porous medium (i.e. large lengths-scale apertures coexisting with much smaller length-scale pores); so if the apertures aligned during the stacking of wipes, wicking behavior was completely different from when the apertures were not aligned. As a result, it was felt by the authors that more study is needed to develop a reasonable theoretical model for wicking in such dual-scale wipes, and such an effort will be undertaken in future.

5.5 Summary and Conclusion

Wicking of liquid under externally imposed liquid pressure into three cellulose wipes is studied experimentally and theoretically. The wicking and wetting parameters of testing wipes were measured to enable a comparison between theoretical predictions and experimental results. Wicking models based on Darcy law and aligned capillary tubes were developed as our theoretical models. A new formula for prediction of suction pressure is presented, which is based on the ratio of mean values of volume and wetted surface-area of particles in the porous

medium. It was seen that the predictions of the capillary model and Darcy law based models were not consistent over the whole range of the externally applied liquid pressure during wicking: the capillary model was accurate at higher applied pressures while the Darcy law based model was better at zero pressure (pure wicking) situations. The cause of this inconsistency may be that the wicking parameters may be affected by the applied pressure in compressible wipes as well as change during the wetting of cellulose-based paper wipes. It also was seen that as the applied pressure increases, its relative effect on the absorption rate of saturation time decreases.

References

1. PK Chattered and BS Gupta .Absorbent Technology. Amsterdam. Elsevier. 2002
2. Y. A, Cengel and J. M. Cimbala .Fluid Mechanics Fundamentals and Applications. McGraw-Hill, 2006:329-331
3. R Masoodi, K M Pillai and P Varanasi. Darcy's Law based Models for Liquid Absorption in Polymer Wicks. J. AIChE. 2007; 53(11): 2769-2782
4. KM Pillai and SG Advani .Wicking Across a Fiber-Bank. J. Colloid and Interface Sci. 1996; 183: 100-110
5. Williams JG, Morris CM and Ennis BC .Polym. Eng. Sci. 1979;14(6): 413-419
6. Anthony J Wheeler, Ahmad R Ganji .Introduction to Engineering Experimentation. Prentice Hall, 1996
7. R Masoodi, K M Pillai and P Varanasi. Role of Hydraulic and Capillary Radii in Improving the Effectiveness of Capillary Model in Wicking. ASME Summer Conference, Jacksonville FL, USA, August 10-14, 2008.

Chapter 6

DARCY'S LAW BASED MODEL FOR WICKING IN PAPER-LIKE SWELLING POROUS MEDIA

6.1 Introduction

Wicking is the spontaneous absorption of a liquid into a porous medium by the action of capillary pressure. An example of wicking is the imbibition of liquids by towels, paper towels, table napkins, wipes, and sponges. Another important example is that of wicking in commercial wicks used by consumer product companies to dispense volatile substances into the air such as room fresheners or insect repellents.

Capillary pressure during wicking occurs as a result of capillary suction, which is created on the walls of the porous media at the interface of wet and dry matrix [1,2]. These forces originate from the mutual attraction of the molecules in the liquid medium and the adhesion of liquid molecules to those in the solid medium [3]; the wicking phenomenon occurs when the adhesion is greater than the mutual attraction. Wicking is the main cause of absorption in the porous materials, although there may be other factors causing absorbency [4].

Wicking performance is an important issue in several industries that deal with liquid-absorbing porous media, including the pulp and paper industry. The most common example is the paper towel, in which water absorption and

retention is the primary goal [1]. There are two traditional models for studying the wicking phenomenon mathematically: 1) The older method uses the Washburn (or Lucas-Washburn) equation [5,6], where the porous medium is assumed to be a bundle of aligned capillary tubes of the same radii; Lately a newer version of this equation has been developed after inclusion of the gravity term [7]. 2) In recent years, a new approach based on Darcy's law has been successfully used to model wicking in porous media such as a sintered polymer wick [8] or bank of fibers [9]. (Darcy' law, a simple formula that relates the average velocity of a liquid to the pressure gradient within a porous medium, was first discovered by Henri Darcy in 1857 [10].)

Wicking is a function of the micro- and macro-structure of porous media, the characteristics of liquid, and a function of time [8]. The general relation between the wicking rate, wicking time, and liquid characteristics is clearly described in the aforementioned conventional wicking models. The relation between the wicking rate and structure of a porous medium is the most challenging, since the structure of porous media show great variations [11]. Several researchers studied the relationship between the wicking rate and the porous medium structure in fibrous materials by analyzing the wicking rates along the fibers [12-14] and across the fibers [9, 15, 16]. Recently, the wicking enhancement in multi-ply paper structure was investigated experimentally [17], where it was shown that this enhancement is most noticeable in the beginning of the wicking process and diminishes gradually. Although several researchers

have tried to find a theoretical equation relating the wicking rate to the microstructure of a porous medium, it still remains a poorly understood problem.

Fiber swelling is an important phenomenon that affects wicking in paper [18], as it is one of the swelling mechanisms that occur during water-fiber interaction in all bio-fiber and plant-based materials such as paper and pulp. Since swelling changes the structure and molecular arrangement of materials, it affects both the wettability and 'wickability' of the porous media [19]. In fact, the swellability of fibers is an important and useful property of paper for the paper industry—the swelling leads to liquid absorption in the paper matrix, which in turn leads to liquid retention inside the porous paper. In paper industry, this liquid holding capacity, which is related to the moisture content after a paper sheet dries, is called Water Retention Value [20].

The swelling effect leads to error if the conventional wicking models such as Washburn equation are employed to predict the wicking rate in swelling porous media [21]. Schuchardt and Berg [22] studied the swelling phenomenon experimentally and modified the Washburn equation for application in some swelling materials. This model, built on the assumption that pore radii in a swelling porous medium decrease linearly with time, compares better with the experimental data than the conventional Washburn model.

In this Chapter, we present a new model based on Darcy's law to predict wicking rates in swelling porous media. Using the volume averaging method, the continuity equation for single-phase flow in swelling porous media is modified to include 1) a sink term, which is related to liquid absorption by dry particles; and

2) a source term, which is related to the rate of change of porosity. We also investigate the dependence of permeability upon porosity, expressed through several permeability models, including the Kozeny-Carman model.

The advantage of using Darcy's law to predict wicking rates compared with the Washburn equation is that Darcy's law provides a modern approach that can be extended into modeling two- or three-dimensional wicking flows [23], while the Washburn equation is limited to one-dimensional wicking due to its origin from the laminar-flow model along a bundle of capillary tubes. By combining the general form of Darcy's law and the continuity equation, any two- or three-dimensional flow in porous media can be modeled. Based on such an approach, the PORE-FLOW[®], a novel, finite-element based numerical simulation, was developed to predict the wicking flow in the three-dimensional and complex geometries [23]. The inclusion of swelling effect in Darcy's-law based model, as proposed in this paper, has the added benefit of easy implementation in such flow-modeling codes, based on Darcy's law and the continuity equation, to study three-dimensional wicking in swelling porous materials.

6.2 Theoretical Details

6.2.1 Wicking in Rigid Porous Media

In rigid porous media, the sizes of the constituent particles and the pores between them remain constant during the wicking process. The two conventional theories for wicking in rigid porous media, one based on the Washburn equation

(also known as the Lucas-Washburn equation) and the other based on Darcy's law, are explained below.

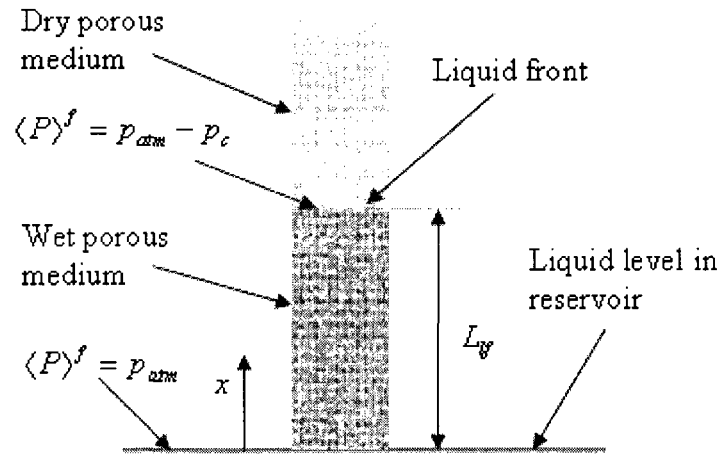


Figure 6.1 A schematic of the wicking setup and the wicking (or liquid-front) height in a porous wick.

6.2.1.1 Washburn Equation

If a porous medium is assumed to consist of a bundle of parallel capillary tubes of the same size, the governing equation for wicking flow, after assuming the Hagen-Poiseuille flow of liquids through such tubes and neglecting the effect of gravity [7], is Washburn equation:

$$L_{wf} = \sqrt{\frac{\gamma D_e \cos(\theta)}{4\mu} t} \quad (6.1)$$

where L_{wf} is the height of the rising liquid-front within the porous medium (see Figure 6.1), μ is the liquid viscosity, γ is the liquid surface tension, θ is contact angle, t is time, and D_e , the effective pore diameter, is obtained through

$$D_e = \frac{D_h^2}{D_c} \quad (6.2)$$

where D_c is capillary pore diameter, and D_h is hydraulic pore diameter. If the capillary and hydraulic diameters are equal, i.e., $D_e = D_h = D_c$, the height of the wicking front changes to

$$L_{yf} = \sqrt{\frac{\gamma D_c \cos(\theta)}{4\mu}} t \quad (6.3)$$

6.2.1.2 Darcy's Law

The single-phase flow of a Newtonian liquid in an isotropic and rigid porous medium is governed by Darcy's law and continuity equation. We have shown in Chapter 2 that in the case of a one-dimensional flow after neglecting the effect of gravity, the use of Eqs (2.8) and (2.9) leads to an equation for liquid-front location in the form of

$$L_{yf} = \sqrt{\frac{2K p_c}{\varepsilon_f \mu}} t^2 \quad (6.4)$$

where ε_f , the porosity of the porous medium, is defined as the ratio of pore volume to the total volume. p_c is the capillary pressure obtained through the well-known Young-Laplace equation.

6.2.2 Wicking in Non-Rigid, Swelling Porous Media

In order to use the above models in swelling porous media, some modification is necessary since the pore radius, porosity, and permeability change during the course of swelling. In fact, these parameters are functions of both time and space in swelling porous media during wicking. The next section describes two

approaches to modify the previous wicking models for application to swelling porous media.

6.2.2.1 Washburn Equation

Schuchardt and Berg [22] assumed the pore radius in the wetted area of the considered porous medium (a composite of cellulose and superabsorbent fibers) will decrease linearly with time as a result of swelling. They used this assumption to modify the Washburn equation and proposed the relation for the wicking rate as

$$L_{if} = \sqrt{\frac{\gamma R_0 \cos(\theta)}{2\mu}} \left[t - \frac{a}{R_0} t^2 + \frac{a^2}{3R_0^2} t^3 \right]^{1/2} \quad (6.5)$$

while using a decreasing hydraulic radius $R_h = R_0 - at$ behind the flow front due to swelling of fibers constituting the porous medium. In this formulation R_h is hydraulic pore radius, R_0 is the initial value of R_h , and a is a constant representing the swelling effect. The details of derivation are presented in Appendix C. Note that upon neglecting the swelling effect (i.e., $a = 0$), Eq (6.5) turns to Eq (6.3), which is the original Washburn equation for rigid porous media.

6.2.2.2 Darcy's Law

For a swelling porous medium, the continuity equation modifies to the form

$$\vec{\nabla} \cdot \langle \vec{V} \rangle = -S - \frac{\partial \varepsilon_f}{\partial t} \quad (6.6)$$

using the volume averaging method. (See Appendix B for details of the derivation.) Note that a negative term on the right causes the liquid to 'disappear' from the interconnected pore-space available for the traveling liquid, while a positive term 'creates' liquid in the same space. The first sink term, $-S$, is created due to the absorption of liquid by the solid matrix. Since the porosity ε_f decreases in a swelling porous medium, the $\partial\varepsilon_f/\partial t$ term is $-ve$; thus, the second term on the right is actually a $+ve$ source term.

If we consider the wicking flow to be one-dimensional, the governing equations (Darcy's law and the modified continuity equation) simplify to

$$\langle u \rangle = -\frac{K}{\mu} \frac{d\langle p \rangle^f}{dx} \quad (6.7)$$

$$\frac{d\langle u \rangle}{dx} = -S - \frac{\partial\varepsilon_f}{\partial t} \quad (6.8)$$

where $\langle u \rangle$ is the volume-averaged Darcy velocity, also known as the specific discharge in the porous media literature [10]. Since S is the rate of liquid absorption by solid matrix and $\frac{d\varepsilon_s}{dt}$ is directly related to the rate of increase of

solid-matrix volume, we propose that S is proportional to $\frac{d\varepsilon_s}{dt}$ (ε_s defined as the ratio of solid volume to the total volume). In other words, we assume S to be

linearly proportional to $\frac{d\varepsilon_s}{dt}$, i.e.,

$$S = b \frac{d\varepsilon_s}{dt} \quad (6.9)$$

where $b = 0$ case signifies 'no absorption of liquid by solid matrix' and $b=1$ case indicates 'the rate of increase of solid-matrix volume is equal to the volumetric rate of liquid absorption by solid matrix'. Therefore, b , to be referred to as the *absorption coefficient*, must fall in the range $0 \leq b \leq 1$ ¹⁵. We also have the following relation between two porosities:

$$\varepsilon_s + \varepsilon_f = 1 \quad (6.10)$$

Substituting Eq (6.9) in Eq (6.8), and then using Eq (6.10) to eliminate ε_s , leads to the following relation for the continuity equation:

$$\frac{d\langle u \rangle}{dx} = (b - 1) \frac{\partial \varepsilon_f}{\partial t} \quad (6.11)$$

If we substitute Eq (6.7) in Eq (6.11), and assume the permeability and porosity to be functions of time only, then we obtain

$$\frac{d^2 \langle p \rangle^f}{dx^2} = G(t) \quad (6.12)$$

where

$$G(t) = (1 - b) \frac{\mu}{K} \frac{d\varepsilon_f}{dt} \quad (6.13)$$

Note that in general the porosity and permeability are expected to be functions of both time (t) and space (x coordinate) in swelling materials. If we consider the global values for porosity and permeability throughout the wetted porous medium, then local effects are neglected and the permeability and porosity can then be just functions of time. Neglecting the local spatial dependence in these parameters simplifies the governing equation (6.12) from a nonlinear partial

¹⁵ One can allow b to be greater than 1 if the increase in solid volume is caused by some other effect other than the migration of volume of the liquid.

differential equation to an ordinary differential equation that can be solved *analytically*. Although this assumption reduces the accuracy of our wicking predictions, the resultant simplification in the wicking model makes it worthwhile to neglect the local effects. After neglecting the effect of gravity with $\rho g L_{lf} \ll p_c$, the boundary conditions for Eq. (6.12) (Figure 6.1) can be deduced to be

$$\langle p \rangle^f (x = 0) = p_{atm} \quad (6.14a)$$

$$\langle p \rangle^f (x = L_{lf}) = p_{atm} - p_c \quad (6.14b)$$

After integrating Eq (6.12) two times and applying the boundary conditions Eqs (6.14a) and (6.14b), the final expression for pressure reduces to

$$\langle p \rangle^f (x, t) = \frac{1}{2} G x^2 - \left(\frac{1}{2} G L_{lf} + \frac{p_c}{L_{lf}} \right) x + p_{atm} \quad (6.15)$$

The liquid-front velocity and the Darcy (filtration) velocity are related through the equation [23]

$$\frac{dL_{lf}}{dt} = \frac{\langle u \rangle}{\varepsilon_{lf}} \Big|_{x=L_{lf}} \quad (6.16)$$

where ε_{lf} is the *surface* porosity at the liquid front. If we assume the surface and bulk porosities to be identical, then, due to the swelling effect, the porosity will decrease progressively from its initial value of the surface porosity at the liquid front, i.e., $\varepsilon_{lf} = \varepsilon_{f_0} = \varepsilon_f(t=0)$. Substitution of Eq (6.7) in Eq (6.16) and considering Eq (6.15) for pressure term leads to the following differential equation

$$\frac{dL_{lf}}{dt} = G_1 L_{lf} + \frac{G_2}{L_{lf}} \quad (6.17)$$

where G_1 and G_2 are just functions of time:

$$G_1(t) = -\frac{K(t) G(t)}{2 \varepsilon_{f_0} \mu} \quad (6.18a)$$

$$G_2(t) = \frac{K(t) p_c}{\varepsilon_{f_0} \mu} \quad (6.18b)$$

Eq. (6.17) can be converted into a linear differential equation by defining y as

$$y = L_{lf}^2 \quad (6.19)$$

Using Eq (6.19), we can transform Eq (23) into a differential equation of the form

$$\frac{dy}{dt} = 2G_1 y + G_2 \quad (6.20)$$

that can be easily integrated using the initial condition $y(t = 0) = 0$. The final form of the solution is

$$y = 2e^{2\int G_1 dt} \int_0^t e^{-2\int G_1 dt'} G_2 dt' \quad (6.21)$$

Substituting G_1 , G_2 and y from Eqs (6.18a), (6.18b), (6.19), respectively, into Eq (6.21), results in

$$L_{lf} = \sqrt{2e^{2\int -\frac{KG}{2\varepsilon_{f_0}\mu} dt} \int_0^t e^{-2\int -\frac{KG}{2\varepsilon_{f_0}\mu} dt'} \frac{Kp_c}{\varepsilon_{f_0}\mu} dt'} \quad (6.22)$$

Substituting G from Eq (6.13) in Eq (6.22), and doing some algebraic operations yields the final relation for liquid front as

$$L_{lf} = \sqrt{\frac{2p_c}{\varepsilon_{f_0}\mu} e^{(b-1)\frac{\varepsilon_f}{\varepsilon_{f_0}}} \int_0^t e^{(1-b)\frac{\varepsilon_f}{\varepsilon_{f_0}}} K(t') dt'} \quad (6.23)$$

Note that for a rigid porous media with no absorption into fibers/particles ($b = 0$) and with the porosity remaining unchanged behind the liquid front ($\varepsilon_f = \varepsilon_{f_0}$), Eq

(6.23) reduces to the ordinary porous-media case of Eq (6.4). For the special case of $b = 1$ when the swelling rate matches the volumetric absorption rate, the wicking relation (6.23) simplifies to

$$L_{ij} = \sqrt{\frac{2p_c}{\varepsilon_{f_0}\mu} \int_0^t K(t') dt'} \quad (6.24)$$

Our main assumptions in deriving Eqs (6.23) and (6.24) are:

1. The absorption rate of liquid in the porous medium is linearly proportional to the rate of change of solid volume fraction.
2. The porosity and permeability are considered globally for the whole wet area; thus, they are functions of time only.
3. The effect of gravity on the wicking phenomenon is negligible.

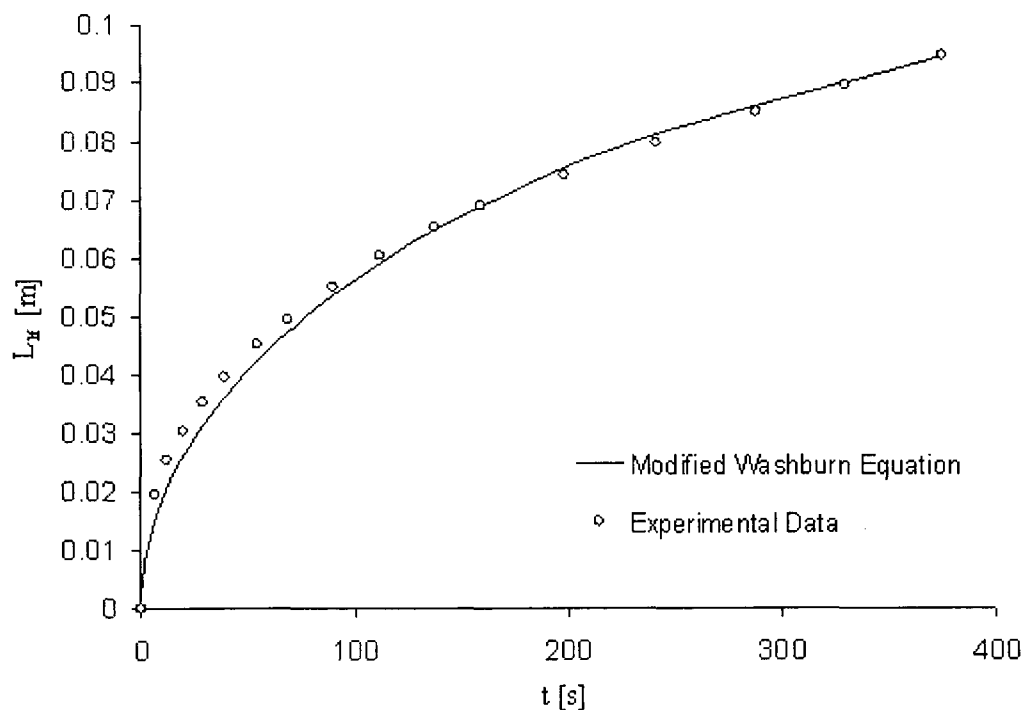


Figure 6.2 Wicking height vs. time plot for water absorption in the 13%FC CMC/Cellulose composite-paper strip [22].

6.3 Results and Discussions

6.3.1 An Experimental Study

Schuchardt and Berg [22] conducted experiments to compare the predictions of their modified Washburn model, Eq (6.5), with the experimental results. Figure 6.2 shows the experimental data and predictions of the modified Washburn equation for wicking water in a composite paper strip of 13%FC¹⁶ CMC¹⁷/Cellulose (i.e., 13% of FC consists of CMC fibers and the rest is made of cellulose fibers). Although there is a minor deviation at the beginning, the theoretical predictions match well with the experimental results as the time passes on.

Table 6.1 The characteristics of test liquid (distilled water) and the values of R_0 and a measured by Schuchardt [21].

Characteristic	Value	Unit
Viscosity of test liquid	0.000911	<i>Kg/m.s</i>
Surface tension of test liquid	0.0723	<i>N/m</i>
Pore radius reduction rate a	8.40E-10	s^{-1}
Initial pore radius R_0	8.80E-07	<i>m</i>

Schuchardt and Berg [21] used two different liquids in their wicking experiments: one that causes swelling in the composites paper during wicking, and one that does not. They compared the measured values for pore radii under swelled and non-swelled conditions at various times, and thus estimated the

¹⁶ FC (or Aquasorb FC) is a type of superabsorbent fiber made by the then Hercules Chemical Company (which may now be known DuPont).

¹⁷ CMC is an acronym for Carboxymethylcellulose.

values of R_0 and a in Eq (6.5). The characteristics of their test liquids, and the measured values of R_0 and a are listed in Table 6.1. Although the modified Washburn equation predicts well in Figure 6.2, it has some limitations—it assumes the hydraulic radius continually reduces, which means the fiber swelling must continue during the wicking time. Therefore, Schuchardt and Bergs' model works as long as the wicking time is not greater than the maximum-permitted swelling time (depending upon the void space between fibers) for individual fibers.

6.3.1.1 Changes in Porosity during Wicking

The porosity was not measured in the above-mentioned experiment. Since the pore radius and its rate of change were measured, we can derive an expression for porosity versus time, as follows. In the capillary model, the porosity is defined as

$$\varepsilon_f = n\pi R_c^2 H \quad (6.25)$$

where H is the length of the porous medium, and n is the number of assumed capillary tubes passing through a unit area of the porous medium. The capillary (pore) radius, R_c , decreases linearly with time as a result of swelling as

$$R_c = R_0 - at \quad (6.26)$$

The initial porosity ε_{f_0} can be similarly defined as

$$\varepsilon_{f_0} = n\pi R_0^2 H \quad (6.27)$$

Comparing Eqs. (6.25) and (6.27) while including Eq (6.26) leads to the following relation for porosity

$$\varepsilon_f = \varepsilon_{f_0} \left(\frac{R_0 - at}{R_0} \right)^2 \quad (6.28)$$

Figure 6.3 plots the relative porosity $\varepsilon_f / \varepsilon_{f_0}$ against time for the composite paper strip of 13%FC CMC/Cellulose using Eq (6.28); it is clear that the porosity and the rate of change of porosity decrease with time.

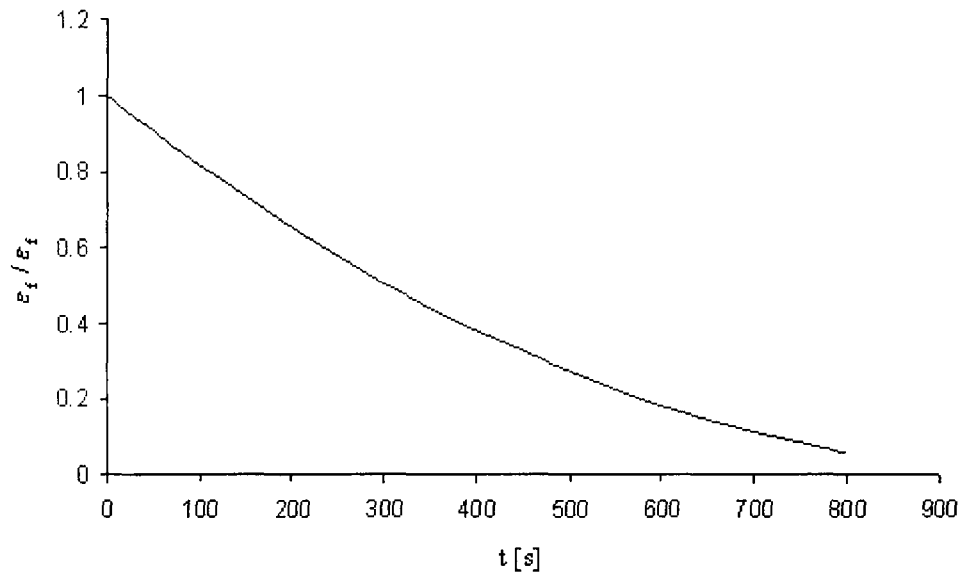


Figure 6.3 Relative porosity $\varepsilon_f / \varepsilon_{f_0}$ versus time plot for the 13%FC CMC/Cellulose composite-paper.

6.3.1.2 Changes in Fiber Size During Wicking

If we assume 13%FC CMC/Cellulose to consist entirely of fibers, we can also derive an expression for fiber size as a function of time from the data presented in the above-mentioned experiment. If we assume the porous medium to consist entirely of parallel fibers, the solid volume fraction ε_s can be formulated as

$$\varepsilon_s = \frac{1}{4} m \pi D_{fb}^2 L_{fb} \quad (6.29)$$

where m is the total number of fibers in a unit cross-sectional area, D_{fb} is the diameter of fibers, and L_{fb} is the length of fibers. As a result, the initial solid volume fraction ε_{s_0} is given by

$$\varepsilon_{s_0} = \frac{1}{4} m \pi D_{fb_0}^2 L_{fb} \quad (6.30)$$

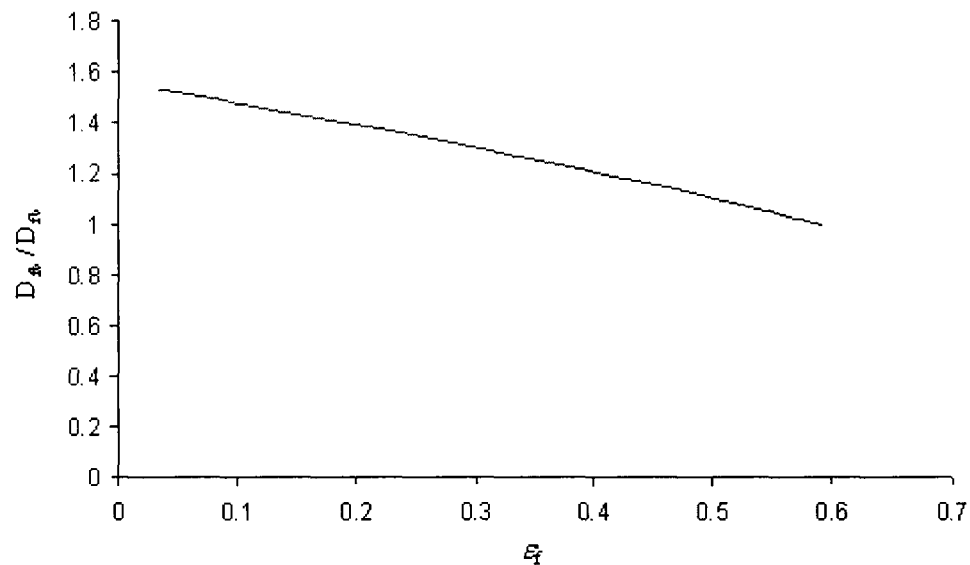


Figure 6.4 Dimensionless fiber diameter D_{fb} / D_{fb_0} versus porosity plot for the 13%FC CMC/Cellulose composite-paper.

On dividing Eq (6.28) with Eq (6.30) while using Eq (6.10) results in the following relation for fiber diameter:

$$D_{fb} = D_{fb_0} \sqrt{\frac{1 - \varepsilon_f}{1 - \varepsilon_{f_0}}} \quad (6.31)$$

Figure 6.4 plots the dimensionless fiber diameter D_{fb} / D_{fb_0} against porosity for the tested material using Eq (6.31); it is clear that the average fiber diameter increases as the porosity decreases during the swelling of the material. Since porosity is a function of time through Eq (6.28), the fiber diameter is also a function of time. Figure 6.5 shows how the fiber diameter is expected to increase with time in 13%FC CMC/Cellulose composite paper, a swelling porous media.

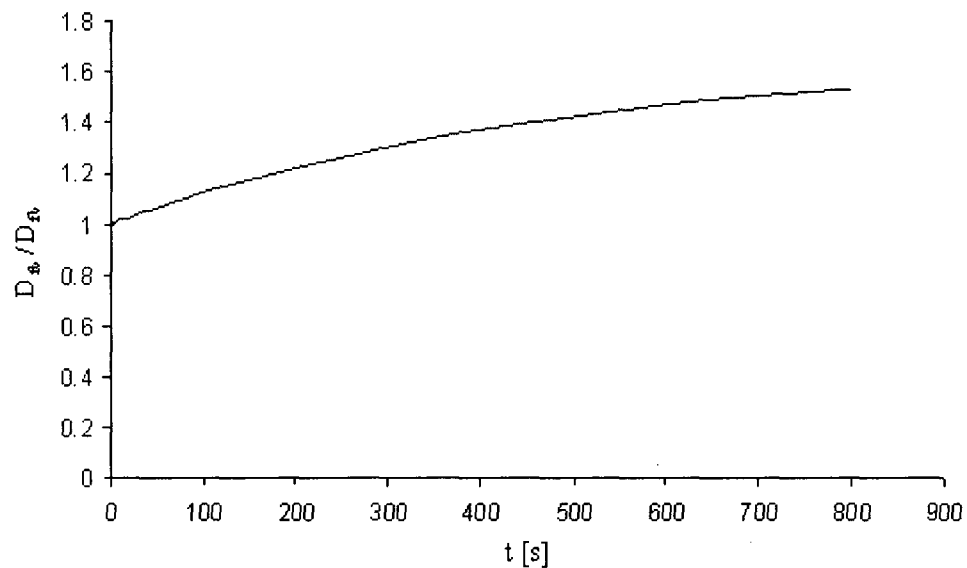


Figure 6.5 Dimensionless fiber-diameter D_{fb} / D_{fb_0} versus time plot for the composite 13%FC CMC/Cellulose paper.

6.3.2 Permeability

In order to predict the Darcy's law-based wicking length given by Eqs (6.23) or (6.24), we need to know how the permeability of the composite paper changes with time. In the capillary model, where the porous medium is assumed to be a bundle of capillary tubes, the permeability can be obtained by comparing Eq (6.3) with Eq (6.4). Note that porosity in Eq (6.4) refers to the porosity at liquid front,

which is the porosity under the non-swelled, initial state, i.e., $\varepsilon_f = \varepsilon_{f_0}$. The relation thus obtained with this assumption is referred to as the capillary-model permeability [11]:

$$K = \frac{l}{8} \varepsilon_{f_0} R_c^2 \quad (6.32)$$

Table 6.2 Different suggested relations for $\phi(\varepsilon_f)$ for porous media consisting of packed particles, where c is an arbitrary constant that depends on the structure of porous media.

Author	Suggested relation for $\phi(\varepsilon_f)$
Blake (1922), Kozeny (1927), Carman (1937) [10]	$c \frac{\varepsilon_f^3}{(1-\varepsilon_f)^2}$
Zunker (1920) [11]	$c \frac{\varepsilon_f}{(1-\varepsilon_f)^2}$
Terzaghi (1625) [11]	$c \frac{(\varepsilon_f - .13)^2}{(1-\varepsilon_f)^{1.3}}$
Fehling (1939) [11]	$c \varepsilon_f^4$
Rose (1945) [11]	$c \varepsilon_f^{4.1}$
Rumpf and Gupte (1971) [11]	$c \varepsilon_f^{5.5}$

Since the capillary pore radius changes with time [Eq (6.26)], this permeability is also a function of time only.

We may also use some empirical and theoretical formulas for estimating the permeability, which are well-established in the literature on porous media. These formulas are generally in the form

$$K = D_f^2 \phi(\varepsilon_f) \quad (6.33)$$

where $\phi(\varepsilon_f)$ is a function of porosity. We have used different empirically obtained or theoretically derived formulas for ϕ , which are listed in Tables 6.2 and 6.3. Table 6.2 shows different suggested relations for $\phi(\varepsilon_f)$ for porous media consisting packed *particles*, while Table 6.3 displays similar formulas for porous media consisting of packed *fibers*.

Table 6.3 Different suggested relations for $\phi(\varepsilon_f)$ for porous media consisting of packed fibers, where c is an arbitrary constant that depends on the structure of porous media.

Author	Suggested relation for $\phi(\varepsilon_f)$
Davies (1952) [11]	$c \frac{1}{(1 - \varepsilon_f)^{1.5} [1 + 56(1 - \varepsilon_f)^3]}$
Chen (1955) [11]	$c \frac{\varepsilon_f}{1 - \varepsilon_f} \ln \frac{0.64}{(1 - \varepsilon_f)^2}$
Bruschke and Advani (1993) [25]	$c \frac{(1 - \eta)^2}{\eta^3} \left(\frac{3\eta \cdot \tan^{-1} \sqrt{(1 + \eta)/(1 - \eta)}}{\sqrt{1 - \eta^2}} + \frac{\eta^2}{2} + 1 \right)^{-1}$ where $\eta = \frac{4}{\pi}(1 - \varepsilon_f)$
Gebart (1992) [26]	$c \left(\sqrt{\frac{1 - \varepsilon_{f_{min}}}{1 - \varepsilon_f}} - 1 \right)^{5.2} \text{ where } \varepsilon_{f_{min}} = 1 - \frac{\pi}{2\sqrt{3}}$

There is a constant factor c in each formula for $\phi(\varepsilon_f)$, which plays an important role and may depend on other aspects of flow through porous media, including the particle-based Reynolds number [27]. Since we have the exact

Table 6.4 The final forms of permeability relations (obtained using $\phi(\varepsilon_f)$ and Eq (6.30)) for porous media consisting of packed *particles*.

Author	Suggested relation for $\phi(\varepsilon_f)$
Blake (1922), Kozeny (1927), Carman (1937) [10]	$K_0 \left(\frac{\varepsilon_f}{\varepsilon_{f_0}} \right)^3 \frac{1 - \varepsilon_{f_0}}{1 - \varepsilon_f}$
Zunker (1920) [11]	$K_0 \frac{\varepsilon_f}{\varepsilon_{f_0}} \frac{1 - \varepsilon_{f_0}}{1 - \varepsilon_f}$
Terzaghi (1625) [11]	$K_0 \left(\frac{\varepsilon_f - 0.13}{\varepsilon_{f_0} - 0.13} \right)^2 \left(\frac{1 - \varepsilon_{f_0}}{1 - \varepsilon_f} \right)^{0.3}$
Fehling (1939) [11]	$K_0 \left(\frac{\varepsilon_f}{\varepsilon_{f_0}} \right)^4 \frac{1 - \varepsilon_f}{1 - \varepsilon_{f_0}}$
Rose (1945) [11]	$K_0 \left(\frac{\varepsilon_f}{\varepsilon_{f_0}} \right)^{4.1} \frac{1 - \varepsilon_f}{1 - \varepsilon_{f_0}}$
Rumpf and Gupte (1971) [11]	$K_0 \left(\frac{\varepsilon_f}{\varepsilon_{f_0}} \right)^{5.5} \frac{1 - \varepsilon_f}{1 - \varepsilon_{f_0}}$

value of K_0 , the permeability of the composite paper at $t = 0$ for the case of no swelling, we have used the ratio of K/K_0 to eliminate the constant c . Since we also used Eq (6.31) to express pore diameter as a function of porosity, the final expression of the permeability is just a function of porosity. Tables 6.4 and 6.5 list the final forms of the theoretical and empirical formulas for permeability of swelling porous media.

Table 6.5 The final forms of permeability relations (obtained using $\phi(\varepsilon_f)$ and Eq (6.30)) for porous media consisting of packed *fibers*.

Author	Suggested relation for $\phi(\varepsilon_f)$
Davies (1952) [11]	$K_0 \left(\frac{1-\varepsilon_{f_0}}{1-\varepsilon_f} \right)^{0.5} \frac{1+56(1-\varepsilon_{f_0})^3}{1+56(1-\varepsilon_f)^3}$
Chen (1955) [11]	$K_0 \frac{\varepsilon_f}{\varepsilon_{f_0}} \ln \frac{0.64}{(1-\varepsilon_f)^2} / \ln \frac{0.64}{(1-\varepsilon_{f_0})^2}$
Bruschke and Advani (1993) [25]	$K_0 \frac{\psi(\eta)}{\psi(\eta_0)} \frac{\eta}{\eta_0} \text{ where } \eta_0 = \frac{4}{\pi} (1-\varepsilon_{f_0})$ and $\psi(\eta) = \frac{(1-\eta)^2}{\eta^3} \left(\frac{3\eta \cdot \tan^{-1} \sqrt{(1+\eta)/(1-\eta)}}{\sqrt{1-\eta^2}} + \frac{\eta^2}{2} + 1 \right)^{-1}$
Gebart (1992) [26]	$K_0 \frac{1-\varepsilon_f}{1-\varepsilon_{f_0}} \left[\left(\frac{\sqrt{1-\varepsilon_{f_{min}}}-1}{\sqrt{1-\varepsilon_f}} - 1 \right) / \left(\frac{\sqrt{1-\varepsilon_{f_{min}}}-1}{\sqrt{1-\varepsilon_{f_0}}} - 1 \right) \right]^{5/2} \text{ where } \varepsilon_{f_{min}} = 1 - \frac{\pi}{2\sqrt{3}}$

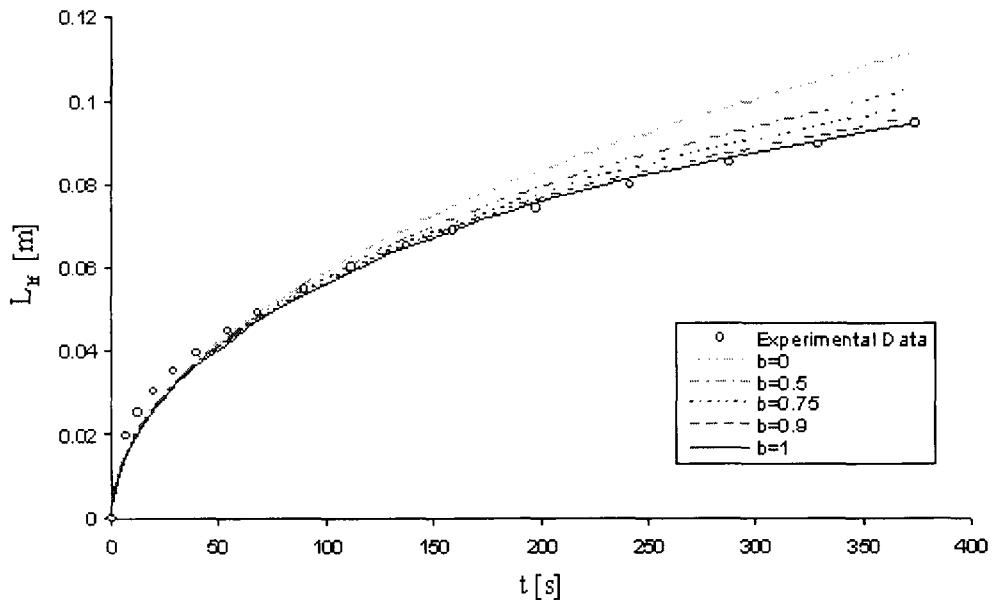


Figure 6.6 Wicking height vs. time plot for water absorption in the 13%FC CMC/Cellulose composite-paper strip using the capillary-model permeability and different values for the absorption coefficient b . Experimental data are from Ref [22].

6.3.3 Wicking Predictions

The derived formula for the height of wicked liquid, Eq (6.23), has the absorption coefficient b , which is directly related to the absorption of liquid by solid matrix of a porous medium. Figure 6.6 plots the growth of wicking height for water using the capillary-model permeability [Eq (6.32)] for different values of b and compares such predictions with Schuchardt and Berg's experimental data [22]. According to the figure, predictions of Darcy's law employing the capillary-model permeability improve with an increase in b : a value of b between 0.9 and 1.0 leads to a very good match with the data. A reason for the increase in the average wicking height can be proffered as follows. Based on Figure 6.6, as b increases from 0 to 1, the distance traveled by the wicking front or the wicking height decreases. Note that as b approaches unity, the net value of the volumetric source term on the right hand side of Eq (6.11) goes to zero, meaning that less liquid is available in the pores to push the liquid-front forward.

Figure 6.7 compares the wicking height predictions by the modified Washburn equation with the modified Darcy's law [Eq (6.24) with the absorption coefficient $b = 1$ and the capillary-model permeability Eq (6.32)]; we note that both the models predict identical growth in wicking heights. It is not surprising to obtain the same predictions from the two models, since the capillary-model permeability is used in the modified Darcy's law approach, while the modified Washburn equation is based on the capillary model [8]. However, since the modified Washburn equation is an accepted model for wicking in a class of swelling porous material, the flawless comparison verifies our key assumption of

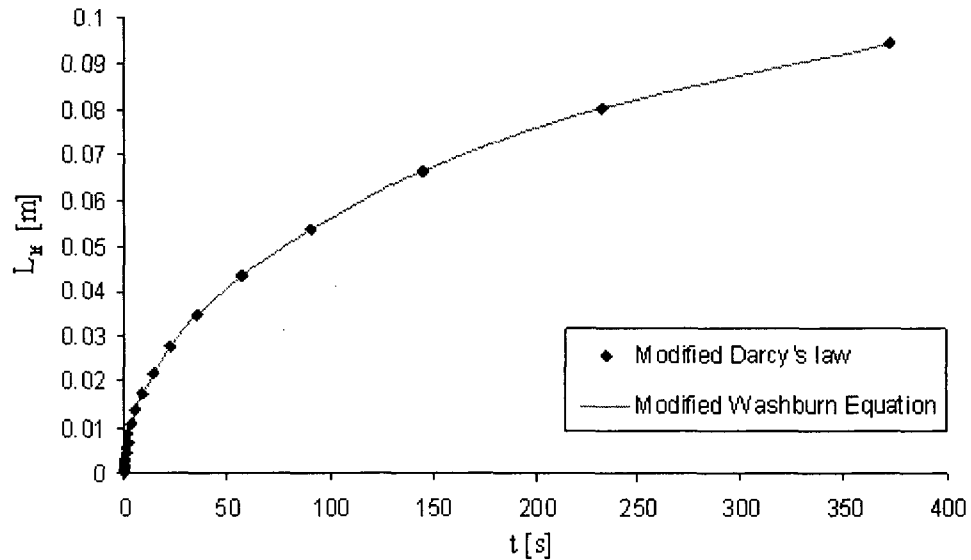


Figure 6.7 A comparison of predictions by the modified Washburn equation (Eq (6.4)) and the modified Darcy's law with ' $b=1$ ' (Eq (6.23)) while using the capillary-model permeability.

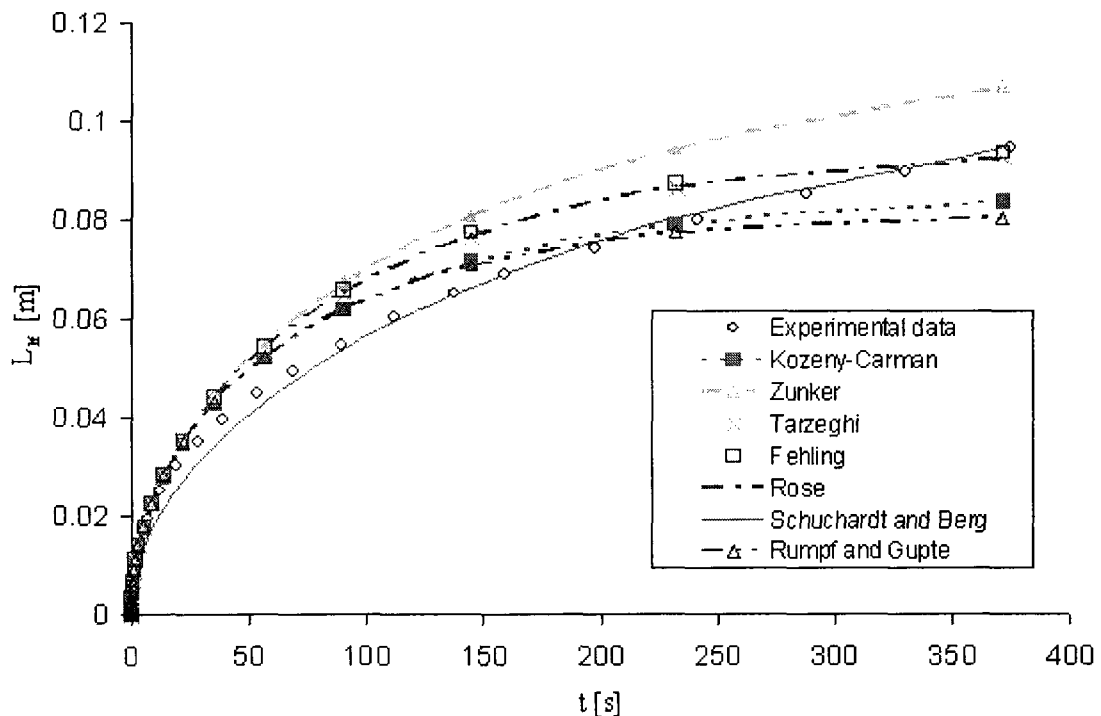


Figure 6.8 Wicking height vs. time predictions for the wicking of water in the 13%FC CMC/Cellulose composite-paper strip using the Darcy's law-based model with different formula for the permeability of *particulate* porous media. The predicted values are compared with the modified Washburn-equation predictions and the experimental data of Schuchardt and Berg [22].

Eq (6.9). In essence, using the capillary model for permeability, and considering b to be unity, leads to the same prediction from Eq (6.24), as given by using Eq (6.4). This indicates that in the newly proposed wicking model based on Darcy's law, the value of 'b' should be either one or very close to one.

Figure 6.8 shows the predictions of wicking height against time for water absorption in the 13%FC CMC/Cellulose composite-paper strip using the different models for permeability for porous media made from particles. Here, Eq (6.24) based on the modified Darcy's law model is used for the wicking prediction, where b is unity. The empirical formulas for permeability as a function of porosity are listed in Table 6.4, while the porosity changes with time according to Eq (6.28) or Figure 6.3. The prediction of the modified Washburn equation is also shown in Figure 6.8 for comparison. It is clear that Schuchardt and Bergs' model matches with the experimental data better than any other models (this is not surprising since the model gets its values of parameters R_0 and a after fitting the experimental data [22]); however, among the empirical formulas used for permeability in the proposed Darcy's law based model, the Terzaghi, Fehling, and Rose formulas fare the best against the experimental data, although the predictions from other formulas are also reasonable.

Figure 6.9 shows the wicking predictions using the different permeability models for fibrous porous media. (The empirically obtained or theoretically derived formulas for these permeability models are listed in Table 6.5.) It is clear that prediction using the capillary model for permeability best agrees with the experimental data. Since we have the measured pore-radius values as a function

of time for this specific experiment from [22], it is not surprising that the capillary model, which relies on these values, performs the best. If we had measured the porosity separately, then we could have seen better predictions from the other models. Among the empirical formulas for permeability, the Davies and Chen model seem to fare well against the experimental data.

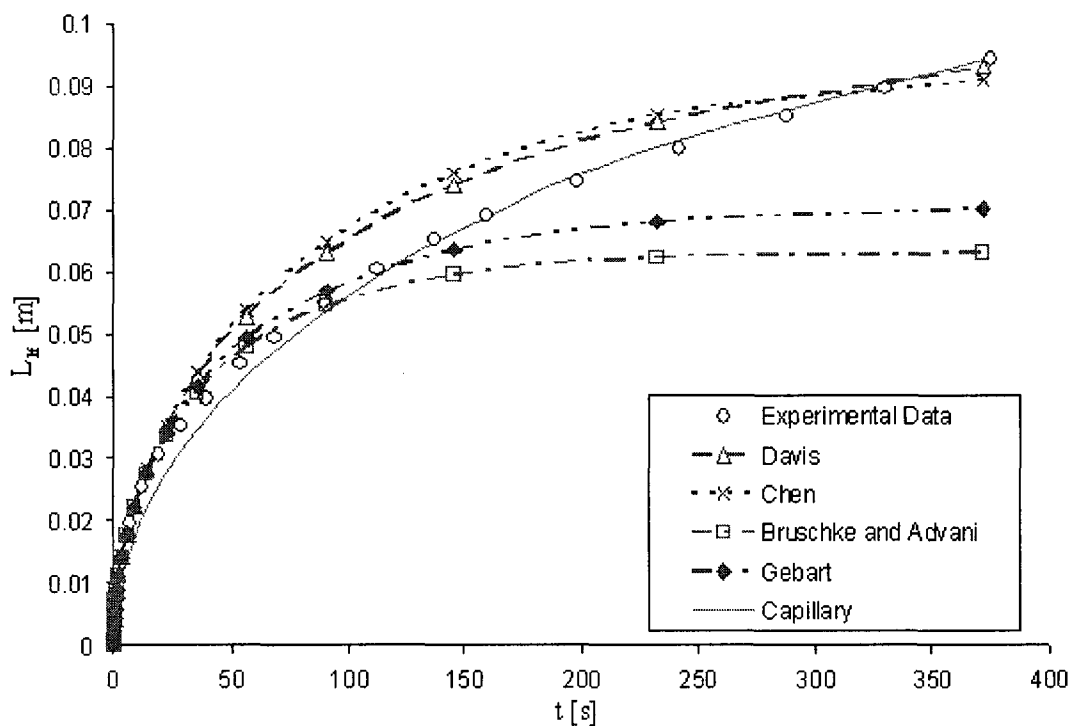


Figure 6.9 Wicking height vs. time predictions for the wicking of water in the 13%FC CMC/Cellulose composite-paper strip using the proposed Darcy's law-based model with different formula for the permeability of *fibrous* porous media. The predicted values are compared with the modified Washburn-equation predictions and the experimental data of Schuchardt and Berg [22].

6.4 Summary and Conclusions

In this chapter, the wicking of liquid into a paper-like swelling porous medium (a composite paper made formed from a network of cellulose and superabsorbent fibers), is studied theoretically. This work is built on a previous

study by Schuchardt and Berg [22], in which a modified Washburn equation was used to predict liquid absorption in the composite paper. Here, we propose a new theoretical approach in which Darcy's law is coupled with a modified continuity equation, characterized by sink and source terms representing the effects of liquid absorption into fibers and their subsequent swelling.

The wicking predictions obtained from the newly proposed wicking model compare well with the previous theoretical predictions of the modified Washburn equation, as well as the experimental data of Schuchardt and Berg [21-22]. It is observed that the proposed model performs the best when it is assumed that the volume of liquid absorbed into the fibers is equal to their volumetric expansion. An estimate of change in porosity with time for the proposed model is obtained from the published data on changes in hydraulic radius with time during wicking in the composite paper. This porosity change, when fed to several pre-existing permeability models, with their permeability values being a function of porosity, gives an estimate of changes in permeability in the paper. Of the several permeability models considered, the models by Terzaghi, Fehling, and Rose for porous media formed from particles, and the models by Davies and Chen for porous media formed from fibers, perform the best when coupled with the proposed wicking model.

The new Darcy's law-based approach has an important advantage over the Washburn equation-based approach, as the former can be extended into two- and three-dimension wicking situations, while the latter Washburn model is restricted to one-dimensional flows [23]. The Darcy's law based approach has

some advantages over other wicking models based on multi-phase flows, as well. The proposed model, since it harnesses the simplicity of single-phase flow, has fewer property values and parameters to be measured; moreover, the property and parameter values for single-phase flows are relatively simpler to measure.

Another advantage of the proposed Darcy's-law based model is its versatility. We have used the model in a preliminary study of liquid absorption in a porous bed of particles made from superabsorbent polymer¹⁸, and it seems that this model can improve wicking predictions in such extremely-swelling materials, as well [30]. We have also applied this theory to model flow in natural-fiber performs used in the liquid composite molding process for making bio-based composites, and our first attempt showed that it also works well for this material [31]. We plan to extend this theory, especially considering other values for the parameter ' b ' of Eq. (9), and study its effectiveness in modeling 2D and 3D flows in the swelling, liquid-absorbing porous media made from natural-fibers.

References

1. Chatterjee P.K. and Gupta B.S., "Absorbent Technology," Amsterdam, Elsevier, 2002
2. Berg John C. "Wettability," New York, Marcel Dekker, 1993
3. Alava M., Dube M. and Rost M., "Imbibition in Disordered Media," *Advances in Physics*. 53, 2, 83-175, 2004
4. Masoodi R., Pillai K.M., and Varanasi P.P., "Effect of Externally Applied Liquid Pressure on Wicking in Paper Wipes" a manuscript submitted to JEFF J., 2009

¹⁸ Superabsorbent polymers are used as extreme water-absorbing substances that swell to many times their original particle dimensions while absorbing many times their weight of water.

5. Lucas R., "Rate of Capillary Ascension of Liquids," *Kolloid Z.* 23, 15, 1918
6. Washburn E.V., "The Dynamics of Capillary Flow", *Phys. Rev.* 17, 273, 1921
7. Masoodi R., Pillai K.M., and Varanasi P.P., "Role of Hydraulic and Capillary Radii in Improving the Effectiveness of Capillary Model in Wicking," ASME Summer Conference, Jacksonville FL, USA, August 10-14, 2008.
8. Masoodi R., Pillai K.M., and Varanasi P.P., "Darcy's Law based Models for Liquid Absorption in Polymer Wicks," *J. AIChE.*, 53(11), 2769-2782, 2007
9. Pillai K.M. and Advani S.G., "Wicking Across a Fiber-Bank", *J. Colloid and Interface Sci.*, 183, 100-110, 1996
10. Bear Jacob, "Dynamics of Fluids in Porous Media," Elsevier Science, 1972
11. Dullien F.A.L, "Porous Media: Fluid Transport and Pore Structure," Academic Press, 1992.
12. Chwastiak S., "A Wicking Method for Measuring Wetting Properties of Carbon Yarn," *J. Colloid Interface Sci.*, 42, 298-309, 1973
13. Scher K.E., Master's Thesis. Dept. of Chemical Engineering. University of Washington. 1983
14. Hodgson K.T. and Berg J.C., "The Effect of Surfactants on Wicking Flow in Fiber Networks" *J. Colloid Interface Sci.*, 121 (1), 22-31, 1988.
15. Fowkes F.M., "Role of Surface Active Agents in Wetting", *J. Phys. Chem.*, 57, 98-103, 1953
16. Williams J.G., Morris C M and Ennis B C .*Polym. Eng. Sci.*, 14(6), 413-419, 1979
17. McDonald P., "Wicking in Multi-ply Structures with Dissimilar Plies", MS. Dissertation, Georgia Institute of Technology, August 2006.
18. Sedef Akinli-Kogak, "The influence of Fiber Swelling on Paper Wetting," MS. Dissertation, The University of Maine, August 2001.
19. Kissa E., "Wetting and Wicking," *Textile Research Journal*, 66, 10,660-668, 1996.
20. TAPPI Useful Methods, "Water Retention Value (WRV)", UM-254, 54-56, TAPPI Press, Atlanta, 1991.
21. Schuchardt, D.R., "The Effects of Fiber Swelling on Liquid Transport in Fibrous Media", Master's Thesis., Dept. of Chemical Engineering, University of Washington, 1989.
22. Schuchardt, D.R., Berg, J.C., "Liquid Transport in Composite Cellulose-Superabsorbent Fiber Network", *Wood and Fiber Science*, 23,3, 342-357, 1990.
23. Masoodi, R., Tan, H. and Pillai, K. M., "Darcy's Law Based Numerical Simulation for Modeling 3-D Liquid Absorption into Porous Wicks", manuscript submitted to *AIChE Journal* for review.

24. Whitaker, Stephen, "The Method of Volume Averaging", Springer, 1998
25. Brusckke, M.V., Advani, S.G., "Flow of generalized Newtonian fluids across a periodic array of cylinders", J. Rheol. 37(3), 479-498, May/June 1993.
26. Gebart, B.R., "Permeability of Unidirectional Reinforcements for RTM", Journal of Composite Materials, 26(8), 1100-1133, 1992.
27. Skartsis, L., Khomani, B. and Kardos, J. L., "Resin flow through fiber beds during composite manufacturing processes. part II: Numerical and Experimental Studies of Newtonian Flow Through Ideal and Actual Fiber Beds," Polym. Eng. and Sci., 32(4), 221-239, 1992.
28. Pillai, K.M., "Governing Equations for Unsaturated Flow in Woven Fiber Mats: Part 1 Isothermal Flows", Composites Part A: Applied Science and Manufacturing, 33, 1007-1019, 2002.
29. Pillai, K.M. and Munagavalsa, M.S., "Governing Equations for Unsaturated Flow through Woven Fiber Mats, Part 2: Nonisothermal Reactive Flows", Composites Part A: Applied Science and Manufacturing, 35, 403-415, 2004.
30. R. Masoodi and Krishna M. Pillai "A preliminary study on modeling wicking in superabsorbent particles," A technical report submitted to Procter & Gamble Service GmbH, Germany, March 2009.
31. R. Masoodi, Krishna M. Pillai and Michael A. Verhagen "Flow Modeling in Natural-Fiber Preforms used in Liquid Composite Molding," Proc. 1st joint American- Canadian International Conference on Composites, Delaware, USA, September 15-17, 2009.

Chapter 7

A GENERAL FORMULA FOR CAPILLARY SUCTION-PRESSURE IN POROUS MEDIA

7.1 Introduction

Wicking is the movement of liquids into porous media under the action of the capillary suction-pressure. The difference in the surface energies of the dry and wet solid matrices leads to the creation of a capillary force at contact lines which is responsible for pulling certain liquids into the porous media. The previous research on the wicking phenomenon has been mainly focused on the relation between the wicking rate and wicking time, the relation between the wicking rate and the porous medium characteristics, and the wettability or the contact angle issues. There are two traditional models for studying the wicking phenomenon mathematically. The older approach is the Lucas-Washburn equation where the porous medium is assumed to be a bundle of aligned capillary tubes of the same radii [1, 2]. Another approach is based on the Darcy's law, which relates the average velocity of a liquid to the pressure gradient within a porous medium [3]. Both approaches assume full saturation behind a clearly-defined liquid-front while the liquid is being pulled into a porous medium as a result of the capillary suction [3, 4]. Note that important parameters for flow modeling such as the saturated permeability and capillary suction-pressure (through the Laplace equation) are easily measurable quantities in the clear-

liquid-front approach. While in the traditional multi-phase flow approach involving the generalized Darcy's laws, the relative permeability and the capillary pressure (as a function of the saturation) are two parameters that cannot be measured easily [3]. The sharp interface approach is also important in the modeling of liquid composites molding processes for manufacturing composite materials as it simplifies the governing equations without the complications of Buckley-Leverett approach [5-7]. The single-phase Darcy's law approach has advantage of being applicable to the three-dimensional flows as well as the swelling porous-media flows [8-10].

The capillary suction-pressure gives rise to the capillary force, which is the driving force in any wicking phenomenon. There have been a few studies on modeling the capillary suction phenomenon at the boundaries of the single-phase flow in porous media. The oldest and well-known relation for the capillary pressure is the Young–Laplace equation that describes the capillary pressure-difference across the interface between two static immiscible fluids, such as water and air, after relating it to the geometry of the surface, the surface energies of the fluids and solid, and the wettability [11, 12]. The Young–Laplace equation is named after Thomas Young, who developed the qualitative theory of surface tension in 1805 [13], and Pierre-Simon Laplace who published the mathematical description later [11]. It might also be called the Young–Laplace–Gauss equation, as Gauss unified the work of Young and Laplace, by deriving the governing differential equation and boundary conditions using the Bernoulli's principles [11].

The assumption of porous medium to be consisting of a bundle of the identical parallel capillary tubes aligned with the liquid direction is the basic idea behind the Young-Laplace equation. This equation can be used even when the radius of the imaginary capillary tubes vary along the liquid-flow direction [14-16]. Young [14] and Staples and Shaffer [15] used the Laplace-Young capillary equation and studied the capillary flow in non-circular capillaries. They used a simple formulation for interface progression in a non-uniform capillary based on the Lucas–Washburn equation. Recently, Liao et al. [16] studied the flow in non-uniform cross-sectional capillaries where, using the Navier-Stokes equations, a nonlinear, second-order differential equation was derived to predict the rise of a liquid in such capillaries. The Young-Laplace equation was shown analytically to be valid for capillary tubes of non-uniform radii.

One of the biggest challenges in using the Young-Laplace equation is the estimation of the capillary radius. Since real porous media with tortuous fluid paths are not bundles of the identical, aligned capillary tubes, so some assumptions must be made to estimate the 'equivalent capillary-radius' for a real porous medium. The most accurate method of estimating the equivalent capillary-radius is the capillary rise experiment, in which the surface energy is balanced by the gravitational potential energy [17, 18]. Masoodi et al. [19] and Chwastiak [20] used the indirect measurement of hydraulic radius to estimate the capillary radius. In this method the pressure drop through the porous medium is measured and the Hagen-Poiseuille law is applied to find the equivalent hydraulic-radius. Studies show that though the hydraulic and capillary radii (or

the wet and dry radii, as named by Chatterjee [21]) are two different characteristics, they are frequently used interchangeably [18, 21].

The analysis of the micrographs of any porous medium is another way of estimating the equivalent capillary-radius. Benltoufa et al [22] and Chatterjee and Gupta [23] fitted circles in the pore space between particles and suggested the circle radii to be considered as the equivalent capillary-radii. Dodson and Sampson [24] defined the capillary radius as the radius of a circle whose perimeter is the same as that of the pores. Indirect measuring of the hydraulic radius is another method used by some researchers [18, 25, 26]. In this method, the pressure drop along the porous medium is measured and then the Hagen-Poiseuille law is employed to calculate the hydraulic radius of the imaginary capillary tubes. Some researchers suggested the radius of the largest sphere (or circle in the case of using a 2-D micrograph) that could be fitted in the inter-particle pore space to be considered the capillary radius [27].

The capillary pressure in fibrous material is another challenge that attracted attention of some researchers. Usually the capillary pressure is considered a function of the porosity, fiber size and orientation, and flow direction. Wicking along the fibers was studied by Chwastiak [20], Amico and Lekakou [28], and Williams et al. [29]. The wicking across the fibers was studied by Senoguz et al [30], Ahn et al. [31], Lekakou and Bader [32], and Pillai and Advani [33]. In all these studies, different expressions for the capillary pressure along- and across-the-fibers were suggested or experimentally validated. The capillary pressure in woven fabrics was also studied experimentally by Ahn et al. [31]. In nonwoven

fabrics, the capillary pressure was found to be a function of porosity, fiber size and orientation, and flow direction [34].

The measurement or estimation of the capillary radius is the key to finding the correct capillary pressure, and thus to modeling the wicking in porous materials accurately. As reviewed above, the capillary-radius prediction is still a challenge and several different methods for estimating it have been presented. The literature survey also showed that some of the models are not consistent with each other. In this Chapter, we present a general theoretical expression for the capillary radius, based on the Young-Laplace capillary-pressure equation. Our goal is to unify some of the previously suggested expressions into a single general relation. Later, we validate the expression by deriving the capillary pressure or capillary radius expressions for some simple cases where the analytical relations and experimental data are available. We also show how this proposed expression can be used to find the capillary radius in complex geometries. One of the advantages of this new approach is the possibility of using images and micrographs of porous media to estimate the local capillary pressure. Furthermore, one can also use the statistical information on particle's size and shape to estimate the capillary radius.

7.2 Derivation of a General Formula for Capillary Suction-Pressure

We apply the energy balance principle to the wicking process to find a general expression for the capillary suction-pressure. For a liquid being absorbed

by a porous medium as a result of the capillary action, the statement of energy balance can be listed as

$$dE_{ds} = dW_c + dE_{ws} + dE_a + dE_k + dW_g + dE_{vs} \quad (7.1)$$

where E_{ds} is the surface energy of the dry surface, W_c is the capillary work, E_{ws} is the surface energy of the wetted surface, E_a is the inertial energy needed to accelerate the liquid from zero to the wicking velocity, E_k is the kinetic energy of the liquid, W_g is the work done against gravity, and E_{vs} is the energy dissipated due to viscosity. The inertial and kinetic energies are usually negligible as the wicking speed is quite low [18]. We can also neglect the gravity work W_g ; however, it is possible to include it later through the Darcy's law if it plays a major role in the wicking process [19]. The viscous dissipation is a significant term that is related to the microstructure of the porous medium and the liquid viscosity. In using the Darcy's law, the effect of such dissipation is included through the permeability and the viscosity, so we can neglect this term at this stage. After dropping the negligible terms, Eq (7.1) reduces to

$$dW_c = dE_s \quad (7.2)$$

where $dE_s = dE_{ds} - dE_{ws}$. Eq (7.2) indicates that the capillary-pressure work is equal to the difference between surface energies of the porous medium before and after getting wet. Note that a wet surface has lower surface energy than a dry surface. Therefore, the right hand side of Eq (7.2) is always positive and is expressible [26] as

$$dE_s = (\gamma_{ds} - \gamma_{ws})dA_{ws,s} \quad (7.3)$$

where γ_{ds} is the surface energy of dry surface, γ_{ws} is the surface energy of wet surface, and $dA_{ws,s}$ is the change in the solid-surface wet area. According to the Young's equation [12], the contact angle and surface energies are related through

$$\cos \theta = \frac{\gamma_{ds} - \gamma_{ws}}{\gamma_l} \quad (7.4)$$

in which γ_l is the surface energy of the liquid and θ is the contact angle of liquid at the solid- liquid interface. Combining of Eqs (7.3) and (7.4) yields the expression

$$dE_s = \gamma_l \cos \theta dA_{ws,s} \quad (7.5)$$

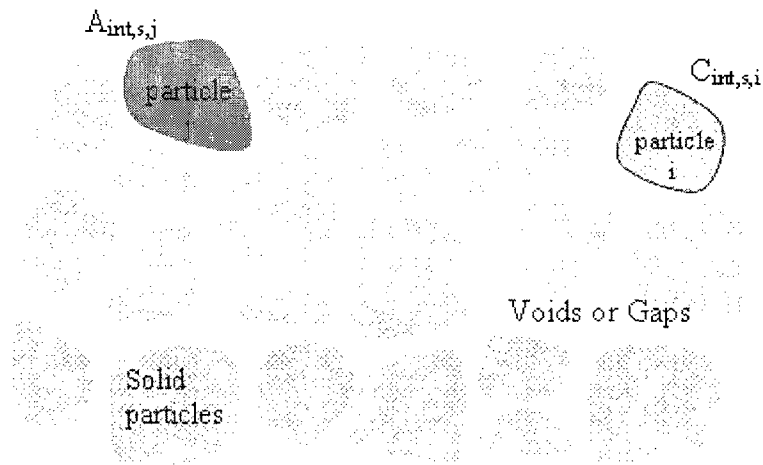


Figure 7.1 A schematic of particles and void areas in a cross-section of the porous medium.

If we assume the porous medium to be composed of particles of different sizes (Figure 7.1), and if $C_{int,s,i}$ is the cross-sectional perimeter of a solid particle 'i' at

the interface, then the total surface-area of the solid matrix wetted by the invading liquid can be approximated as

$$dA_{ws,s} = \sum_i C_{int,s,i} dh_f \quad (7.6)$$

where dh_f is the small increment caused by the liquid-front movement. The summation is over all particles at the interface. Note that we assumed the perimeters of particles at interface, $C_{int,s,i}$, to remain constant during the interval of dh_f . If we further define $C_{int,s}$ to be the total cross-sectional perimeter of solid particles at the interface in so called the representative elementary area or REA¹⁹, i.e. $C_{int,s} = \sum C_{int,s,i}$, then Eq (7.6) simplifies to

$$dA_{ws,s} = C_{int,s} dh_f \quad (7.7)$$

On replacing $dA_{ws,s}$ of Eq (7.5) with the expression from Eq (7.7), we get

$$dE_s = \gamma_l \cos \theta C_{int,s} dh_f \quad (7.8)$$

The work by the capillary pressure to move the fluid front by dh_f is given by

$$dW_c = F_c dh_f \quad (7.9)$$

where F_c is the capillary force that pulls the liquid front through the pores of the porous medium. According to the definition of pressure, the capillary force is related to the capillary pressure through the relation

$$F_c = P_c A_{int,v} \quad (7.10)$$

¹⁹ REA is typically much bigger than the solid particle in a porous medium and is often employed to average flow-variables while modeling flow through porous media [3].

where $A_{int,v}$ is the total void area at the interface. The cross-sectional area of solid particles, $A_{int,s} = \sum A_{int,s,i}$, and the cross-sectional area of the void space,

$A_{int,v} = \sum A_{int,v,j}$, are related through

$$A_{int,v} = \frac{\varepsilon}{1-\varepsilon} A_{int,s} \quad (7.11)$$

where ε is areal porosity²⁰. Combing of Eqs (7.9), (7.10) and (7.11) transforms the capillary-work expression to

$$dW_c = P_c \frac{\varepsilon}{1-\varepsilon} A_{int,s} dh_f \quad (7.12)$$

On using Eqs (7.8) and (7.12) in Eq (7.2), the following relation is obtained for the capillary suction-pressure.

$$P_c = \frac{2\gamma_l \cos(\theta)}{R_e} \quad (7.13)$$

Here R_e , the equivalent capillary-radius, is defined as

$$R_e = 2 \frac{A_{int,s}}{C_{int,s}} \frac{\varepsilon}{1-\varepsilon} \quad (7.14)$$

Eq (7.13) gives the local value of the capillary pressure by estimating the local equivalent capillary-radius using Eq (7.14)²¹. (Note that definition of Eq (7.14) is based on the geometry of solid particles in the porous medium.) The equivalent

²⁰ The 'area' porosity averaged over a length, perpendicular to the area, is identical to the volume-based porosity [3] where the latter is defined as the ratio of the total pore-volume (within a representative averaging volume or REV of the porous medium) to the REV volume.

²¹ Hassanzadeh and Gray [35] suggested the use of a statistical average in the vicinity of a considered point in the porous medium and rewrote Eq (7.13) as $P_c = 2\langle\gamma_l\rangle \cos(\langle\theta\rangle) / \langle R_e \rangle$ where the brackets represent the averaging of quantities within an REV.

capillary radius, which is defined at the liquid-air interface, can also be related to the geometry of void spaces through

$$R_e = 2 \frac{A_{int,v}}{C_{int,v}} \quad (7.15)$$

which is also a definition of the hydraulic radius. Note that the total perimeter of solid particles, $C_{int,s}$ is equal to the total perimeter of the void spaces, $C_{int,v}$ (Figure 7.1), and the sectional areas of solid particles, $A_{int,s}$ and void space, $A_{int,v}$ are related through Eq (7.11). In other words, Eqs (7.14) and (7.15) are identical.

7.3 Verification of the Capillary-Pressure Relation

In order to verify the general capillary-pressure relation of Eq (7.13) (or more specifically, Eqs (7.14) and (7.15)), we will show that for some simple cases, where we already have other verified formulas for the capillary pressure, the capillary-pressure relations obtained using the newly proposed expression are identical to the established formulas.

7.3.1 Flow in the Porous Media with a Constant Ratio of the Volume to Wetted Area in Particles

Suppose there is a porous medium with the following assumptions:

1. The medium is composed of randomly distributed particles of the same shape but different sizes.
2. The ratio of volume to surface area for all particles is a constant.
3. The porous medium is homogeneous.

A medium composed of aligned parallel-fibers is an example of such a porous medium. Assume V_s and S_s to be the volume and surface areas of particles in an interfacial volume²². If L is the thickness of the interfacial volume, then employing the third assumption, one can propose that

$$A_{int,s} = \frac{nV_s}{L} \quad (7.16a)$$

$$C_{int,s} = \frac{nS_s}{L} \quad (7.16b)$$

where n is the number of particles within the interfacial volume. Note that Eqs (7.16a) and (7.16b) estimate the averages of the interfacial area and perimeter; but since the medium is homogeneous, so the local interfacial area and perimeter are deemed identical with their averages. Based on the first and second assumptions, we have

$$\Gamma = \frac{V_s}{S_s} = \frac{A_{int,s}}{C_{int,s}} \quad (7.17)$$

where Γ is the ratio of the volume to surface area of solid particles, which is a constant based on the second assumption. Using Eq (7.17) result with Eqs (7.14) and (7.13) leads to a relation for the capillary pressure as

$$P_c = \frac{1 - \varepsilon}{\varepsilon} \frac{\gamma_l \cos(\theta)}{\Gamma} \quad (7.18)$$

Eq (7.18) is identical to the expression for P_c derived and experimentally validated by Masoodi and Pillai for modeling the wicking flow in wipes [10].

²² Interfacial volume is an imaginary volume of a certain thickness at the liquid-front location, parallel to the sharp interface.

7.3.2 Flow along Capillary Tubes with a Fixed Radius

It is common to follow the Lucas-Washburn approach and assume a porous medium composed of aligned capillary tubes [1, 4]. If such imaginary capillary tubes have the same radius r_c , then

$$A_{\text{int},v} = n\pi r_c^2 \quad (7.19a)$$

$$C_{\text{int},v} = n(2\pi r_c) \quad (7.19b)$$

On using Eqs (7.19a) and (7.19b) in Eq (7.15), one gets the equivalent capillary radius as

$$R_e = r_c \quad (7.20)$$

On substituting Eq (7.20) into Eq (7.13), we can express the capillary pressure as

$$P_c = 2 \frac{\gamma_l \cos(\theta)}{r_c} \quad (7.21)$$

which is identical to the famous Young–Laplace relation for capillary pressure [24].

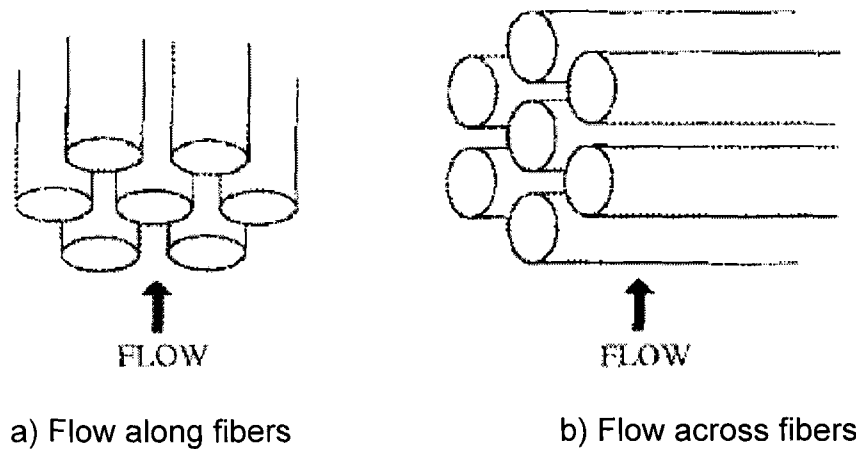


Figure 7.2 Flow through a fiber-bank.

7.3.3 Flow along a Bank of the Same-Radius Fibers

In the composite processing community, the flow of resin along or across a bank of parallel fibers is a convenient idealization for modeling the wetting of fibers. For the case of flow along a homogeneous bank of the same-size fibers (Figure 7.2a), the sectional area and perimeter of fibers at the interface are

$$A_{int,s} = n\pi r_{fb}^2 \quad (7.22a)$$

$$C_{int,s} = 2n\pi r_{fb} \quad (7.22b)$$

where n is the number of fibers and r_{fb} is the radius of fibers. Using Eqs (7.22a) and (7.22b) in Eq (14) gives the equivalent capillary radius as

$$R_e = \frac{\varepsilon}{1-\varepsilon} r_{fb} \quad (7.23)$$

Substitution of R_e from Eq (7.23) in Eq (7.13) gives the following expression for the capillary pressure for flow along fibers

$$P_c = 2 \frac{1-\varepsilon}{\varepsilon} \frac{\gamma \cos(\theta)}{r_{fb}} \quad (7.24)$$

which is identical to the expression used by Chwastiak [20], Amico and Lekakou [28], Williams et al. [29], and Ahn et al. [31] for wicking along a bank of parallel fibers.

7.3.4 Flow across a Bank of the Same-Radius Fibers

For flow across a bank of uni-radial fibers (Figure 7.2b), the maximum sectional area and perimeter of fibers at the interface are

$$A_{int,s} = 2nl_{fb}r_{fb} \quad (7.25a)$$

$$C_{int,s} = 2n(l_{fb} + 2r_{fb}) \quad (7.25b)$$

Since the radius of fibers r_{fb} can typically be taken to be negligible in comparison to the fiber length l_{fb} , i.e. $l_{fb} \gg 2r_{fb}$, therefore, by neglecting the second term on the right side of Eq (7.25b) and by using Eqs (7.25a) and (7.25b) in Eq (7.14), the equivalent capillary radius is determined as

$$R_e = 2r_{fb} \frac{\varepsilon}{1 - \varepsilon} \quad (7.26)$$

Replacing the capillary equivalent radius in Eq (7.13) with this expression yields the following expression for the capillary pressure across fibers

$$P_c = \frac{1 - \varepsilon}{\varepsilon} \frac{\gamma_l \cos(\theta)}{r_{fb}} \quad (7.27)$$

which is identical to the expression suggested and verified for flow across a fiber-bank by Senoguz et al [30], Ahn et al. [31], and Lekakou and Bader [32]²³.

7.3.5 Flow across a Porous Medium Made of Spherical Particles

Some porous substances, such as sand or commercial wicks, can be thought of as composed of spherical particles of different sizes. For an isotropic porous medium composed of compact spherical particles with different radii, we can estimate the averages of interfacial area and perimeter as

$$A_{int,s} = \frac{\frac{4}{3} \pi \int_0^{\infty} r^3 \phi(r) d(r)}{L} \quad (7.28a)$$

²³ Pillai and Advani derived an equation for capillary pressure across a fiber-bank, which is similar to Eq (7.27) but without porosity term in denominator [33]. The reason of such a difference is that they related the capillary pressure to capillary forces through the relation $F_c = P_c A_{int}$, which is perhaps less accurate than Eq (7.10) used here.

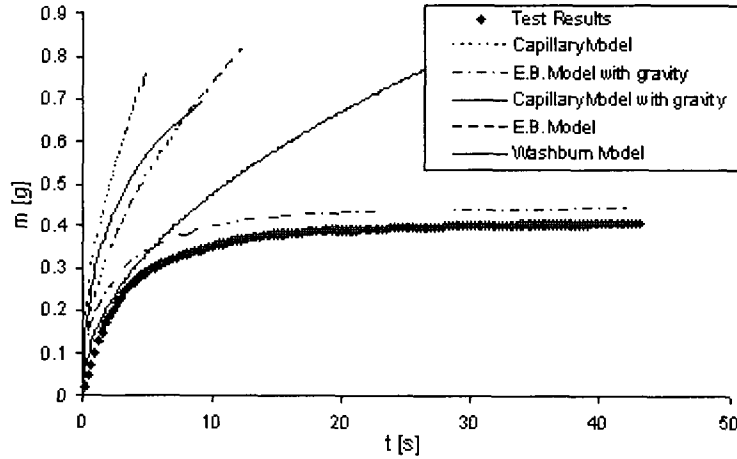


Figure 7.3 Wicking predictions using the Darcy's law and different models for the capillary suction-pressure. The wick was put in contact with a liquid at one end while the other end was connected to a microbalance to measure the weight of the wick changing as a function of time. The E.B. Model with gravity, where the capillary pressure was estimated using Eq (7.34), predicted the best results [16]. The variable m is the absorbed mass in grams and t is time in seconds.

$$C_{m,t,s} = \frac{4\pi \int_0^{\infty} r^2 \phi(r) d(r)}{L} \quad (7.28b)$$

where L is the thickness of the interfacial volume and $\phi(r)$ is the probability density function for radius r , such that

$$\int_0^{\infty} \phi(r) d(r) = 1 \quad (7.29)$$

Note that since a finite number of different radii are often present in a typical porous medium, the use of the probability density function turns the discrete radii into a continuous function and hence we can use the integrals. Using Eqs (7.28a) and (7.28b) in Eq (7.14) gives the equivalent capillary radius as

$$R_e = 2 \frac{r_{sp}}{3} \frac{\varepsilon}{1-\varepsilon} \quad (7.30)$$

where r_{sp} , the effective spherical radius, is obtained from the expression

$$r_{sp} = \frac{\int r^3 \phi(r) d(r)}{\int r^2 \phi(r) d(r)} \quad (7.31)$$

On substituting of Eq (7.30) in Eq (7.13), the capillary-pressure expression changes to

$$P_c = 3 \frac{1 - \varepsilon}{\varepsilon} \frac{\gamma_l \cos(\theta)}{r_{sp}} \quad (7.32)$$

Eq (7.32) is identical to the equation that was derived and experimentally validated for wicking in polymer wicks by Masoodi and Pillai [19] (Figure 7.3). In case all spherical particles have the same radius, then from Eq (7.31), it is clear that r_{sp} is identical to the radius of particles and Eq (7.32) is identical to another expression reported by Dullein [26].

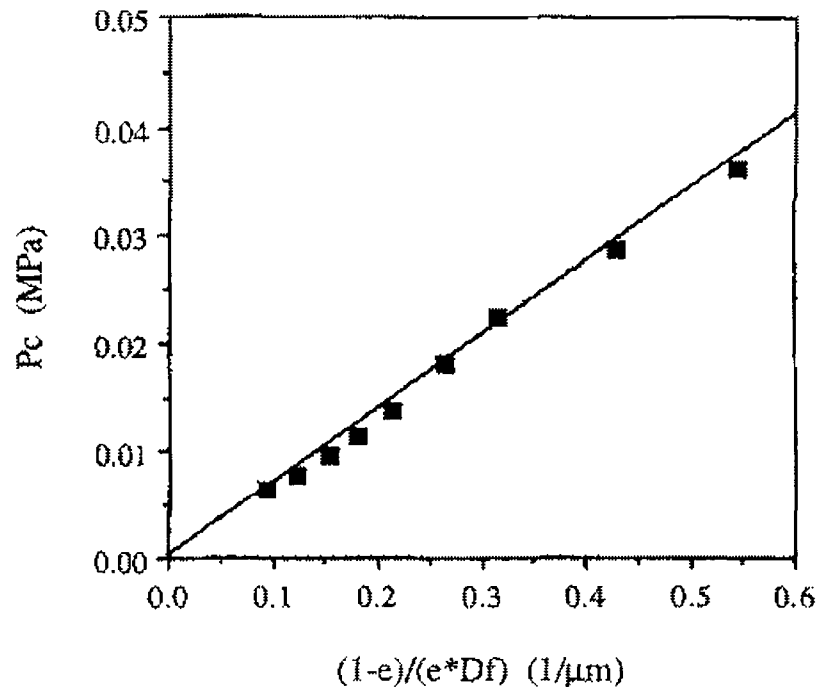


Figure 7.4 A previous experimental study on the estimation of the capillary pressure in woven fiber-mats [31] showed a linear relation between the capillary pressure and $(1 - \varepsilon)/\varepsilon D_f$. Here different types of woven fiber-mats were used to measure the capillary pressure using the method of rising liquid-front.

7.3.6 Flow in Woven Fibermats

Ahn et al. [31] did some flow experiments with a set of woven fabrics and showed that the relation between the capillary pressure and the term $(1-\varepsilon)/(\varepsilon D_f)$ is linear as seen in Figure 7.4. (D_f is the average diameter of fibers.) It proves that Eq (7.14) is valid for woven fiber-mats as well. We expect the equation for the equivalent capillary radius to be similar to Eq (7.26) with a coefficient between 1 and 2 for woven fiber-mats.

7.4 Applications of the Suggested Formula

After the validation of our suggested model, we now show how it can be used in research and industrial applications. In this section, we will briefly describe some applications of the suggested general expression for capillary pressure.

7.4.1 Deriving New Expressions for Capillary Pressure

One of the intended applications of proposed capillary-pressure formula is the derivation of new capillary-pressure expressions for novel kinds of porous media for which we do not have such expressions. Here, we show how the suggested general formula can be applied to derive specific expression for capillary pressure in porous media with complex microstructures.

7.4.1.1 Flow Along Capillary Tubes of Different Radii

Assume a porous medium to be composed of capillary tubes aligned with the flow; if such capillary tubes have a spectrum of discrete radii, then using Eq (7.15), one can find the equivalent capillary radius to be

$$R_e = \frac{\sum n_i \pi r_{c,i}^2}{\sum n_i \pi r_{c,i}} \quad (7.33)$$

where n_i is the number of capillary tubes corresponding to the radius $r_{c,i}$. If we replace the number of capillary radius, n_i , with probability density function $\phi(r)$, then the summation turns into an integration and the equivalent capillary radius can then be expressed as

$$R_e = \frac{\int_0^{\infty} r^2 \phi(r) d(r)}{\int_0^{\infty} r \phi(r) d(r)} \quad (7.34)$$

Note that if the radii of capillary tubes are equal, then Eq (7.34) turns to Eq (7.20).

Use of Eq (7.34) in Eq (7.13) yields a new expression for the capillary pressure that should be effective in a medium made of a range of capillary tubes.

7.4.1.2 Flow Along a Bank of Variable-Radii Fibers

Assume a porous medium to be composed of a bank of fibers of different radii, then using Eq (7.14) and the same methodology that was used for Eq (7.23), we can derive the equivalent capillary radius to be

$$R_e = \frac{\varepsilon \sum n_i \pi r_{fb,i}^2}{1 - \varepsilon \sum n_i \pi r_{fb,i}} \quad (7.35)$$

If we replace the discrete set of radii by a continuous spectrum of radii, then the summation will change to integration and the frequency n_i corresponding to the fiber radius $r_{fb,i}$ will be replaced with a probability density function $\phi(r)$. Consequently the expression for the equivalent capillary-radius will change to

$$R_e = \frac{\varepsilon \int_0^{\infty} r^2 \phi(r) d(r)}{1 - \varepsilon \int_0^{\infty} r \phi(r) d(r)} \quad (7.36)$$

Note that if the radii of all fibers are equal, then Eq (7.36) changes to Eq (7.23).

Use of this expression in Eq (7.13) yields a correspondingly new expression for the capillary pressure.

7.4.1.3 Flow Across a Bank of Variable-Radii Fibers

Assuming the porous medium to be composed of parallel fibers of different radii, we can use Eq (7.14) to derive the equivalent capillary-radius for flow across such a fiber bank as

$$R_e = 2 \frac{\varepsilon}{1 - \varepsilon} \frac{\sum n_i l_{fb} r_{fb,i}}{\sum n_i (l_{fb} + 2r_{fb,i})} \quad (7.37)$$

Once again for $l_{fb} \gg 2r_{fb,i}$ Eq (7.37) can be simplified to

$$R_e = 2 \frac{\varepsilon}{1 - \varepsilon} \frac{\sum n_i r_{fb,i}}{N} \quad (7.38)$$

where $N = \sum n_i$ is the total number of fibers. On using the probability density function, $\phi(r)$, the expression for equivalent capillary radius changes to

$$R_e = 2 \frac{\varepsilon}{1 - \varepsilon} \int_0^{\infty} r \phi(r) d(r) \quad (7.39)$$

Note that if the radii of all fibers are equal, then Eq (7.39) changes to Eq (7.26).

Use of this expression in Eq (7.13) will yield a correspondingly new expression for the capillary pressure.

7.4.2 Using Experimental Measurements to Estimate the Capillary Suction-Pressure

There are some experimental methods, such as the mercury porosimetry, that estimate the pore-size distribution in a porous medium. We can use the relations suggested here, i.e. Eqs (7.33) to (7.39), to use the pore-size distribution for estimating the capillary suction-pressure. We can also use Eq (7.36) or (7.39) to estimate the capillary pressure after using the fiber-radius distribution. One obvious application is the flow through a fiber-bank where one can use the probability density function for fiber radii or the histogram for fiber radii to estimate the equivalent capillary radius, which then leads us to the capillary suction-pressure.

One important application of the developed equation for the equivalent capillary radius is the use of micrographic photos of the porous medium to directly measure the equivalent capillary radius using Eq (7.14) or (7.15). The previous methods were using the radius of the largest sphere that fits the pores [27], the radius of a circle with equivalent area [22, 23], the radius of a circle with equivalent perimeter [24], and the hydraulic radius [25, 26]. Our method based on Eq (7.14) or Eq (7.15) is developed using the energy balance principle. This method proposes a unified approach applicable to any complex porous material that may be significantly inhomogeneous.

7.4.3 Study Changes in the Capillary Suction-Pressure

If we define the significant length-scale in the porous medium at the liquid-gas interface as the ratio of the liquid cross-sectional area and the wetted perimeter, i.e. $\lambda = A_{int} / C_{int}$, then such length-scales of solid particles and void spaces can be expressed as

$$\lambda_s = \frac{A_{int,s}}{C_{int,s}} \quad (7.40a)$$

$$\lambda_v = \frac{A_{int,v}}{C_{int,v}} \quad (7.40b)$$

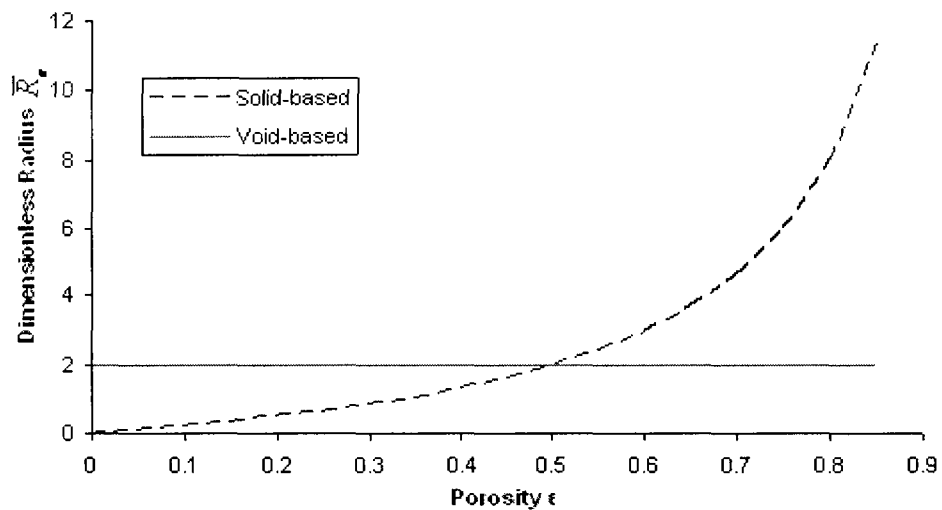
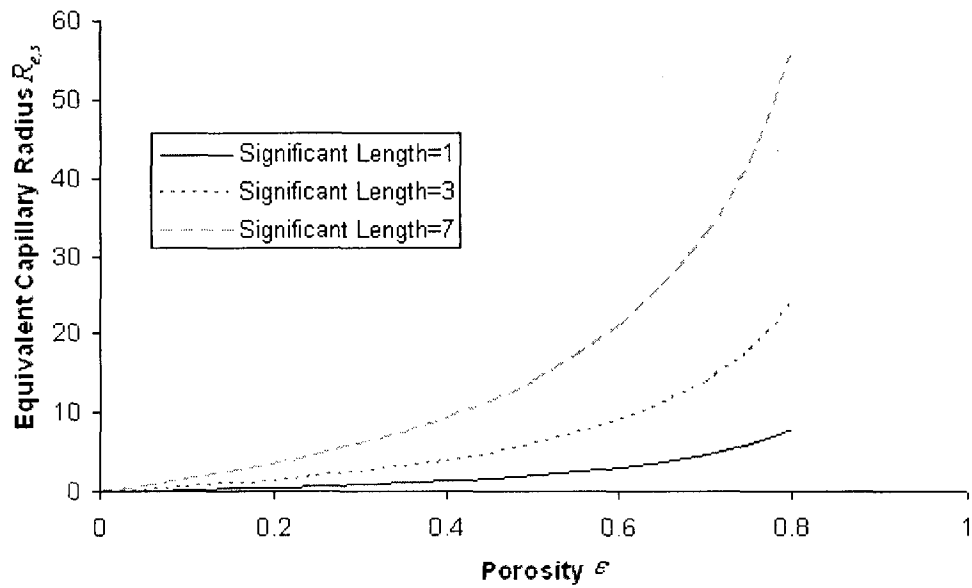
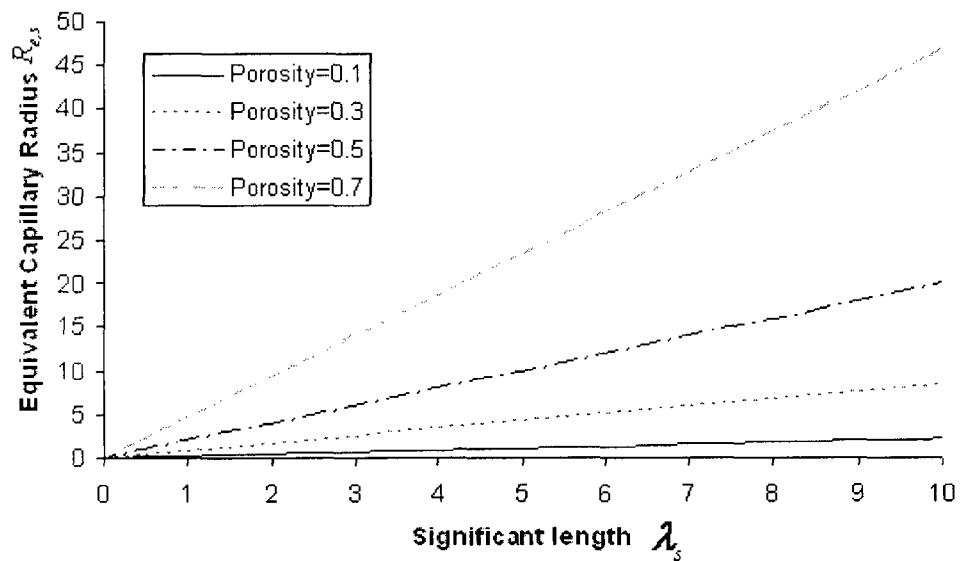


Figure 7.5 Change in the dimension-less capillary radius (\bar{R}_c) with porosity.



a) The porosity is varying while the significant length is kept constant.



b) The significant length is varying while the porosity is kept constant.

Figure 7.6 Changes in the solid-based equivalent capillary radius with the porosity and the solid-based significant length.

A nondimensional capillary radius can be defined as $\bar{R}_e = R_e / \lambda$. Therefore, the solid-based and void-based dimensionless capillary radii are expressible as

$$\bar{R}_{e,s} = \frac{R_e}{\lambda_s} = 2 \frac{\varepsilon}{1-\varepsilon} \quad (7.41a)$$

$$\bar{R}_{e,v} = \frac{R_e}{\lambda_v} = 2 \quad (7.41a)$$

through the use of Eqs (7.14) and (7.15). Figure 7.5 shows how the dimensionless capillary radii vary with porosity. As porosity increases, the solid-based capillary radius increases, while the void-based capillary radius remains a constant. Figures 7.6 and 7.7 show how the equivalent capillary radii (dimensional form) change with the porosity and significant lengths. Figure 7.6a shows that when the solid-based significant length remains a constant, the equivalent capillary radius increases as porosity increases. It also shows that the relative effect of porosity change on the equivalent capillary radius increases as the porosity increases. In the other words, the sensitivity of capillary radius to the porosity increases as the porosity increases. Figure 7.6b shows that when the porosity remains a constant, the equivalent capillary radius increases as the solid-based significant length increases. It also shows that the solid-based significant length linearly affect the capillary radius.

Figure 7.7a displays that when the void-based significant length remains constant, the equivalent capillary radius remains at a fixed value while the porosity increases. Figure 7.7b shows that when the porosity remains constant, the equivalent capillary radius increases linearly with the void-based significant length. For example, if the void-based significant length is 7, then for all porosities the equivalent capillary radius is 14. Both Figures 7.6b and 7.7b indicate that the capillary radius increases with the significant length, which

according to Eq (7.13) leads to a lower capillary pressure. The effect of these changes can be better seen in the dimensionless capillary pressure. If we define a dimensionless capillary pressure as

$$\bar{P}_c = \frac{P_c}{2\gamma_l \cos(\theta) / \lambda} \quad (7.42)$$

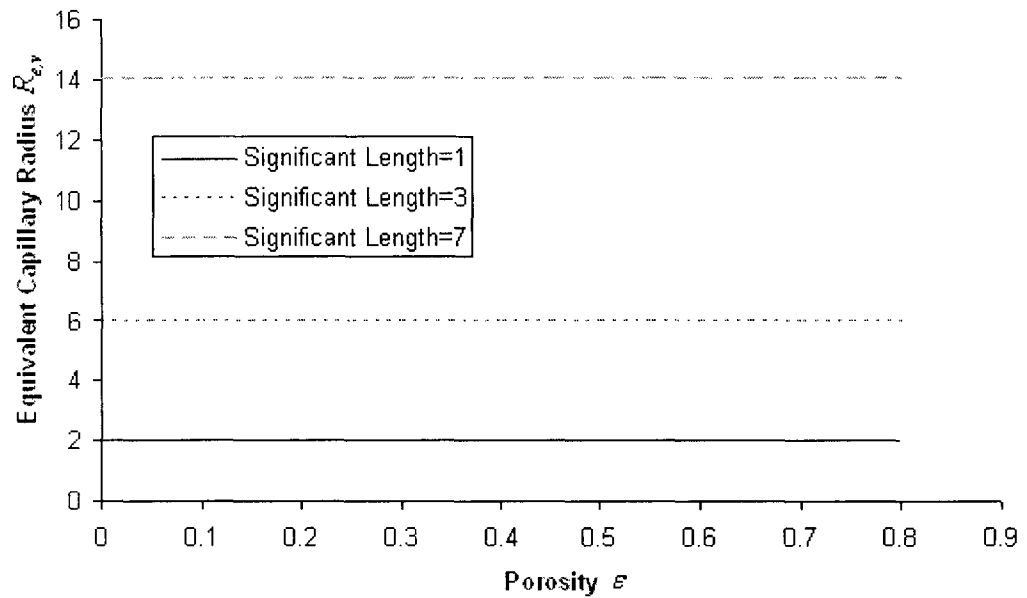
then the solid-based and void-based dimensionless capillary pressures are

$$\bar{P}_{c,s} = \frac{1-\varepsilon}{2\varepsilon} \quad (7.43a)$$

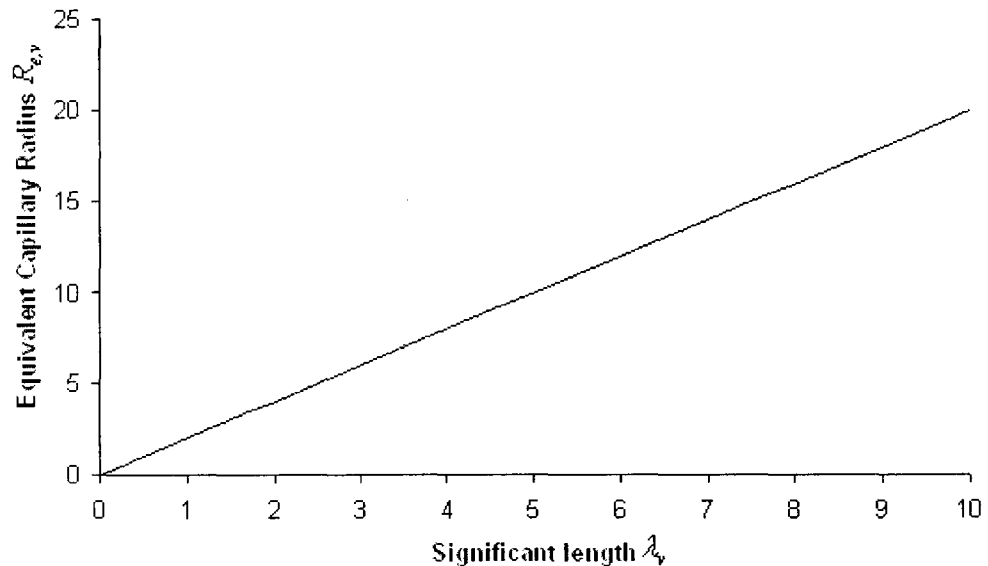
$$\bar{P}_{c,v} = \frac{1}{2} \quad (7.43b)$$

Figure 7.8 displays how these pressures change with porosity: the solid-based capillary pressure decreases as the porosity increases, while the void-based capillary pressure remains a constant. Both values of capillary pressures are identical when the porosity is 0.5. It also shows that for porosities less than 0.5, the solid-based capillary pressure is larger than void-based capillary pressure. For porosities above 0.5, this is opposite, meaning the void-based capillary pressure is the larger one.

In this section, we showed the general forms of the dimensionless capillary pressure and studied its change with porosity. The dimensionless formulation is important as it is a general formula that can be applied to any kind of porous medium. One important potential application of the above formulas for the capillary pressure is in the design of absorbing media or in the estimation of the capillary suction-pressure in porous media.



a) The porosity is varying while the significant length is kept constant.



b) The significant length is varying while the porosity is kept constant.

Figure 7.7 Changes in the void-based equivalent capillary radius with the porosity and the void-based significant length.

For example, assume a vertical wick is being designed to deliver a liquid from a reservoir to the atmosphere. If the size and shape of the beads as well as the wick size are known, then the porosity for the wick is needed to complete the

formulation. Since the length of the wick is known, so the minimum capillary pressure required to raise the liquid to the top of the wick is estimated using $P_c = \rho g l$ where l is the length of the wick. Since bead parameters are known, so λ_s can be calculated using Eq (7.40a), and then one can find \bar{P}_{cs} using Eq (7.42). Finally one can find the required porosity through the use of Eq (7.43a).

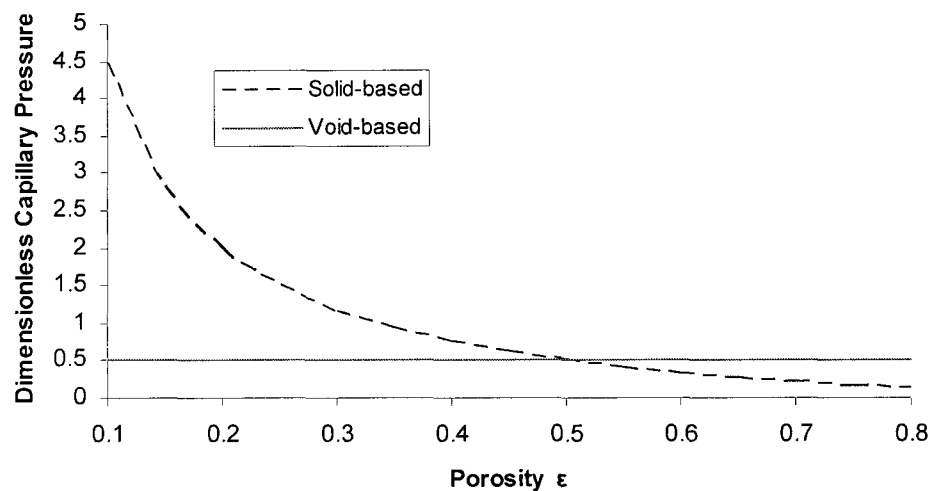


Figure 7.8 The relation between the dimensionless capillary pressure and the porosity.

7.5 Summary and Conclusion

Application of the energy balance principle during the wicking process in a porous medium leads to the development of a general expression for the capillary suction-pressure for porous media flows involving a sharp liquid-air interface or a liquid front. The developed formula for the capillary pressure is studied as a function of the microstructure of the porous medium. To validate the

suggested formula, six different cases from the literature with valid expressions for the capillary suction-pressure were studied. It was shown that the newly suggested formula reduces to the cited expressions for the capillary suction-pressure for the studied cases.

The new proposed equation was also used to derive expressions for the capillary pressure in three different porous media composed of particles or voids with different size distributions. The proposed formula was shown to be applicable to such complex porous media as well. The suggested model was shown to apply to both the homogeneous and inhomogeneous porous media. One important application of the proposed formula is the possibility of using the macrographs of porous media directly to estimate the capillary suction-pressure.

We also studied the dimensionless capillary radius and capillary pressure. It was shown that dimensionless pressure decreases as the porosity and significant length-scale increases. It was also shown that the solid-based dimensionless capillary pressure is a decreasing function of the porosity, while the void-based dimensionless capillary pressure is constant for all kinds of microstructures in porous media. The proposed expression for the capillary pressure can be used to design high-efficiency absorbing materials such as wicks.

References

1. Lucas R., "Rate of Capillary Ascension of Liquids," *Kolloid Z.* 23, 15, 1918
2. Washburn E.V., "The Dynamics of Capillary Flow", *Phys. Rev.* 17, 273, 1921
3. Bear Jacob, "Dynamics of Fluids in Porous Media," Elsevier Science, 1972

4. Robert A. Greenkorn, "Flow Phenomena in Porous Media," Marcel Dekker, New York, 1983
5. S.E. Buckley and M.C. Leverett, "Mechanism of fluid displacements in sands". Transactions of the AIME (146): 107–116, 1942
6. K. M. Pillai and S. G. Advani, "Modeling of Void Migration in Resin Transfer Molding Process", ASME winter meeting, Atlanta (GA), Sep. 1996.
7. Hua Tan, Krishna M. Pillai, "Processing Composites for Blast Protection" In: Blast protection of civil infrastructures and vehicles using composites, edited by N Uddin, Woodhead Publishing limited, Cambridge, 2010.
8. Masoodi, R., Pillai, K.M. and Tan, H., "Darcy's Law Based Numerical Simulation for Modeling 3-D Liquid Absorption into Porous Wicks," Accepted for publication in AIChE Journal.
9. Masoodi, R. and Pillai, K.M., "Darcy's Law based Model for Wicking in Paper-Like Swelling Porous Media," AIChE Journal, Published online, DOI: 10.1002/aic.12163, Jan 20, 2010.
10. Masoodi, R., Pillai, K.M. and Varanasi, P.P., "The Effect of Hydraulic Pressure on the Wicking Rate into the Wipes," Accepted for publication in the Journal of Engineered Fibers and Fabrics.
11. Finn, Robert, "Capillary Surface Interfaces," Notices of the AMS, 46 (7), 770-781, 1999.
12. Berg, J. C. "Wettability," Dekker, New York, 1993
13. Young, T "An essay on the cohesion of fluids. Philos. Trans," R. Soc. London 95, 65-87, 1805.
14. Wen-Bin Young, "Analysis of capillary flows in non-uniform cross-sectional capillaries," Colloids and Surfaces A: Physicochem. Eng. Aspects 234, 12, 2004.
15. Thomas L. Staples and Donna G. Shaffer, "Wicking flow in irregular capillaries," Colloids and Surfaces A: Physicochemical and Engineering Aspects, 204, 1-3, 239-250, 2002
16. William W. Liou a, Yongqing Peng a, Peter E. Parker, "Analytical modeling of capillary flow in tubes of non-uniform cross section," Journal of Colloid and Interface Science 333, 389–399, 2009.
17. Trong Dang-Vu and Jan Hupka, Characterization of Porous Materials by Capillary Rise Method, Physicochemical Problems of Mineral Processing, 39, 47-65, 2005.
18. Masoodi, R., Pillai K.M., and Varanasi P.P., "Role of Hydraulic and Capillary Radii in Improving the Effectiveness of Capillary Model in Wicking," ASME Summer Conference, Jacksonville FL, USA, August 10-14, 2008.

19. Masoodi, R., Pillai, K.M., and Varanasi, P.P., "Darcy's Law based Models for Liquid Absorption in Polymer Wicks," *J. AIChE.* 53, 11, 2769-2782, 2007.
20. Chwastiak S. "A Wicking Method for Measuring Wetting Properties of Carbon Yarn" *J. Colloid Interface Sci.* 42, 298-309, 1973.
21. PK Chatterjee "Absorbency: Amsterdam/New York. Elsevier. 1985
22. Sofien Benltoufa, Faten Fayala, Sassi BenNasrallah, "Capillary Rise in Macro and Micro Pores of Jersey Knitting Structure," *Journal of Engineered Fibers and Fabrics*, 3, 3, 47-54, 2008.
23. Chatterjee P.K. and Gupta B.S., "Absorbent Technology," Amsterdam, Elsevier, 2002
24. Dodson, C. T. J., and W. W. Sampson., "Modeling a Class of Stochastic Porous Media", *Applied Mathematics Letters*, 10 (2), 87 – 89, 1997.
25. D. Rajagopalan, A.P. Aneja, and J.M. Marchal, Modeling Capillary flow in complex geometries, *Textile Res. J.* 71(91), 813-821 2001
26. Dullien F.A.L, "Porous Media: Fluid Transport and Pore Structure," Academic Press, 1992.
27. Lombard, G., Rollin, A., and Wolff, C., Theoretical and Experimental Opening Sizes of Heat-bonded Geotextiles, *Textile Research Journal*, 208, 1989.
28. S.C. Amico and C. Lekakou, Axial Impregnation of a fiber Bundle, Part 2: Theoretical Analysis, *Polymer Composites*, 23, 2, 264-273, 2002.
29. Williams JG, Morris CM and Ennis BC "Liquid Flow Through Aligned Fiber Beds," *Polym. Eng. Sci.* 14(6), 413-419, 1979.
30. M. T. Senoguz, F. D. Dungan, A. M. Sastry and J. T. Klamo "Simulations and Experiments on Low-Pressure Permeation of Fabrics: Part II—The Variable Gap Model and Prediction of Permeability" *Journal of Composite Materials*, 35,. 14, 1285-1322, 2001.
31. Ahn, K.J., Seferis, J.C. and Berg, J.C. "Simultaneous measurements of permeability and capillary pressure of thermo setting matrices in woven fabric reinforcements. *Polymer Composites*, 12 (3) 146-152, 1991.
32. C. Lekakou and M.G. Bader, Mathematical modeling of macro and micro infiltration in resin transfer moulding (RTM), *Composites Part A* 29A, 29-37, 1998.
33. KM Pillai and SG Advani .Wicking Across a Fiber-Bank. *J. Colloid and Interface Sci.* 183, 100-110, 1996.
34. H. S. Kim and B. Pourdeyhimi, In-Plane Liquid Distribution in Nonwoven Fabrics: Part 2 Simulation, *Int. Nonwoven J.* 12(2), 29-33, 2003.
35. Hassanizadeh, S.M and W.G. Gray, "Thermodynamic basis of capillary pressure in porous media," *Water Resour. Res.*, 29, 3389-3405, 1993.

Chapter 8

FLOW MODELING IN NATURAL-FIBER PREFORMS USED IN LIQUID COMPOSITE MOLDING

8.1 Imbibition

Polymer composite materials are replacing many of old conventional materials nowadays. Fiber-reinforced composite polymers have several advantages over conventional materials, such as low weight, low cost, and easy processing. In recent years, many researchers started investigating using natural fibers instead of inorganic common reinforcement fibers [1]. Natural fibers have some advantages over synthetic fibers such as lower cost, acceptable properties, lighter weight and recyclability [2].

Liquid Composite Molding (LCM), especially Resin Transfer Molding (RTM) which involves injecting a liquid resin into a closed mold containing compressed reinforcing material, is a common method used by engineers in producing natural-fiber reinforced thermosets [1]. The application of Jute fibers as reinforcement was studied by Rowell et. al. [3] and O'Dell [4], where they showed that jute composite can be used in a large number of applications.

The modeling of liquid flow in RTM has been studied by several researchers [5, 6]. One of the important parameters in RTM flow modeling is permeability, which is a tensor and is measured using 1-D and radial flow methods [7, 8]. Studies have showed plant fibers such as jute can swell in liquids by about 22%

of the initial fiber volume [9]. The swelling phenomenon adds another difficulty to the permeability measurements. The previous studies on liquid modeling through jute fiber reinforcement composites assumed that the permeability remains constant during the mold-filling process while ignoring liquid absorption and swelling [10-13].

As shown above, nobody has studied the liquid transport in jute fibers after incorporating the fiber swelling phenomenon. We have suggested a model for permeability that worked for modeling the liquid flow in cellulose based swelling materials [14]. The suggested variable permeability model worked well for the wicking predictions in such media. Here we apply the same approach to model the liquid flow in swelling natural-fiber reinforcements. We assume a simple function for permeability and show how it improves the flow modeling, when used with a swelling-causing liquid. We have used two liquids, where one leads to swelling while the other does not affect the fiber diameters. This preliminary study shows that with some assumptions one can estimate the changes in permeability with time and use the estimated function to improve the liquid flow modeling in LCM involving natural fibers.

8.2 Mathematical Theory

8.2.1 Flow Modeling in Rigid Porous Media

The single-phase flow in an isotropic and rigid porous medium is governed by Darcy's law and the continuity equation of the form

$$V = -\frac{K}{\mu} \nabla P \quad (8.1)$$

$$\nabla \cdot \mathbf{V} = 0 \quad (8.2)$$

where \mathbf{V} and P are volume-averaged liquid velocity and pore-averaged pressure, respectively [15]. It is shown that in the case of a one-dimensional flow in a medium with constant permeability and with a constant driving pressure in the form of a steady inlet-pressure, the combination of Eqs (8.1) and (8.2) leads to an equation for liquid-front location in a 1-D flow mold [16] of the form

$$X_f = \sqrt{\frac{2 K P_{in} t}{\varepsilon_0 \mu}} \quad (8.3)$$

where X_f is the x coordinate of liquid front, ε_0 is the initial porosity (which is a constant here), and P_{in} is the constant inlet-pressure.

8.2.2 Flow Modeling in Non-Rigid, Swelling, Porous Media

For a non-rigid, swelling porous-medium, Eq. (8.2), the continuity equation, is modified to the following form to include structural change due to swelling as well as the sink or source effects due to liquid absorption [14].

$$\nabla \cdot \mathbf{V} = -S - \frac{\partial \varepsilon}{\partial t} \quad (8.4)$$

As was proposed in Ref [14], we assume S to be linearly proportional to $\frac{dv_f}{dt}$, i.e.,

$$S = b \frac{dv_f}{dt} \quad (8.5)$$

The coefficient b , which we called the absorption coefficient, must fall in the range $0 \leq b \leq 1$. Combining Eqs. (8.1) and (8.4) after employing Eq. (8.5) for the

sink (suction of liquid into fibers) term leads to following analytical relation for liquid front [14]:

$$X_f = \sqrt{\frac{2P_{in}}{\varepsilon_0\mu} e^{(b-1)\frac{\varepsilon}{\varepsilon_0}} \int_0^t e^{(1-b)\frac{\varepsilon}{\varepsilon_0}} K(t') dt'} \quad (8.6)$$

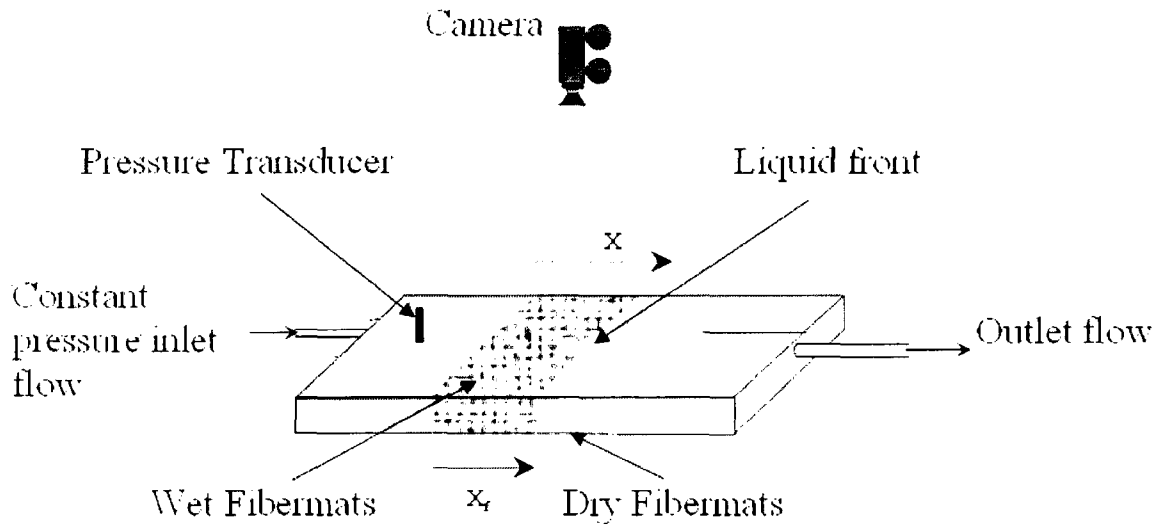
The details of derivation Eq (8.6) are in Ref [14]. (Note that in deriving Eq (8.6), the pressure drop driving the flow came from the inlet pressure P_{in} ; while deriving a similar expression in Ref [14], the pressure drop driving the wicking flow came from the suction pressure induced at the flow-front. In the present derivation, the suction pressure is ignored due to its much smaller magnitude compared to the inlet pressure.)

For the special case of $b = 1$, when the swelling rate of fibers matches the volumetric absorption rate into the fibers, the relation (8.6) simplifies to

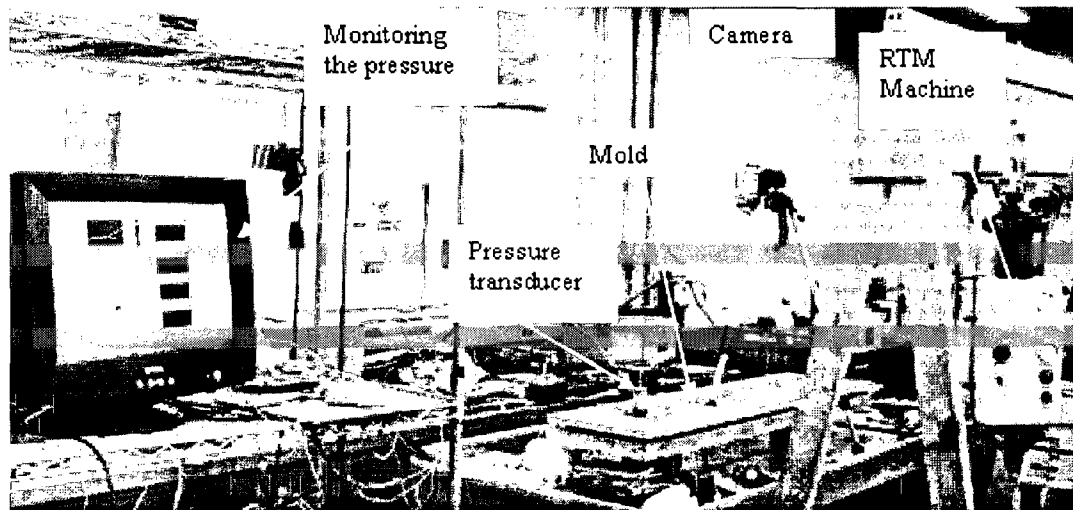
$$X_f = \sqrt{\frac{2P_{in}}{\varepsilon_0\mu} \int_0^t K(t') dt'} \quad (8.7)$$

Note that Eq. (8.7) was used in our predictions. Note that in the case of having a constant permeability in fiber preform, Eq. (8.7) reduces to Eq. (8.3). Our main assumptions in deriving Eq. (8.6) are as follows:

1. The absorption rate of liquid by fiber mats is linearly proportional to the rate of change of fiber volume fraction, i.e. Eq. (8.5).
2. The porosity and permeability are considered to be constant through out the whole wet fibermats and are only function of time, i.e. $\varepsilon = \varepsilon(t)$, $K=K(t)$.
3. The effect of gravity on the liquid transport is neglected.



a) A schematic of the 1-D flow test setup.



b) A photo of the test setup.

Figure 8.1 The experimental setup used for permeability measurement and liquid front tracking during 1-D flow in a flat RTM mold.

8.3 Experimental Study

In our experimental study, we have used a common 1-D flow test setup and a RTM machine (Figure 1). The RTM machine was a Hypaject model MK1 that

was connected to a shop air source of 6 bars. Both test liquids were drawn into the machine, and then injected into the mold at a constant pressure. The RTM machine had the possibility to set the injection pressure to a desired constant pressure. Reinforcement for the experiment consisted of sections of jute gunny bags obtained as waste from a coffee shop. As shown in Figure 8.1, several layers of jute fiber mats were stacked in the middle of the flow channel to create a fiber preform. The flow with constant pressure enters the front area of the mold and moves through the fiber mats. A transducer is used to record the pressure of liquid entering the fiber preform. A camera placed on top of the transparent top-plate of the mold is used to track the liquid-front location; so we were able to record the liquid-front location as a function of time by reviewing the movies.

We have used two different liquids in our tests—motor oil and diluted corn syrup. The jute fibers do not swell in motor oil while they swell in diluted corn syrup. Our effort is to show how we can theoretically predict liquid-front location in case of using a swelling-causing liquid. The reason for using diluted corn-syrup is to match the viscosity of the syrup with that of the motor oil (which is similar to that of a thermosetting resin used in RTM) while at the same time having the fiber-swelling property. The viscosity of motor oil at the test temperature was found to be 245 mPa.s; in order to reach this viscosity, we had to add water to the corn syrup such that 20% of the final solution was water.

8.3.1 Measuring the Porosity and Permeability

Porosity is the ratio of void volume to the whole volume of the compressed fiber-preform. The importance of porosity is that it indicates the percent of the mold volume that should be filled by resin. We measured the porosity of the mold volume that should be filled by resin. We measured the porosity of the preform when the mold was stacked with the fibermats. One layer of jute fiber mat with known dimensions was inserted into a burette filled with a known volume of motor oil. The difference between the volume before and after inserting the material was measured (see Figure 8.2). Since the number of layers in the mold is known, the total volume of the jute fibers can thus be computed and the overall porosity can be estimated. We used 8 layers of jute fiber-mats in the mold to obtain a preform porosity of 0.5 for our tests.

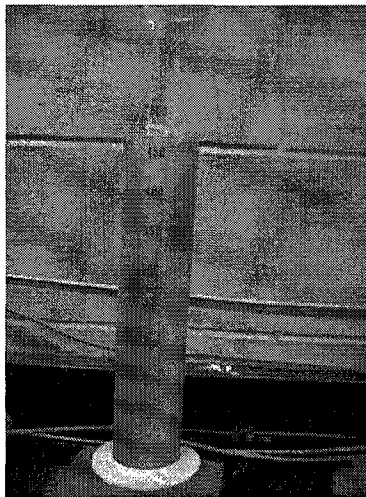


Figure 8.2. Estimation of fiber volume (which is used later to measure porosity) by measuring the difference in liquid volumes in a graduated cylinder before and after the submergence of fiber mats.

Since jute fibers do not swell in motor oil, so the permeability of jute layers should remain constant during 1-D tests with the oil. We measured the inlet

pressure and volume flow-rate of the passing liquid under steady-state conditions, and then the permeability was measured by using the following relation for steady-flow:

$$K_0 = \frac{Q\mu L_f}{AP_{in}} \quad (8.8)$$

The reason for using the subscript zero for permeability in this measurement is that K_0 is also equal to the initial ($t=0$) permeability for the case with diluted corn-syrup, a swelling-causing liquid. In the case of using diluted corn syrup, we estimated the permeability right after the liquid-front has reached the end of fiber preform length, L_f at time t_{end} . If we name this permeability to be K_{end} , we can then estimate it as

$$K_{end} = \frac{Q\mu L_f}{AP_{in}} \quad (8.9)$$

In this estimation, we assumed steady-state flow conditions, and neglected the effect of liquid absorption on the overall flow-rate Q during the transient mold-filling process.

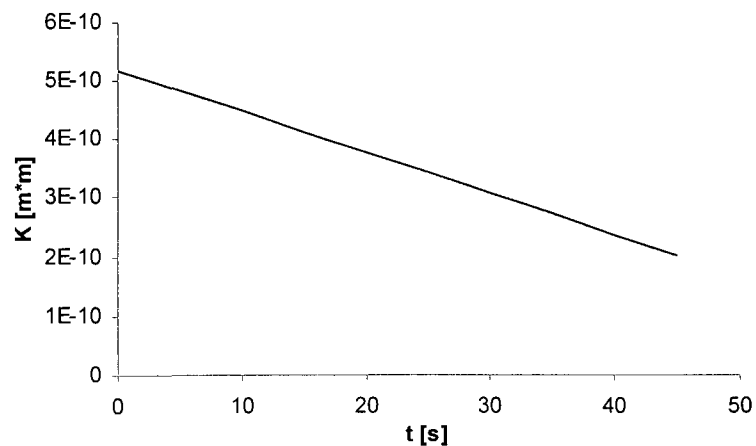


Figure 8.3 The permeability change predicted by Eq (8.10).

Note that in Eq. (8.8), we used motor oil, while in using Eq. (8.9), we used the diluted corn syrup. Since we need to have permeability as a function of time to be able to use Eq. (8.7), here we simply assumed the permeability to be a linear function of time, i.e. $K = C_1 + C_2t$. We can use the values of the measured K_0 , K_{end} , and t_{end} to find the constants in this permeability function. Therefore, the final relation for permeability is

$$K(t) = K_0 + \frac{K_{\text{end}} - K_0}{t_{\text{end}}} t \quad (8.10)$$

The measured values for K_0 , K_{end} , and t_{end} are $4.816 \text{ e-}10 \text{ m}$, $2.51\text{e-}10 \text{ m}$, and 44 s . Figure 8.3 shows how the permeability is assumed to change linearly based on Eq. (8.10) and above-motioned measured values.

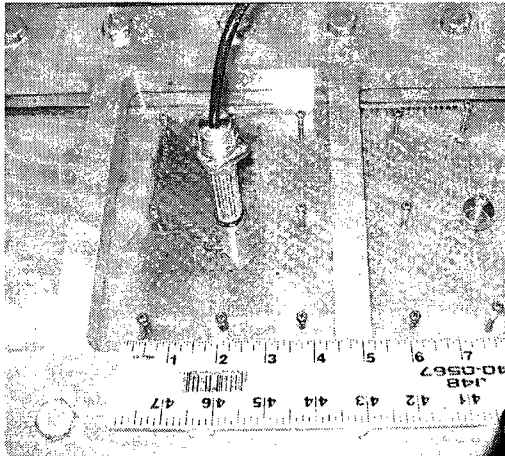


Figure 8.4 Estimation of liquid-front location in jute fiber mats during 1-D flow in the test setup.

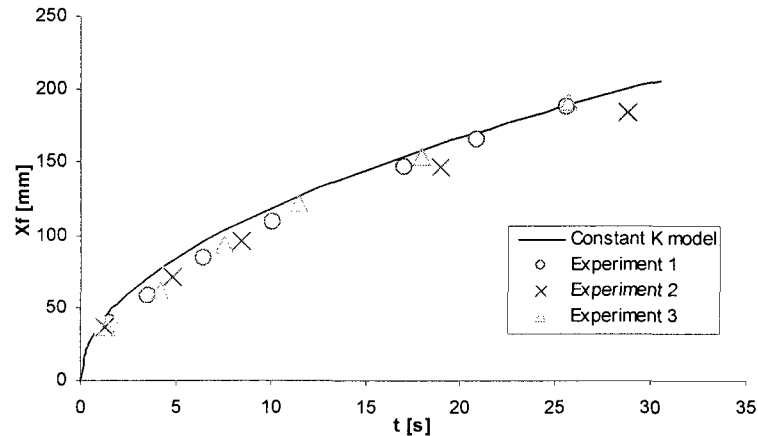


Figure 8.5 A comparison of the theoretical prediction of liquid-front location as a function of time with the experimental observations for the case of using motor oil as test liquid in the absence of fiber swelling.

8.3.2 Measuring the Liquid-Front Position

The liquid-front tracking was done by reviewing the recorded movies. We had used a scale alongside the fiber mats in the flow mold (Figure 8.4), and by comparing the liquid-front location with the scale we were able to find the x coordinate (along the flow direction) of the liquid front at each time. (A stop watch was used to keep time which was filmed along with the liquid front in the movie.)

8.4 Results and Discussion

The theoretical prediction of the liquid-front position for the case of using motor oil as a test liquid (which does not induce swelling in jute fibers) is shown in Figure 8.5; it indicates a very good predictions. However, there are some variations as the time passes, but the predictions are still very good. The plausible reason for some variations and differences could be uneven nature of

flow front (Figure 8.4) related to 1) inherent inhomogeneity in the jute mats, and 2) slight differences in the structure of the fiber mats used in various layers.

Figure 8.6 shows the difference between predictions of the constant permeability model, Eq. (8.3), and the variable permeability model, Eq. (8.7). In the beginning, both the models behave in an identical manner; but as the time passes, the new model predictions are lower than that of the fixed permeability model. As the front progresses, fibers swell and the permeability decreases, and one can expect a deceleration of front—this is what is shown by the variable permeability model.

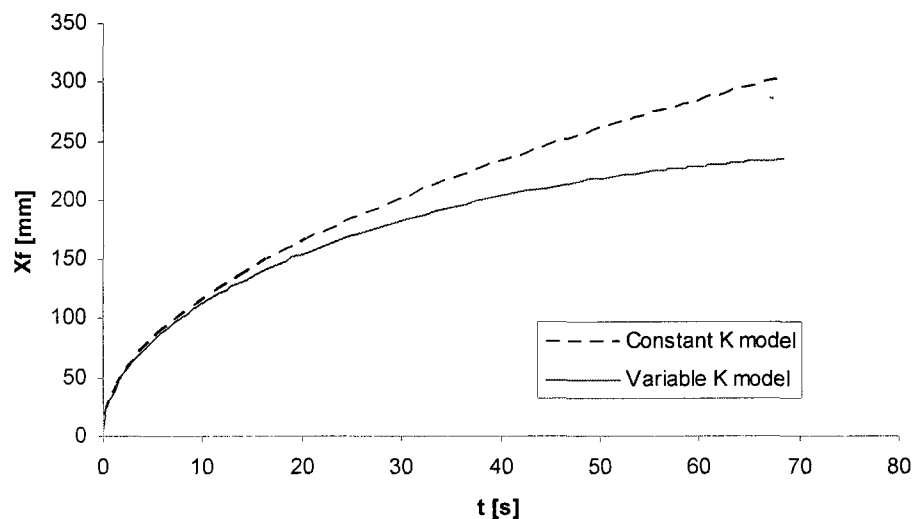


Figure 8.6. A comparison of theoretical predictions for the cases of non-swelling and swelling fibers using the constant and variable K models, respectively.

The variable permeability model is compared with the experimental results in Figure 8.7. It shows that the predictions are in general quite accurate—although there is some inaccuracy initially, but this difference decreases with time. It also observed that predictions of the fixed K model are a little higher than the

experimental data, while predictions of the variable K model are closer to the experimental data and hence more accurate.

We would like to comment on the observed difference between predictions and experiments in the beginning in Figure 8.7—note that the differences decrease with time. The reason is that though we assumed the pressure to remain constant throughout the experiment, it was not constant in the beginning of our experiments—the injection pressure was observed to be less than the desired pressure due to a limitation of our injection setup. This led to higher theoretical predictions vis-a-vis the experimental data.

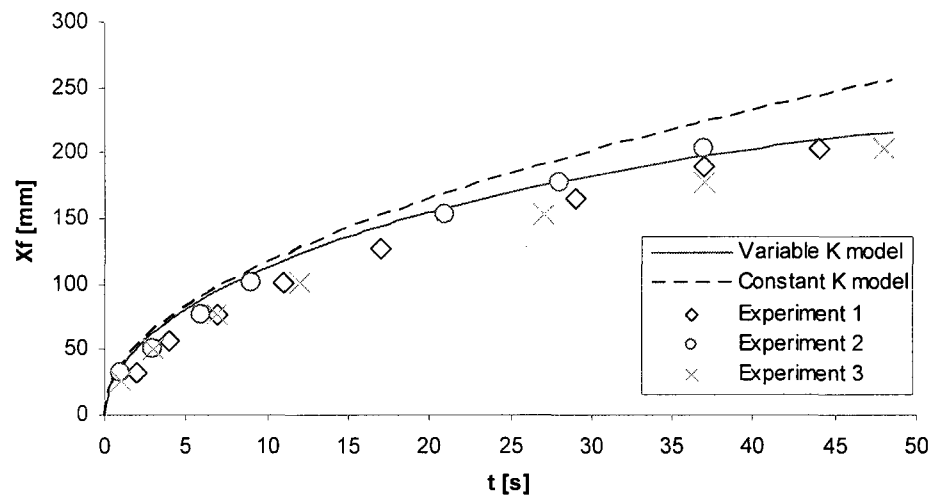


Figure 8.7. A comparison of the theoretical prediction of liquid-front location as a function of time with the experimental observations for the case of using diluted corn-syrup as test liquid which is accompanied by fiber swelling.

The variable K model, which has been proven to be quite accurate, assumes a simple, linear variation of permeability with time. Because of its simplicity, we did not expect it to have very accurate results; however, we were pleasantly

surprised as it was shown to be quite accurate. Note that the two constants in the linear model were easy to estimate through the use of just two experimentally-obtained permeability values. If we had used a more complex higher-degree model, we would have needed many more permeability values to find its coefficients which in turn would have rendered it less practical.

It is to be noted that in our variable K model, we assumed the porosity and permeability to be functions of time only. However, to be precise, they will be a function of both time and space. In such a situation, one will have to employ an RTM mold-filling simulation to solve Eqs. (8.1) and (8.4) together to predict liquid flow in our 1-D mold. So our analytical 'variable K' model precludes the need for such a simulation after adopting some simplifying assumptions.

8.5 Summary and Conclusion

The one dimensional flow of test liquids is successfully studied through a bed of jute fibers. Two different test liquids, the motor oil and water-diluted corn syrup, were used in the 1-D, constant injection-pressure experiment. The latter induced a swelling in the jute fibers while the former did not cause any change. The constant permeability model was obtained after assuming the permeability to be a constant and using the traditional mass-balance equation. The variable permeability model was obtained after assuming the permeability to be decreasing linearly with time and using the modified mass-balance equation after including the effects of liquid absorption and fiber swelling. The constant permeability model was found to be quite acceptable for the flow of motor oil, a

swelling inhibiting liquid. However the variable permeability model was found to be more accurate for the flow of water-diluted corn syrup, a swelling inducing liquid. However, further experiments with a more reliable injection-pressure setup are needed for further validation of these conclusions.

References

1. R. Umer a, S. Bickerton a, A. Fernyhough. 2007. "Wood Fiber mats as Reinforcements for Thermosets" in Handbook of Engineering Biopolymers, Fakirov S. and Bhattacharyya D. eds. Munich: Hanser Gardner, pp. 693-713
2. Joshi S.V., Drzal L.T., Mohanty A.K., and Arora S. 2004. "Are natural fiber composites environmentally superior to glass fiber reinforced composites", Composites: Part A, 35: 371-376.
3. Roger Rowell, Jane O'Dell, R. K. Basak, and M. Sarkar, 1997, "Applications of Jute in Resin Transfer Molding", www.fpl.fs.fed.us/documnts/pdf1997/rowel97h.pdf
4. Jane L. O'Dell, 1997, "Natural Fibers in Resin Transfer Molded Composites", www.fpl.fs.fed.us/documnts/pdf1997/odell97b.pdf
5. Tucker CL, Dessenberger RB. 1994. "Governing equation for flow and heat transfer in stationary fiber beds", in Flow and Rheology in Polymer Composites Manufacturing, Advani SG, ed. Amsterdam: Elsevier, pp. 257-323
6. Hua Tan and Krishna M. Pillai. 2010 "Processing composites for blast protection", in Blast protection of civil infrastructures and vehicles using composites, N Uddin, ed. Cambridge, Woodhead, (in press).
7. Tonmoy Roy, Hua Tan and Krishna M. Pillai. 2007 "A method to estimate the accuracy of 1-D flow based permeability measuring devices," Journal of Composite Materials, , 41(17): 2037-2055.
8. Hua Tan and Krishna M. Pillai, 2009 "A method to estimate the accuracy of radial flow based permeability measuring devices," Journal of Composite Materials (In press)
9. Roger M. Rowell and Harry P. Stout, 1998, "Jute and Kenaf," www.fpl.fs.fed.us/documnts/pdf1998/rowel98e.pdf
10. L. Nilsson and S. Stenstrom. 1997, "A Study of the Permeability of Pulp and Paper," Int. J. Multiphase Flow, 23(1): 131-153

11. R. Umer a, S. Bickerton a, A. Fernyhough. 2007, "Characterizing wood fiber mats as reinforcements for liquid composite molding processes", *Composites: Part A*, 38: 434–448
12. R. Umer a, S. Bickerton a, A. Fernyhough. 2008, "Modeling the application of wood fiber reinforcements within liquid composite molding processes," *Composites: Part A*, 39: 624–639
13. Rodriguez E, Giacomeilli F and Vazquez A. 2004, "Permeability-Porosity Relationship in RTM for Different Fiberglass and Natural Reinforcements", *J. Com. Mat.* 38(3): 259-268.
14. R. Masoodi, Krishna M. Pillai. 2009, "Darcy Model for Wicking in Paper-Like Swelling Porous Media", a manuscript submitted to *AIChE* journal.
15. Whitaker, Stephen, 1998, *The Method of Volume Averaging*, Springer, pp. 161-177
16. Masoodi R., Pillai K.M., and Varanasi P.P. 2007, "Darcy's Law based Models for Liquid Absorption in Polymer Wicks," *J. AIChE.*, 53(11): 2769-2782

Chapter 9

DARCY'S LAW BASED NUMERICAL SIMULATION FOR MODELING 2-D LIQUID ABSORPTION INTO PAPER-LIKE SWELLING POROUS MEDIA

9.1 Introduction

In chapter 6, a method to improve the predictions of liquid absorption in paper-like swelling porous media was presented where the Darcy's law and continuity equation were used as the governing equations [1]. The continuity equation was modified to include the effects of swelling and liquid absorption in the form of two right-hand-side terms for the rate of porosity change and a sink effect [2]. The global values for permeability throughout the wetted porous medium were considered, while neglecting the local variations. Neglecting spatial dependence in the permeability and porosity simplified the governing equation and turned it into an ordinary differential equation that could be solved analytically. However, this assumption, though it simplifies the wicking model, reduces the accuracy of the model.

Another approach is the use of Locus-Washburn (or Washburn) equation, which may apply for simple 1-D geometries [3,4]. The swelling effect leads to an error if the conventional Locus-Washburn equation is employed to predict the wicking rate in swelling porous media [5]. Therefore Schuchardt and Berg [6] modified the Locus-Washburn equation for application in some swelling materials

where they assumed the pore radii in a swelling porous medium to decrease linearly with time, as a result of the swelling. However, as observed in the experimental study published by Wiryana and Berg [7], this assumption is not accurate sometimes.

In general, the Darcy's law based approach is the better approach as it can be extended to 2-D and 3-D flows [8,9]. However, in the case of complex geometries, the analytical solution of the governing equations may not be possible. Another advantage of the Darcy's law based approach is the possibility of employing numerical simulations for predicting wicking in complex geometries. Among the different numerical methods, the finite element method has been extensively employed for modeling flows in porous media [10]. There are several commercial softwares that can model fluid flow in porous media using FEM, such as COMSOL and ANSYS; these software can easily model saturated single-phase flows in simple rigid porous substances, but none of them can incorporate the swelling effects in the flow model. Therefore, they can not model flows in non-rigid porous media such as superabsorbent polymers, cellulose fibers, and paper napkins.

In this chapter, we are going to model a two-dimensional liquid flow in a porous network of cellulose fibers and powdered superabsorbents. PORE-FLOW[®], a computer program developed in the Laboratory for Flow and Transport Studies in Porous Media at the University of Wisconsin-Milwaukee [11], is employed to solve the governing equations. PORE-FLOW[®] is a comprehensive computational fluid dynamics (CFD) tool focused primarily on solving the flow

infiltration/wetting of porous media type problems. The Finite Element/Control Volume (FE/CV) method is implemented in the code to simulate single-phase flow behind a clearly observable moving-boundary. The algorithm is efficient and robust for solving the moving-boundary problems in complex domain geometries. We will show how to estimate the local permeability of swelling matrix, which assumed to be identical to the permeability of each element in the FE/CV simulation. The estimated function for the permeability will be used to predict the absorption rate in the swelling porous medium using PORE-FLOW[®]; the comparison of the numerical predictions and experimental results indicates a rather good accuracy in the predictions. Later, we will suggest some ways of improving the permeability estimation in order to increase the accuracy of numerical predictions.

9.2 Experimental Study

This research is based on a experimental study conducted at the University of Washington where Wiryana and Berg [7] studied experimentally the wicking of water into paper strips consisting of cellulose fibers and different proportions of powdered carboxymethyl cellulose (CMC) superabsorbent. They used four different weight percentages of CMC (0%, 10%, 20%, and 30%) in the paper stripes used in the wicking tests. In order to see the swelling effect, they studied wicking with two different liquids: n-Octane, as the reference non-swelling

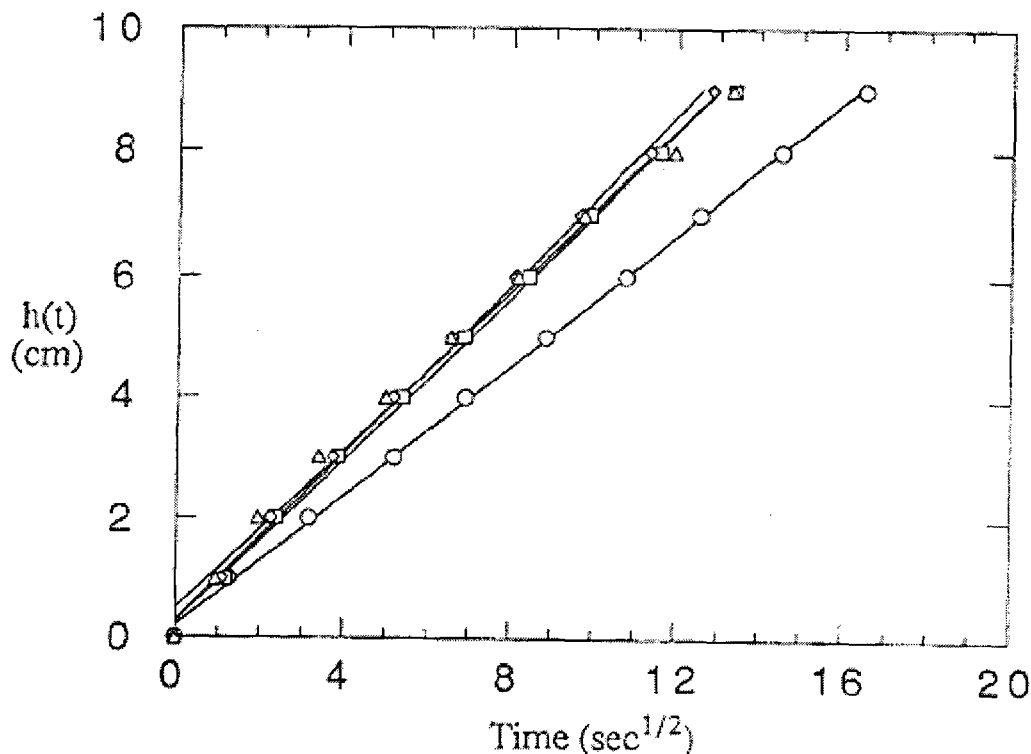


Figure 9.1 Wicking distance vs. time for n-Octane. (○) 0% CMC; (□) 10% CMC; (◇) 20% CMC; (△) 30% CMC [7]

liquid, and water, as the swelling liquid²⁴. The experiments showed no swelling in the matrix material with n-Octane while there was swelling with water. They also observed that the swelling rate increased with the percentage of CMC. Figure 9.1 shows their wicking test results with n-Octane—the linearity of the curves prove that there is no swelling with n-Octane. Figure 9.2 shows the same test with water—here the wicking curves clearly deviated from the linear pattern. This deviation increases as the percentage of CMC increases. (Increasing the CMC percentage means increasing the percentage of the superabsorbent material, which swell rapidly when put in contact with water-based liquids.)

²⁴ The term swelling liquid means that the liquid induces swelling in the considered porous material.

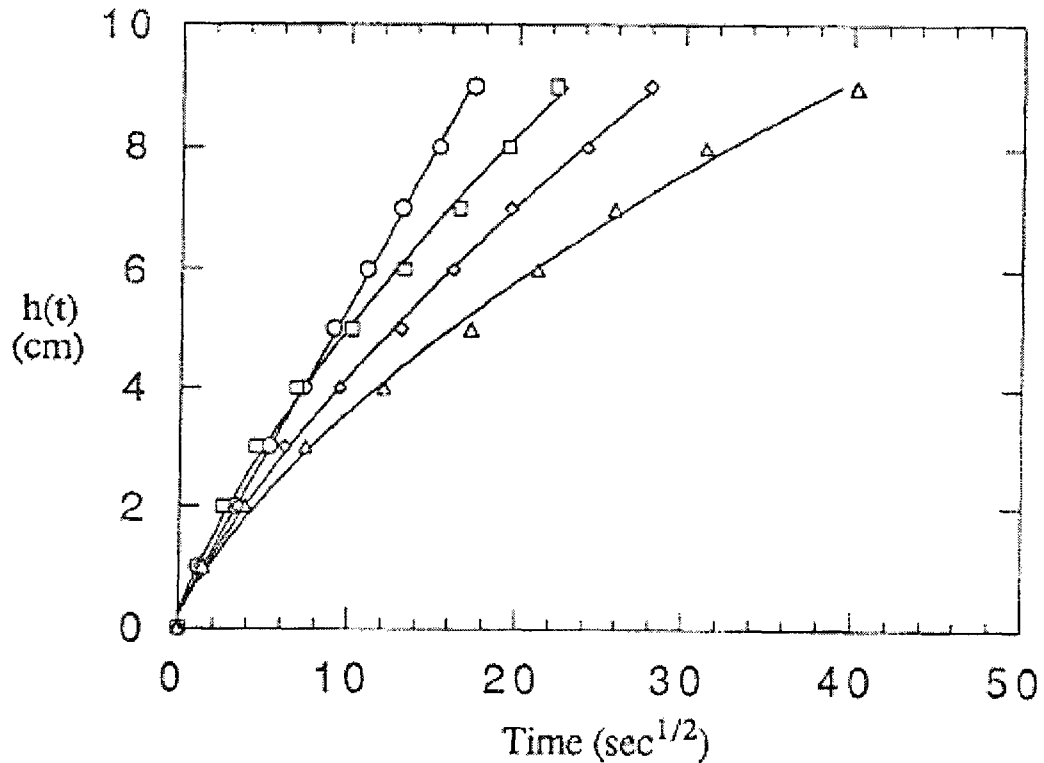


Figure 9.2 Wicking distance vs. time for water. (○) 0% CMC; (□) 10% CMC; (◇) 20% CMC; (△) 30% CMC [7]

9.3 Theory of Wicking

We assumed that there is a clear liquid-front during wicking in the test material. Hence we applied the Darcy's law based model to predict the single-phase flow behind the liquid front. As we discussed in Chapter 1, the Darcy's law, for the flow of a single liquid in an isotropic porous medium under isothermal conditions is

$$\langle \vec{V} \rangle = -\frac{K}{\mu} \vec{\nabla} \langle P \rangle^f \quad (9.1)$$

where $\langle \vec{V} \rangle$ and $\langle P \rangle^f$ are the volume-averaged liquid velocity and the pore-averaged modified pressure, respectively. K is the permeability of the porous

medium while μ is the liquid viscosity. Note that in general the permeability is a function of both time and space in swelling materials. The other governing equation for the flow of an incompressible liquid in a porous medium is the macroscopic continuity or mass-balance equation. It was shown in Chapter 6 that the modified continuity equation for swelling porous media is

$$\bar{\nabla} \cdot \langle \vec{V} \rangle = -S - \frac{\partial \varepsilon}{\partial t} \quad (9.2)$$

where S is the sink term and ε is the porosity. It was shown that the sink term and the porosity are related to each other, and so the above equation was simplified to

$$\bar{\nabla} \cdot \langle \vec{V} \rangle = (b - 1) \frac{\partial \varepsilon}{\partial t} \quad (9.3)$$

It was shown in chapter 6 that b , *the absorption coefficient*, is very close to one [2], so we assume $b=1$ here (i.e., the volumetric rate of liquid absorption is equal to the volumetric rate of matrix expansion). As a result, the continuity equation simplifies to

$$\bar{\nabla} \cdot \langle \vec{V} \rangle = 0 \quad (9.4)$$

If the liquid viscosity is considered to be a constant, then a combination of Eq. (9.1) with Eq. (9.4) leads to the following equation for the modified pressure:

$$\bar{\nabla} \cdot (K \bar{\nabla} \langle P \rangle^f) = 0 \quad (9.5)$$

Based on Figure 9.3, the pressure boundary-conditions can be expressed as

$$\langle P \rangle^f (x = 0) = p_{atm} \quad (9.6a)$$

$$\langle P \rangle^f (x = L_f) = p_{atm} - p_c + \rho g L_f \quad (9.6b)$$

The relation between the front speed and the volume-averaged liquid velocity [12] is

$$\bar{v}_f = \frac{\langle V \rangle}{\varepsilon} \quad (9.7)$$

On solving Eq (9.5), the pressure field is determined, and then the application of Eq (9.1) along with Eq (9.7) gives the liquid-front velocity. Knowing the liquid front velocity, one can find the liquid-front location. Since permeability is a function of both time and space in swelling porous materials, so finding an analytical solution for Eq (9.5) is very difficult and hence numerical solutions are needed.

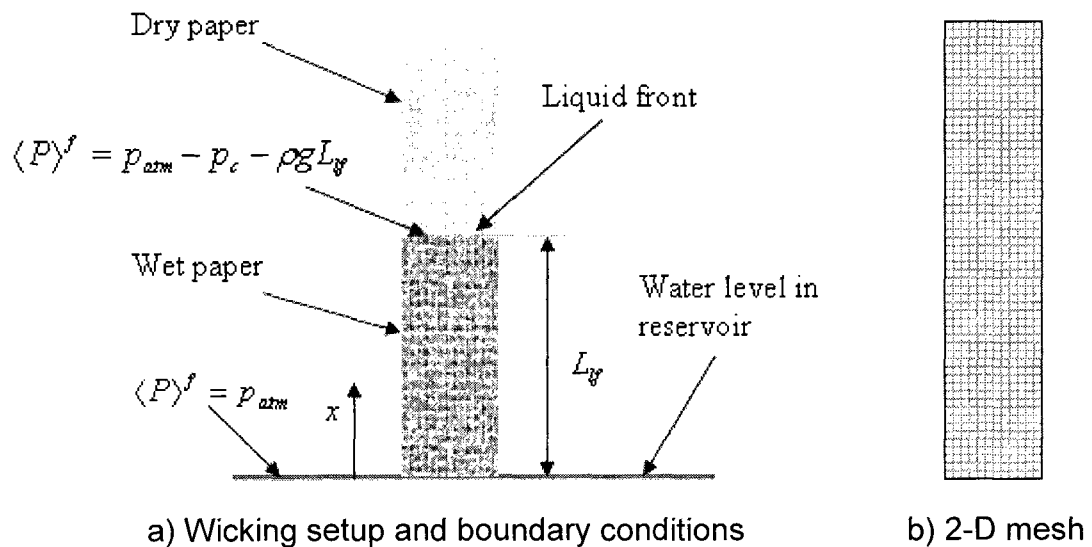


Figure 9.3 A schematic of the wicking setup and the 2-D mesh used in the numerical simulation

9.4 Numerical Simulation

We used PORE-FLOW[®] for numerically modeling the liquid flow in swelling porous media. In the algorithm employed by PORE-FLOW[®], the transient fluid-flow in porous medium involving a moving-boundary (i.e., a flow

front) is divided into multiple time steps. After assuming a quasi-steady condition during each time step, Eq (9.5) is first solved for the modified pressure in the wet region that has been saturated by the moving liquid-front. Then the computed pressure field is used to estimate the velocity field through Eq (9.1); later the velocity field is used to find the new location of the liquid front at each time-step. (Further details on the PORE-FLOW[®] algorithm are given in Chapter 4.)

Note that since the flow is essentially one-dimensional in our problem, a 2-D flow simulation is enough to capture the fluid flow in the considered geometry (see Figure 9.3b). The only difficulty here is the dependence of permeability in the wetted region behind the flow-front on time and space. Since the permeability of each element in the finite element mesh used for the simulation can be defined, this dependence reduces to just that of time²⁵ in each element. Therefore, we need to find the permeability of each element as a function of time.

Permeability of an element, before it gets 'wet' and its matrix starts swelling, is defined as the initial permeability, K_0 . Once the element has been passed by the liquid front and its matrix has been wetted, the matrix starts swelling and the porosity (defined as the ratio of the pore volume to the total volume) begins reducing, the permeability reduces with time. If t_{wet} is the time when an element gets wet²⁶ by the moving liquid-front, then we can propose the following general form for the permeability of each element as

²⁵ The time here refers to the time the element has been wetted since the passage of the liquid front through it.

²⁶ When the control volume defined around a finite element node is dry or empty, the filling factor is '0'; when it is wet or filled, the filling factor is '1'.

$$K_t = \begin{cases} K_0 & t < t_{wet} \\ fn(t - t_{wet}) & t \geq t_{wet} \end{cases} \quad (9.8)$$

The accuracy of the numerical predictions is highly dependent to the accuracy of the estimated K_0 and $fn(t - t_{wet})$. In the following section, we will explain our approach to estimating these parameters from the experimental results published by Wiryana and Berg [7].

Table 9.1. The properties of test liquids [5].

Characteristic	Unit	n-Octane	Water
Viscosity μ	<i>Pa.s</i>	0.000911	0.000522
Surface Tension γ	<i>N/m</i>	0.0723	0.0212
Contact Angle θ	<i>Degree</i>	0	0

9.4.1 Estimating the Wicking Parameters

In order to solve Eq (9.5), we need the permeability and the capillary (suction) pressure at the front. If we use the Young-Laplace equation to estimate the capillary pressure, then the needed parameters are the capillary radius R_c , the viscosity μ , the surface tension γ , and the contact angle θ . The properties of the liquids used in the experiment are given in Table 9.1 [5]. Wiryana and Berg measured the contact angle to be zero for both the liquids [7]. To estimate the capillary radius, we used the Lucas-Washburn equation, Eq (3.7). Based on Lucas-Washburn equation, we can write the following expression for the wicking tests with n-Octane:

$$L_w = \sqrt{\frac{\gamma R_c \cos(\theta)}{2\mu}} \sqrt{t} \quad (9.9)$$

Therefore, if we measure the slope of the fitting lines in the Figure 9.1, it should be equal to $\sqrt{\frac{\gamma R_c \cos(\theta)}{2\mu}}$. Since we know every parameters except R_c in this expression, so we can calculate the capillary radius R_c . The obtained results are presented in Table 9.2.

Table 9.2. The wicking parameters of test specimen estimated from Figure 9.1 plots.

% of CMC in test specimen	Capillary radius R_c [m]	Initial permeability K_0 [m ²]
0%	1.5 e-6	2.82 e-13
10%	2.47 e-6	7.65 e-13
20%	2.47 e-6	7.65 e-13
30%	2.47 e-6	7.65 e-13

To estimate the permeability, we can use the same approach using the Darcy's-law based formulation for wicking. Considering the Eq (2.21), we can write the following expression for the wicking tests showed in Figure 9.1:

$$L_w = \sqrt{\frac{4K_0 \gamma \cos(\theta)}{\varepsilon_0 \mu R_c}} \sqrt{t} \quad (9.10)$$

Once again, we can use the measured slopes of the fitted lines of Figure 9.1 to find the value of $\sqrt{\frac{4K_0 \gamma \cos(\theta)}{\varepsilon_0 \mu R_c}}$. Here ε_0 , the initial porosity, is 0.59 for all materials [7]. All other parameters in the expression are known except the permeability K_0 . The permeability thus measured could be equated to the initial permeability, K_0 ,

as there were no swelling effects present in the wicking tests with n-Octane. The measured initial permeabilities are listed in Table 9.2

9.4.2 Estimating the Local Permeability Change

In order to have theoretical (analytic or numeric) predictions for the experimental wicking data showed in Figure 9.2, we should include the swelling effects in terms of a model for the local change in permeability with time in the theoretical models. If we use the methodology explained in chapter 6, and consider the global values for permeability, then Eq (6.24) can be employed to predict the liquid-front location as

$$L_{lf} = \sqrt{\frac{2p_c}{\varepsilon_0\mu} \int_0^t K(t') dt'} \quad (9.11)$$

If we use the average values of permeability and raise both the sides of the equation to a power of 2, then Eq (9.11) simplifies to

$$L_{lf}^2 = \frac{2p_c K_{ave}}{\varepsilon_0\mu} t \quad (9.12)$$

The use of Eq (9.12) with the liquid-front-vs-time experimental data given in Figure 9.2 yields different values for the global (average) permeability as a function of time. We have used such linear equations on the best-fitted curves of L_{lf}^2 vs t to find the global permeabilities, K_{ave} , and the corresponding elapsed-time, t_i , for regular liquid-front increments (i.e., $L_0, 2L_0, 3L_0, \dots, nL_0$ at times t_1, t_2, \dots, t_n). Later we used these estimated permeabilities to approximate the permeability change in the first increment L_0 at the different times. Here is the method that was used:

For time interval $t = 0$ till $t = t_1$:

We can neglect the swelling effect due to a small time-increment and assume the permeability of the first increment of length L_0 to be identical to the initial permeability,

i.e., $K_1 = K_0$.

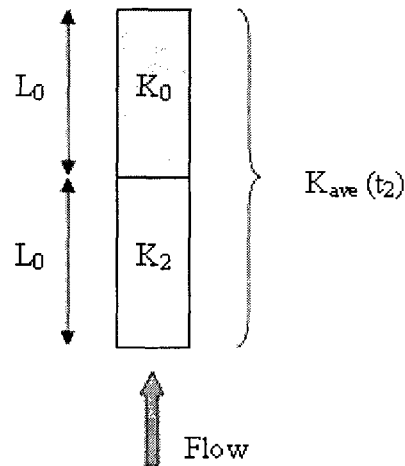


Figure 9.4 The permeabilities of the first and second parts at time $t = t_2$ along with the average permeability of the system at time $t = t_2$

For time interval $t = t_1$ till $t = t_2$:

Consider the Figure 9.4 for this time increment; the upper (second) part of length L_0 just got wet so its permeability is still K_0 , but the permeability of the lower (first) part is unknown. The global permeability that we have estimated using the experimental data at time $t = t_2$ is $K_{ave}(t_2)$. Now, we can use the method explained in Appendix B to calculate the permeability of the first part K_2 through the relation

$$\frac{L_0}{K_2} + \frac{L_0}{K_0} = \frac{2L_0}{K_{ave}(t_2)} \quad (9.13)$$

Therefore, the permeability of the first part at this time interval will be

$$K_2 = 1 / \left(\frac{2}{K_{ave}(t_2)} - \frac{1}{K_0} \right) \quad (9.14)$$

For time interval $t = t_2$ till $t = t_3$:

With an approach similar to the one explained above, we can find the permeability of the first part in the third time interval as well using the formula

$$\frac{L_0}{K_3} + \frac{2L_0}{K_{ave}(t_2)} = \frac{3L_0}{K_{ave}(t_3)} \quad (9.15)$$

Therefore, the permeability of the first part at this time interval will be

$$K_3 = 1 / \left(\frac{3}{K_{ave}(t_3)} - \frac{2}{K_{ave}(t_2)} \right) \quad (9.16)$$

For time interval $t = t_{n-1}$ till $t = t_n$:

Using the same approach, we get following expression for the permeability of the first part in the n^{th} time interval.

$$K_n = 1 / \left(\frac{n}{K_{ave}(t_n)} - \frac{n-1}{K_{ave}(t_{n-1})} \right) \quad (9.17)$$

We have used above mentioned approach to find the local changes in the permeability of the first part, i.e., K_0 to K_n over the time t_1 till t_n . This local permeability change is assumed to be equal to the time-varying permeability of the each finite element in the FE mesh after it gets wet by the advancing flow-front. The best-fitting curves were used to turn the point-wise permeability values to continuous functions of time to be able to be used in the FE/CV algorithm of PORE-FLOW[®] with varying time-steps. Table 9.3 shows the equations for the best-fitting curves that were obtained as the permeability function for each wetted element.

Table 9.3 The estimated equations for permeability change in the first part (assumed to be identical to the permeability of each wetted element) when water was used as the wicking liquid.

% of CMC in test specimen	Permeability function $\times 1e14 [m^2]$
0%	$0.02660044 t - 0.987185274 t^{1/2} + 13.9383114$
10%	$3.290189145 e^{91.48534841 / (t + 34.23242083)}$
20%	$0.59 / (0.01300368063 t^{0.4456958577} + 0.01307771327)$
30%	$157.7577211 / (t + 3.670593901) + 2.156661895$

9.5 Results and Discussion

Our goal is to use the computer code PORE-FLOW[®] (developed in-house) to predict 3-D wicking in swelling porous materials. The time-varying functions found for the permeability (Table 9.3) provide a value for the permeability of any wetted elements after any elapsed time. After knowing the permeability of the wetted elements and the capillary suction-pressure on the liquid front, we were able to use PORE-FLOW[®] for numerical predictions. Note that although the porosity of any swelling porous-medium is also varying as a result of the swelling and liquid absorption, but since we do not have any porosity term in the governing equations²⁷, so we did not model the changes in the medium porosity with time. The only porosity term that is needed is the initial porosity (porosity before swelling), which is used to estimate the capillary suction-pressure on the liquid front. Since the time steps in the numerical simulation are small, so we

²⁷ Since we assumed $b=1$ in Eq (9.3), so the porosity term was deleted from the continuity equation.

assumed the porosity at the liquid-front elements to be identical to the initial porosity of the test specimen, i.e., the porosity of the dry medium before the onset of swelling.

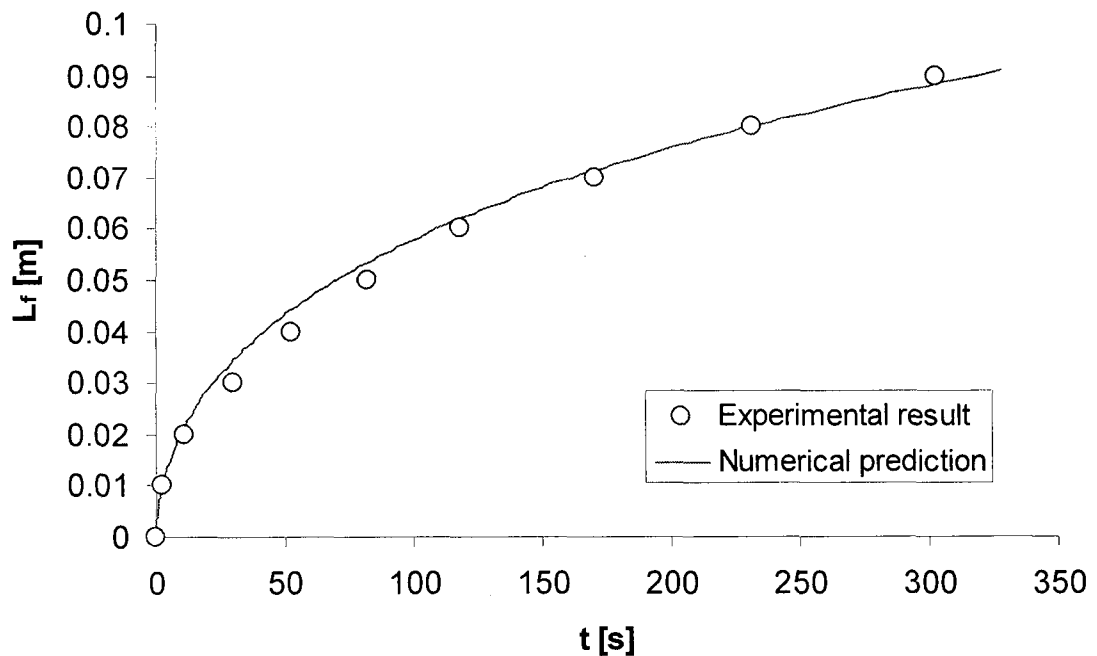


Figure 9.5 The experimental data and numerical prediction for 0% CMC

Figure 9.5 compares the numerical predictions and experimental data for the test material with 0% CMC. It shows that the numerical predictions are very accurate for this material. The slight difference between the experimental and numerical results is to be expected due to the use of several assumptions and simplifications in our theoretical /numerical model. It indicates that though these assumptions are broadly valid, we have lost some accuracy in each assumption or simplification. One such simplification is the use of the average permeability in Eq (9.10) instead of a time-varying permeability function.

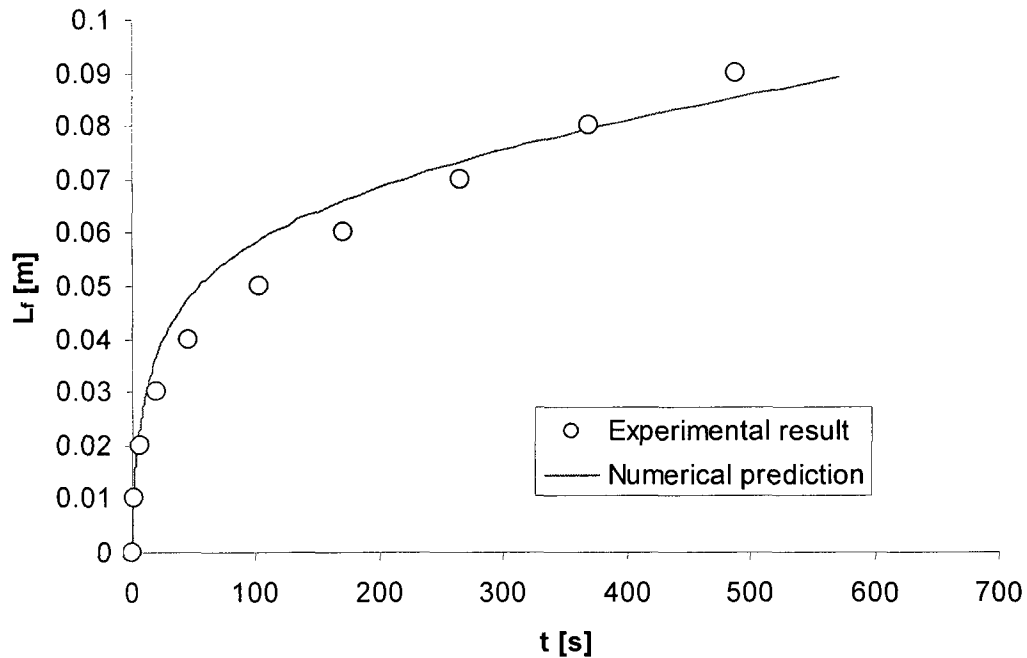


Figure 9.6 The experimental data and numerical prediction for 10% CMC

Figure 9.6 shows the same comparison for the wicking tests with 10% CMC. Here, although the accuracy is still reasonable, it is not as good as in the previous figure. It is apparent that the accuracy of our theoretical/numerical model is good at the beginning but it decreases till $t = 80$ s. After that, the accuracy increases till $t = 400$ s and then it starts to decrease again.

In Figure 9.7 the trend is different from previous figures. Here, the numerical prediction is good till $t = 250$ s, after which its accuracy begins to decrease. Note that this is for the case in which there are 20% superabsorbent fibers, which results in a higher swelling rate than the previous experiments. As mentioned in the previous section, we employed the curve-fitting procedures while developing the permeability functions. We believe that such fitting procedures caused some errors as the fitted curves do not usually match the

data at all points. Therefore, using the data file with advanced interpolation methods such as the use of splines can improve the accuracy of the permeability functions.

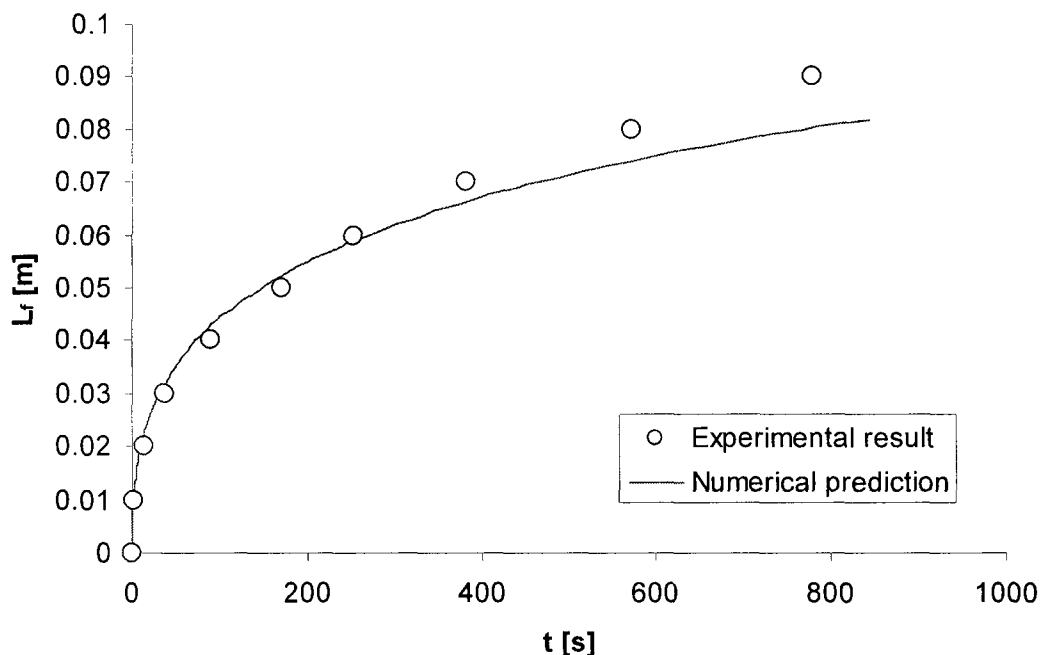


Figure 9.7 The experimental data and numerical prediction for 20% CMC

The numerical predictions for wicking in the material with 30% CMC is shown in Figure 9.8. A very good agreement between the experimental data and simulation is achieved. There is still a slight error here, presumably due to the use of curve fittings. Note that in this last case, the highest percentage of superabsorbent material (30% of CMC) is present in the paper, and hence the highest rate of swelling occurs in this case. Considering this fact, our prediction should be considered as an excellent theoretical/numerical prediction.

The comparisons presented in Figures 9.5 to 9.8 establish the accuracy of our computer code PORE-FLOW[®] for wicking predictions in swelling porous

media. We would restate the three sets of assumptions used in the present study:

1. Replacement of the transient permeability with an average permeability in Eq (9.11)
2. Use of a fitting curve to find the equal intervals for the wicking lengths
3. Use of mathematical equations in best-fitting curves while developing the local permeability functions in Table 9.3

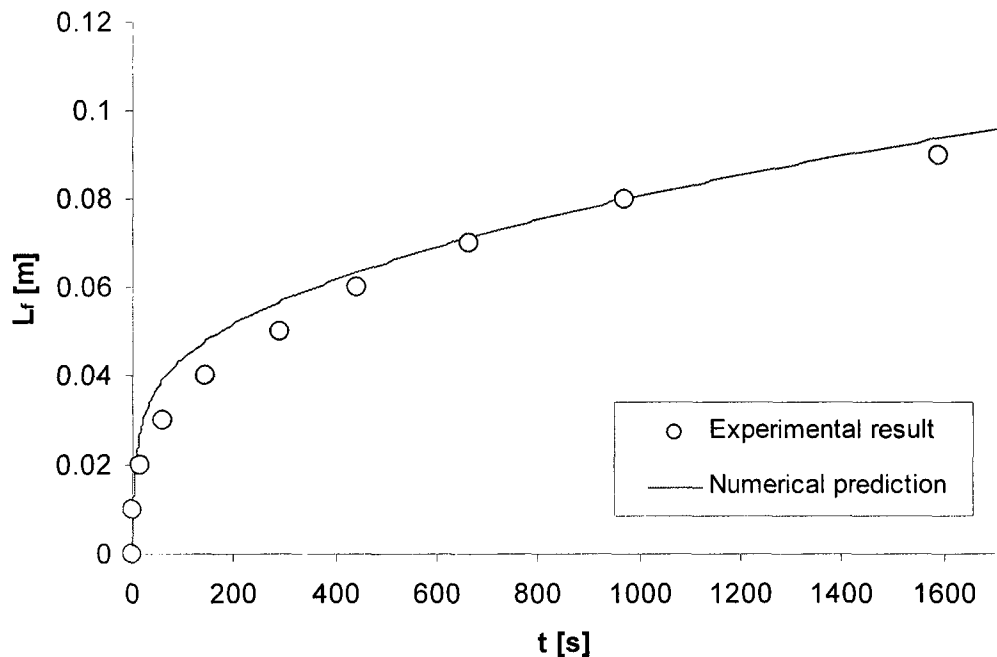


Figure 9.8 The experimental data and numerical prediction for 30% CMC

Use of these three assumptions is likely to be the cause of some errors in the final wicking predictions, but the numerical results show that such errors are not significant. In future, attempts should be made to further reduce the errors accruing from the above assumptions. Using small time-steps in the wicking simulation improves the accuracy of the first assumption. Finding the better fitting

curves such as the spline functions can improve the accuracy of the second assumption. For the third assumption, the use of the experimental data file and the spline interpolations (instead of using the mathematical relations) is likely to improve the accuracy.

As a final note on this topic of prediction errors, we would like to add that our theoretical model proposed through Equations (9.1) to (9.4) involves a fundamental assumption that the particles of a porous medium are fixed in space while undergoing swelling during the wicking process. In the cited work of Wiryana and Berg [7], the swelling experiments were conducted with paper strips where swelling would lead to an increase in the thickness of the strips²⁸ and is likely to cause small displacements of the fibers constituting the porous medium. As a result, the use of the proposed flow model will incur a slight in-built error, however small it may be.

9.6 Summary and Conclusions

We have proposed a theoretical/numerical model to predict wicking in a swelling, liquid-absorbing porous medium. The model is validated against the previous published experimental data by Wiryana and Berg [7] on wicking in composite paper made of a network of cellulose fibers and different percentage of the superabsorbent CMC. Due to the swelling of matrix in such a porous medium, the porosity and permeability vary with time and space. We developed a method to estimate the local permeability changes in porous materials using the

²⁸ No information on the change in the thickness of the paper strips used in their experiments was provided by Wiryana and Berg [7].

experimental data on wicking rate. A method to estimate the capillary suction pressure at the flow fronts was also proposed. The local permeability functions and the capillary suction-pressure expression were used to predict the wicking rate as a function of time using PORE-FLOW[®] [11], a computer program based on the FE/CV filling algorithm and developed at the University of Wisconsin-Milwaukee. The numerical predictions compare well with the experimental data. Some ways to improve the accuracy of numerical predictions through the use of improved better fitting functions are suggested. In general, this study demonstrated the efficacy of a numerical simulation based on the FE/CV algorithm and employing a sharp liquid-front assumption in predicting the wicking rate in the swelling porous media. It is important to add here that this is the first time that such a simulation is used to model the liquid flow in a swelling porous medium during the wicking process.

References

1. Jacob Bear .Dynamics of Fluids in Porous Media. Elsevier Science, 1972
2. Masoodi, R. and Pillai, K.M., "Darcy's Law based Model for Wicking in Paper-Like Swelling Porous Media," *AIChE Journal*, Published online, DOI: 10.1002/aic.12163, Jan 20 2010.
3. Lucas R. "Rate of Capillary Ascension of Liquids," *Kolloid Z.*, 23, 15, 1918.
4. E.V. Washburn. The Dynamics of Capillary Flow. *Phys. Rev.* ,17, 273, 1921.
5. Schuchardt, D.R., "The Effects of Fiber Swelling on Liquid Transport in Fibrous Media", Master's Thesis., Dept. of Chemical Engineering, University of Washington, 1989.
6. Schuchardt, D.R., Berg, J.C., "Liquid Transport in Composite Cellulose-Superabsorbent Fiber Network", *Wood and Fiber Science*, 23,3, 342-357, 1990.

7. Wiryana, S., Berg, J.C., "The Transport of Water in Wet-Formed Networks of Cellulose Fibers and Powdered Superabsorbent", *Wood and Fiber Science*, 23,3, 456-464, 1991.
8. Masoodi, R., Pillai, K.M. and Varanasi, P.P., "Darcy's Law based Models for Liquid Absorption in Polymer Wicks," *AIChE Journal*, Vol 53, No. 11, 2769-2782, 2007.
9. Masoodi, R., Tan, H., and Pillai, K.M., "Darcy's Law Based Numerical Simulation for Modeling 3-D Liquid Absorption into Porous Wicks," to appear in *AIChE Journal*.
10. Chen, Z., Huan, G., and Ma, Y., "Computational Methods for Multiphase Flows in Porous Media," Society for Industrial and Applied Mathematics, 2006.
11. <http://www4dev.uwm.edu/porous/>
12. CI Tucker and RB Dessenberger .Governing Equation for Flow and Heat Transfer in Stationary Fiber beds. In: SG Advani .Flow and Rheology in Polymer Composites Manufacturing. Elsevier Science, 1994: Ch8

Chapter 10

SUMMARY, CONTRIBUTIONS, AND FUTURE WORK

10.1 Summary

Imbibition or wicking, which is the absorption of a liquid by a porous medium due to the capillary suction pressure, is the focus of the present study. Both the conventional theories of wicking, i.e., the Locus-Washburn equation and the Darcy's law based formulation, are presented as models for the wicking process. First the imbibition in general is studied and then some special cases where the imbibitions or wicking plays an important role are considered. The first such case considered is the modeling the flow of liquids in polymer wicks. A formula based on the energy balance principle is proposed to predict the capillary suction-pressure in a porous medium made of spherical particles, such as the polymer wicks. The capillary model was also modified to improve its accuracy by making a difference between the capillary and hydraulic pore radii. Later, we employed our in-house developed software PORE-FLOW[®], based on the finite element/control volume algorithm, to numerically model the three-dimensional wicking of liquids into wicks and explore the effect of change in wick shapes on the phenomenon.

The effect of an external hydrodynamic pressure on wicking into a stack of paper wipes was studied next. In this analytical and experimental study, the performance of both the Darcy's law based formulation and the Washburn

equation were explored vis-à-vis the results of experiments conducted by us: the former behaved well under zero external pressure while the latter seemed to improve at higher external pressures.

The capillary suction-pressure applied on the liquid-fronts in porous media was studied theoretically. A general formula to predict the capillary suction-pressure in any porous medium, after including the effect of the microstructure of a porous medium, was suggested. It was shown that the expressions derived from the newly proposed formula for some simple cases are identical with the available expressions in the literature.

The imbibition in the liquid absorbing, swelling porous media was another topic that was studied. A theoretical model based on Darcy's law was proposed to model the wicking in paper-like swelling porous media. In this study, the continuity equation was modified to include the effect of swelling and liquid absorption. The predictions of the newly proposed theory were found to be identical to the predictions of the modified Washburn equation developed by Schuchardt and Berg for swelling media [1], as well as were found to satisfy their experimental data. Later, the same approach was employed to model the flow of a water-based test liquid through a fiber mat made of natural fibers. The comparison of the Darcy's law based theoretical predictions with the experimental results for the 1-D injected flow showed that the proposed model for swelling porous-media has a higher accuracy as compared to the conventional model for rigid porous-media. The software PORE-FLOW[®] was adapted to model the flow through swelling porous media such that the wicking of water in paper

strips containing superabsorbent materials could be simulated numerically. A new method was developed to estimate the local, time-dependent permeability in such swelling media. The numerical results compared well with the experimental data from a previous published study.

10.2 Contributions

Some of the important scientific contributions resulting from this Ph.D. dissertation, which were published in established technical journals and presented in international conferences, are as follows:

- First serious study of the Darcy's law based model, employing the assumption of single-phase flow behind a well-defined liquid-front and driven by the capillary suction-pressure applied at the front, for the wicking/imbibition applications
- Modification of the Darcy's law based model for modeling wicking in liquid-absorbing, swelling porous media through a new continuity equation with sink/source terms obtained through the application of the volume averaging method and through the use of time-dependent forms for the permeability and porosity [7]
- First application of the finite element/control volume (FE/CV) algorithm for the modeling of wicking/imbibition in both the rigid and swelling porous media through our in-house code PORE-FLOW[®] [5, 9]
- Application of the wicking/imbibition flow-model, developed for wicking in the swelling porous media, to model the resin flow in natural fibermats

subjected to swelling [8]

- A new validated formula for predicting the capillary suction-pressure in porous media made of spherical particles with different radii [2]
- A new validated formula for predicting the capillary suction-pressure in isotropic porous media with a constant value of the volume to surface-area ratio of the particles [3]
- A new verified capillary model, in which the capillary and hydraulic radii are treated as two independent parameters that should be measured separately, for wicking in porous media [4]
- The novel idea of using a reduction in the cross-sectional area of the cylindrical porous wicks to change the delivery rates [5]
- A general formula to predict the capillary suction pressure in a porous medium based on its microstructure [6]
- A new method to predict changes in the local permeability of swelling porous substances using the experimental data for wicking rate [9]

10.3 Future Work

Imbibition of liquids by porous media is a broad area that needs specific research for each special application. In this work, some applications were considered and the appropriate theories were developed to study the imbibition or wicking processes in them. There are still some areas that need more research to complete the current study. Following are our suggestions for future work:

- We used single-phase flow modeling to study wicking into the polymer wicks. Another approach is employing the two-phase flow model through the use of the Richard's Equation for moisture transport²⁹. Such an approach is appropriate if no sharp front is visible during wicking—around 40% of cases studied in [2] were of this type. Such an approach, which is also called the unsaturated flow approach, is definitely worth exploring for the 'diffuse front' cases in wicking.
- A general formula for the capillary suction-pressure in porous media has been proposed in this work which was validated by comparing its predictions with some other expressions verified previously for specific porous media. However, more experiments need to be done to verify its applicability to porous substances with complex microstructure.
- In the modeling of wicking in swelling materials, we adopted the global permeability (i.e., the average permeability of the wetted region as a function of time only) to simplify the governing equations. It is obvious that this reduces the accuracy. Another attempt should be made in analytical modeling after including both the space and time dependence in the permeability model (i.e., the local permeability in the wetted region changes as a function of time as well as a function of distance from the flow-front) and study how it works.
- Another part of the future work should be devoted to improving the numerical simulation of wicking in the swelling porous media. One should

²⁹ The Richard's equation is similar to the heat equation and is used to model the diffusion-like transport of moisture in porous media [10]. It is derived from the unsaturated-flow equations to model the flow of water in the capillary fringe near a saturated zone.

use smaller wicking-height intervals during the local permeability estimation. Using small time steps and better interpolation methods, such as the use of splines, should also improve the accuracy of the local permeability estimation.

- One can study the fiber swelling under microscope and use it to estimate the porosity and permeability changes in fibermats. The results of such a study can be employed to model liquid flow in the swelling natural fibermats or in the cellulose-fiber networks.

References

1. Schuchardt, D.R., Berg, J.C., "Liquid Transport in Composite Cellulose-Superabsorbent Fiber Network", *Wood and Fiber Science*, 23,3, 342-357, 1990.
2. Masoodi, R., Pillai, K.M. and Varanasi, P.P., "Darcy's Law based Models for Liquid Absorption in Polymer Wicks," *AIChE Journal*, 53, 11, 2769-2782, 2007.
3. Masoodi, R., Pillai, K.M. and Varanasi, P.P., "The Effect of Hydraulic Pressure on the Wicking Rate into the Wipes," to appear in *Journal of Engineered Fibers and Fabrics*.
4. Masoodi, R., Pillai K.M., and Varanasi P.P., "Role of Hydraulic and Capillary Radii in Improving the Effectiveness of Capillary Model in Wicking," *ASME Summer Conference*, Jacksonville FL, USA, August 10-14, 2008.
5. Masoodi, R., Pillai, K.M. and Tan, H., "Darcy's Law Based Numerical Simulation for Modeling 3-D Liquid Absorption into Porous Wicks," to appear in *AIChE Journal*.
6. Masoodi, R. and Pillai, K.M., "A General Formula for Capillary Suction-Pressure in Porous Media," a manuscript submitted to the *Journal of Porous Media*.
7. Masoodi, R. and Pillai, K.M., "Darcy's Law based Model for Wicking in Paper-Like Swelling Porous Media," *AIChE Journal*, Published online, DOI: 10.1002/aic.12163, Jan 20, 2010.
8. Masoodi, R., Pillai, K.M. and Verhagen, M.A., "Flow Modeling in Natural-Fiber Preforms used in Liquid Composite Molding," *Proc. 1st joint*

American-Canadian International Conference on Composites, Delaware, USA, September 15-17, 2009.

9. Masoodi, R. and Pillai, K.M., "A Darcy's Law Based Numerical Simulation for Modeling 3-D Liquid Absorption in Paper-Like Swelling Porous Media," a manuscript to be submitted to AIChE Journal.
10. Bear, J., "Dynamics of Fluids in Porous Materials," American Elsevier, 1972.

Appendix A

CAPILLARY PRESSURE FOR AN ISOTROPIC POROUS MEDIA WHEN THE RATIO OF VOLUME TO SURFACE AREA OF PARTICLES IS A CONSTANT

Here in order to find the suction pressure, we apply the energy balance principle to wicking. The amount of energy needed to raise the liquid in porous medium is equal to the sum of the viscous energy dissipated by the fluid, the energy spent on accelerating the fluid from zero to the wicking speed, and the energy needed to overcome the gravity. The inertial energy can be neglected as the speed of liquid is very low. We also neglect the gravity effects at this stage because we can include it later in the Darcy's law. So the reduction of free surface energy is equated to the viscous dissipation energy when the liquid moves within the porous medium. As the liquid moves through the porous medium, it reduces the dry surface area and so increases the wetted surface area. If γ_{ds} stands for surface energy in dry surface and γ_{ws} stands for surface energy in wetted surface areas, then viscous dissipation energy will be

$$(\gamma_{ds} - \gamma_{ws})dA = -dW_{vs} \quad (\text{A-1})$$

in which dA is interfacial area and w_v is viscous work done during the flow of the liquid.

According to Young's equation, the relation between the contact angle and surface energy is given by

$$\cos \theta = \frac{\gamma_{ds} - \gamma_{ws}}{\gamma} \quad (\text{A-2})$$

in which γ is represents the surface energy of the liquid and θ is contact angle. Combination of Eq. (A-1) and Eq. (A-2) leads to the following expression for viscous dissipation energy.

$$-dW_{vs} = \gamma \cos \theta dA \quad (\text{A-3})$$

If V_s and A are the volume and surface area of solid particles, let us define the suction pressure parameter Γ as

$$\Gamma = \frac{V_s}{A} \quad (\text{A-4})$$

which leads to the following expression for change in surface area:

$$dA = \frac{dV_s}{M} \quad (\text{A-5})$$

If we approximate the three-dimensional pore structure in paper as something generated by extruding a two dimensional micrograph (as shown schematically in Figure A-1) along the vertical direction, Γ can be equated to the ratio of the particle cross-sectional area to its perimeter. Hence V_s can be related to porosity through

$$dV_s = A_{cs} dh (1 - \varepsilon) \quad (\text{A-6})$$

where A_{cs} is the cross-sectional area of the porous medium perpendicular to the fluid flow velocity. Combination of Eqs. (A-5) and (A-6) leads to the following expression for interfacial surface area:

$$dA = \frac{A_{cs} dh (1 - \varepsilon)}{\Gamma} \quad (\text{A-7})$$

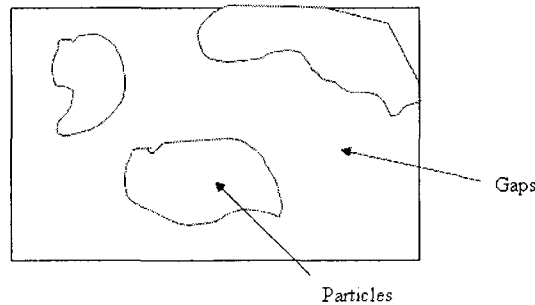


Figure A-1 A schematic of particles and void areas in the cross-section of a porous medium.

We assumed Γ stays constant during the wetting which is valid if change in the size of particles/fibers is small along the thickness direction. Substituting dA from Eq. (A-7) into Eq. (A-3) gives the final form of dissipation energy as

$$-dW_{vs} = \gamma \cos \theta \frac{A_{cs} dh(1-\varepsilon)}{\Gamma} \quad (\text{A-8})$$

The mechanical work needed to move the fluid by dh is

$$dW_m = F_p dh \quad (\text{A-9})$$

where F_p is the pulling force that ‘pulls’ the liquid front through the porous medium. As per the definition of suction pressure, this pulling force should be equal to $p_s \cdot \varepsilon A_{cs}$. So we can write

$$dW_m = p_s \varepsilon A_{cs} dh \quad (\text{A-10})$$

As per energy balance, the total energy of system after moving the front liquid into the porous medium should be equal to its initial zero value. So the summation of the left sides of Eqs (A-8) and (A-10) should be zero, i.e. $dW_{vs} + dW_m = 0$. The resultant final expression for the suction pressure is

$$p_s = \frac{\gamma_l \cos(\theta) (1-\varepsilon)}{\Gamma \varepsilon} \quad (\text{A-11})$$

Appendix B

PERMEABILITY OF A HYBRID SYSTEM

We have measured the permeability of the hybrid (wipes + fritted glass) system in my test setup in Chapter 5 using the falling head permeameter. However in order to estimate the permeability of only the wipes, the hybrid system will be treated as two porous media that are in series as follows.

First we measure the permeability of porous fritted glass (K_p) and hybrid system (K) separately using the falling head permeameter described in Chapter 5. If K_w is designated as the permeability of the stack of wipes, L_w is the length of the wipe stack in the cylinder and L_p is the length of porous fritted glass (see *Figure 5.1*), then Darcy's law will lead to:

$$Q = \frac{K \Delta P}{\mu L} \quad (\text{B-1})$$

where Q is flow rate, ΔP is steady state pressure drop occurring in the hybrid system, and $L (= L_p + L_w)$ is the total length of composite system. As the flow rates within the porous fritted glass and the wipe stack are the same, so

$$Q = \frac{K_w (\Delta P)_w}{\mu L_w} = \frac{K_p (\Delta P)_p}{\mu L_p} \quad (\text{B-2})$$

Note that the total pressure loss ΔP will be equal to the summation of the individual pressure drops in the both media:

$$(\Delta P)_w + (\Delta P)_p = \Delta P \quad (\text{B-3})$$

If the pressure drop terms from Eqs (B-1) and (B-2) are put into Eq. (B-3), we get

$$\frac{L_w}{K_w} + \frac{L_p}{K_p} = \frac{L_w + L_p}{K} \quad (\text{B-4})$$

So the overall hybrid permeability K is the harmonic mean of the two constituent permeabilities, K_w and K_p . From Eq. (B-4) the final expression for the permeability of wiper K_w is

$$K_w = \frac{L_w K_p K}{(L_w + L_p) K_p - L_p K} \quad (\text{B-5})$$

Appendix C

DERIVATION OF THE MODIFIED WASHBURN EQUATION FOR SWELLING MEDIA

Schuchardt and Berg [1] assumed that the radius of parallel tubes decreases linearly with time as a result of swelling. Based on this assumption, the capillary and hydraulic radii were proposed to be

$$R_c = R_0 \quad (\text{C-1a})$$

$$R_h = R_0 - at \quad (\text{C-1b})$$

Note that the capillary radius is taken to be a constant, as it is in the incoming dry part of the porous medium where the liquid front is just beginning to wet the matrix during wicking, while the hydraulic radius is deemed to decrease as a result of swelling. Substituting of Eqs (C-1a) and (C-1b) in Eq (3.6) and neglecting the gravity effect leads to

$$\frac{2\gamma \cos(\theta)}{R_0} = \frac{8\mu L_{if}}{(R_0 - at)^2} \frac{dL_{if}}{dt} \quad (\text{C-2})$$

On separating the variables and rearranging, we have

$$\frac{\gamma \cos(\theta)}{4\mu R_0} (R_0 - at)^2 dt = L_{if} dL_{if} \quad (\text{C-3})$$

Integrating Eq (C-3) while using the initial condition of $L_{if}(t=0) = 0$ results in the modified Washburn equation of the form proposed by Schuchardt and Berg [1]:

$$L_{if} = \sqrt{\frac{\gamma R_0 \cos(\theta)}{2\mu} \left[t - \frac{a}{R_0} t^2 + \frac{a^2}{3R_0^2} t^3 \right]^{1/2}} \quad (\text{C-4})$$

Reference

1. Schuchardt, D.R., Berg, J.C., "Liquid Transport in Composite Cellulose-Superabsorbent Fiber Network", Wood and Fiber Science, 23,3, 342-357, 1990.

Appendix D

DERIVATION OF THE VOLUME-AVERAGED CONTINUITY EQUATION FOR LIQUID-ABSORBING, SWELLING POROUS MEDIA

For a single-phase flow in a porous medium, the point-wise continuity equation for fluid flow through the pores of the porous medium can be written as

$$\frac{\partial \rho_f}{\partial t} + \vec{\nabla} \cdot (\rho_f \vec{V}_f) = 0 \quad (\text{D-1})$$

where ρ_f and \vec{V}_f are density and velocity of fluid, respectively. The volume averaging of Eq (D-1) in a term-by-term fashion within a representative elementary volume (REV) [1] leads to

$$\left\langle \frac{\partial \rho_f}{\partial t} \right\rangle + \left\langle \vec{\nabla} \cdot (\rho_f \vec{V}_f) \right\rangle = 0 \quad (\text{D-2})$$

Two averaging theorems are employed to convert the average of time and space derivatives to the derivatives of time and space. Using any fluid-flow related quantity q_f in a porous medium, the first and second averaging theorems [2,3], respectively, can be described as

$$\langle \nabla q_f \rangle = \nabla \langle q_f \rangle + \frac{1}{Vol} \int_{A_{fs}} q_f \vec{n}_{fs} dA \quad (\text{D-3})$$

$$\left\langle \frac{\partial q_f}{\partial t} \right\rangle = \frac{\partial \langle q_f \rangle}{\partial t} - \frac{1}{Vol_f} \int_{A_{fs}} q_f \vec{V}_{fs} \cdot \vec{n}_{fs} dA \quad (\text{D-4})$$

Here, A_{fs} is fluid-solid interface area, \vec{n}_{fs} is the unit normal vector on the fluid solid interface pointing from fluid phase to the solid phase, and \vec{V}_{fs} is the velocity of fluid-solid interface (see Figure D-1). The first and second terms on the right hand side of Eq (D-2) can be expanded using the first and second average theorems, Eqs (D-3) and (D-4), as

$$\frac{\partial \langle \rho_f \rangle}{\partial t} - \frac{1}{Vol} \int_{A_{fs}} \rho_f \vec{V}_f \cdot \vec{n}_{fs} dA + \vec{\nabla} \cdot \langle \rho_f \vec{V}_f \rangle + \frac{1}{Vol} \int_{A_{fs}} \rho_f \vec{V}_f \cdot \vec{n}_{fs} dA = 0 \quad (D-5)$$

Rearranging Eq (D-5) gives the following form for the volume-averaged continuity equation.

$$\frac{\partial \langle \rho_f \rangle}{\partial t} + \vec{\nabla} \cdot \langle \rho_f \vec{V}_f \rangle + \frac{1}{Vol} \int_{A_{fs}} \rho_f (\vec{V}_f - \vec{V}_{fs}) \cdot \vec{n}_{fs} dA = 0 \quad (D-6)$$

The term $\vec{V}_f - \vec{V}_{fs}$ is the relative velocity of fluid with respect to the solid surface of the particles. In the other words, the surface integral, which is evaluated at the fluid-solid interface, is the rate of absorption of a liquid by the porous-medium fibers (or particles). In superabsorbent-fiber networks undergoing swelling, the liquid is absorbed by the fibers. Eq (D-6) is the general continuity equation for flow in a deforming porous media undergoing liquid absorption by solid fibers or particles.

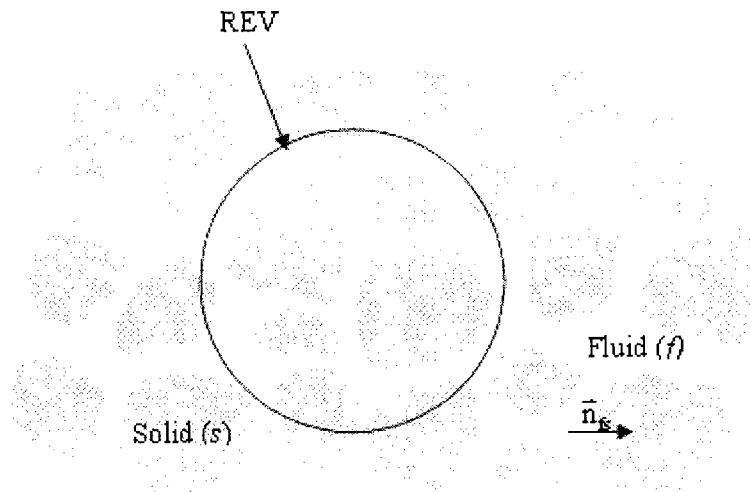


Figure D-1. A schematic showing a spherical representative elementary volume (REV), the solid particles, the fluid region, and the unit normal vector \vec{n}_{fs} (which is on the fluid-solid interface and is directed from the fluid phase to the solid phase) in a porous medium.

For an *incompressible* liquid, the density can be removed from the terms of Eq (D-6) and the continuity equation reduces to

$$\frac{\partial \langle I \rangle}{\partial t} + \vec{\nabla} \cdot \langle \vec{V}_f \rangle + S = 0 \quad (D-7)$$

with

$$S = \frac{I}{Vol} \int_{A_{fs}} (\vec{V}_f - \vec{V}_{fs}) \cdot \vec{n}_{fs} dA \quad (D-8)$$

such that the sink term S is defined to be the ratio of volumetric rate of liquid absorption within an REV to the total volume of REV. Since $\langle I \rangle = \varepsilon_f$, so Eq (D-7) can be simplified to the following final form for the flow of an incompressible liquid in a swelling, liquid-absorbing porous medium.

$$\vec{\nabla} \cdot \langle \vec{V}_f \rangle = -S - \frac{\partial \varepsilon_f}{\partial t} \quad (D-9)$$

Reference

1. Whitaker, Stephen, "The Method of Volume Averaging", Springer, 1998
2. Pillai, K.M., "Governing Equations for Unsaturated Flow in Woven Fiber Mats: Part 1 Isothermal Flows", Composites Part A: Applied Science and Manufacturing, 33, 1007-1019, 2002.
3. Pillai, K.M. and Munagavalsa, M.S., "Governing Equations for Unsaturated Flow through Woven Fiber Mats, Part 2: Nonisothermal Reactive Flows", Composites Part A: Applied Science and Manufacturing, 35, 403-415, 2004.

Appendix F

PRESSURE CHANGE UNDER A FLAT WIPE AT A SMALL ANGLE OF ATTACK

As the angle of attack is small during the wiping motion, so the lubrication approximation can be applied. Based on the lubrication approximation theory, following assumptions should be made to simplify the Navier-Stokes equations for a thin liquid film sheared between two surfaces:

- The effects of curvature of surfaces are negligible.
- Fluid properties (viscosity and density) are constant and isentropic.
- Flow is laminar.
- Flow is moving between two surfaces that are 'almost parallel'; that means the angle between the two surfaces is very close to zero.
- The pressure change across the film is small and negligible.
- The rate of change of any velocity component along the film can be neglected in comparison with the rate of the same velocity component across the film.
- Flow is predominantly two-dimensional.

After applying the above assumptions, the simplified Navier-Stokes equation will be

$$\frac{\partial P}{\partial x} = \mu \frac{\partial^2 u}{\partial y^2} \quad (\text{F-1})$$

where P is pressure, u is velocity component in the x direction, and μ is the fluid viscosity. Since P supposed to be a function of x , so this equation can be integrated twice with respect to y to get

$$u = \frac{y^2}{2\mu} \frac{\partial P}{\partial x} + Ax + B \quad (\text{F-2})$$

Here A and B are either constants or functions of x , which should satisfy the boundary conditions. Based on the schematic setup presented in Fig. F-1 where the wipe is considered fixed and the fluid is moving with the velocity U toward it, the no-slip condition at the lower surface results in

$$u(x,0) = -U \Rightarrow B = -U \quad (\text{F-3})$$

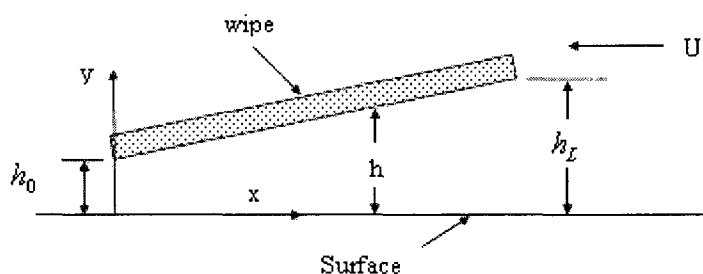


Figure F-1. A schematic of cleaning a surface by a flat wipe at a small angle of attack

In order to find A , Beavers and Joseph boundary condition should be applied at the interface of the porous wipe and the open channel below. Applying this boundary condition at the wipe-fluid interface leads to

$$\left. \frac{\partial u}{\partial y} \right|_{y=h} = s(u+U) \Big|_{y=h} \quad (\text{F-4})$$

where $s = \alpha / \sqrt{K}$, α is the dimensionless slip coefficient, and K is the wipe permeability. Using Eqs (F-2) and (F-3) in (F-4) allows us to estimate A as

$$A = -\frac{\lambda_1 h}{2\mu} \frac{\partial P}{\partial x} \quad (\text{F-5})$$

in which

$$\lambda_1 = \frac{2 - sh}{1 - sh} \quad (\text{F-6})$$

Using Eqs (F-3) and (F-5) with Eqn (F-2) yields final form of velocity equation as

$$u(x, y) = \frac{1}{2\mu} \frac{\partial P}{\partial x} (y^2 - \lambda_1 y h) - U \quad (\text{F-7})$$

To find the v component of the velocity at the top of the liquid film, the continuity equation can be applied. For 2-D incompressible fluid, the continuity equation is

$$\frac{\partial u}{\partial x} + \frac{\partial v}{\partial y} = 0 \quad (\text{F-8})$$

Integrating Eqn (F-8) from 0 to h along the y direction gives $v(x, h)$ as

$$v(x, h) = \int_0^h dv = - \int_0^h \frac{\partial u}{\partial x} dy \quad (\text{F-9})$$

To integrate the right hand side, Leibnitz rule will be applied. Accordingly,

$$\frac{\partial}{\partial x} \int_a^b f(x, y) dy = \int_a^b \frac{\partial f(x, y)}{\partial x} dy + f(x, b) \frac{db}{dx} - f(x, a) \frac{da}{dx} \quad (\text{F-10})$$

Using Eqn (F-10), the following derivation can be achieved:

$$\int_0^h \frac{\partial u}{\partial x} dy = \frac{d}{dx} \int_0^h u dy - u(x, h) \frac{dh}{dx} + u(x, 0) \frac{d0}{dx} \quad (\text{F-11})$$

Since angle of attack is small, so $\frac{dh}{dx}$ is small and negligible; last term also vanishes due to the no-slip condition at the lower surface. Using the expression for $u(x, y)$ from Eqn (F-7) for integration on the right hand side, we get

$$\int_0^h u dy = \lambda_2 \frac{\partial P}{\partial x} - Uh \quad (\text{F-12})$$

in which

$$\lambda_2 = \frac{h^3}{12\mu} (2 - 3\lambda_1) \quad (\text{F-13})$$

Using Eqns (F-12) and (F-11) in Eqn (F-9) leads to

$$v(x, h) = -\frac{d}{dx} \left(\lambda_2 \frac{\partial P}{\partial x} - Uh \right) \quad (\text{F-14})$$

If the flow into the wipe is assumed to be just in the vertical direction, which appears correct for small angle of attack, the mass balance of fluid flow under and into the wipe gives the equation

$$U(h_L - h_0) = v(x, h)L \quad (\text{F-15})$$

where L is length of the wipe. And as the angle is small, L can be considered equal to the horizontal projection of the wipe. Using Eqn (F-14) into Eqn (F-15) gives us

$$\frac{d}{dx} \left(\lambda_2 \frac{\partial P}{\partial x} - Uh \right) = -\frac{U(h_L - h_0)}{L} \quad (\text{F-16})$$

Integrating the above equation two times gives the following equation for pressure distribution:

$$\int_0^x dP = \int_0^x \frac{Uh - \frac{U(h_L - h_0)}{L}x + C}{\lambda_2} dx \quad (\text{F-17})$$

If pressures at the inlet and outlet are assumed to be zero, i.e. $P(0) = 0$ and $P(L) = 0$, then

$$P(L) = 0 \Rightarrow C = -\frac{\int_0^L \frac{Uh - \frac{U(h_L - h_0)}{L}x}{\lambda_2} dx}{\int_0^L \frac{dx}{\lambda_2}} \quad (\text{F-18})$$

Substitution of the above equation in the Eqn (F-17), while using Eqns (F-6) and (F-13), yields the final expression for pressure distribution as

$$P(x) = \int_0^x \frac{Uh - \frac{U(h_L - h_0)}{L}x - \int_0^L \frac{Uh - \frac{U(h_L - h_0)}{L}x}{\frac{h^3}{12\mu} \left(2 - 3\frac{2-sh}{1-sh}\right)} dx}{\frac{h^3}{12\mu} \left(2 - 3\frac{2-sh}{1-sh}\right)} dx \quad (\text{F-19})$$

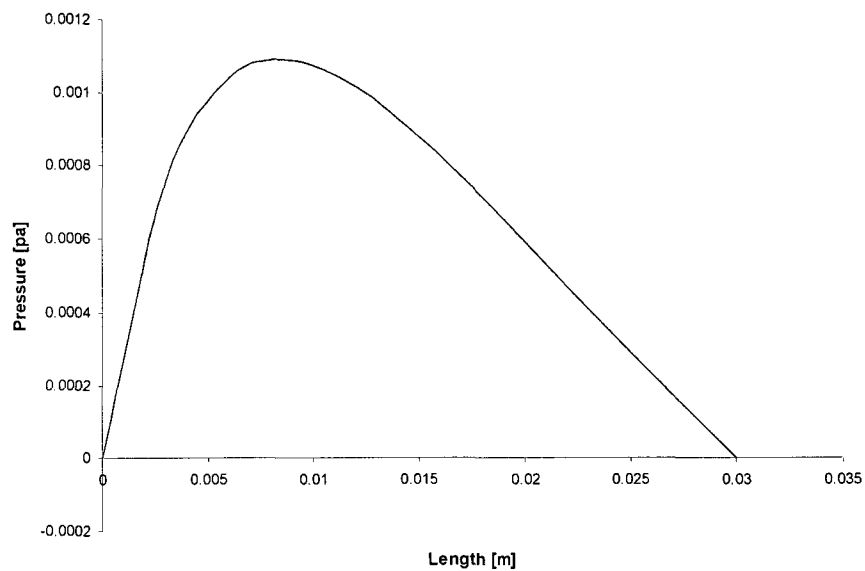


Figure F-2. Predicted pressure distribution for a wipe using Eqn (F-19).

CURRICULUM VITAE

Name: Reza Masoodi

Place of birth: Eghlid, Fars, Iran

EDUCATION

- Bachelor of Science, Amirkabir University of Technology, Iran, September 1996
Major: Marine Engineering
- Master of Science, University of Tehran, Iran, February 2002
Major: Mechanical Engineering

Dissertation Title: Modeling Imbibition of Liquids into Rigid and Swelling Porous Media

PUBLICATION

A) Published/Accepted Journal Papers

1. **Masoodi, R.**, Pillai, K.M. and Varanasi, P.P., "The Effect of Hydraulic Pressure on the Wicking Rate into the Wipes," to appear in *Journal of Engineered Fibers and Fabrics* (in print).
2. **Masoodi, R.**, Tan, H, and Pillai, K.M., "Darcy's Law Based Numerical Simulation for Modeling 3-D Liquid Absorption into Porous Wicks," to appear in *AICHE Journal* (in print).
3. Vechart, A., **Masoodi, R.**, and Pillai, K.M., "Design and Evaluation of an Idealized Porous Medium for Calibration of Permeability Measuring Devices," *Advanced Composites Letters*, Vol. 19, No. 1, 35-49, 2010 .
4. **Masoodi, R.** and Pillai, K.M., "Darcy's Law based Model for Wicking in Paper-Like Swelling Porous Media," *AICHE Journal*, Published online, DOI: 10.1002/aic.12163, Jan 20 2010.
5. Mohseni-Languri, E., Taherian, H., **Masoodi, R.**, and Reisel, J.R., "An Energy and Exergy Study of a Solar Thermal Air Collector," *Thermal Science*, Vol 13, No. 1, 205-216, 2009.
6. Mohseni-Languri, E., Gorji-Bandpy, M. and **Masoodi, R.**, "A Numerical Study of Flow and Temperature Fields in Circular Tube Heat Exchanger with Elliptic Vortex Generators," *Thermal Science*, Vol 12, No. 2, 129-136, 2008.
7. **Masoodi, R.**, Pillai, K.M. and Varanasi, P.P., "Darcy's Law based Models for Liquid Absorption in Polymer Wicks," *AICHE Journal*, Vol 53, No. 11, 2769-2782, 2007.

B) Submitted Journal Paper

1. **Masoodi, R.**, Pillai, K.M., "A General Formula for Capillary Suction Pressure in Different Porous Media," submitted to the *Journal of Porous Media*.

C) Manuscript in Preparation

1. **Masoodi, R.**, Tan, H, and Pillai, K.M., "Darcy's Law Based Numerical Simulation for Modeling 2-D Liquid Absorption into paper-like swelling porous media," to be submitted to *AIChE Journal*.
2. **Masoodi, R.** and Pillai, K.M., "An Analytical and Numerical Study of Pressure Change Under a Flat Wipe," to be submitted to *AIChE Journal*.

D) Technical Reports

1. **Masoodi, R.** and Pillai, K.M., "Wicking in pre-swelled superabsorbent particles," a technical report submitted to *Procter & Gamble Service GmbH*, Germany, April 2009.
2. **Masoodi, R.** and Pillai, K.M., "A preliminary study of wicking modeling in superabsorbent particles," a technical report submitted to *Procter & Gamble Service GmbH*, Germany, March 2009.
3. **Masoodi, R.** and Pillai, K.M., "A New Model to Predict the Liquid Absorption Rate in Polymer Wicks," a technical report submitted to *S.C. Johnson & Son Inc*, USA, July 2007.

E) Conference Papers

1. Languri, E.M., Moore, R.D., **Masoodi, R.**, Pillai, K.M., and Sabo, R., "An Approach to Model Resin Flow through Swelling Porous Media made of Natural Fibers," Proc. *10th International Conference on Flow Processes in Composite Materials (FPCM10)*, Monte Verità, Ascona, CH – July 11-15, 2010.
2. Languri, E.M., Bennett III, G. L., **Masoodi, R.**, and Pillai, K.M., "A Reference Porous Medium made by Rapid Prototyping as a Calibration Tool for Permeability Measurement," Proc. *10th International Conference on Flow Processes in Composite Materials (FPCM10)*, Monte Verità, Ascona, CH – July 11-15, 2010.
3. **Masoodi, R.**, Pillai, K.M. and Verhagen, M.A., "Flow Modeling in Natural-Fiber Preforms used in Liquid Composite Molding," Proc. *1st joint American-Canadian International Conference on Composites*, Delaware, USA, September 15-17, 2009.
4. Verhagen, M.A., Duelge, T., Pillai, K.M. and **Masoodi, R.**, "A Study of Change in Properties of Polymer Composite after the Replacement of Glass with Jute Fibers," Proc. *1st joint American- Canadian International Conference on Composites*, Delaware, USA, September 15-17, 2009.

5. **Masoodi, R.**, Pillai K.M., and Varanasi P.P., "Role of Hydraulic and Capillary Radii in Improving the Effectiveness of Capillary Model in Wicking," *ASME Summer Conference*, Jacksonville FL, USA, August 10-14, 2008.

F) Poster

1. **Masoodi, R.**, Pillai, K.M. and Tan, H., "Numerical Simulation of Wicking in Porous Media Using the Clear-Front Porous-Media Flow Model," *1st Int. Conference on Challenges of Porous Media and the inaugural meeting of the International Society for Porous Media*, Kaiserslautern, Germany, March 11-14, 2009.



Major Professor

5/10/2010

Date